MODELING DEBRIS-COVERED GLACIER DYNAMICS IN THE KARAKORAM HIMALAYA

A Dissertation

by

DA HUO

Submitted to the Office of Graduate and Professional Studies of
Texas A&M University
in partial fulfillment of the requirements for the degree of

DOCTOR OF PHILOSOPHY

Chair of Committee,	Michael P. Bishop
Committee Members,	Andrew Klein
	Anthony Filippi
	Jyh-Charn Liu
Head of Department,	David Cairns

August 2020

Major Subject: Geography

ABSTRACT

Recent studies have not achieved a general consensus on how debris-covered glaciers (DCGs) in the central Karakoram Himalaya respond to climate change. Many climate-glacier dynamics cannot be explained by existing models due to the use of oversimplified parameterizations and inappropriate assumptions. This research focuses on improving numerical models for DCGs and understanding the nature of DCG dynamics using simulations to provided new insights into the sensitivity of a DCG system to radiative forcing in the central Karakoram.

Simulations based on the Baltoro Glacier in the central Karakoram indicate that the variability in surface ablation on a DCG is regulated by the feedbacks between surface morphology, melting, and debris flux. The topographic influence on surface ablation is non-negligible for DCGs because surface topography controls irradiance and debris thickness distribution. Results also highlight the importance of debris thickness and gravitational debris flux in governing surface ablation.

Supraglacial lake simulations over the ablation zone of the Baltoro Glacier suggest that supraglacial lakes make a significant contribution (more than 20%) to the total ice-mass loss over the ablation season. Gravitational debris flux and surface topography control lake development, and the presence of supraglacial lakes increases the nonlinearity of the glacier's response to radiative forcing, which are represented as an acceleration in ablation rate, total ice-mass loss, and the lowering of surface altitude over the ablation season.

Simulation results suggest that DCGs in the central Karakoram are actively responding to radiative forcing. The positive feedback between supraglacial lake expansion and ablation may be the main cause for many critical transitions found in temporal and spatial variations in ablation, lake volume, ice volume, ice-flow speed, and mass balance. Collectively, simulations show that even though the magnitude of ice loss on a debris-free glacier is typically higher, the subsystems of a DCG show more critical state transitions and higher spatio-temporal variability, which suggest that DCGs are more sensitive to radiative forcing than previously thought, and some DCGs may exhibit higher sensitivity to climate forcing than debris-free glaciers.

DEDICATION

To my family, my mentors, and my friends who have supported me throughout my doctorate program.

ACKNOWLEDGMENTS

I would like to thank my advisor Professor Michael Bishop for his consistent support and guidance throughout this research, his advice and encouragement has been invaluable and made this work possible. Thanks also to Professor Andrew Klein, Professor Anthony Filippi, Professor Jyh-Charn Liu, Dr. Zhaohui Chi, and Brennan Young for providing advice and help.

Thanks should also go to my wife Shiqiu Lu, and my parents, who have been extremely supportive of me throughout this entire process.

I am also grateful to the Department of Geography and Professor Michael Bishop for the research and teaching assistantships and funding.

CONTRIBUTORS AND FUNDING SOURCES

Contributors

This work was supervised by a dissertation committee consisting of Professor Michael P. Bishop, Professor Andrew Klein and Professor Anthony Filippi of the Department of Geography and Professor Jyh-Charn Liu of the Department of Computer Science and Engineering.

Chapter2 of this dissertation consists of work submitted to Treatise on Geomorphology, 2nd edition (under review), which is a product of collaboration with Dr. Michael Bishop, Dr. Zhaohui Chi, and Brennan Young.

All other work conducted for the dissertation was completed by the student independently.

Funding Sources

This research was completed without outside financial support.

NOMENCLATURE

ASTER	Advanced Spaceborne Thermal Emission and Reflection Radiometer
Cosi-corr	Co-registration of Optically Sensed Images and Correlation
DCG	Debris-Covered Glacier
DEM	Digital Elevation Model
DFG	Debris-Free Glacier
ELA	Equilibrium-Line Altitude
HMA	High-Mountain Asia
SIA	Shallow Ice Approximation

TABLE OF CONTENTS

Page

LIST OF FIGURES

FIGURE Page

LIST OF TABLES

TABLE Page

1. INTRODUCTION

1.1 Overview

Debris-covered glaciers in the high-mountain Asia (HMA) play a critical role in governing water resources, natural hazards, mountain geodynamics and landscape evolution [10, 11, 12, 13, 14]. There is general consensus that the dynamics of a debris-covered glacier system is governed by a variety of controlling factors including climate, topography, and debris load [15, 16, 17, 18, 19]. Studies have focused on several important questions regarding glacier erosion and sediment fluxes [20, 21, 22, 18, 23]; climate-glacier dynamics and mass balance[13, 24, 16]; and meltwater production and drainage [25, 26]. Investigators have noted that debris-covered glacier systems are extremely complex due to numerous subsystem interactions, such as the feedbacks between surface ablation, topography and debris flux that significantly controls supraglacial lake development [27, 28], and the coupling between ice-flow, erosion and topography that governs sediment transport, glacier evolution and topographic evolution [29]. Externally, these glacier subsystems are also governed by forcing factors including climate, basin topography, hillslope sediment-transport and tectonics [30, 15, 17, 19]. Previous studies, however, have not adequately addressed such complexity, as most of the aforementioned works only partially characterize glacier systems, which leads to a large degree of uncertainty associated with evaluating and understanding of controlling factors, predicting glacier-system state, and assessing the sensitivity of debris-covered glaciers to climate change.

Numerical modeling efforts represent the only reasonable way to explore complex glacier dynamics, as field data and remote-sensing observations are difficult to acquire and do not permit spatio-temporal decoupling of parameters and feedbacks. Unfortunately, most existing numerical models [24, 16, 17] do not accurately characterize parameters and processes such as albedo, surface irradiance, surface ablation, supraglacial lake development, and sediment fluxes. System coupling and feedback mechanisms (e.g., the ablation-topography-irradiance feedback and the ice flow-

erosion-topography feedback) are also often neglected in these models. As a result, variation in the completeness of parameterization schemes raise issues and produce potentially conflicting understandings of climate-glacier dynamics in HMA. For example, most researchers agree that debris insulation makes a glacier less sensitive to climate change. Recent observations and simulations, however, show that some debris-covered glaciers have exhibited accelerated thinning despite the presence of supraglacial debris [31, 32, 16]. This effectively represents the "debris-covered glacier anomaly" that has been described by [33], where ablation rates for debris-covered glaciers are similar in magnitude to "clean-ice" glaciers, and therefore it appears that debris-covered glaciers may be more sensitive to climate change than previously thought. Present-day models do not explain this phenomenon because many processes have not been accounted for. Studies have also found that Karakoram glaciers may exhibit anomalous responses to climate (for example, the increases in ice mass and annual ice-flow velocities) compared to glaciers in other parts of the Himalaya [34, 35, 9], which suggests that these glaciers may be sensitive to changes in mass loading due to precipitation, and could be responding to precipitation forcing over shorter time frames than those postulated by glaciological theory. Current models, however, do not explain the mechanisms that govern Karakoram glacier dynamics, largely due to the oversimplified parameterization schemes and inappropriate assumptions used in these models [9]. Therefore, better numerical models are needed to provide insights into climate-glacier dynamics in the Karakoram Himalaya.

1.2 Research Objectives and Hypotheses

The main objective of this research is to advance our understanding of debris-covered glacier (DCG) dynamics and to evaluate the sensitivity of DCG systems to various forcing factors in the central Karakoram Himalaya using numerical simulations. Specific research objectives and questions include:

1. Investigate the role of debris cover and gravitational debris flux on the magnitude and spatial variability of surface ablation rates. This will be accomplished by developing and evaluating a new approach that accounts for temporally-linked climate forcing, topographic evolution, gravitational debris transport, and surface albedo variations caused by solar geometry, and sediment miner-

alogical mixing. Specifically, the objective is to determine what role the debris cover plays in regulating ablation by quantifying the impacts of debris cover type and heterogeneity, debris thickness variations, and gravitational debris flux rate on surface ablation using simulations. Given that topography also governs the sediment fluxes, it is important to understand how initial topographic conditions influence debris fluxes and surface ablation given the topography-irradiance-debris flux-ablation feedback. Simulations will be used to investigate the coupling dynamics between these parameters and processes, and also highlight the differences in ablation dynamics between a debris-covered glacier and a debris-free glacier.

Simulations will help provide insight into the degree to which gravity-driven debris fluxes alters the surface topography and albedo, thereby regulating the ablation rate. Results will provide valuable insights into the following questions: Do the above-mentioned processes and feedback accelerate ice-mass loss and make a glacier more sensitive to radiative forcing? Does variation in the debris-flux rate impact morphology, ablation and meltwater production? How does topographic forcing govern the surface ablation dynamics? Does the glacier system evolve to represent higher degrees of spatial and temporal complexity?

It is expected that the debris cover plays a more important role in glacier-system evolution than has previously been reported in the literature. Ablation patterns are expected to evolve to greater levels of spatial variation, that collectively over time could spatially oscillate thereby contributing to overall downwasting. Temporal variability in ablation is also expected to increase as modification of the topography can facilitate more meltwater, absorption of energy by debris and therefore higher ablation rates. Such questions can only be investigated via numerical simulations. It is expected that debris-covered glacier systems can reach rapid nonlinear changes in ice-mass loss compared to debris-free glaciers given radiative forcing.

2. Understand the role of supraglacial lakes in ablation dynamics and the controlling factors in lake development. Supraglacial lakes can rapidly evolve and alter the morphology of the glacier surface, and the degree to which they contribute to ice loss, sediment transport, and topographic evolution are poorly understood. These questions will be addressed by developing and evaluating a

new parameterization scheme that addresses the energy-balance and ablation for lakes, supraglacial drainage, and discharge that will be integrated with the sediment-flux and ablation models.

Simulations will be used to evaluate the specific role that supraglacial lakes have on glacier surface ablation dynamics. To date, we really do not know to what degree do supraglacial lakes contribute to surface ablation and glacial thinning, given that sediment flux-topography oscillations could also theoretically contribute to glacier thinning. Simulations will also be used to explore the couplings between lake expansion, ice-cliff retreat, gravitational debris flux, and topographic evolution that may significantly accelerate ice loss on DCGs.

It is expected that supraglacial lakes and surrounding ice-cliffs exhibit higher ablation rates than most debris-covered areas, and make significant contributions to heterogeneous thinning of the ablation zone over the melting season depending upon the size distribution and number of lakes present. The presence of water and lake expansion should dramatically change the glacier surface morphology and result in more ice-mass loss. The change in surface albedo will alter the energy input into the system and facilitate sediment transport to enhance debris thinning and increases in ablation at the debris-ice interface. Surface and marginal streams should form during the ablation season, thereby modifying the topography and altering other surface processes. It is expected that supraglacial lake formation and evolution dramatically causes rapid nonlinear change in the glacier surface morphology and magnitude of ice loss over time. This is anticipated to be a system threshold that governs the stability of glacier subsystem and dictates system state.

3. Glacier ice-flow dynamics have long been recognized to be a critical component of climate-glacier dynamics and an indicator of glacier state [36]. Consequently, an important objective is to understand the role of ice-flow in regulating ice and sediment transport, basal erosion and topography evolution which is the basis for many glacial processes. This will be addressed by developing and evaluating an integrated parameterization scheme that accounts for ice-flow, basal glacier erosion, and debris advection governed by ice-velocity field. Multiple simulations will be used to answer the following research questions: 1) To what degree does ice-flow influence glacier mass balance and debris transport? 2) What is the spatial variability and magnitude of the basal

erosion rate? 3) Is englacial debris transport sensitive to the change in basal topography? 4) How long does it take entrained sediment to make its way to the glacier surface?

Simulations will be used to explore ice-flow dynamics and its impact on glacier subsystems. It is expected that ice-flow plays a critical role in governing overall dynamics of a DCG because it is responsible for supraglacial and englacial debris advection, surface topography evolution, glacier erosion, and mass flux from the accumulation zone which controls the ice volume of the glacier.

4. Assess DCG system sensitivity to radiative forcing and understand critical transitions and controlling factors that govern major DCG subsystems using integrated modeling. Simulation will be used to identify critical nonlinear transitions that exist in DCG subsystems that indicate high sensitivity to radiative forcing. Results will also provide comparisons to determine if a DCG system can be more sensitive to radiative forcing than a debris-free glacier system in the central Karakoram.

This will be achieved by performing tipping point analysis on temporal and spatial variations of DCG subsystems (including surface ablation, supraglacial lakes, ice volume, ice-flow velocity, and mass balance) to identify early warning signals that indicate critical system transitions as a proxy for sensitivity to radiative forcing. Tipping point analysis can capture the effects of positive feedbacks that lead to rapid changes in a glacier subsystem, therefore, this type of analysis is a better approach to characterize system sensitivity than traditional metrics such as terminus states and overall mass balance.

It is expected that DCGs in the Karakoram are actively responding to climate change, even though their terminus positions may be considered stable due to debris loads. More tipping points are expected to be found in a DCG system than in a DFG system as tipping points are early indicators of critical transitions that are mostly caused by positive feedbacks between ablation and supraglacial lake expansion. More tipping points are also expected to be identified when examining parameter spatial variation in altitude profiles for DCGs compared to DFGs, caused by heterogeneous debris loads and supra-glacial lake distributions. Collectively, it is hypothesized that even though the magnitude of ice loss on a DFG is typically higher, a DCG exhibits more

critical state transitions and higher spatio-temporal variability, which suggests a higher level of sensitivity to radiative forcing.

1.3 Research Significance

It is widely known that DCG dynamics in HMA govern water resources, natural hazards and mountain geodynamics [14, 15]. Unfortunately, these systems are extremely complex, and a multitude of positive and negative feedbacks regulate glacier fluctuations and system evolution. Currently, there is still no agreement on the state and fate of Karakoram glaciers due to uncertainties in climate, topographic and debris-load forcings and the aforementioned Karakoram and "debris-covered glacier" anomalies. This research provides numerical simulations to potentially permit better understandings of the complexities associated with DCGs, and help identify the key forcing factors that regulate glacier response to climate, and identify indicator metrics for evaluating nonlinear responses in glacier-system evolution in the central Karakoram Himalaya. This research can contribute to scientific inquiry and practical problem solving related to water resources, food security, geohazards, geodynamics, geomorphology, and glaciology issues.

From a methodological perspective, the parametrization schemes and integration of various models developed in this research account for numerous processes, feedback mechanisms and forcing factors that have been neglected or over-simplified in existing glacier system models. Examples include the use of radiation-transfer models that account for local and meso-scale topographic effects of surface irradiance; a relatively comprehensive debris transport system including gravity-driven debris flux and ice-flow driven debris flux; mineral spectral reflectance mixing and temporal surface albedo variation caused by sediment flux, meltwater production, and supraglacial drainage and lake evolution; supraglacial discharge; basal-debris production due to erosion; and topographic controls on erosion rate and englacial debris transport. Therefore, this research explores the subsystem couplings and characterizes feedback mechanisms between multiple parameters, processes and subsystems, many of which have never been discussed in the existing literature. Innovative numerical approaches are used to address the associated characterization and modeling issues, which will significantly facilitate new insights and future studies.

1.4 Research Activities

The Baltoro Glacier in the central Karakoram of Pakistan is used to evaluate glacier subsystem response to forcing factors and to investigate system coupling and feedback mechanisms through integrated model simulations. The research will be systematically broken into chapters that focus on the investigation of a particular set of processes and feedbacks.

Chapter 2 addresses issues associated with characterizing and modeling DCGs. It essentially represents background information for understanding the nature of the problem, and identifying specific glacier modeling issues that need to be addressed based on a detailed review of the literature and existing models and studies. Specifically, multiple numerical modeling issues associated with glacier-system components are discussed, and preliminary simulation results are incorporated into the discussion to demonstrate various concepts. This includes discussion of the surface-energy balance, debris loads and sediment transport, ablation dynamics, supraglacial hydrology, ice-flow dynamics and glacial erosion. We also highlight numerous modeling issues regarding subsystem coupling, feedback mechanisms, model input and validation, and identify important research questions for understanding complex DCGs.

Chapter 3 addresses surface-ablation dynamics. The ablation dynamics of a DCG represents a multitude of processes and feedbacks that involve microclimate, debris loads, topography, meltwater production and drainage. Most existing ablation models either over-simplify these surface conditions or heavily rely on meteorological and remote-sensing measurements. This chapter address these issues using a solar radiation-driven glacier surface ablation model that more fully characterizes surface-irradiance conditions that are govern by topographic variations and ablation dynamics, by accounting for temporally-linked radiative forcing, topographic evolution, sediment mixing, and gravitational debris transport (other factors that also influence surface ablation dynamics such as supraglacial lakes, meltwater drainage and ice-flow dynamics will be addressed in subsequent chapters). Simulations are used to investigate the processes and feedbacks that govern surface-ablation rates, to understand the influence of sediment flux on mass balance over the glacier and to explain the observed heterogeneous downwasting of DCGs in the Karakoram.

Chapter 4 addresses the dynamics of supraglacial meltwater drainage and lake development. Supraglacial lakes and meltwater transport play an important role in the mass-balance of DCGs [37, 38, 39]. Researchers have found that ponding is caused by surface ablation under a differential surface lowering condition, and the increasing lake areas can significantly magnify surface ablation rates [38, 40]. Existing models, however, often neglect supraglacial lakes [4, 24], which could be one of the reasons why we cannot explain the high-magnitude downwasting on some debris-covered Himalayan glaciers [31, 16]. This chapter investigates the dynamics of supraglacial lakes and the supraglacial hydrology-morphology interactions using numerical simulations. Specifically, a new parameterization scheme is developed that incorporates supraglacial drainage and lake evolution into the surface-ablation model to quantify the impact of supraglacial lakes on surface ablation, to understand the coupling mechanisms between supraglacial hydrology and supraglacial morphology, and associated time scales, and to investigate the favored conditions for supraglacial lake formation. This work will enable us to quantify the influence of supraglacial lakes on ablation dynamics and a glacier's nonlinear responses to radiative forcing.

Chapter 5 addresses ice-flow dynamics and DCG system sensitivity to radiative forcing. Ice-flow dynamics regulates glacier mass distribution, flow velocity, basal erosion and glacier geometry. For a DCG, ice-flow also controls debris production and transport. In this chapter, we investigate ice-flow dynamics and merge them with other sub-models to simulate glacier subsystem responses to radiative forcing. Most importantly, simulation results from the integrated model are analyzed using a tipping point analysis approach to understand the sensitivity of DCG subsystems to forcing factors. Glacier subsystem responses are evaluated from temporal and spatial perspectives, to identify the controlling factors that cause rapid nonlinear changes in a DCG system. Identifying early indicators (tipping points) of critical system changes and comparing DCG systems to debris-free systems is the focus of this chapter.

Finally, Chapter 6 will include an overview of the research and a summary of all the major conclusions from this work. In addition, this chapter will make recommendations for future research and compare our findings to current understandings of DCG dynamics presented in the literature.

2. NUMERICAL MODELING ISSUES FOR UNDERSTANDING COMPLEX DEBRIS-COVERED GLACIERS

2.1 Abstract

Debris-covered glaciers play a critical role in governing mountain geodynamics and relief production. Numerous process and system couplings regulate glacier dynamics at various scales, and understanding glacier sensitivity to climate change is notoriously difficult. Consequently, numerical models are needed to investigate the ablation, accumulation and sediment-transport dynamics that govern glacier morphometric responses to climate forcing. This chapter addresses glacier modeling issues for characterizing surface-energy balance, ablation, meltwater production, supraglacial debris fluxes, ice-flow dynamics and glacial erosion. We highlight numerous modeling issues regarding specific processes, subsystem coupling and feedbacks, model input and validation, and identify research directions.

2.2 Introduction

Debris-covered glaciers play a fundamental role in governing mountain geodynamics and regulate geohazards and resource availability [10, 11, 12, 13, 14]. Consequently, they are studied extensively by the geomorphology, glaciology, and hydrology communities, as investigators seek to address important questions regarding glacier erosion, sediment fluxes, landforms and relief production [20, 21, 22, 18, 23]; climate-glacier dynamics and mass balance [13, 24, 16]; and meltwater production and drainage [25, 26]. Research has focused on the identification and characterization of the most significant processes and controlling factors that govern glacier systems and their responses to climate change. There is general consensus that climate, topography, and debris load represent important factors in governing debris-covered glacier dynamics [15, 16, 17, 18, 19]. Furthermore, it is important to note that glacier systems are extremely complex due to glacier-system couplings that are also coupled with external topographically-forced systems involving radiative and precipitation forcing, topographic and far-field tectonic stresses, and sediment-transport dy-

namics [30, 15, 17, 19]. Such complexity contributes to a large degree of uncertainty associated with determining the impact of controlling factors, predicting the state of these systems, and assessing the sensitivity of debris-covered glaciers to climate change. The inherent spatio-temporal scale-dependent dominance of processes and feedbacks can presently only be accounted for through numerical modeling, as field data and remote-sensing observations do not permit spatio-temporal decoupling of factors and assessment of process-form responses over large areas.

The complexity of glacier systems when viewed from empirical statistical-based studies, can lead to uncertainty and ambiguity in our understanding of controlling factors. This is in part due to the lack of key spatio-temporal datasets needed to characterize the scale dependencies of processes and feedback mechanisms. Furthermore, assumptions in characterizing parameters, process mechanics, and the exclusion of parameters and systems in analysis and modeling efforts may influence the significance or validity of results, as important positive and negative feedback mechanisms may not have been accounted for. This may explain conflicting understandings and variable explanations regarding climate forcing [9], the role of morphometric controlling factors [41, 42, 43], process rates [16, 23], glacier state [44], and system responses over time [17, 18]. For example, studies have shown that debris cover governs surface melting [45, 46], and it is generally thought that debris insulation reduces debris-covered glacier sensitivity to climate change. This understanding, however, does not account for the mass loading (accumulation) dynamics that drives ice-flow velocities. Mass loading is sensitive to changes in precipitation, which is a major component of the climate system. Numerous investigators have reported that there have been increases in ice mass and annual ice-flow velocities in the Karakoram [34, 35, 9], which suggests that the glaciers could be responding to precipitation forcing over shorter time frames than those postulated by glaciological theory. If this is the case, then glacier sensitivity to climate change must also account for accumulation and flow dynamics. Unfortunately, most analysis and modeling efforts do not, or cannot accurately account for climate-system dynamics and orographic precipitation due to the need for high-resolution topographic data that governs circulation patterns and precipitation processes.

Furthermore, we lack fundamental data on the lithological variations of debris loads on glaciers, do not have reliable estimates on debris-depth variations, do not typically account for gravitational and ice-flow sediment-transport fluxes, and do not account for boundary-layer dynamics driven by the surface-energy balance. The assumption of a linear thermal gradient for the debris load promotes the conclusion of insulation given increasing debris thickness. Recent observations and simulations, however, show that some debris-covered glaciers have exhibited accelerated thinning despite the presence of supraglacial debris [31, 32, 16]. This effectively represents the "debris-covered glacier anomaly" that has been described by [33], where ablation rates for debris-covered glaciers are similar in magnitude to "clean-ice" glaciers, and it appears that debris-covered glaciers could be more sensitive to climate change than previously thought. This can also be explained by sediment fluxes that alter debris-load distributions and depth that govern spatial variability in ablation rates and further promote meltwater sediment transfer (i.e., supra-fluvial processes). Where debris depths are large, it is possible that surface heating can be accentuated, thereby initiating atmospheric convective motion [47, 48]. This could result in precipitation which makes it way to the ice-surface given porous debris loads, thereby increasing the ablation rate. Unfortunately, the timing and periodicity of such forcing mechanisms are not known with any degree of certainty.

Supraglacial ponding is another overlooked process for debris-covered glaciers. Supraglacial lakes play an important role in glacier mass-balance as well as glacial hydrology [37, 38, 39]. Researchers have found that ponding is caused by surface ablation under a differential surface lowering condition, and the number of ponds are increasing on some large debris-covered glaciers [23]. Studies have also indicated that the spatial density of supraglacial ponds is directly related to the degree of thinning because the collapse of englacial water channel roofs leads to a high degree of vertical thinning [38]. Unfortunately, many of these important mechanisms have not been adequately studied and are often neglected in existing glacier models and simulations by the geomorphological community (e.g.,[49, 16, 17, 18]).

Recent simulations highlight the importance of system coupling and feedbacks for understanding debris-covered glaciers [17]. For example, a potential feedback involving ice-flow, erosion and

topography may have a significant impact on glacier evolution in the Himalaya [29]. The system coupling between sub-glacial processes and sediment-transport dynamics is also important, yet largely remain unknown [50]. Numerical simulations are needed to investigate these processes, feedbacks and their spatio-temporal scale dependencies. Unfortunately, multiple components of this complex system have not been adequately represented in modeling efforts, which poses a challenge to our current understanding of debris-covered glaciers and magnifies the uncertainty in current climate-glacier sensitivity assessments [51, 52, 50, 17, 19].

Given that numerical modeling is one of the most powerful methods for exploring complex glacier dynamics [50, 17, 18], the primary objective of this chapter is to describe important processes and components of the debris-covered glacier system that need to be accounted for in modeling efforts. We specifically review existing models of glacier system components and identify issues associated with characterizing parameters and estimating process rates, so that we can better understand the fundamental processes that govern glacier responses. We utilize simulation results from Karakoram glaciers to demonstrate the concepts, parameters and processes discussed in this chapter. Finally, we recommend new research directions to facilitate future studies.

2.3 Glacier System Components and Issues

Numerous components of the geomorphological system regulate glacier mass balance, surface process rates and topographic evolution. This includes the coupling of climate, surface process and tectonic systems [36, 50, 17, 19]. Characterization of numerous subsystems is required, which includes the surface-energy budget, landscape erosion and sediment-transport dynamics, glacier ablation dynamics, ice-flow dynamics, and glacier erosion and uplift dynamics. In this section, we address these subcomponents with respect to modeling and issues.

2.3.1 Surface-Energy Budget

The surface-energy balance governs ablation rates and meltwater production on a debris-covered glacier. The energy balance at the debris/air interface can be written as [53, 45]:

$$Q_s + Q_l + Q_h + Q_e + Q_c = 0, \tag{2.1}$$

where Q_s is the net short-wave radiation flux, Q_l is the net long-wave radiation flux, Q_h is the net sensible-heat flux, Q_e is the net latent-heat flux, and Q_c is the conductive heat flux into the debris which governs the ablation rate. Note that in a distributed model, heat-flux terms must be computed at the beginning of each iteration due to the changing topography, albedo, and surface temperature.

For glacier surfaces that are covered by lakes or ponds, the ablation process is more complex. Sakai et al. [38] developed an energy-balance model to estimate the melting caused by supraglacial lakes:

$$Q_s + Q_l + Q_h + Q_e + Q_{in} - Q_{out} - \Delta Q_t - Q_i - Q_d = 0, \tag{2.2}$$

where $Q_s + Q_l + Q_h + Q_e$ is the net heat flux at the lake surface, Q_{in} is the input heat flux from meltwater inflow into the lake, which in most cases, can be neglected [38], Q_{out} is the output heat flux from the water outflow from the lake, which dominates the englacial ablation caused by lakes [38], ΔQ_t is the change in heat storage of the lake, Q_i is the conductive heat flux into the bare-ice areas under the water surface, and Q_d is the conductive heat flux into the debris-covered areas under the water surface.

Many glacier models do not account for the full surface-energy budget conditions, and most do not account for the influence of supraglacial lakes governing the ablation rate (e.g., [49, 24, 17, 18]). This potentially results in underestimation of the ablation rate and the degree of glacier thinning, which governs ice depth and erosion rates.

Net radiation fluxes dominate glacier-surface-energy balance and significantly control surface ablation rates [36, 45]. The net short-wave radiation flux and the net long-wave radiation flux can be computed as:

$$Q_s = (E_d + E_d + E_t)(1 - \alpha), \tag{2.3}$$

$$Q_l = \varepsilon_a \sigma T_0^4 - \varepsilon_s \sigma T_s^4 + \varepsilon_t \sigma T_t^4, \tag{2.4}$$

where E_b is the direct/beam irradiance from the sun, E_d is the diffuse-skylight irradiance, E_t is the adjacent-terrain irradiance, and α is the surface albedo. For the long-wave radiation fluxes, ε_a, ε_s and ε_t are the emissivity for the air, glacier surface and adjacent terrain, respectively, σ is the Stefan-Boltzmann constant, T_0 is the air temperature which is a function of altitude, T_s is the surface temperature, and T_t is the surface temperature of the surrounding terrain, which represents the long-wave adjacent-terrain irradiance that is not usually accounted for. Air temperature can be measured at-site or can be estimated based on climate reanalysis data. Surface temperature modeling is required, as it can be highly variable over time. The long-wave adjacent-terrain irradiance can also be significant, as debris surface temperatures have been recorded to range from about 20^oC to 35^oC during the day [54, 55], resulting in non-negligible irradiance for certain locations, assuming Lambertian (isotropic) emission of energy. Researchers have noted that long-wave irradiance contributes to the high-magnitude ablation on ice cliffs [54].

Regarding the short-wave component, surface irradiance is often not accounted for as the irradiance components are strongly governed by multi-scale topographic effects and are wavelength dependent [56]. Furthermore, surface albedo estimates are not usually accounted for, as this requires information on area and intimate surface-matter composition mixtures, and on variations in the surface bi-directional reflectance distribution function (BRDF) that is also governed by solar geometry and topography. Glacier surface albedo generally decreases over time during the ablation season [36], and sediment fluxes (i.e., changes in composition, thermal and reflectance properties, topography and ablation rate) and moisture conditions also cause spatio-temporal variability in surface albedo.

The dominant surface-irradiance component is the direct-beam irradiance (E_b). Many surface

ablation models only account for the direct-beam irradiance under assumptions of simplified solar geometry, surface albedo and topographic effects (e.g., [13, 49, 24]). These assumptions often yield unrealistically homogeneous patterns of ablation rates over glaciers. Complex topography in the Himalaya causes significant variation in surface irradiance over short distances due to extreme relief and cast shadows [16]. Furthermore, minor variations in one variable, when multiplicatively coupled with other prominent governing parameters (e.g., atmospheric and a multitude of topographic factors), generates significant variation in E_b. The parameterization scheme for an exact computation is:

$$E_b(\lambda) = E^0(\lambda)T^{\downarrow}(\lambda)cosiS, \tag{2.5}$$

where E^0 is the exo-atmospheric irradiance, which is modified by the Earth-Sun distance correction factor, λ is the wavelength of light, $T^{\downarrow}$ is the downward total transmittance, $cosi$ is the cosine of the incidence angle of illumination (i), and S is a binary coefficient that accounts for cast shadows being present ($S = 0.0$) or absent ($S = 1.0$) on the landscape. The exo-atmospheric conditions are governed by orbital parameters such as the eccentricity of the orbit, the obliquity of the Earth's axis and the longitude of the Earth's perihelion [56].

The atmosphere attenuates the solar beam via gaseous absorption and molecular and aerosol scattering [57, 58]. Atmospheric processes are highly wavelength dependent and controlled by spatio-temporal variations in various atmospheric constituents including aerosols, and water vapor [59, 58].

The atmospheric transmittance should account for the primary constituents, such that $T^{\downarrow}$ can be computed as [60]:

$$T^{\downarrow}(\theta_s, \lambda) = T_r(\theta_s, \lambda)T_a(\theta_s, \lambda)T_g(\theta_s, \lambda)T_o(\theta_s, \lambda)T_w(\theta_s, \lambda), \tag{2.6}$$

where T_r represents transmittance due to Rayleigh scatter, T_a is transmittance due to aerosol scattering, T_g is transmittance due to primary gas absorption, T_o is transmittance due to ozone absorp-

tion, T_w is transmittance due to water-vapor absorption, and θ_s is the solar-zenith angle. The total atmospheric transmittance is a function of the total optical depth of the atmosphere that is related to the hypsometry of the topography, such that variations in topographic relief can cause mesoscale variations in the atmospheric optical depth and volumetric scattering of radiation.

It is also necessary to address local topographic effects that account for the relationship between the solar and terrain geometry. Specifically, the incidence angle of illumination (i) between the sun and normal to the ground surface is defined as:

$$cosi = cos\theta_s cos\theta_t + sin\theta_s sin\theta_t cos(\phi_t - \phi_s), \tag{2.7}$$

where θ_s is the apparent solar-zenith angle that accounts for altitude variations and atmospheric refraction given the atmospheric temperature and pressure profiles, θ_t represents the terrain slope angle, ϕ_s is the solar-azimuth angle, and ϕ_t is the terrain slope-azimuth angle. Calculation of cos i is possible with the use of a digital elevation model (DEM). The solar geometry is also governed by orbital parameters that vary over time. Finally, the meso-scale relief structure of the topography, coupled with temporally-dependent solar geometry, governs the presence of cast shadows on the landscape. Ray-tracing algorithms can be used to account for this influence on E_b [61, 62, 63, 64]. This component is highly variable over the diurnal cycle.

The net sensible-heat flux and the net latent-heat flux terms can be computed as [45]:

$$Q_h = \rho_0(\frac{P}{P_0})cA_t u_w(T_0 - T_s), \tag{2.8}$$

$$Q_e = (\frac{0.622\rho_0}{P_0})L_e A_t u_w(e_z - e_s), \tag{2.9}$$

where ρ_0 is the air density at sea-level, P is the air pressure at altitude, P_0 is the standard air pressure at sea level, c is the specific-heat capacity of air, u_w is the wind speed, L_e is the latent heat of evaporation of water, e_z is the vapor pressure of air above the surface, e_s is the vapor pressure at the glacier surface, and A_t is a dimensionless transfer coefficient defined by [45].

Information about atmospheric surface wind direction and speed is difficult to obtain, and is usually estimated based upon using climate stations in the field. Nevertheless, surface irradiance, temperature and roughness variations usually cause significant variation in wind direction and speed over glaciers [65].

2.3.2 Sediment Transport and Debris Loads

Supraglacial debris plays a crucial role in glacier surface ablation and morphological evolution [66, 45, 18]. Supraglacial debris thickness can be spatially heterogeneous due to debris transport by ice-flow, gravitational movement, and hydrological processes [18, 67, 23]. Scale-dependent sediment-transport processes also control glacier topography, the mass-balance gradient, ice-velocity gradient due to load stress, and glacial drainage [68, 69]. Although several approaches have been developed to estimate the distribution of debris thickness (e.g., [4]), to understand the effects of debris on surface ablation (e.g., [4, 49, 24]), and to model debris transport on glacier surfaces (e.g., [18, 17]), there are still many unknowns associated with the properties of supraglacial debris, and many related processes have not been accounted for in existing numerical models.

2.3.2.1 Supraglacial Debris

The source of supraglacial debris can be of aeolian, mass movement, fluvial, and/or glacial in origin depending upon environmental conditions. Aeolian transport and deposition of sediment can occur from the adjacent landscape and from supraglacial deposits. Mass movement processes from the adjacent terrain can be significant over time, including landslides [50], snow avalanches [70], and rockfalls from hillslopes and headwalls [50]. Physical and chemical weathering also provide debris that can be incorporated into surface runoff contributions and redistribution of sediment via supra-fluvial erosion and transport. Ablation dynamics and meltwater production also produce more debris, as englacial debris loads become part of the supraglacial debris load. Glacial erosion at the glacier bed also encapsulates debris into the englacial debris load. Finally, gravity and ice-flow dynamics provide the two dominant forms of glacier debris-load transport excluding the basal

debris load which is primarily transported by subsurface glacial hydrological mechanisms and pathways. Studies have pointed out that, for most valley glaciers in the Himalaya, headwall and sidewall erosion is the primary source of supraglacial debris [71, 20]. Oversteepened hillslopes on headwalls and surrounding sidewalls can deliver large amounts of rock and sediment onto glacier surfaces and are transported to lower altitudes due to gravity and/or ice/water transport (i.e., ice flow and supra-fluvial processes). A typical headwall erosion rate ranges from 0.5 to 2 mm yr-1 [18]. Hillslope erosion rates are also regulated by the relief and slope angles, and topography controls rock resistance to erosion and the locations where debris can be deposited onto the glacier surface. Tributary glaciers also contribute to debris input, especially at glacier-tributary junctions [72]. Ultimately the production of debris is governed by a variety of factors such as topographic stress, lithology, and various erosion mechanisms within a basin.

Supraglacial debris depths are highly variable and can range from several millimeters to over 5 meters thick [73, 74]. From a surface planimetric perspective, the spatial heterogeneity in debris thickness is also an important factor that can regulate surface ablation and meltwater production, thereby governing the production and distribution of supraglacial lakes and ice cliffs [75, 17]. Researchers have also indicated that the water content in in the debris cover also affects sub-debris ablation [48].

Many studies have documented a negative relationship between debris thickness and ablation rate due to insulation by a thick debris layer (e.g. [76, 66, 2]). These studies, however, did not account for the melt-enhancing effect of thin debris due to the higher absorption of solar radiation by debris and conduction of heat into the underlying ice [3, 2, 77].

For many temperate mountain glaciers, debris loads over the terminus can limit glacial recession [72, 78, 52, 18] because debris loads are much thicker at the terminus due to increased surface melting at lower altitudes, and the accumulation of the upwelling englacial debris load due to the upward flow of ice [79, 80, 81]. Several studies have confirmed that a heavily debris-covered terminus allows the glacier to extend further below the ELA than a clean-ice glacier [52, 18].

Several approaches have been developed to estimate the distribution of debris thickness. Mi-

halcea et al.[4] and Juen et al.[82] derived debris thickness from land surface temperature based on regressions equations using field measurements. Zhang et al.[49] use surface thermal resistance computed from satellite date as a proxy for debris thickness. Rounce et al.[83] developed an integrated method to estimate debris thickness, which involves DEM differencing, ice-flow modeling and energy-balance modeling. It is important to note that these approaches are site-specific and only yield instantaneous debris thickness distribution that corresponds to the acquisition time of imagery.

Ice-flow dynamics govern the transport of debris from high-altitude regions to the terminus over a large spatio-temporal scales, and simulating the sediment flux requires an accurate characterization of ice-flow velocity to account for supra- and englacial loads (e.g., [18, 17]). Gravity-driven debris flux, however, operates over a small spatio-temporal scale and is sensitive to the changes in glacier surface topography. Therefore, gravitational sediment transport governs the local debris thickness that collectively accounts for the spatial distribution of the debris load. This process is non-trivial especially when the surface topography is changing rapidly during the ablation season. Unfortunately, gravity-driven debris flux is usually neglected in glacier simulations, as the topography of the sediment and ice must be allowed to evolve and be temporally coincident with variations in surface irradiance and ablation. In addition, future models should also account for the mixing mechanism under debris flux, which alters the thermal and reflectance properties (such as thermal resistance and albedo) of the glacier surface.

Most existing numerical models, however, assume static debris thickness during the simulation period (e.g., [4, 49, 13, 24]), which increases the uncertainty in estimating ablation rates and accounting for topographic variation that governs surface irradiance. Modeling should integrate these components to accurately predict ablation rates, characterize thinning patterns, and explore feedbacks at the glacier surface. Accounting for process-morphology dynamics is essential for understanding glacier-system sensitivity to climate change and the role that individual glaciers play in the every evolving geomorphological system. Better characterization of debris properties including thickness, grain size, mineralogical mixtures, and water content is also required for future

studies [84, 45].

2.3.2.2 Ice-Flow and Gravity-Driven Debris Fluxes

Glaciers not only transport ice, but also transport debris from the active erosion zone to depositional basins [50]. A complete picture of glacial-debris transport consists of three components: surface debris flux; englacial debris flux; and basal debris flux [78]. Due to our limited knowledge of basal processes, most numerical models only consider the supraglacial and englacial debris transport (e.g., [18]).

The most recent ice-flow based debris-transport model was developed by Anderson and Anderson [18]. They modeled englacial and supraglacial debris advection under a steady debris input to understand the mechanisms in the debris–glacier–climate system. Simulations indicated that debris has significant control on glacier length and gradients of ice discharge, ice thickness, and surface velocities. Their model demonstrated that high debris flux slows down the glacier and contributes to extending its length. This model describes the transport of supraglacial debris in the ice-velocity field as an advection process:

$$\frac{\partial h_d}{\partial t} = -\nabla \cdot (h_d \mathbf{u_s}), \tag{2.10}$$

where h_d is the thickness or concentration of surface debris, t is time, and $\mathbf{u_s}$ is surface ice velocity. Similarly, englacial debris transport can be modeled as an advection process governed by the englacial velocity field, which in the x-z plane can be written as [18]:

$$\frac{\partial C}{\partial t} = -\frac{\partial (u_x C)}{\partial x} - \frac{\partial (u_z C)}{\partial z} - \frac{C}{h_c}\frac{\partial h_c}{\partial t} - \frac{u_x C}{h_c}\frac{\partial h_c}{\partial x}, \tag{2.11}$$

where C is the debris concentration in each cell and u_x and u_z are the horizontal and vertical ice velocity, respectively. h_c is the cell height in a given ice column. The first and second terms on the right represent the advection process. The third and fourth terms represent the variations of debris concentration due to vertical and longitudinal ice thickness changes. The use of advection is valid for glacial debris transport because advection is defined as the transport of a substance due

to the bulk motion of a fluid, and glacier ice is a form of a viscoelastic fluid that is the basis for all modern glacier modeling studies.

Supraglacial debris movement (such as sliding and slumping) occurs on hillslopes and on glacier surfaces [50]. Field observations have identified sediment sliding or slumping off steepening ice cliffs due to ice-cliff retreat and supraglacial lake expansion [85, 43]. Gravity-driven debris flux can dominant the local thickness distribution of supraglacial debris especially during the ablation season when the surface topography is constantly changing under rapid melting. From a mass flux perspective, the change of debris thickness over time can be estimated as:

$$\frac{\partial h_d}{\partial t} = \frac{q_{in} - q_{out}}{A_c}, \tag{2.12}$$

where q_{in} and q_{out} are the sediment fluxes into and out of a grid cell, respectively, and A_c is the planimetric area of a grid cell. The flux out of a grid cell can be represented as:

$$q_{out} = A_s u, \tag{2.13}$$

where A_s is the cross-sectional surface area which the flux passes through, u is the velocity of supraglacial sediments, which can be solved from force analysis, such as the approach for modeling unsteady gravity-driven debris flow by Chen and Lee [86], which accounts for gravity, internal friction and basal resistance. A multiple flow-direction algorithm can be used to determine the direction of sediment movement on the glacier surface based on sloping conditions. Specifically, sediment from a given grid cell flows to multiple neighboring cells [87]. Therefore, the total sediment flux into a given grid cell is:

$$q_{in} = \sum_{i=1}^{8} f_i \cdot q_{out,i}, \tag{2.14}$$

where f_i is the fraction of flow into grid cell i, such that:

$$f_i = \frac{max(0, \theta_{t,i}^p) l_i}{\sum_{j=1}^{8} max(0, \theta_{t,j}^p) l_j}, \tag{2.15}$$

where cells i and j are neighbors of the source cell, $\theta_{t,i}$ is the slope gradient from the central grid cell to its neighbor i, p is a flow-partition exponent, and l_i modifies the function to ensure even distribution in circular contours on a hypothetical conical surface.

Many unknowns limit our understanding of supraglacial debris. In order to accurately account for debris effects in glacier models, several issues need to be addressed: 1) The pathways and rates of glacial debris discharge from the ablation area are not well constrained. Current models cannot explain the full sediment balance at the glacier terminus [88]. 2) The hydrological controls on debris transport is largely unknown [89]. 3) Debris flux simulations are sensitive to errors in initial inputs and boundary conditions. An accurate debris-thickness distribution, however, is difficult to estimate given that field measurements have sampling limitations and remote-sensing approaches usually suffer from high uncertainty. The debris supply rates from surrounding hillslopes are also largely unknown. 4) Supraglacial debris consists of sediments with different lithology, grain size and moisture content [66]. Future models should take these properties and their mixing dynamics into account. 5) A very thin debris layer and the debris-ice interface are strongly affected by meltwater and ice, where cohesion and refreezing effects can significantly restrict debris particle movement. 6) Future models also need to differentiate debris flux behaviors, such as non-turbulent plastic behavior versus fluid behavior [50].

2.3.3 Ablation Dynamics

An accurate modeling of ablation dynamics needs to account for various forcing factors that regulate the surface-energy balance (i.e., irradiance, albedo, debris, topography). The energy balance at the glacier surface is the basis for modeling ablation rates under radiative forcing. For a bare-ice glacier, the surface that regulates the energy balance is the air-ice interface, however, for a debris-covered glacier, two surfaces need to be taken into account: the air-debris interface, and the debris-ice interface.

The ablation dynamics of a debris-covered glacier represents a multitude of processes and feedbacks that must account for debris loads, topography and surface hydrology and microclimate. Although thick debris loads generally suppress melting, ablation rates for a debris-covered glacier can still be high [31, 16]. Thin debris cover enhances ablation, and transition zones usually contain moisture-laden debris that absorb more energy thereby causing relatively high ablation rates. Studies also found the average ablation rate for a glacier to be similar between debris-covered ice and clean ice in the Hindu Kush-Karakoram-Himalaya. Immerzeel's [32] basin-scale simulations over the Baltoro Glacier predicted a significant increase in total runoff, downwasting and retreat throughout the twenty-first century despite thick debris cover. Simulations [16] also suggested that the debris cover on a Himalayan glacier can promote ablation such that the debris-covered area contributes more per unit area to the total runoff than the clean-ice portion. Recent studies also found that ice cliffs and supraglacial lakes significantly accelerate differential melting on debris-covered glaciers [38, 52, 17, 90, 91].

Simplistic approaches for estimating ablation rates, such as empirical regression and degree-day modeling heavily rely on weather-station data, and therefore are highly site-specific and may not characterize surface property spatio-temporal variation [92, 45]. Consequently, more recent studies are based upon the evaluation of surface-energy balance components via modeling. For example, recent energy-balance approaches [45, 13] are capable of predicting the internal temperature of debris loads at any location and provide satisfactory ablation rate estimates. Other studies also incorporate remote-sensing imagery to address the debris effect (e.g., [4, 49]), where the thermal resistance of the debris is estimated. It should be noted that this approach does not account for the debris fluxes, as it represents an instantaneous estimate of the debris load. Existing numerical models do not provide satisfactory explanations to empirical findings, indicating that debris load dynamics require further study and numerical modeling at a scale that characterizes rapid change in surface conditions.

Based on the energy balance at the ice/air interface, the melt rate at a bare-ice surface under temperate conditions can be calculated as [45, 49]:

$$M_i = \frac{Q_s + Q_l + Q_h + Q_e}{\rho_i L_f}, \tag{2.16}$$

where M_i denotes the ablation rate of ice, L_f is the latent heat of fusion for ice, and ρ_i is the density of ice. The energy balance at the debris/ice interface can be written as [53]:

$$Q_m = Q_c^{\downarrow} - Q_c^{'}, \tag{2.17}$$

where Q_m is the heat flux used for sub-debris ice ablation, $Q_c^{\downarrow}$ is the conductive heat flux from the debris, and $Q_c^{'}$ is the conductive heat flux towards the ice that is not used for ablation. Since we assume the ice is at its melting point, the conductive heat is negligible [36]. Under the assumptions of constant heat storage and a linear debris-temperature gradient, Q_m during the ablation season can be computed using the one-dimensional heat-flux equation described by Fourier's law [53, 45]:

$$Q_m = k_d \frac{(T_s - T_i)}{h_d} = \frac{T_s - T_i}{R}, \tag{2.18}$$

where k_d is the thermal conductivity of the debris, T_i is the ice temperature, h_d is debris thickness, and R is the thermal resistance of the debris layer, which can be estimated from thermal imagery or field data. T_s can be computed for debris-covered areas at each iteration by solving the surface-energy balance equation, and set to melting temperature for bare-ice surfaces. Then, the sub-debris melt rate (M_s) can be computed as [53, 45]:

$$M_s = \frac{Q_m}{\rho_i L_f}. \tag{2.19}$$

Note that this parameterization scheme only accounts for radiative-forcing, and a more rigorous scheme would also need to account for liquid precipitation, sublimation, water-phase transitions, and other climate factors that govern surface ablation during the night.

Figure 2.1 shows simulated ablation rates as a function of debris thickness for a Himalayan glacier using the aforementioned parameterization scheme. Estimated rates are compared with

field measurements on several Himalayan glaciers, including Barpu Glacier [1], Khumbu Glacier [2], and Rakhiot Glacier [3]. The simulated rates are reasonably similar to field measurements. The critical debris thickness at which the sub-debris ablation rate equals that of bare-ice usually ranges from 0.02 to 0.1m [23], and the modeled critical debris thickness is 0.03m, which falls into a reasonable range.

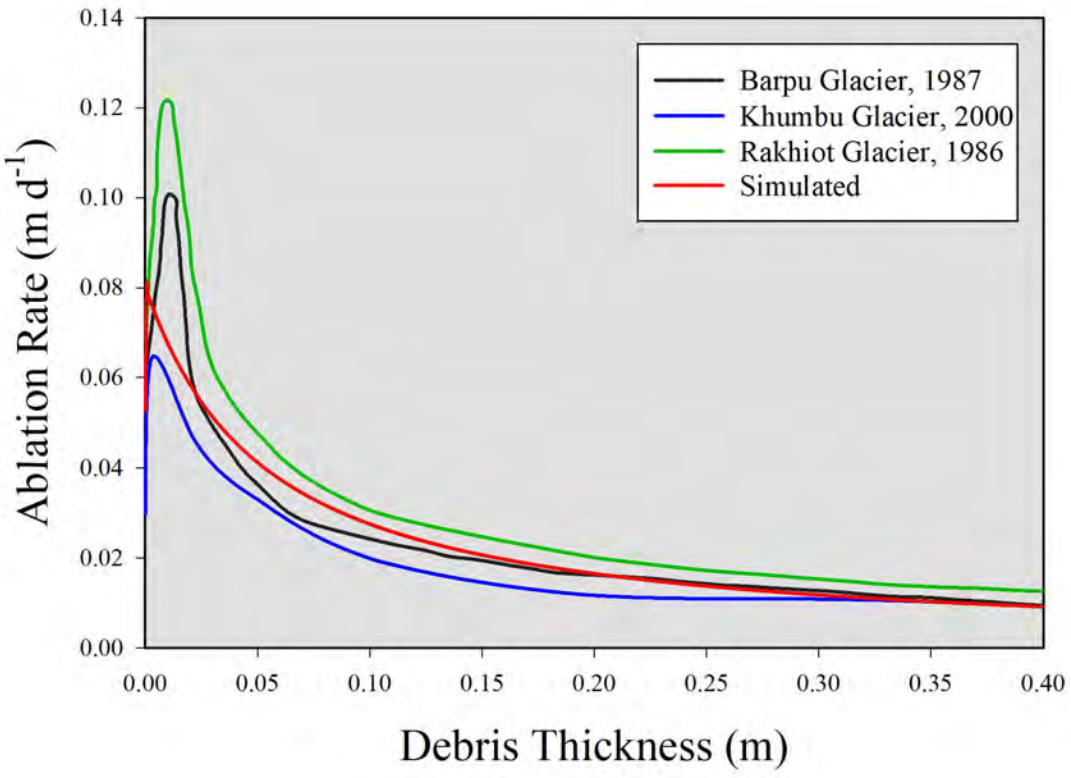

Figure 2.1: June-averaged simulated ablation rate as a function of debris thickness (red) compared to field measurements on Himalayan glaciers: Barpu Glacier [1], Khumbu Glacier [2], and Rakhiot Glacier [3].

Studies have suggested that glacier thinning dominates the mass loss of debris-covered glaciers [78], and that thinning variability is spatially heterogeneous [38, 27, 17]. Figure 2.2 depicts simulated surface ablation rates compared to the remote-sensing-based estimates [4]. Both results show suppressed ablation in the terminus region and higher ablation around inter-moraine valleys.

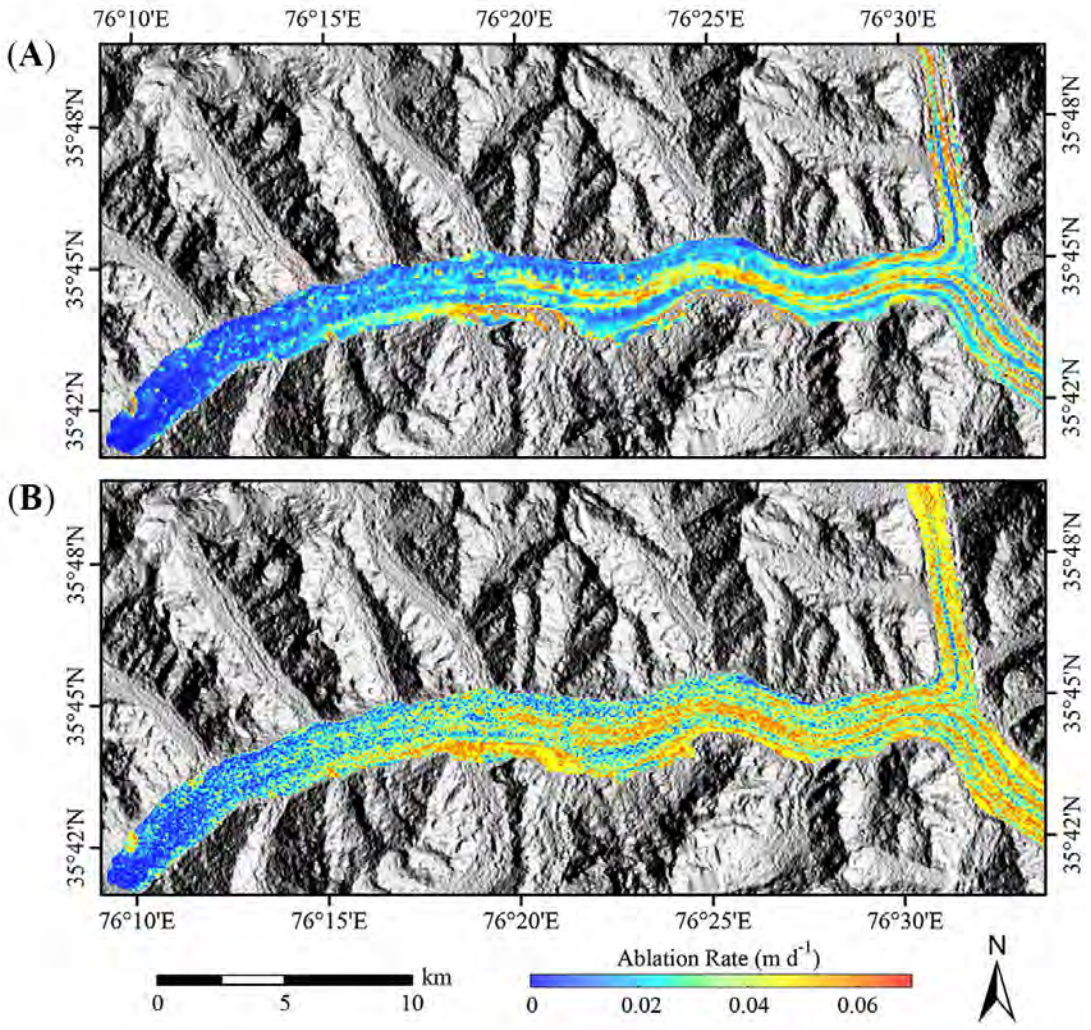

Figure 2.2: Ablation rates over the debris-covered Baltoro Glacier in Pakistan using (A) the remote-sensing-based approach by Mihalcea et al. [4], and (B) a radiation-driven model based upon accounting for variations in the direct and diffuse-skylight irradiance components. Both models use the same initial debris-thickness distribution, which was estimated for August 14th, 2004 by Mihalcea et al. [4]. Note that a major limitation of the remote-sensing-based approach is that it can only estimate instantaneous ablation rates due to the lack of multi-temporal satellite imagery.

The estimated ablation rates are commonly higher in the areas of clean ice or thin debris cover. Given high melting rates, more sediments are exposed by ice melting, and the surface debris concentration is likely to increase over time [93, 80, 18].

Although many approaches have been developed to model the surface-energy balance and ablation rates, researchers have suggested that mass-balance estimates for many Himalayan glaciers

are still inaccurate [15]. To improve the mass-balance estimates for debris-covered glaciers, future work is warranted on the following modeling issues: 1) The complex ablation dynamics of ice-cliffs and supraglacial lakes are over-simplified in existing models. 2) The ablation caused by precipitation is often neglected or underestimated because debris cover can warm surface water before it percolates through, and the warmed water can contribute to significant surface and englacial melting. 3) The non-linear temperature profile and water-phase changes within the debris cover have not been accounted for. 4) Surface temperature and the albedo distribution should be continuously modeled rather than being restricted by instantaneous estimates utilizing remote-sensing imagery. This will require modeling of the BRDF. 5) Sublimation also contributes to mass loss, it occurs at all temperatures and dominates in cold environments, however, sublimation is often neglected in many models.

2.3.4 Supraglacial Hydrology

Glacier hydrology describes the production, storage and transport of water on glaciers [50]. Supraglacial and englacial fluvial systems can regulate glacier mass balance by forming supraglacial lakes, expanding water channels, altering debris thickness distribution, and transporting the heat stored in debris. Subglacial hydrology (including basal water pressure, basal ablation and basal drainage) has a significant influence on basal sliding and erosion, which impacts glacier evolution at a larger time scale. Unfortunately, many of englacial and subglacial processes have not been adequately studied or modeled, and there remain many unknowns about englacial and subglacial conditions [42, 43].

Supraglacial meltwater production is very sensitive to atmospheric and surface morphological conditions. Water transport and storage are key processes that alter morphology and glacier thinning. Surface meltwater is usually transported via stream channels during the ablation season and can also be temporarily stored in supraglacial lakes [36]. Differential ablation and meltwater transport produces undulations and relief of the ice surface, which encourages the formation of supraglacial lakes in depression areas [38, 75, 39, 42, 43]. Studies also indicate that many supraglacial lakes are hydrologically connected [42, 43].

2.3.4.1 Supraglacial Lakes

Supraglacial lakes are found on many debris-covered glaciers [23], and their evolution will most likely accelerate given current atmospheric temperature trends [75]. Glacier morphological changes due to glacier thinning may also further increase the number of supraglacial lakes on glaciers [94, 52]. Nevertheless, we do not accurately know the baseline status for any particular glacier regarding the evolution of lakes, as they are controlled by numerous mechanisms. Understanding lake dynamics provides valuable insights into glacier sensitivity to climate change [41, 75, 19, 23]. Recent studies have concluded that ponding is caused by surface ablation under a differential surface lowering condition, and that the number of ponds are increasing on some of the largest glaciers [23].

Supraglacial lakes exhibit a lower albedo than surrounding areas [8], which allows them to absorb more solar energy, rapidly melting the ice and expanding the lake area. Previous studies have estimated that the ablation rates around the lakes can be much higher than that of most debris-covered areas, therefore supraglacial lakes can be a significant contributor to the total ablation [38, 40]. Furthermore, a dense spatial distribution of lakes often increases glacier thinning because they form a large number of englacial channels, and the collapse of the englacial channel roofs creates new lakes that further accelerate ablation and thinning.

Numerical modeling of supraglacial lake evolution is challenging, and current models (e.g., [8]) neglect many processes that governs lake evolution (e.g., back-wasting of ice-cliffs, englacial drainage, topography and debris-thickness variations). The filling and draining cycles control the evolution of supraglacial lakes [75, 42, 43], and rapid draining can happen when a lake intersects with englacial conduits. Surface conditions (bare-ice or debris-covered) also regulate the growth rate of lakes [75]. Modeling lake temperatures can also be difficult, which is a challenge for estimating the amount of ice loss that is related to supraglacial lakes.

2.3.4.2 *Supraglacial Water-Flow Modeling*

Water flow and supraglacial lake development can be numerically investigated using high-resolution DEMs. Basic approaches for flow-path determination have been successfully applied on the Lirung Glacier in the Himalaya to study the connectivity of supraglacial ponds [43]. Lüthje et al. [8] developed a model that characterized supraglacial lake evolution on the Greenland ice-sheet margin based on surface ablation and surface-drainage dynamics. The supraglacial water level can be estimated as:

$$\frac{\partial h_w}{\partial t} = He(h)(\frac{\rho_i M_l}{\rho_w} - D\nabla \cdot (h_w \nabla z_i)), \tag{2.20}$$

where h_w is water depth above the ice surface, $He(h)$ is a Heaviside function to prevent negative water depth, ρ_i is the density of ice, ρ_w is the density of water, D is a tuning parameter, and z_i is the ice-surface elevation.

Field studies suggest that meltwater can travel long-distances in active marginal and sub-marginal channels [42]. These channels may be bounded between ice and valley walls, as the surface elevation of glacier margins is typically lower than at the center of the glacier, and melt-water can accumulate in these channels while flowing towards the terminus. Figure 2.3 depicts simulation results of the surface water level over the ablation zone of the Baltoro Glacier, in which both marginal streams are produced from water transport.

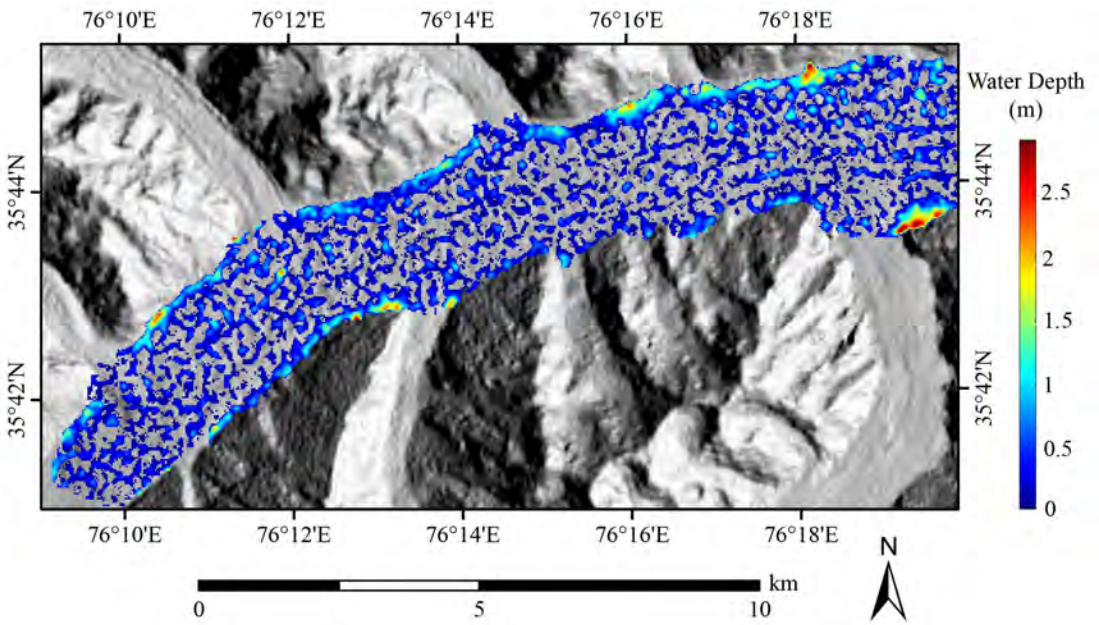

Figure 2.3: Simulated supraglacial water depth (on top of ice surface) in the ablation zone at 13:00 on June 3rd, 2004. Areas with a water depth less than 5mm is considered dry. Note that the marginal streams form in the ablation zone on both sides of the glacier.

The travel time for meltwater to drain out of the glacier ranges from days to hours, depending on the location where the meltwater is generated [36]. Studies have found a 3-7 hour time lag between the peak of melt and the peak of discharge in Greenland during the ablation season [95]. The time lag is usually smaller in the ablation season when the discharge reaches its maximum in late July or early August [36]. This time delay is due to multiple factors, such as the amount of snow, firn, and debris along the path, as well as the time for subglacial and englacial conduits to develop. Otherwise, the travel speed on ice is similar to the speed in open channels [36]. Due to the water storage in the glacier, runoff does not represent the total meltwater production [36]. As our model does not account for those mechanisms, our simulation results (Figure 2.4) represent the fastest drainage situation.

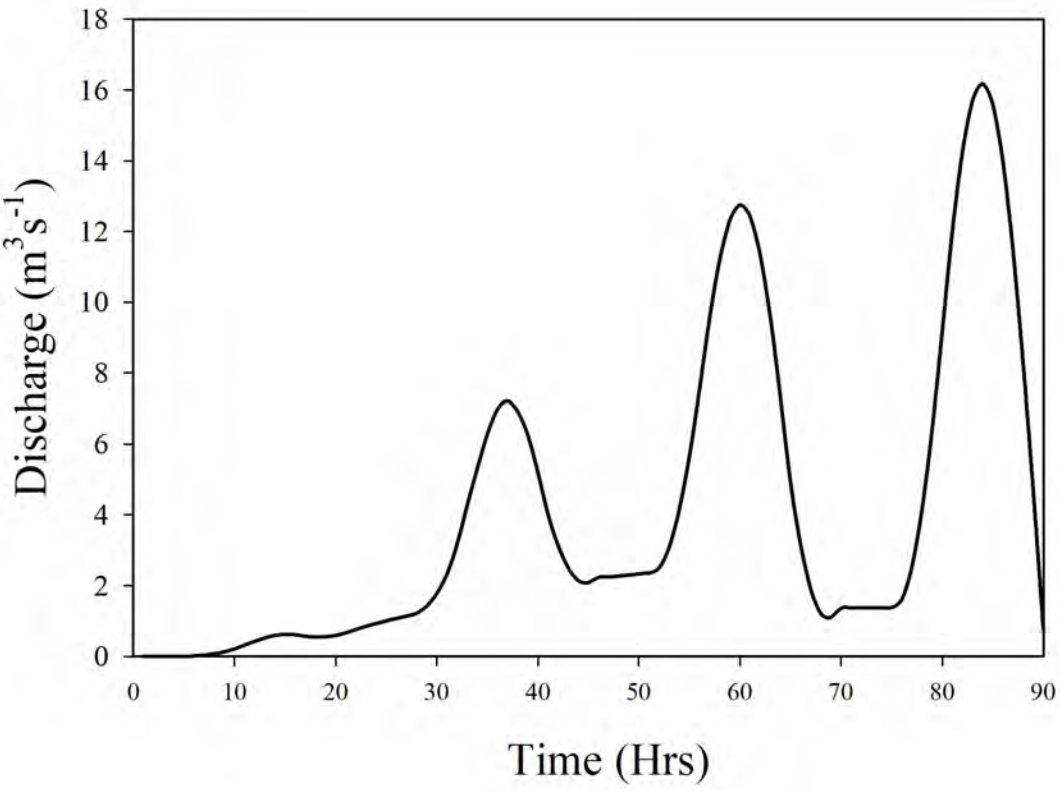

Figure 2.4: Simulated discharge of water flow from the terminus of the Baltoro Glacier. Timing of simulation starts from 12AM, June 1st, 2004 to 6PM, June 4th, 2004. Note that these simulation results only account for supraglacial drainage, and are the result of the assumption that supraglacial water transport does not contribute to the englacial water storage and transport components.

Improved numerical models are required to generate new knowledge about glacial hydrology, accounting for such structures and processes as the formation and evolution of supraglacial lakes, hydrological connectivity through englacial channels, and hydrological debris transport on, under, and through glaciers.

2.3.5 Ice-Flow Dynamics

Ice-flow dynamics regulate ice-mass distribution, transport and geometry changes (length, width and thickness) of glaciers. Prognostic ice-flow simulation is key for understanding glacier responses to forcing factors [50]. Ice-flow not only governs its velocity and geometry, but also partially controls erosion and debris production. Numerous studies have indicated that signifi-

cant ice-flow can occur on heavily debris-covered glaciers that exhibit relatively stable termini [35, 68, 96]. This may be the result of tributary contributions to ice discharge, high-altitude mass loading, and/or basal sliding due elevated basal meltwater and basal-water pressure [68].

Ice-flow velocity is governed by ice thickness, that is regulated by the mass flux and surface and basal ablation rates. Unfortunately, information regarding bed topography and ice depths is not readily available, yet critical for ice-flow modeling [50]. Direct measurements of the bed topography heavily depend on geophysical surveys (e.g., seismic and radio sounding), which are usually time-consuming, expensive and logistically challenging [97]. Ice depth may, however, be approximated with numerical modeling. For example, Farinotti et al. [98] indicated that ice thickness can be estimated from the mass-conservation equation using apparent mass-balance distribution in the ice-flow catchments. Mass-balance distribution, however, can be difficult to estimate, especially for debris-covered glaciers. Therefore, many modelers use surface velocities to infer ice thickness (e.g., [99, 97]), and associated optimization approaches have also been developed to improve accuracy of ice thickness estimates [100]. Many of these methods are discussed briefly by Farinotti et al. [101], who concluded that ice thickness estimates are strongly dependent on the quality of input data, choice of parameters, and the approaches that utilize additional datasets (such as surface flow velocity) do not perform better than approaches that require less data.

Once the ice thickness is known or approximated, most glacier models use the shallow-ice approximation (SIA) to compute the velocity distribution and glacier geometry evolution (e.g., [102, 103, 104, 18]). Generally, SIA assumes no debris cover and no basal sliding.

The shallow-ice approximation assumes a glacier has a small depth-to-width ratio and glacier ice can be modeled as an incompressible viscous and isotropic fluid [36, 104]. The mass-continuity equation is the foundation of an ice-flow model:

$$\frac{\partial H}{\partial t} = M_g - \nabla \cdot \mathbf{Q}, \tag{2.21}$$

where H is the ice thickness, M_g is the glacier mass balance. The flow of ice is characterized by a velocity field (u_x,u_y,u_z), which consists of the vertical velocity (u_z) and the horizontal veloci-

ties (u_x,u_y). The horizontal ice flux, $\mathbf{Q}$, is a product of ice thickness and the vertically averaged horizontal velocity $\overline{\mathbf{U}}$:

$$\mathbf{Q} = \overline{\mathbf{U}} H. \tag{2.22}$$

Based on the widely used SIA [102] and non-sliding assumptions, the ice-flow velocity field can be calculated based on mass continuity, Glen's flow law, and basal-stress balance. If we take the ice-flow factor as a constant, then the horizontal velocity field can be written as [104]:

$$(u_x, u_y) = -\frac{2A(\rho_i g)^n}{n+1}[H^{n+1} - (z_i - z)^{n+1}] \mid \nabla z_i \mid^{n-1} \nabla z_i, \tag{2.23}$$

where A is the ice-flow factor (ice softness), ρ_i is the density of ice, g is gravitational acceleration, n is the stress exponent (typically, n = 3). H is ice thickness ($H - z$ is the depth within the ice), and z_i is ice-surface elevation. Under this non-sliding shallow-ice approximation, the ice thickness can be estimated from surface velocity, and Figure 2.5 is an example of modeled ice thickness for the Baltoro Glacier based on this equation.

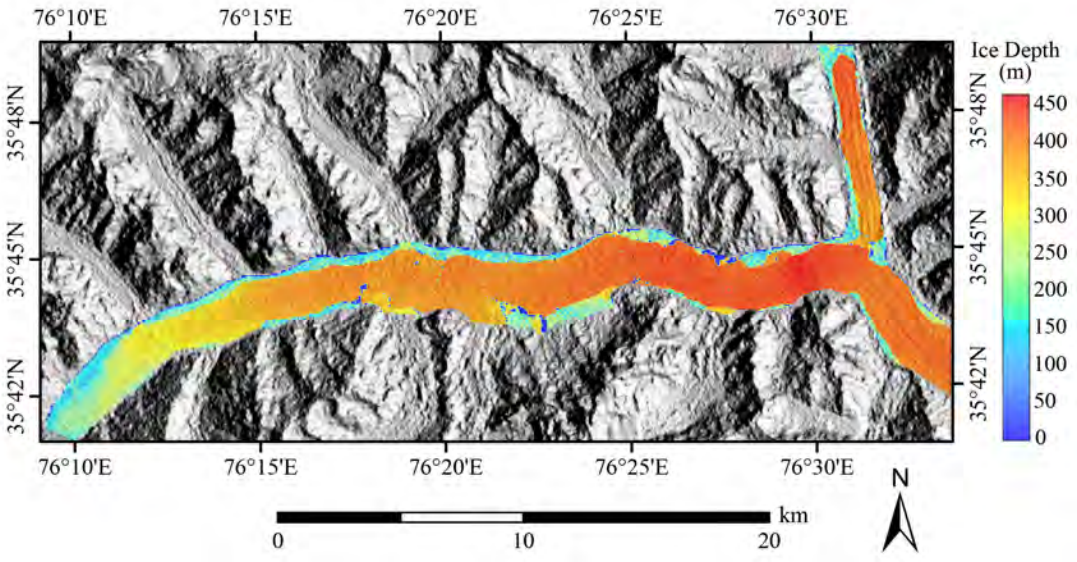

Figure 2.5: Modeled ice thickness for Baltoro Glacier based on the ice thickness-surface velocity relationship using the non-sliding shallow-ice approximation.

For a simplified non-sliding x-z plane model, the horizontal velocity as a function of depth can be computed from:

$$u_x = \frac{1}{2}A(\rho_i g sin\theta_t)^3(H^4 - (H-z)^4), \tag{2.24}$$

where θ_t is the slope angle of the glacier. This equation has been validated against several field observations (e.g. [105]), and Figure 2.6 is an example of the modeled horizontal velocity as a function of depth within the ice based on equation 2.24.

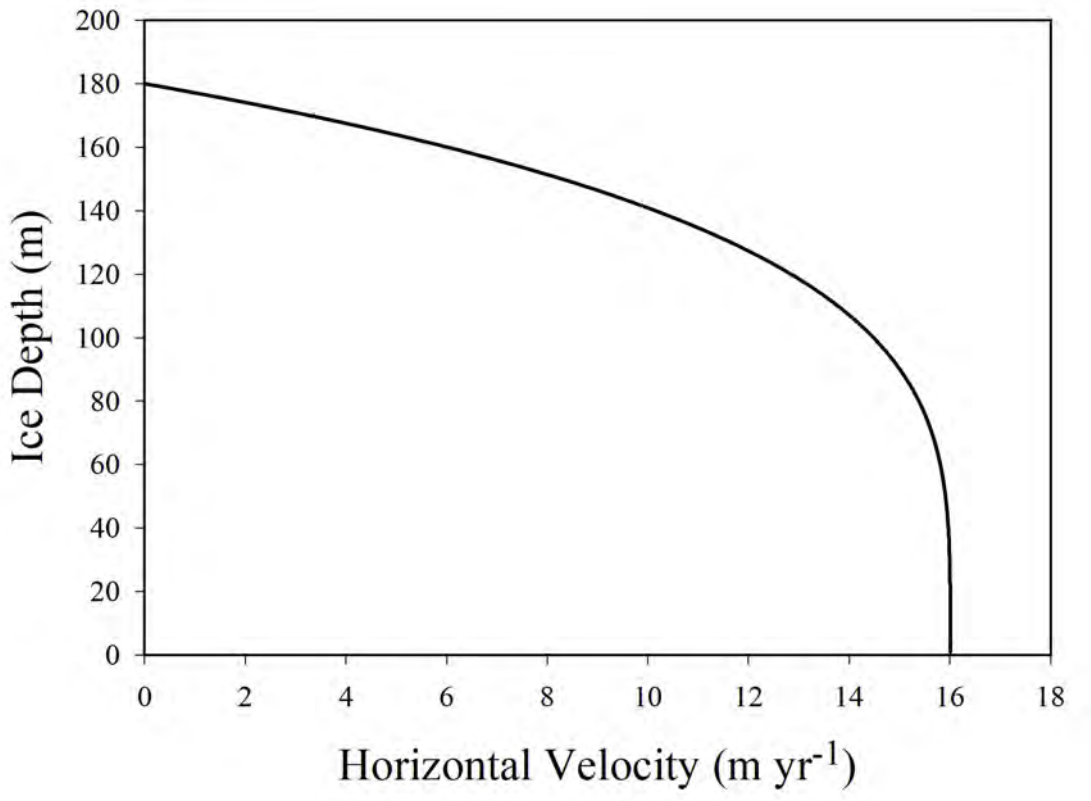

Figure 2.6: Modeled horizontal velocity as a function of ice depth for a hypothetical 180m thick glacier (assuming no basal sliding and a 3-degree constant slope angle for both the surface and basal topography of the glacier).

After substituting equation (2.22) and equation (2.23) into equation (2.21), we have the equa-

tion that describes the rate of ice-thickness change over time given the SIA:

$$\frac{\partial H}{\partial t} = M_g + \nabla \cdot (\frac{2A(\rho_i g)^n}{n+1} H[H^{n+1} - (z_i - z)^{n+1}] \mid \nabla z_i \mid^{n-1} \nabla z_i). \tag{2.25}$$

Figure 2.7 depicts SIA-based ice flow and thickness simulations, in which a hypothetical glacier retreats over time (Figure 2.7B) under a constant mass-balance condition (Figure 2.7A).

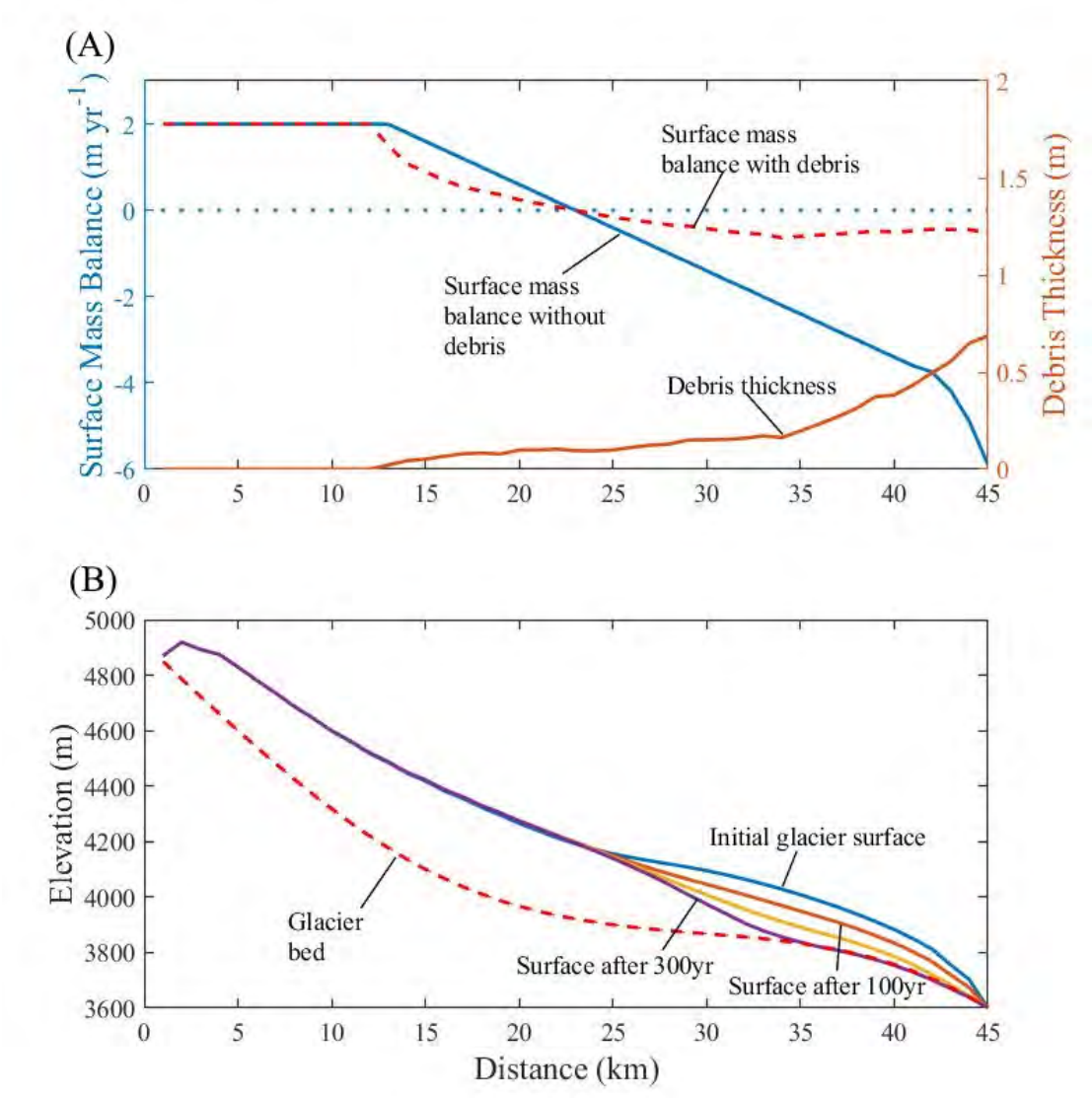

Figure 2.7: Ice thickness simulation based on the non-sliding SIA for a hypothetical debris-covered glacier. (A) Surface mass balance with and without debris cover (only the insulation effect of debris cover is considered here). (B) Glacier retreat over 300 years.

Shallow-ice approximation, a second-order approach, produces reasonable results compared to observations of large ice sheets (e.g., [106, 107]). The SIA approach may, however, be inaccurate for modeling glaciers in complex topography [108]. More advanced higher-order ice-flow models take into account the effects of rugged basal topography (e.g., the integrated second-order shallow-ice approximation developed by Egholm et al. [108]), and appear promising for modeling narrow glaciers in steep terrain. Herman et al. [103] indicated that ice-flow models can also be integrated with erosion models to accurately delineate the evolution of alpine valleys. They integrated several types of erosion processes (fluvial incision, glacier erosion and hillslope diffusion) into an ice-flow model[109] and their simulation results successfully characterized erosion patterns governed by glacial cycles, which demonstrated greater capability in studying the evolution of the Southern Alps in New Zealand. Another improved ice-flow model was developed by Bueler and Brown [104]. Their model takes basal melt and temperature-adjusted ice properties into account, and is mathematically suitable for long-term high-resolution simulations.

Several limitations exist in many models: 1) Most ice-thickness estimates suffer from significant errors [100], and over-simplified bed shapes are often used; 2) The traditional SIA assumes no debris load and no sliding at the bed, which is unrealistic for debris-covered glaciers; 3) Many models do not account for complex topographic factors and the effects of basal debris on ice-flow [110]; 4) Feedback mechanisms have not been fully integrated, to account for example, the feedback between ice-flow, basal erosion and frictional heating; and 5) Many ice-flow models use constant ice temperature and ice softness to characterizes the rheology of glacier ice (e.g., [18]), however, ice rheology can vary significantly as a function of ice temperature [36], therefore, this assumption introduces uncertainty into simulation results. In addition, new approaches are needed for full 3D velocity modeling that accounts for rugged bed topography, tributary glacier mass flux, and debris-covered stagnant termini. Systematic improvements are required in order to characterize the interactions among ice-flow, ablation, erosion, debris production and transport.

2.3.6 Glacier Erosion

Glaciers and glacier erosion represent a major component of alpine geomorphological systems [111]. It is necessary to include erosion processes into numerical models of debris-covered glaciers because: 1) Glacier erosion governs the evolution of glacial valleys and relief production over larger timescale, which controls ice-flow dynamics [103]; 2) Erosion modifies the morphology of glacial valleys which regulates radiation and precipitation forcing; and 3) Basal erosion is an important source of basal and englacial debris. Glacial erosion is thought to scale with ice depth and ice velocity at the ice-bedrock interface, and the basal erosion rate ε_b can be characterized as [109, 112]:

$$\varepsilon_b = K_g u_{bs}^l, \tag{2.26}$$

where K_g is the glacial erosion constant, u_{bs} is the basal sliding speed, and the exponent l is taken to be 1 based on [111, 112]. The basal sliding speed can be computed as [113]:

$$u_{bs} = u_0 e^{1-\frac{\tau_c}{\tau_b}}, \tag{2.27}$$

where u_0 is the typical sliding velocity (5-20 myr^{-1}), τ_c is the reference basal stress, and τ_b is the basal shear stress.

Glacial erosion must account for basal morphometric conditions such that the erosion rate modifies the topography vector normal to the basal slope angle and azimuth topographic direction. This process-form relationship enables simulation of the production of U-shaped glacier valleys that typically form over approximately a 100 k time frame [111]. Furthermore, the prevailing thought that glacier erosion rates are relatively high has sparked significant debate in the literature regarding the role and magnitude of fluvial versus glacial erosion in mountain geodynamics and topographic evolution [74, 22, 114]. Assessing the magnitude of modern-day glacier erosion is notoriously difficult, as supraglacial, englacial, and basal-load processes and debris components must be accurately accounted for, given a large number of feedbacks and complex spatio-temporal

dynamics. While it is generally assumed that higher erosion rates are associated with glaciation, it is not clear how the role of accelerated meltwater production during deglacierization may regulate glacier denudation rates. Basal glacio-fluvial processes most likely vary in dominance during such changes in climate forcing. Glacier erosion is also strongly controlled by relief production and topographic stress conditions thereby reducing rock resistance to abrasion and plucking. More comprehensive glacier system modeling studies to explore the scale-dependent nature of glacier erosion and topographic evolution is sorely needed.

2.4 Coupled Systems

A multitude of feedback mechanisms and coupled systems complicate our understanding of debris-covered glaciers [51, 19]. Many processes operate at very different spatio-temporal scales, making them difficult to investigate in the field. Therefore, numerical modeling plays a significant role in studying feedbacks and system interactions.

2.4.1 Supraglacial System

The supraglacial system involves complex couplings between topography, surface irradiance, precipitation, ablation, and sediment fluxes (Figure 2.8). Surface irradiance is partially controlled by the local and meso-scale topographic properties that have been conditioned by paleoclimate conditions and operational scale dependencies of various geomorphological systems. Surface-energy balance conditions can affect ablation rates thereby altering the topography and topographic forcing on irradiant fluxes. External hillslope sediment erosion and transport contribute to the debris load, which regulates the ablation, and supraglacial gravitational-based sediment fluxes and meltwater transport of debris also alters the debris load and topography, changing topographic forcing on irradiant fluxes. The ponding of surface water also contributes to ablation irrespective of the presence of debris and debris depth, which is governed by topography, generating more relief that governs irradiant fluxes. Precipitation also governs ablation irrespective of debris and the mechanism can be external (i.e., frontal, orographic) or caused by convective lifting due to debris and surface temperatures, regulated by topography, debris depth and debris-moisture conditions.

From a modeling perspective, the surface topography and ablation rates are interdependent and must be updated at each iteration.

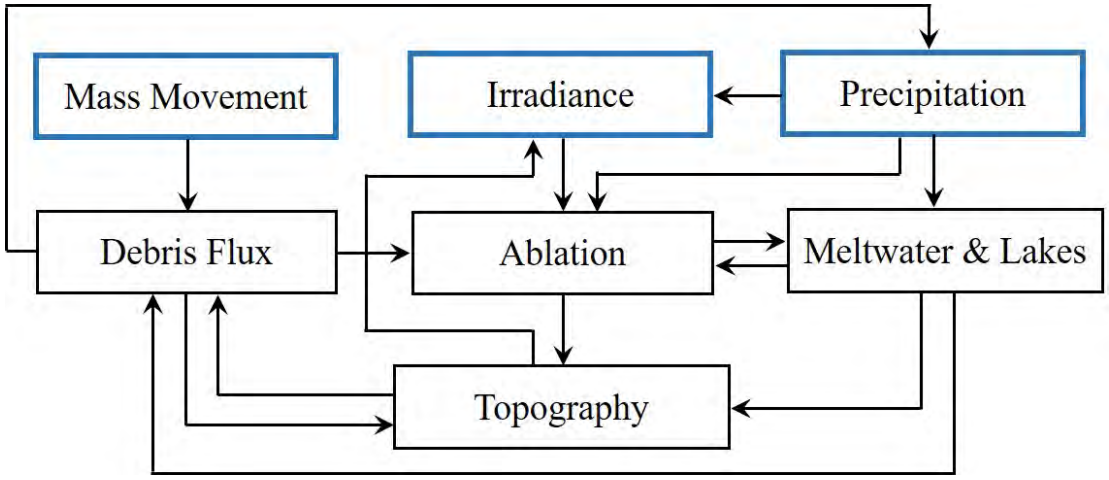

Figure 2.8: Diagram illustrating the feedback mechanisms involving multiple surface processes of the supraglacial system that alters the topography, which in turn governs the magnitude of ablation. Pathways are highlighted to demonstrate various feedbacks. External processes are listed at the top of the diagram and drive internal mechanisms that regulate ablation dynamics.

Several positive feedbacks govern the evolution of supraglacial lakes. For example, the heterogeneous glacier thinning facilitates the formation of supraglacial lakes, which then enhances glacier thinning [17, 33]. This mechanism is regulated by the slope gradient of the glacier, as water transport is enhanced with steeper gradients, and ablation and ponding is enhanced with lower gradients. This is largely controlled by ice-mass fluxes that govern the magnitude of glacier erosion, which in turn governs the basal topographic gradient. Another positive feedback is associated with ice cliffs around supraglacial lakes, where thin debris on cliffs accelerate ablation causing ice cliff retreat, thereby causing lake expansion and further acceleration of thinning [20, 27]. Such complex feedback dynamics and coupling may result in debris-covered glaciers being more sensitive to climate change than previously thought.

2.4.2 Subglacial System

External climate mechanisms coupled with bed topography influence ice-flow, basal erosion and basal ablation. The bed topography is slowly evolving due to differential glacier erosion caused by variations in ice-flow dynamics, such that erosion is most likely at a maximum near the ELA due to relatively high ice depths and flow velocities [115, 116]. The relatively high erosion coupled with isostatic and/or tectonic uplift generates more relief which increases topographic stresses which decreases rock resistance to erosion. Consequently, climate and tectonic forcing facilitates high-magnitude glacier erosion, although the effective spatio-temporal operational scales of these couplings is not known with any certainty, and are most likely highly variable depending upon the geological setting. This feedback mechanism is significant over larger time scales.

Basal erosion also contributes to basal debris input and transport, which over long time periods influences surface ablation, as basal debris can eventually re-emerge at the surface [18]. At lower altitude, the magnitude of erosion most likely decreases as ablation, ice-flow velocities and topographic stress conditions may decrease the efficiencies of abrasion and quarrying. It is assumed that most glacier erosion parameterization schemes collectively account for the aforementioned processes, although quarrying is dependent on subglacial temperature conditions and the degree of rock fracturing [117, 118]. Furthermore, it is difficult to model basal hydrological conditions that govern basal sliding, as high basal water pressure lubricates the ice-bedrock interface [36], and fluvial transport of debris can cause erosion and deposition at the base. Higher ice-flow velocity generates more frictional heating that further increases basal water pressure [50]. Therefore, the interactions between ice-flow, basal hydrology and frictional heating form a positive feedback as described by Benn and Evans [50].

Collectively, most subglacial processes are interrelated (Figure 2.9), although details about basal erosion, sliding, subglacial ablation, basal hydrology and their process mechanics with sediment transport and ice-flow have not been adequately studied [50]. Consequently, many research questions need to be addressed towards improving numerical models.

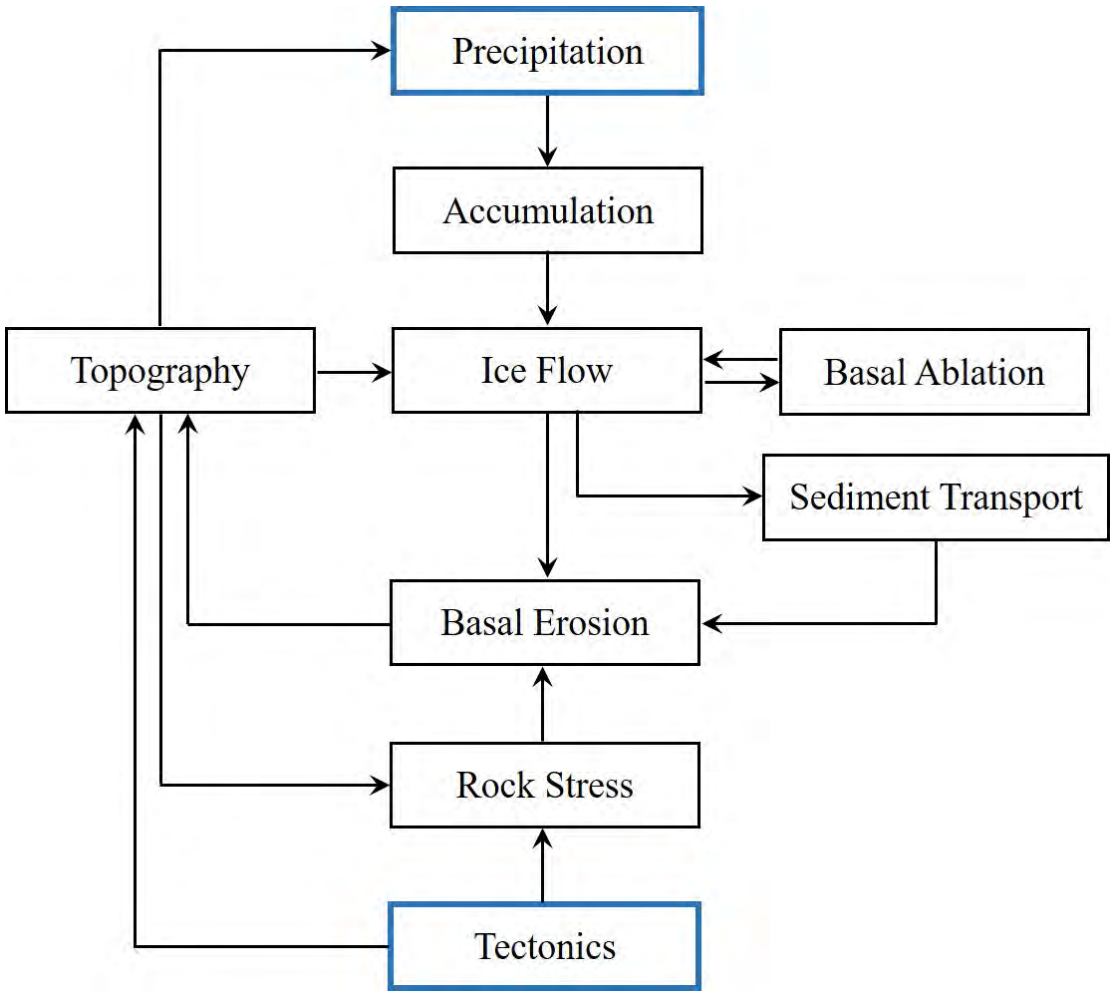

Figure 2.9: Subglacial system conceptual diagram of processes that govern ice-flow dynamics, basal ablation and glacier erosion. Pathways are highlighted to demonstrate various feedbacks. More basal parameters are required to better characterize processes and basal feedback mechanisms. Glacier erosion is driven by the interaction of climate, surface and tectonic processes.

2.4.3 Glacier System and Sensitivity to Climate Change

Collectively, a debris-covered glacier is a complex system with internal and external processes and feedbacks that govern glacier dynamics (Figure 2.10). It is difficult to accurately characterize the forcing factors, as they can exist at multiple scales. Interactions between numerous subsystems cause problems, as parameterization schemes may not account for numerous parameters and their relationships. Such is the case in modeling debris-covered glaciers, as many debris-flux parameters have not been taken into consideration, although various debris-related feedbacks can significantly

govern glacier states and evolution [119, 19, 17].

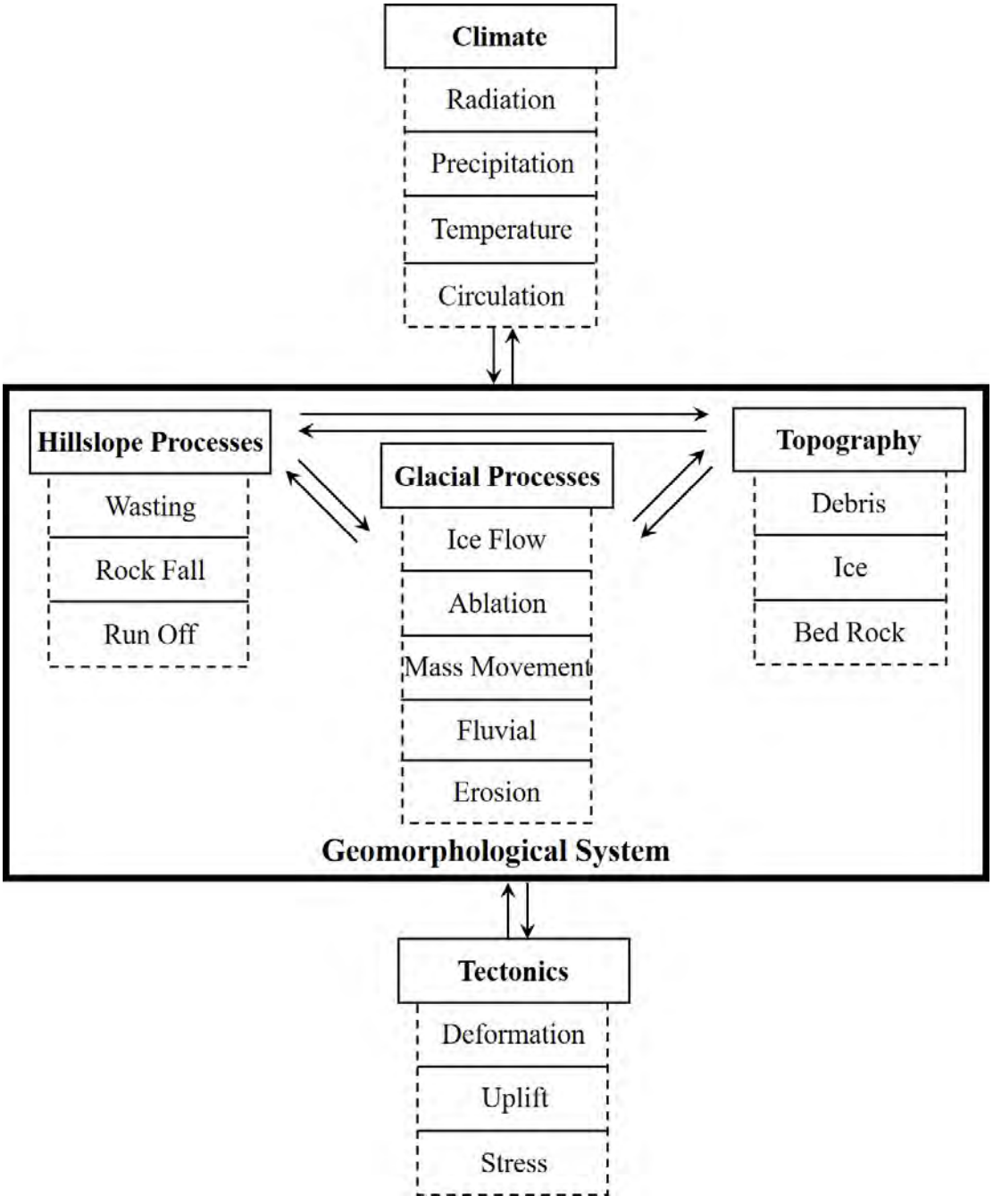

Figure 2.10: Glacier system conceptual diagram of climate, surface and tectonic processes that interact to govern glacier system state and evolution. Pathways are highlight to demonstrate forcing factors and system interdependencies.

More sophisticated models are warranted to better understand the basal and englacial system coupling. Developing and testing these models require numerical solutions to account for thermal-mechanical dynamics, such as the ice-flow velocity and heat-advection feedback [50]. Another direction for numerical modeling studies is to focus on the couplings within a particular subsystem to address specific questions, such as the ice-cliff retreat-supraglacial lake evolution and calving dynamics [36]. From an implementation perspective, new numerical schemes and computational optimization strategies are necessary in order to support these complex-system simulations.

Further research is also required to determine what type of glacier responses can be used to evaluate glacier sensitivity to climate change. Important conceptual and technical questions that must be addressed include: 1) How should we evaluate glacier responses to radiation and precipitation forcing? 2) Can various subsystems like ablation, ice-flow, hydrology, or erosion dynamics actively respond to climate change? 3) Over what time periods do these subsystems respond? 4) Do we need to evaluate the entire system, and use traditional properties such as mass balance variation to characterize sensitivity to change? More accurate characterization of parameters, processes, and system couplings may permit us to investigate these questions.

From another perspective, processes and coupled systems govern the spatio-temporal geometry of glaciers and the morphometry of their surfaces. Fundamentally, process dictates morphometry, and the compositional make-up of glaciers ensures high-magnitude lability compared to other landscape surfaces dominated by rock or hillslope sediments. This suggests that morphometric parameters may be useful indicators of glacier sensitivity to change if morphometric properties adequately characterize subsystem components or integrated systems (e.g., ablation, ice flow, debris fluxes).

We demonstrate this concept by conducting glacier simulations that account only for ablation dynamics, comparing a debris-free and debris-covered glacier over a portion of the ablation season. Specifically, we characterize the temporal variability of glacier surface area in the ablation zone accounting for sediment fluxes and water-induced ablation caused by supraglacial lakes (Figure 2.11).

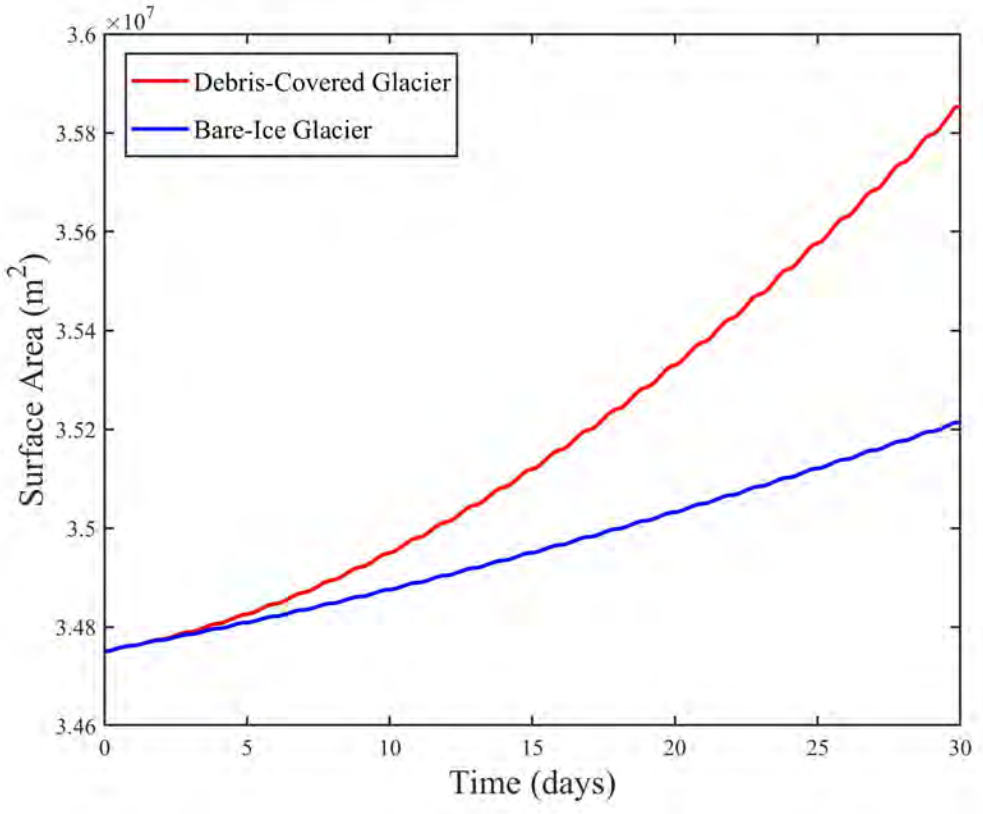

Figure 2.11: Simulation of ablation dynamics on the Baltoro Glacier during a portion of the ablation season and resulting glacier surface-area changes for a debris-covered and debris-free glacier. Simulation results are for a 30-day period starting from July 1, 2004. Surface area significantly increases for a debris-covered glacier compared to a debris-free glacier, suggesting that the surface-morphology response on a debris-covered glacier is very sensitive to ablation dynamics and climate forcing.

The simulation results clearly reveal that the surface area of a debris-covered glacier increases at a higher rate than a debris-free glacier. Relief caused by differential ablation increases the surface area, as supraglacial lakes and sediment transport fluxes due to topographic forcing causes greater morphological change. We might expect this example to be validated in terms of morphological change if we examine other glacier morphological properties. Ice-flux dynamics, however, should also be accounted for, as ice flow will regulate the surface-area distribution, glacier-slope profile and potentially other geometry parameters. Such non-linear responses, however, strongly suggest that process-form relationships on debris-covered glaciers may represent an indication of

critical transitions in glacier responses to climate forcing.

2.5 Model Inputs, Constraints and Validation

Initial conditions, constraints and validation of modeling efforts is essential for characterizing parameters and prediction of glacier conditions. Field data can be extremely valuable for prescribing parameter values and constraining simulation results. Validation, however, is often difficult, given large uncertainties in the magnitude of parameters, parametrization schemes, characterization of scale dependencies and assumptions regarding initial conditions. New developments in geospatial data science such as advancements in sensor technologies, remote-sensing platforms, and spatial analysis and modeling capabilities provide additional data/information for establishing initial conditions and validation of glacier parameters and boundary conditions.

2.5.1 Glacier Mapping

Remote sensing of glaciers has been an active research area involving the thematic mapping of glacier and their properties, as well as estimation of glacier-surface morphometry and ice-flow conditions [30, 120, 121, 122, 123]. Glacier mapping of debris-covered glaciers is a notoriously difficult task, as supraglacial debris-loads exhibit similar spectral characteristics as rocks and sediment of the surrounding terrain [30, 124, 125, 126]. Nevertheless, glacier outlines and surface and ice-flow properties can be very valuable in establishing initial conditions for simulation, validating various simulated properties, and determining glacial states via the estimation of termini advancement and retreat rates.

Glacier mapping is fraught with difficulties, as multispectral data should be preprocessed appropriately to remove environmental information related to the atmosphere and topographic effects [127, 56]. This involves anisotropic-reflectance correction to address multi-scale topographic effects that cause spectral variations to be associated with relief, shadows, and local topographic conditions. Unfortunately, many empirical approaches exist that can be utilized in an attempt to reduce the error in mapping glaciers, but they do not effectively account for a multitude of topographic effects [56]. Consequently, researchers have relied upon spectral features and image

ratioing as a basis for mapping glaciers from spectral imagery.

More recently, investigators have recognized the importance of using digital elevation models and topographic information with spectral data for improved glacier mapping (e.g., [124, 125]). First-order and second-order morphometric parameters can be very useful in delineating the boundaries of debris-covered glaciers [30, 125], and object-oriented analysis and the use of terrain objects offers promising mapping capabilities [30, 124]. Active research currently involves the evaluation of a variety of information themes, and the use of advanced pattern-recognition approaches (e.g., [128, 129]). Regardless, accurately mapping boundary locations for assessment of fluctuations rates and states requires more deterministic analysis approaches rather than the use of empirical pattern-recognition approaches that also involve uncertainty analysis.

Assessment and mapping of supra-glacial debris loads is also important. For example, Scherler et al.[29] utilized the ratio of Landsat TM near-infrared bands (TM4/TM5) to help discriminate between debris-covered and debris-free ice, and focused mainly on the longitudinal glacier profiles of percent of debris-covered area, glacier velocity, and local slope angle to infer stronger coupling between hillslope and glacier processes in steep terrain. Ojha et al.[130] identified slopes with potential for shedding debris onto the glacier surface by manual digitization based on slope angle and slope contours derived from the ASTER GDEM2 dataset, but found the relationship between these potential source slopes to be highly region-dependent and not morphometrically controlled. Gibson et al.[131] utilized numerous Landsat and ASTER satellite images to manually map debris cover and trace it back to its source. Although these studies are useful for gaining a conceptual understanding of the sources and mechanisms of debris cover and its influence on glacier behavior, numerical models are required to predict debris loading on glacier surfaces over time, as well as debris entrainment on and in the ice [17], to gain greater quantitative insight into glacier dynamics and glacier sensitivity to changing climate conditions [19].

Thermal imagery can be used to estimate debris thickness on glaciers. For example, Mihalcea et al.[4] described a relationship between debris thickness and surface temperature approximated from ASTER surface kinetic temperature data over the Baltoro Glacier. Such relationships assume

that debris depth is related to thermal resistance and the assumption of a linear thermal gradient is used. It is unclear to what degree the particle-size distribution, local topographic conditions, and debris moisture would influence the accuracy of such an approach, given extreme variability in all of these conditions over a glacier surface. Furthermore, the presence of boulder fields represents an extreme condition modifying the thermal gradient. Nevertheless, debris-depth conditions can be extrapolated and estimated for initial conditions.

Supraglacial meltwater streams and ponds can also be mapped from high-resolution imagery depending upon the geographic scale of the feature [132]. Gibson et al.[131] used false-color composites and the normal difference water index with the ASTER near-infrared and first shortwave-infrared bands (NDWI = NIR - SWIR/NIR + SWIR) to assist manual mapping of supraglacial water bodies and debris cover. Miles et al.[43] utilize geomorphometry to model the hydrology of the glacier surface and identify hydrological sinks in order to assess supraglacial ponding and the development of conduits to englacial flow. Mapping hydrological micro-basins on the glacier surface in this way is useful for object-oriented analysis for insight into ablation dynamics, including changes in supraglacial lake or pond size, shape, and the direction of water-body enlargement (e.g., [133, 43]). Such information about the frequency, density and evolution of lakes can be compared with numerical simulations. Meltwater streams on and off glacier can also be compared with simulated drainage conditions.

2.5.2 Ice-flow Velocities

Ice flow is a vital variable for dynamic modeling of debris-covered glaciers [52, 17, 18]. The simulation of sediment fluxes is highly dependent upon an accurate characterization of ice-flow rate to account for supra- and englacial loads [18, 17]. In addition, reduced ice-flow rate can be used to identify glacial stagnation [128]. Hence, observed surface ice-flow rates can be used as validation of the simulation of ice-flow parameters (i.e., velocity and direction).

With the advent of Global Positioning System (GPS) technology, temporally continuous GPS measurements have become popular in ice-flow monitoring, commonly supplanting field surveying to monitor ice-flow rates [134]. The accuracy of in-situ GPS measurements, however, can be

deteriorated by ionospheric delay, and inaccuracies in the satellite orbit, and clock information [135]. Such in-situ measurements are also time-consuming and only provide a discrete set of distributed velocity measurements. Remote-sensing technologies and imagery can be used to address this spatial problem.

Feature tracking using spectral imagery provides a solution for ice-velocity derivation by measuring the displacements based on the location of identical surface features from sequential images [136, 137, 138, 139, 140, 141]. Surface features are represented by the patterns of a group of individual pixels. By shifting small search windows across each single band image pair, the displacement of the dominant feature within the window is computed through the normalized covariance correlation method [142]. Although image matching is not limited by topography, prerequisite of enough cumulative displacements, appropriate time intervals between images should be considered in data selection in order to obtain high-accuracy ice velocity estimates (Figure 2.12).

Satellite microwave remote sensing, particularly Synthetic Aperture Radar (SAR), provides advantages of high accuracy flow-rate estimation and all-weather monitoring [143]. Two complex SAR images of the same surface area acquired at slightly different orbit configurations are combined to exploit the interferometric phase difference occurring between the acquisition time intervals. The phase differential interferometry (ψ) contains contributions from several independent terms, such as topography (ψ_t), displacement (ψ_d), atmosphere (ψ_a), system noise (ψ_n), flat-Earth (ψ_f) and is generally presented as a linear summation given as:

$$\psi = \psi_t + \psi_d + \psi_a + \psi_n + \psi_f, \tag{2.28}$$

If all the other four terms ψ_t, ψ_f, ψ_a, and ψ_n are negligible from the interferogram, then the motion-related phase (ψ_d) can be derived to exploit a displacement map. However, the Interferometric SAR (InSAR) method is highly dependent upon an accurate DEM, which is commonly unavailable for many debris-covered glaciers. The typical accuracy of Differential SAR Interferometry (DInSAR) - derived velocity measurements is $1\ mmyr^{-1}$ [144]. However, the DInSAR method is limited by high-phase noise, which can cause problematic phase unwrapping due to dis-

continuities and inconsistencies [145]. DInSAR is limited by severe topography and availability of suitable data.

Regardless of which approach is utilized to generate velocity estimates, simulated surface velocity profiles can be compared to the observed profile velocities to evaluate parameterization schemes for producing reliable estimates. For example, in Figure 2.13, the flow velocities are more similar at lower altitudes near the terminus and variations could be caused by the use of constant parameters such as the ice softness and basal sliding, and basal topography departures from surface topography. Differences at high altitude are due to simulations that do not account for tributary glaciers and their mass influx, which contribute to the much higher observed velocities.

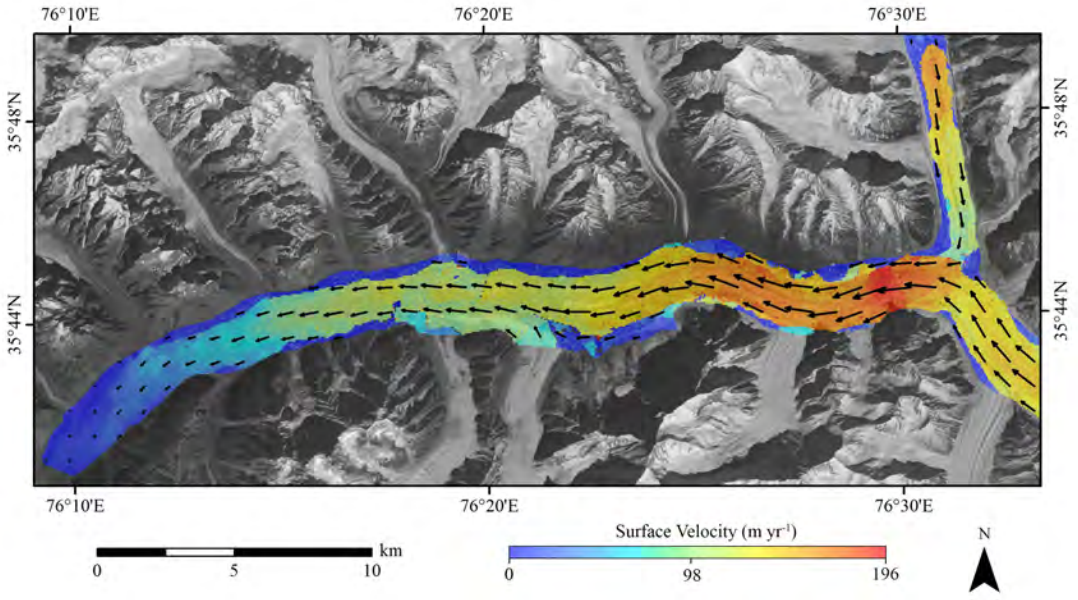

Figure 2.12: Example of the estimated surface ice-flow velocity field of the Baltoro Glacier using image matching. Two Landsat-8 OLI panchromatic images acquired on November 3, 2013 and October 21, 2014 were processed using the Co-registration of Optically Sensed Images and Correlation (COSI-Corr) software package [5].

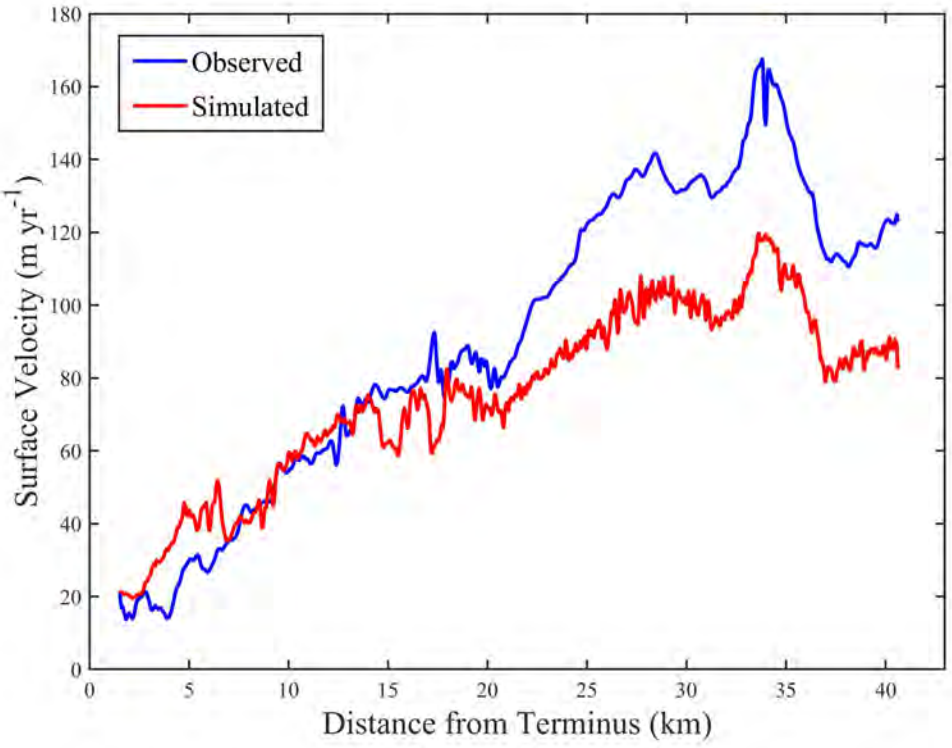

Figure 2.13: Comparison between the simulated ice-flow velocity profile and the observed velocity profile for the Baltoro Glacier along the flow line.

2.5.3 DEM Differencing

DEM differencing can also be used to estimate ice-mass loss given the ablation dynamics on a glacier. The mass losses can be compared to simulation results to determine the validity of estimates and to further elucidate on the dominant controlling factors governing negative mass balance conditions.

Specifically, glacier ice-volume changes may be approximated directly from comparing multi-temporal DEM datasets [133, 122, 43], assuming negligible change in basal bedrock conditions, the two DEMs are well spatially co-registered, and the DEMs do not collectively exhibit any systematic or random variations caused by sensor or acquisition methods (i.e., vertical resolution and error are less than the magnitude of the change in ice-surface altitude). The ice-mass balance, characterization of the accumulation zones and ablation zones, and approximation of the elevation

of glaciers' equilibrium line altitude (ELA) may be approximated with this differencing method (e.g., [146]). Differential DEMs have also be utilized to characterize the evolution of supraglacial water bodies and their impact on glacier ablation [133, 43].

Differential DEMs may likewise be used to measure the volume of material involved in significant mass wasting events from the hillslopes in glacial valleys that contribute debris to the glacier surface. For example, Immerzeel et al. [133] utilized off-glacier altitude values to validate their photogrammetric differential DEMs and glacier-change models and characterized off-glacier elevation difference, but a similar approach over a large time step could capture off-glacier behavior in relation to debris production. Contribution of valley slope material to the glacial debris load must otherwise be back-calculated from an estimation over debris volume by mapping debris cover and estimating debris thickness, or by modeling hillslope processes.

2.6 Conclusions

Understanding debris-covered glacier dynamics is notoriously difficult due to many interacting systems and forcing mechanisms. Empirical statistical analysis of variables does not adequately characterize the complexity of glacier systems given operational scale dependencies governing system interactions. Consequently, numerical modeling is required to provide insights into complex processes and interactions that govern glacier geometry, morphometry, mass balance and topographic evolution. Unfortunately, there are numerous issues that are associated with empirical parameterization schemes and not accounting for key parameters and feedbacks, that limit our understanding and capability to predict process rates and glacier sensitivity to climate change. Our discussions and simulations highlight the importance of: 1) radiative, precipitation and topographic forcing; 2) debris production and transport; 3) characterization of numerous processes that govern ablation dynamics including debris-flux, meltwater transport, and supraglacial lakes development; 4) accurate ice thickness and velocity modeling, 5) multi-scale parameters, feedback, and subsystem and systems coupling that regulate glacier system states; and 6) initial conditions and validation of simulations.

Glacier subsystem dynamics operate over a wide range of spatio-temporal scales, and it is im-

portant that parameters are computed at appropriate scales, such that the integration or interactions of various processes account for temporal dependencies that govern spatio-temporal variation. This requires the selection of an appropriate time step for subsystem simulations. For example, ice-flow-erosion dynamics could be computed over a larger time step (e.g., one-year interval) to account for topographic evolution over the basin, but higher temporal variations in ablation, meltwater production and supraglacial lake evolution operates over smaller spatial scales and requires a much smaller time step in simulations. It can be challenging to reconcile the vastly different simulation scales in an integrated model that involves multiple subsystem couplings and feedbacks. Another associated issue is digital representations and model implementation, as many of the aforementioned processes can be computationally expensive given larger spatial and temporal scales (e.g., the climate-glacier-topography dynamics) or smaller time steps (e.g., a surface drainage model). Addressing this issue will also require the development of new data structures, numerical schemes and optimization approaches (e.g., parallel computing).

Similarly, we need to design multiple simulation scenarios to study the responses (and sensitivity) of debris-covered glaciers to different forcing factors and geometric and morphological initial conditions. More realistic initial conditions must be used in simulations, and geospatial data can be used to validate and help improve the accuracy of parameterization schemes and subsystem coupling. For example, studies have found that surface ablation rates are highly variable on debris-covered glaciers [6, 91], most likely caused by heterogeneous debris distribution and the presence of supraglacial lakes. To simulate glacier dynamics and system states, we need to know realistic distributions of debris thickness, englacial load and paleo-topographic conditions that govern ablation dynamics. This information, however, is not adequately known [119]. Remote sensing plays an important role in addressing this issue as many glacier surface features and properties can be estimated using remote-sensing approaches. Glacier characterization using high-resolution remote-sensing data can also be very useful for validation of simulation results, which represents another research direction for future studies.

Recent simulations have highlighted the importance of system coupling and feedbacks for

debris-covered glaciers [17, 147]. Simulated processes form a net of interactions between radiative and precipitation forcing, topographic evolution, glacial hydrology, and debris cover and sediment transport. Unfortunately, additional processes and feedbacks are neglected or oversimplified in existing models, magnifying the uncertainty in our current climate-glacier sensitivity assessments. Modeling these feedback mechanisms may help explain some field observations, such as the accelerated downwasting on Himalayan debris-covered glaciers [31, 32, 16] and the advancement of many glaciers in the Karakoram [15, 127, 19, 9]. New parameterization schemes and more numerical simulations are needed to determine if subsystems of a debris-covered glacier (e.g., ice-flow velocities, sediment fluxes, and supraglacial lakes) are actively responding to climate forcing, and if glaciers in different geographic locations exhibit similar or different dynamics, thereby indicating magnitude and gradient variations in glacier sensitivity to climate change.

3. UNDERSTANDING DEBRIS-COVERED GLACIER ABLATION DYNAMICS IN THE CENTRAL KARAKORAM HIMALAYA USING DEBRIS-FLUX AND ABLATION MODELING

3.1 Abstract

It is generally thought that debris-covered glaciers are not as sensitive to climate change due to their debris insulation, however, recent studies show that many debris-covered glaciers exhibit accelerated surface thinning despite the presence of supraglacial debris. Existing numerical models do not explain rapid glacier thinning because complex surface dynamics that incorporate topographically controlled sediment flux and surface irradiance, debris properties and related feedback mechanisms have not been rigorously accounted for. Most existing ablation models either oversimplify these surface conditions or heavily rely on meteorological and remote-sensing measurements. In this study, we address these issues using a solar radiation-driven glacier-surface ablation model that more fully characterizes ablation dynamics by accounting for temporally-linked radiative forcing, surface topographic evolution and gravity-driven sediment flux. Simulation results based on the Baltoro Glacier in the Karakoram Himalaya indicate the following: 1) The topographic influence on surface ablation is non-negligible for debris-covered glaciers because glacier-surface topography controls irradiance and gravitational debris flux. The overall ablation on a debris-covered glacier tends to increase in response to high-frequency topographic variations due to faster sediment flux; A bare-ice glacier, however, exhibits decreased overall ablation in response to high-frequency topographic variations due to its high sensitivity to topographic shading. 2) Gravity-driven surface debris flux plays an important role in debris-thickness redistribution which governs ablation rates. A faster debris flux under gravity tends to increase the overall surface ablation. 3) A debris-covered glacier can exhibit high temporally and spatially variable surface ablation due to heterogeneous debris-thickness and debris flux. A bare-ice glacier has higher overall ablation but exhibits much less spatio-temporal variability. 4) Surface-ablation dynamics on

a debris-covered glacier is regulated by active system couplings and feedbacks between surface morphology, melting, and debris flux. Consequently, certain locations on a debris-covered glacier may be more sensitive to radiative forcing than previously thought.

3.2 Introduction

Glaciers in High Asia govern regional water resources, ecosystem sustainability at lower altitudes, geohazards, and play an important role in landscape evolution [10, 11, 12, 13, 14, 9]. Unfortunately, debris-covered glaciers are extremely complex, and we lack fundamental knowledge about controlling factors and feedback mechanisms [119, 9]. Such complexity can only be accounted for by numerical modeling efforts, where coupled forcing factors like climate, topography and debris loads can be accounted for in parameter representation schemes (e.g., [17, 16]). Fundamental to understanding glacier-system complexity is characterization of ablation dynamics, as debris flux and multi-scale topographic effects govern radiation forcing, which governs ablation and alters ice topography forming a complex feedback which may be extremely sensitive to seasonal or annual forcing. Currently, most glaciers are responding to world-wide atmospheric warming [148, 14, 119, 15, 32]. Nevertheless, there is significant debate about the sensitivity of debris-covered glaciers versus debris-free glaciers [31, 32, 16], and it is unclear as to what the concept of sensitivity represents, and quantitatively what represents a forcing-response with respect to glacier systems, and what are the forcing-response times we might expect for various components of a glacier system.

Investigating glacier dynamics and the aforementioned issues in the Himalaya is notoriously difficult due to a multitude of governing factors that are thought to regulate glacier fluctuations and morphological conditions [17, 19]. These include radiative and precipitation forcing, topography, debris cover, and potentially other geological factors (e.g., tectonics). The supraglacial debris load is known to be an important controlling factor on glacier ablation dynamics and glacier morphology [23, 24]. Nevertheless, detailed information about debris-load properties, such as mineralogical composition, thermal properties, reflectance properties, debris-load depth, depth spatial variability, and debris flux rates are not known with any degree of certainty [29, 9], which poses a

challenge to our understanding of the magnitude of glacier processes and morphological dynamics [41, 52, 17, 19]. Furthermore, lithological variation can cause significant mineralogical compositional spatial variation which governs albedo, the surface-energy balance and ablation. Given atmospheric warming, it is generally thought that debris cover insulates a glacier and reduces its sensitivity to climate change [24, 46, 18]. Recent observations and simulations, however, show that Himalayan glaciers have exhibited accelerated surface thinning despite the presence of supraglacial debris [31, 32, 16].

To improve our understanding of ablation dynamics for debris-covered glaciers, it is necessary to understand the role that debris cover and the gravitational debris flux has on ablation dynamics in order to address questions related to glacier mass balance, glacier sensitivity to climate change, glacier-surface process-form relationships, and glacier-surface process regimes. It is also necessary to investigate the extent to which gravitational sediment flux governs the spatial variability of supraglacial debris-thickness and how debris lithology affects albedo and the glacier surface-energy balance. Field studies have found that surface ablation rates are highly variable on debris-covered glaciers [6, 91], likely due to heterogeneous debris distribution, melt-enhancing effects of a thin debris layer, and the presence of supraglacial lakes. Existing models (e.g., [4, 13, 49, 24]), however, fail to quantify and explain such variability due to oversimplification of glacier-surface conditions. Furthermore, the coupling of sediment flux, ablation and glacier-surface morphology most-likely form positive feedbacks that accelerate melting during the ablation season. These mechanisms are often neglected or oversimplified in existing models, magnifying uncertainty in empirical-based climate-glacier sensitivity assessments.

Therefore, the overall objective of this research is to develop a new glacier ablation model that addresses the aforementioned issues by accounting for temporally-linked radiative forcing, surface-morphological evolution and gravity-driven sediment flux to better understand debris-covered glacier ablation dynamics. We use the Baltoro Glacier in the central Karakoram Himalaya in Pakistan to evaluate, validate, characterize and discuss various issues related to ablation dynamics. Our specific research objectives include: 1) evaluate debris-flux rate forcing on surface

ablation over the ablation season; 2) evaluate topographic forcing on surface ablation over the ablation season; and 3) quantify the degree to which topography, debris cover and debris flux governs the spatial and temporal variation in ablation rate over the short-term ablation season given radiative forcing.

3.3 Background

3.3.1 Surface Irradiance

Glacier-surface ablation is primarily governed by short-wave solar radiation [36]. Surface irradiance consists of: 1) direct solar-beam irradiance; 2) diffuse-skylight irradiance; and 3) adjacent-terrain irradiance. Each of these components is strongly governed by multi-scale topographic effects, and the latter two are also regulated by the land-cover spatial structure and the bi-directional reflectance distribution function (BRDF).

Direct solar-beam irradiance is the major contributor to glacier surface-energy and is controlled by the Earth-Sun distance, altitude, local topographic conditions, and meso-scale topographic relief [60, 149]. Diffuse-skylight irradiance is primarily caused by atmospheric scattering, and local topographic variations and basin topographic relief caused by paleo-glacier erosion dynamics that modulates this irradiance component with altitude [150, 149, 19]. The adjacent-terrain irradiance is also governed by complex topographic geometry, atmospheric attenuation, and land cover structure, and is usually not accounted for given the complexity of estimating the BRDF and lack of data regarding temporally-variant landcover, biophysical properties, and solar geometry. Most studies do not account for the multi-scale topographic effects that govern irradiance given the inherent complexity of parameterization schemes and computational issues. Nevertheless, all three components govern glacier geometry and ablation rates in the Karakoram Himalaya, although very few studies actually account for the primary irradiance components (i.e., Direct and sky-light irradiance), but such multi-scale topographic conditions must be accounted for along with solar geometry variations [19].

Most ablation models only account for the direct-irradiance component under assumptions of

simplified solar geometry, surface albedo and local topographic effects (e.g., [13, 49, 24]). These assumptions often yield unrealistically homogeneous patterns of ablation rates over glaciers, because complex topography in the Himalaya causes significant variation in surface irradiance over short distances due to extreme relief and cast shadows, and topographic shielding variations with altitude [16, 56]. Furthermore, minor variations in one radiation parameter, when multiplicatively coupled with other prominent governing parameters (e.g., atmospheric and topographic variation), generates significant variation in surface irradiance conditions [56]. To better simulate the shortwave energy input into a glacier surface-energy balance model that governs ablation, our modeling of surface irradiance accounts for the first two dominant surface irradiance components, including cast shadows, local topography and topographic shielding.

3.3.2 Supraglacial Debris and Debris Flux

Supraglacial debris plays a crucial role in glacier-surface melting [45, 4, 49, 24, 46]. Many studies have documented a negative relationship between debris-thickness and ablation rate due to insulation by a thick debris layer (e.g.[76, 66, 2]). These studies, however, did not account for the melt-enhancing effect of thin debris due to the higher energy absorption of debris and conduction of heat into the underlying ice [3, 2, 77].

Debris-thickness can be spatially heterogeneous due to multiple factors such as hillslope input from steep valley slides, ice-flow debris transport that can increase or decrease debris depth, incorporation of the englacial debris load due to melting, sediment transport due to meltwater production and surface drainage, ice-cliff development and sediment gravity flow [20, 27, 17]. In the Karakoram Himalaya, debris depths are highly variable, and can be more that 3 m thick [73, 74]. Spatially variant sediment-transport processes also control glacier topography, the mass-balance gradient, ice-velocity gradient due to load stress, and glacial drainage [68, 69, 55].

Ice-flow dynamics govern the transport of debris from high-altitude regions to the terminus over large spatial (the entire glacial valley) and temporal (decades and centuries) scales, and simulating the sediment flux requires an accurate characterization of ice-flow velocity to account for supra- and englacial loads (e.g., [18, 17]). Another form of sediment transport on a glacier surface

is gravitational movement [50], which operates over a smaller spatio-temporal scale and is heavily influenced by the near-surface morphological properties of the debris and ice-surface topography. Therefore, gravitational sediment-transport governs the local debris-thickness that collectively accounts for the spatial distribution of the debris load to rapidly changing ice and debris topography due to differential ablation.

Unfortunately, the gravity-driven debris flux is usually neglected in glacier simulations, as the topography of the sediment and ice must be allowed to evolve and be temporally coincident with variations in surface irradiance and ablation. In this study, we demonstrate that the gravity-driven debris flux can lead to significant spatial variation in the debris load over an ablation season, which enhances differential ablation and glacial thinning over a debris-covered glacier. Furthermore, we account for debris-load matter variations and mixing that causes changes in the thermal and reflectance properties of the debris, thereby altering the spatial distribution of ablation rates.

3.3.3 Surface Ablation

It is generally thought that debris-covered glaciers are less sensitive to climate change due to debris insulation [66, 2]). This may be the result of oversimplified assumptions and a lack of understanding of the dominant processes and feedback mechanisms that regulate ablation rates and glacier morphological conditions, which have yet to be fully modeled and understood [30, 15, 19]. Some recent studies suggest that although thick debris loads generally suppress melting, the overall ablation on a debris-covered glacier can still be high [31, 16]. Transition zones from debris to ice are usually characterized by a systematic change in the debris depth due to gravitational sediment transport. Shallow debris enhances ablation, and transition zones usually contain moisture-laden debris that absorb more energy and also exhibit relatively high ablation rates. Kaab et al. [31] also found the average ablation rate for a glacier to be similar between debris-covered ice and clean ice in the Hindu Kush-Karakoram-Himalaya. Immerzeel's [32] basin-scale simulations over the Baltoro Glacier predicted a significant increase in total runoff, downwasting and retreat throughout the twenty-first century despite thick debris cover. Simulations [16] also demonstrated that the debris cover on a Himalayan glacier can promote ablation such that the debris-covered area contributes

more per square meter to the total runoff than the clean-ice portion. Recent studies also found that ice cliffs and supraglacial lakes significantly accelerate differential melting on debris-covered glaciers [38, 52, 17, 90, 91].

Traditional approaches for computing the ablation rate, including the degree-day factor approach, the use of climate station data at a particular altitude, and the use of low-resolution global or regional climate models, cannot adequately account for topographic variation or topography-climate coupling necessary for characterizing complex glacier ablation dynamics [92, 45]. In addition, temporally-variant debris-thickness due to sediment transport has not been adequately characterized over the ablation season. Improved parameterization schemes must integrate these components to accurately predict ablation rates, map downwasting patterns, and explore numerous process feedbacks that govern the magnitude of the ablation rate. Accounting for process-morphology dynamics is essential for better understanding glacier-system sensitivity to diurnal, seasonal and decadal radiative forcing, and the role that individual glaciers play in the every evolving geomorphological system, as paleo-glacier dynamics and erosion have established the topographic forcing controls that govern modern-day surface irradiance and debris production conditions of basin hillslopes. Our parameterization schemes will enable us to more rigorously evaluate the role that debris-load composition and transport has on glacier topography and meltwater production, as we account for debris mineralogical composition, gravitational sediment transport and compositional mixing that governs albedo, debris depth and ablation at the ice-debris interface.

3.4 Methods

3.4.1 Data

We simulate the surface ablation dynamics on the Baltoro Glacier under modern-day and hypothetical conditions to answer our research questions. The Baltoro Glacier is a notable debris-covered glacier located in the central Karakoram Himalaya, and is one of the largest temperate glaciers in the world outside the polar regions. We selected Baltoro Glacier because quantitative estimates of surface ablation rates and debris-thickness distribution have been produced (e.g.,

[6, 4, 23]), and it is large enough to be observed using satellite remote-sensing techniques.

Specifically, the glacier-surface topography is acquired from a digital elevation model, which is generated based on stereo-correlation from Advanced Spaceborne Thermal Emission and Reflection Radiometer (ASTER) satellite data using SILCAST software at a 30-meter spatial resolution. The initial surface temperature is acquired from the ASTER surface kinetic temperature product. All ASTER data were acquired on August 14, 2004, (ID 00308142004054614) in order to maintain temporal consistency and to calibrate with the field measurements at the time of fieldwork by Mihalcea et al. [6]. Air temperature is acquired from the NCEP-CFRS reanalysis product in the central Karakoram [151] adjusted by the mean diurnal measurement by Collier et al. [147] on Baltoro Glacier in the ablation season of 2005. A vertical lapse rate of $0.0065 Km^{-1}$ is used to account for the decrease of air temperature with increasing altitude following Reid and Brock [13].

3.4.2 Surface Irradiance

We use an energy-balance approach to model surface ablation, in which solar radiation and the thermal irradiant flux from the atmosphere are the main radiative-forcing components for ice melting. These two energy fluxes received by the glacier surface are the net short-wave radiation flux (Q_s) and the net long-wave radiation flux (Q_l). The total short-wave surface irradiant flux in our model consists of two components: 1) the direct solar-beam irradiance; and 2) the diffuse-skylight irradiance. The direct solar-beam irradiance, E_b, can be written as:

$$E_b(\lambda) = \int_{\lambda_1}^{\lambda_2} E^0(\lambda) T^{\downarrow}(\theta_s, \lambda) cosi d\lambda, \tag{3.1}$$

where E^0 is the mean exo-atmospheric spectral irradiance given by [60], $T^{\downarrow}$ is the total downward atmospheric transmittance, which is a function of wavelength (λ) and solar zenith angle (θ_s), and $cosi$ is the cosine of the local illumination angle governed by local topography and solar geometry. Note that the wavelength range for integration is $0.3\mu m$ – $3\mu m$.

The total atmospheric transmittance is calculated as [60]:

$$T^{\downarrow}(\theta_s, \lambda) = T_r(\theta_s, \lambda)T_a(\theta_s, \lambda)T_g(\theta_s, \lambda)T_o(\theta_s, \lambda)T_w(\theta_s, \lambda), \tag{3.2}$$

where T_r is transmittance due to Rayleigh scattering, T_a is the transmittance due to aerosol scattering, T_w is transmittance due to water-vapor absorption, T_o is transmittance due to ozone absorption, and T_g is transmittance due to primary-gas absorption. The paleo-glacier erosion conditions due to climate forcing are responsible for relief production in a basin, and this governs the magnitude of the downward atmospheric transmittance, as it decreases at lower altitudes and with an increasing solar zenith angle. The cosine of the local illumination angle is the dominant factor that governs E_b [149] and is defined as:

$$cosi = cos\theta_s cos\theta_t + sin\theta_s sin\theta_t cos(\phi_t - \phi_s), \tag{3.3}$$

where θ_t represents the terrain slope angle, ϕ_s is the solar-azimuth angle, and ϕ_t is the terrain slope-azimuth angle. The solar zenith and solar azimuth angles are calculated for every grid cell using the NOAA Solar Position algorithm in MATLAB.

Our model also accounts for the diffuse-skylight irradiance (E_d), which is computed following [149]:

$$E_d = E_{dh}V_d, \tag{3.4}$$

where E_{dh} is the isotropic diffuse-skylight irradiance for a horizontal surface defined by Bird and Riordan [60], and V_d is the skyview factor as defined by Dozier and Frew [149]. In the computation of V_d, we used an azimuth interval of 5-degree as the step size, which was found to be generally acceptable by Li [152]. Collectively, this model accounts for both local ($cosi$) and meso-scale (V_d) topographic effects on surface irradiance.

3.4.3 Surface-Energy Balance and Ablation

Ablation rates are calculated based upon the surface-energy balance. The energy balance at the debris/air (or the ice/air) interface can be written as [53, 45]:

$$Q_s + Q_l + Q_h + Q_e + Q_c = 0, \tag{3.5}$$

where Q_h is the net sensible-heat flux, Q_e is the net latent-heat flux, and Q_c is the conductive heat flux into the debris which governs sub-debris ablation. Note that in this 2-D distributed model, heat flux terms are computed at the beginning of each iteration due to the changing topography, albedo, and surface temperature.

The net-radiation fluxes (Q_s, Q_l) at the glacier surface can be computed as:

$$Q_s = (E_b + E_d)(1 - \alpha), \tag{3.6}$$

$$Q_l = \varepsilon_a \sigma T_a^4 - \varepsilon_s \sigma T_s^4, \tag{3.7}$$

where α is the surface albedo described in the section 3.4.5, ε_a and ε_s are the emissivity for air and glacier surface respectively, σ is the Stefan-Boltzmann constant, T_a is the air temperature that is a function of elevation (z), and T_s is the surface temperature.

The net sensible-heat flux and the net latent-heat flux terms are computed as [45]:

$$Q_h = \rho_0 (\frac{P}{P_0}) c A_t u_w (T_a - T_s), \tag{3.8}$$

$$Q_e = (\frac{0.622 \rho_0}{P_0}) L_e A_t u_w (e_z - e_s), \tag{3.9}$$

where ρ_0 is the air density at sea-level, P is the air pressure at altitude, P_0 is the standard air pressure at sea level, c is the specific-heat capacity of air, u_w is the wind speed, L_e is the latent heat

of evaporation of water, e_z is the vapor pressure of air above the surface, e_s is the vapor pressure at the glacier surface, and A_t is a dimensionless transfer coefficient defined by Nicholson and Benn [45].

Based on the energy balance at the ice/air interface, the melt rate for bare ice under temperate conditions can be calculated as:

$$M_i = \frac{Q_s + Q_l + Q_h + Q_e}{\rho_i L_f}, \tag{3.10}$$

where. L_f is the latent heat of fusion for ice, and ρ_i is the density of ice.

The energy balance at the debris/ice interface is [53]:

$$Q_m = Q_c^{\downarrow} - Q_c^{'}, \tag{3.11}$$

where Q_m is the heat flux used for sub-debris ice ablation, $Q_c^{\downarrow}$ is the conductive heat flux from the debris, and $Q_c^{'}$ is the conductive heat flux towards the ice that is not used for ablation. Since we assume the surface ice is at its melting point during the ablation season, $Q_c^{'}$ is negligible [36]. Under the assumptions of constant heat storage and a linear debris-temperature gradient, Q_m during the ablation season can be computed using the one-dimensional heat-flux equation described by Fourier's law [53, 45]:

$$Q_m = \frac{(T_s - T_i)}{R}, \tag{3.12}$$

$$R = \frac{h_d}{k_d}, \tag{3.13}$$

where T_i is the ice temperature, h_d is debris-thickness, R is the thermal resistance of the debris layer as a function of debris-thickness, and k_d is the thermal conductivity of debris, which is held constant in our simulations. T_s is computed for debris-covered areas at each iteration by solving the surface-energy balance equation (Equation 3.5), and set to melting temperature for bare-ice

surfaces. Then, the sub-debris melt rate M_s can be computed as [53, 45]:

$$M_s = \frac{Q_m}{\rho_i L_f}. \tag{3.14}$$

The topography is altered by lowering the elevation by Δz_i after each iteration (with a time step of Δt) based upon the ablation rate and surface slope:

$$\Delta z_i = M_s \Delta t cos\theta_t. \tag{3.15}$$

In this radiation-driven model, the ablation rate is governed by the diurnal variation in irradiance, therefore, the time step must be small enough to capture the diurnal variation. The sensitivity tests (Figure 3.1) demonstrate that a larger time step leads to more generalization in ablation rate estimates. In study, a time step of one-hour is used to produce a more accurate characterization of ablation over the ablation season.

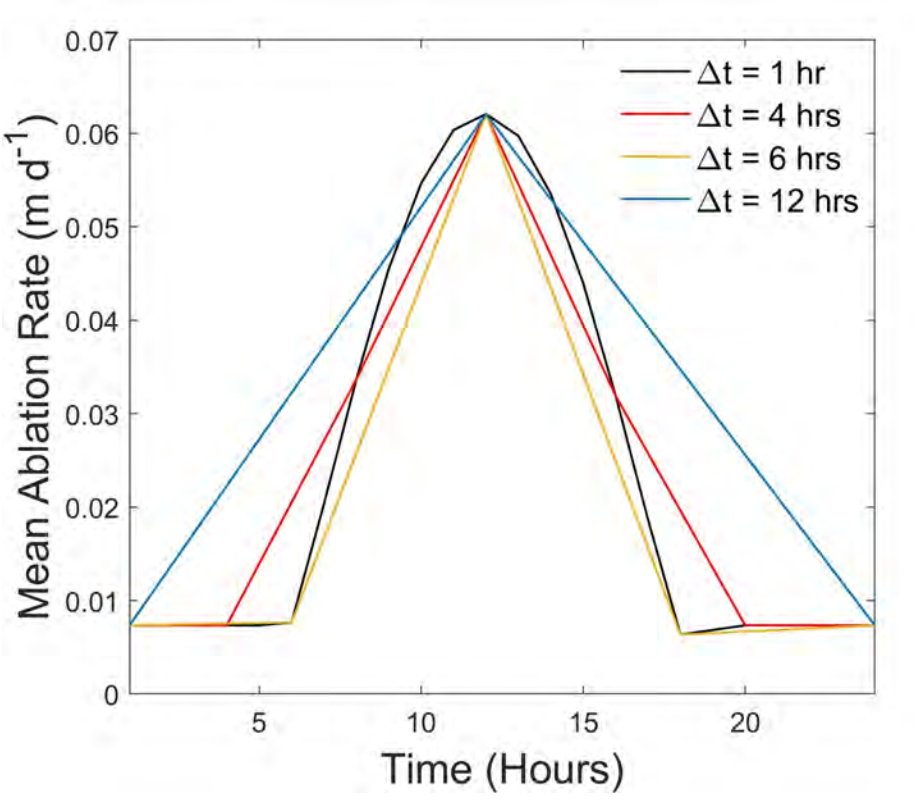

Figure 3.1: Sensitivity tests illustrating how different time steps influence the simulated surface ablation rate. The ablation rates here represent the averaged magnitudes over the Baltoro Glacier on June 1st, 2004. Note that a larger time step leads to more generalization in ablation rate estimates.

3.4.4 Gravity-Driven Debris Flux

Supraglacial debris is mobile under gravity [50], especially during the ablation season when the surface topography is constantly changing due to melting. Our parameterization scheme neglects the ice-flow component of debris transport because we focus on the redistribution of debris over a relatively short period of time, which is governed by gravity and local topographic change. From a mass-flux perspective, the change of debris-thickness is estimated as:

$$\frac{dh_d}{dt} = \frac{-q_{out}}{A_c}, \tag{3.16}$$

where q_{in} and q_{out} are the sediment fluxes into and out of a grid cell, respectively, and A_c is the planimetric area of a grid cell. The flux out of a grid cell can be represented as:

$$q_{out} = A_s u, \tag{3.17}$$

where A_s is the cross-sectional surface area which the flux passes through, and u is the velocity of the debris. The momentum equation is used for solving velocity from force analysis:

$$F = \frac{d(mu)}{dt}, \tag{3.18}$$

where F is the net force applied on the debris column, m is the mass of debris in each grid cell, and $dt(\Delta t)$ is the time step used in the scheme. The discrete form of the momentum equation can be written as:

$$\Delta u = (1 - M)\frac{F\Delta t}{\rho_d V}, \tag{3.19}$$

where Δu represents the change in the flux rate. A tuning parameter (M) is used here to control the flux rate and account for the change of mass during each time step following [153]. The bulk density of debris (ρ_d) is assumed to be constant, and V is the volume of the debris block. The value for M used for simulations was determined by a sensitivity analysis discussed at the end of this section. Very thin debris cover is governed by more complex dynamics: the sediment/debris is strongly affected by meltwater and ice, where cohesion and refreezing effects can significantly restrict debris particle movement. For simplicity, this model assumes that the output discharge for grid cells with a debris-thickness less than 0.5cm is zero due to the cohesion effect. In addition, we assume that sediment velocity is not maintained after entering a new grid cell, due to complex depositional mixing.

To estimate net force applied on each debris column, we adopt the force analysis for unsteady gravity-driven debris flow characterized by Chen and Lee [86], which accounts for gravity, internal friction and basal resistance for each finite moving debris column. Based on this model, the unit net force acting on a debris column F can be written as:

$$F_x = \rho_d g[\frac{z_x}{z_x^2 + z_y^2 + 1} - k\frac{dh}{dx} - \frac{1}{\sqrt{z_x^2 + z_y^2 + 1}}\frac{u_x}{\sqrt{u_x^2 + u_y^2 + 1}}(1 - r_u)tan\varphi], \tag{3.20}$$

$$F_y = \rho_d g[\frac{z_y}{z_x^2 + z_y^2 + 1} - k\frac{dh}{dy} - \frac{1}{\sqrt{z_x^2 + z_y^2 + 1}}\frac{u_y}{\sqrt{u_x^2 + u_y^2 + 1}}(1 - r_u)tan\varphi], \tag{3.21}$$

where ρ_d is sediment density, g is the gravitational acceleration constant (a function of latitude and altitude), z_x and z_y are the first derivatives of ice-surface elevation in the x and y directions, respectively, h is the height of debris in the column, k is the lateral Earth-pressure ratios in active state as defined by Chen and Lee [86], u_x and u_y are the velocity components along the x and y axes, r_u is the constant pore-pressure ratio, and φ is the dynamic internal friction angle of the debris. In equations (3.20) and (3.21), the first term on the right represents the gravitational force, which is obtained by projecting the gravity force onto the vector normal direction of the ice surface. The second term represents the intercolumn force, which describes the internal friction of debris particles. It is computed as the difference of the lateral Earth pressure acting on both sides of a column [154, 155]. The third term represents the basal resistance force, which is a frictional rheological model in terms of an effective stress, (i.e., the resisting shear stress at the base of the flowing mass is a fraction of the total normal stress [153]).

A multiple flow-direction algorithm is then applied to determine the direction of sediment discharge. Specifically, sediment from a given grid cell (the focus) flows to multiple neighboring cells [156, 87]. Therefore, the total sediment flux into a given grid cell is:

$$q_{in} = \sum_{i=1}^{8} f_i \cdot q_{out,i}, \tag{3.22}$$

where f_i is the fraction of flow into grid cell i:

$$f_i = \frac{max(0, \theta_{t,i}^p) l_i}{\sum_{j=1}^{8} max(0, \theta_{t,j}^p) l_j}, \tag{3.23}$$

where cells i and j are neighbors of the source cell, $\theta_{t,i}$ is the slope gradient from the central grid cell to its neighbor i, p is a flow-partition exponent, and l_i modifies the function to ensure even distribution in circular contours on a hypothetical conical surface.

The sediment flux model was evaluated by a sensitivity analysis to determine a reasonable flux rate due to the lack of comprehensive field measurements. We analyzed two scenarios: 1) Sediment transport on a hypothetical U-shaped valley (Figure 3.2); and 2) The discharge of a thick debris layer under different M values (Figure 3.3). Note that the gravitational sediment transport on a glacier surface is much slower than other types of gravitational flows such as landslides, due to cohesion and refreezing effects that significantly slow down particle movement. We compared multiple simulation results with field observations on the Baltoro Glacier in 2005 and determined that M = 0.99 provides a reasonable flux rate that is conservative, given the change in debris depth over time.

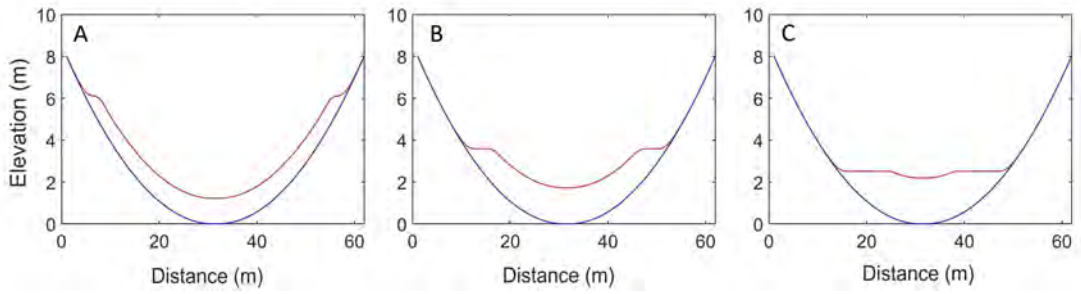

Figure 3.2: Mass movement sediment flux simulation on a hypothetical U-shaped depression. Blue curves represent valley topography and red curves represent the sediment surfaces after (A) 72 hours, (B) 120 hours, and (C) 144 hours.

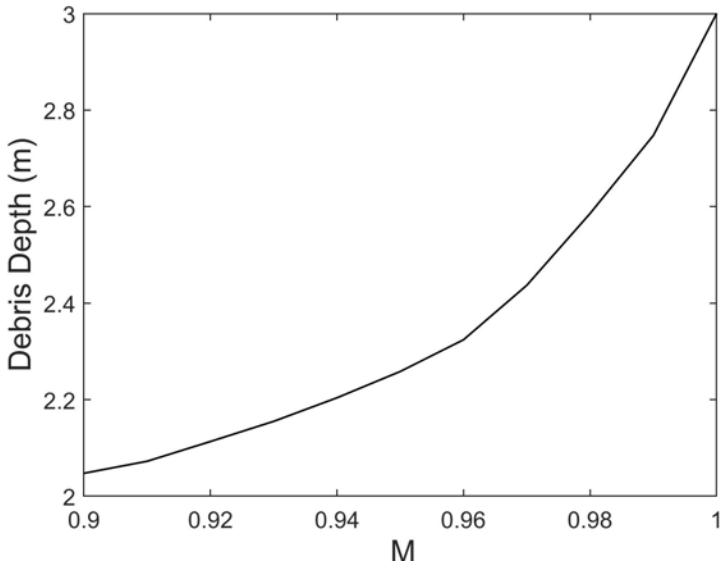

Figure 3.3: Sensitivity test illustrates how the tuning parameter M controls gravitational sediment flux rate. Results show the final debris depth of a 10-day simulation for a 20-degree inclined ice-plane initially covered by 3m thick debris.

3.4.5 Surface Albedo

Surface albedo is an important parameter that governs the amount of net short-wave radiation flux at the glacier surface, and exhibits significant spatio-temporal variability on a debris-covered glacier [157, 158]. We use a radiation transfer approach [159] to compute the broadband surface albedo (α):

$$\alpha = \frac{\int_{\lambda_1}^{\lambda_2} L(\lambda)}{\int_{\lambda_1}^{\lambda_2} E(\lambda)}, \tag{3.24}$$

where E is the total short-wave irradiance, and L is the reflected surface radiance, which, based on an isotropic (Lambertian) assumption, can be written as [160]:

$$L(\lambda) = r_{mc}(\lambda)\frac{E(\lambda)}{\pi}, \tag{3.25}$$

where r_{mc} is the spectral reflectance of the mineralogical composite representing the debris, which

is considered as a composite reflectance of different minerals. The mineral types and distributions are estimated based on the debris rock type map over the Baltoro Glacier [23], based on which, the supraglacial debris mostly consists of gneiss (about 53%), granite (about 30%), and schist metasediment (about 17%), except for the areas with tributary input, which are mostly covered by granite, and the medial moraine area, which is mostly covered by schist. If a grid cell is not debris-covered, then a constant albedo of 0.39 is used based on field measurement[66].

Meltwater can affect the surface albedo if the amount of meltwater is large enough to take up all the pore spaces in the debris and appear near the surface. We account for capillary action and transport of water towards the surface by comparing the debris porosity ε to the volume fraction of meltwater produced f_w:

$$\varepsilon = 1 - \frac{\rho_b}{\rho_p}, \tag{3.26}$$

$$f_w = \frac{V_w}{V_t}, \tag{3.27}$$

where ρ_b is the bulk density of debris, ρ_p is the particle density, V_w is the volume of meltwater generated within one time step, and V_t is the total volume of that grid cell given debris height which fluctuates based on debris-thickness distribution.

If f_w is equal to or greater than ε, we consider the meltwater has made its way to the surface, then spectral reflectance is updated as follows:

$$r_c(\lambda) = \begin{cases} r_{mc}(\lambda), & \text{if } f_w < \varepsilon \\ \varepsilon r_w(\lambda) + (1-\varepsilon) r_{mc}(\lambda), & \text{if } f_w \geq \varepsilon \end{cases} \tag{3.28}$$

where r_c is the composite spectral reflectance, and r_w is the reflectance of water. This approach assumes a thorough mixing of water and minerals, and the areal fraction of water is governed by porosity.

Supraglacial sediment flux changes the mineralogical distributions on the glacier surface, and

therefore alters the surface albedo. Consequently, we use a weighted-average spectral mixing model to describe the mixing of minerals and water due to sediment flux at each grid cell:

$$r^{'}_{mc}(\lambda) = \sum_{i=1}^{8} \frac{V_{in,i}}{V_t} r_{c,i}(\lambda) + (1 - \sum_{i=1}^{8} \frac{V_{in,i}}{V_t}) r^{c,f}(\lambda), \tag{3.29}$$

where $V_{in,i}$ is the volume of input debris from the neighboring cell i, $r_{c,i}$ is the composite spectral reflectance of the neighboring cell i, and $r_{c,f}$ is the composite spectral reflectance of the focus. Such that $r^{'}$ becomes r_{mc} for the next iteration.

We also calibrate the initial mineral compositions and spatial distributions using the broadband albedo estimated from remote-sensing analysis. Specifically, we performed the narrowband to broadband conversion of surface albedo based on the approach by [161] using the ASTER imagery, and confirmed that the values are close to our estimates using the radiation-transfer approach.

Constants and default parameters	Symbol	Value SI Units
Grid cell area	A_c	30x30 m^2
Specific heat capacity of air	c	1010 $Jkg^{-1}K^{-1}$
Vapor pressure at glacier surface	θ_z	611 Pa
Emissivity of air	ε_a	0.8
Emissivity of debris	ε_s	0.97
Acceleration of gravity	g	9.81 ms^{-2}
Debris thermal conductivity	k_d	1.00
Latent heat of evaporation of water	L_e	2.39 $\times 10^6 Jkg^{-1}$
Latent heat of fusion for ice	L_f	3.34$\times 10^5 Jkg^{-1}$
Surface roughness length	l_0	0.01 m
Flow-partition exponent	p	1.00
Air pressure at site	P	61075 Pa
Standard air pressure at sea level	P_0	101325 Pa
Dynamic internal friction angle of the debris	φ	0.34 rad
Lateral earth pressure ratios in active state	k	1.01
Constant pore-pressure ratio	r_u	0.5
Air density at sea-level	ρ_0	1.29 kgm^{-3}
Bulk density of debris	ρ_d	1600 kgm^{-3}
Density of ice	ρ_i	910 kgm^{-3}
Particle density of debris	ρ_p	2650 kgm^{-3}
Stefan-Boltzmann constant	σ	5.67$\times 10^{-8} Wm^{-2}K^{-4}$
Ice temperature	T_i	273.15 K

Table 3.1: Constants and default parameter values used in simulating ablation dynamics for the Baltoro Glacier in the central Karakoram Himalaya.

3.4.6 Simulation Scenarios and Initial Conditions

Three scenarios with sub-scenarios are simulated for an ablation season to answer various questions associated with the research objectives. Table 3.1 lists the parameters that are considered as constants in the simulations. All the simulation scenarios are listed in Table 3.2, and they are simulated with an one-hour time step over the ablation season in 2004 (06-01-2004 – 09-28-2004).

The first group of sub-scenarios addresses the topographic influence on surface ablation rates, in which we assume the glacier surface is a bare-ice surface. Surface ablation under four different surface topographic conditions are simulated: 1) Default surface topography from the DEM; 2) Low-frequency topographic undulations on a plane surface; 3) Moderate-frequency topographic undulations on a plane surface; and 4) High-frequency topographic undulations on a plane surface.

The modern-day surface topography (Figure 3.4A) is acquired from an ASTER DEM. The artificial topography (Figure 3.4B,C,D) are generated by adding hummocky undulations to best-fit plane of the modern-day topography. The following equation is used to create the topographic periodicity with different spatial frequencies such that:

$$z_i = A_z sin(kx)cos(ky) + z_p, \tag{3.30}$$

where the amplitude (A_z) is set to 50m, k controls the spatial frequency of the undulations (for low to high frequencies, k = 0.06, 0.12, 0.24m^{-1} respectively), x, y represents the distance (in terms of number of pixels) in horizontal and vertical directions respectively, and z_p is the elevation of an inclined plane.

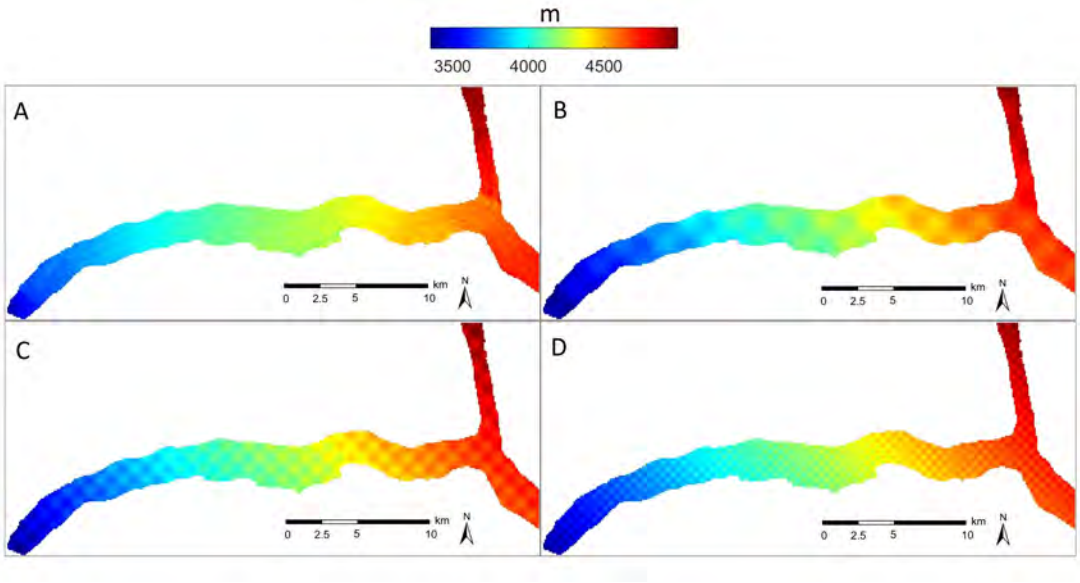

Figure 3.4: Four types of initial ice surface topography used in the simulations. (A) The modern-day topography acquired from the DEM. (B) The hypothetical topography with low-frequency (k = 0.06) undulations. (C) The hypothetical topography with moderate-frequency (k = 0.12) undulations. (D) The hypothetical topography with high-frequency (k = 0.24) undulations.

The second group of sub-scenarios investigates surface ablation rate variability with respect to varying supraglacial debris conditions (thickness and flux rate). Three thickness variations (Figure 3.5) with three different flux rates conditions are simulated, which account for 9 sub-scenario cases: homogeneous thin debris with low/moderate/high debris flux rates; homogeneous moderate debris-thickness with low/moderate/high debris flux rates; and homogeneous thick debris with low/moderate/high debris flux rates.

The initial supraglacial debris-thickness conditions evaluated include: a theoretical condition of homogeneous debris cover at three thicknesses (Figure 3.5) along the central flow line, and the actual debris-thickness distribution (Figure 3.6), which were estimated from thermal remotely-sensed data.

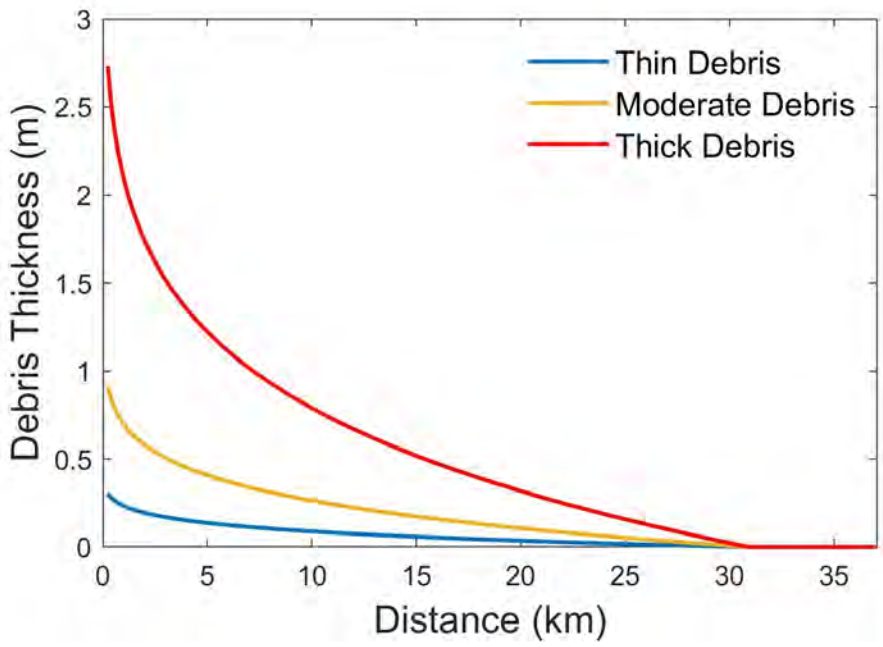

Figure 3.5: Hypothetical debris-thickness conditions used in the HMD (homogeneous debris-thickness in lateral direction) simulations.

The actual supraglacial debris-thickness over the Baltoro glacier (Figure 3.6) was computed from ASTER surface kinetic temperature data following the approach by Mihalcea et al. [4], which is based on in-situ measurements on the glacier surface. Specifically, they found an empirical relationship between supraglacial debris-thickness and surface temperature over the Baltoro Glacier:

$$h_d = exp(0.192T_s - 58.7174). \tag{3.31}$$

In simulations, each grid cell on the glacier surface is classified into two categories: debris cover or bare-ice. The associated ablation rates are computed separately in the model as previously mentioned. The bare-ice condition is determined as $h_d < 1cm$, following Mihalcea et al. [4].

Figure 3.7A shows the initial spatial distribution of debris minerals, such that the albedo at each grid cell is computed based on the spectral reflectance of that rock-type or composite (Figure 3.7B). The mineralogical classification and spatial distribution are derived from the lithologi-

cal/minerological study of the Baltoro Glacier [23], and calibrated using remote-sensing analysis as previously mentioned.

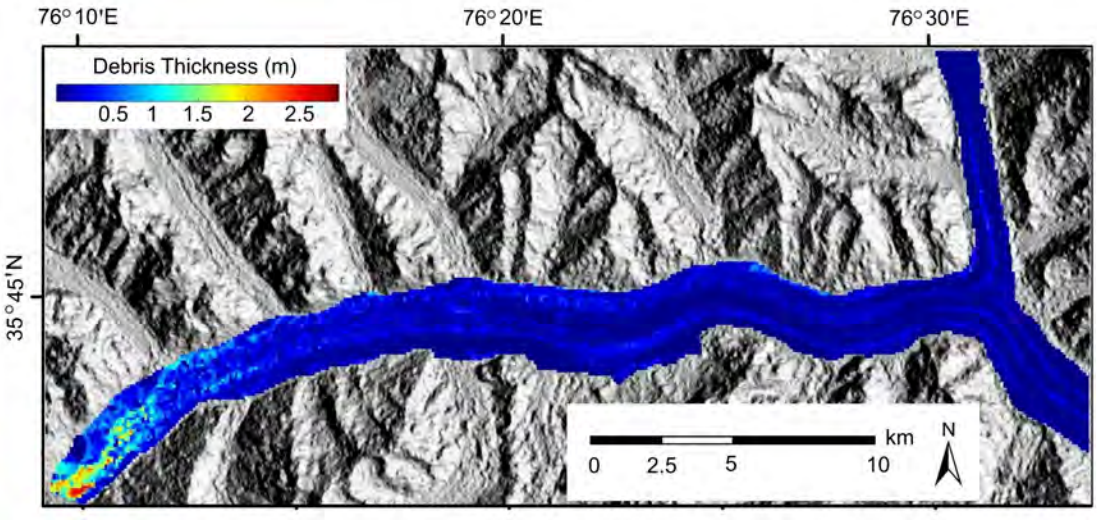

Figure 3.6: The initial debris-thickness distribution for the HTD (heterogeneous debris-thickness) simulations.

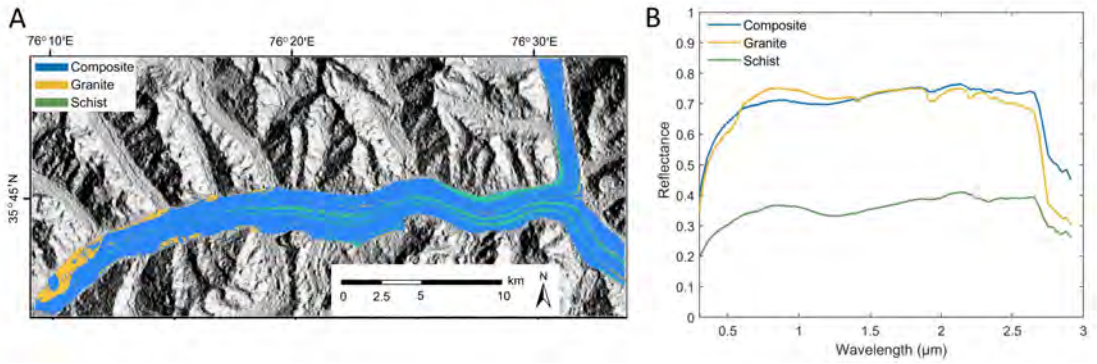

Figure 3.7: The initial debris condition including (A) rock type distribution, and (B) the spectral reflectance curves for each rock type are used for estimating surface albedo.

The third group of sub-scenarios investigates surface ablation rate variability with respect to

heterogeneous debris-thickness distributions. A realistic debris-thickness (Figure 3.6) and lithological distribution (Figure 3.7A) over the Baltoro Glacier is used, and topographic variation is also considered, similar to the first group of sub-scenarios.

Simulation	Debris Thickness	Surface Topography	Debris Flux Rate
BI-1	Bare-ice	Modern-day	N/A
BI-2	Bare-ice	HL	N/A
BI-3	Bare-ice	HM	N/A
BI-4	Bare-ice	HH	N/A
HTD-1	Heterogeneous	Modern-day	Moderate
HTD-2	Heterogeneous	HL	Moderate
HTD-3	Heterogeneous	HM	Moderate
HTD-4	Heterogeneous	HH	Moderate
HMD-1	homogeneous thin	Modern-day	Low
HMD-2	homogeneous thin	Modern-day	Moderate
HMD-3	homogeneous thin	Modern-day	High
HMD-4	homogeneous Moderate	Modern-day	Low
HMD-5	homogeneous Moderate	Modern-day	Moderate
HMD-6	homogeneous Moderate	Modern-day	High
HMD-7	homogeneous Thick	Modern-day	Low
HMD-8	homogeneous Thick	Modern-day	Moderate
HMD-9	homogeneous Thick	Modern-day	High

Table 3.2: List of simulation scenarios. The M value (Equation 3.19) for low, moderate, and high debris fluxes are 0.9967, 0.99, and 0.97 respectively. HL, HM, HH stands for the hypothetical topography with low, moderate, and high frequency undulations respectively.

The initial conditions include defining the surface topography, debris-load thickness, debris

mineralogical conditions and atmospheric temperature. A uniform atmospheric temperature condition is used for all scenarios. The temporal variation in air temperature over the ablation season (Figure 3.8) in the study area (central Karakoram) is derived from published results [147, 151].

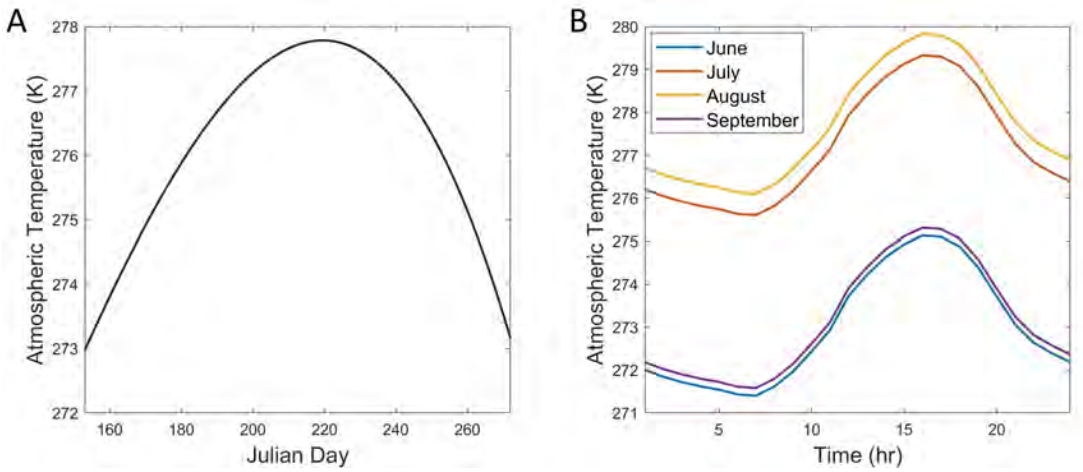

Figure 3.8: Atmospheric temperature used in all simulations. (A) Ablation season temperature variations. (B) Mean diurnal temperature variations for each month.

3.5 Results

3.5.1 Surface Irradiance

The magnitude of short-wave irradiance is governed by diurnal and seasonal variations. Figure 3.9A. shows the seasonal trend of simulated daily maximum short-wave irradiance over the Baltoro Glacier. During the simulated ablation season in 2004, the maximum direct-beam irradiance was 937.62Wm^{-2} and the maximum diffuse-skylight irradiance over the ablation season was 73.07Wm^{-2} (average was 56.33Wm^{-2}). The total short-wave irradiance peaked on June 22. The modeled diurnal variation of surface irradiance is reasonably accurate, as we compared simulated values to field measurements (Figure. 3.9B). The modeled irradiance values are, on average 10% lower than the measurements made by Mihalcea et al. [6], but are otherwise a good fit. The discrepancy is most likely due to the adjacent-terrain irradiance component, which was not modeled

in the simulations, and the simplified atmospheric conditions used in our model related to aerosol conditions and precipitable-water vapor concentrations.

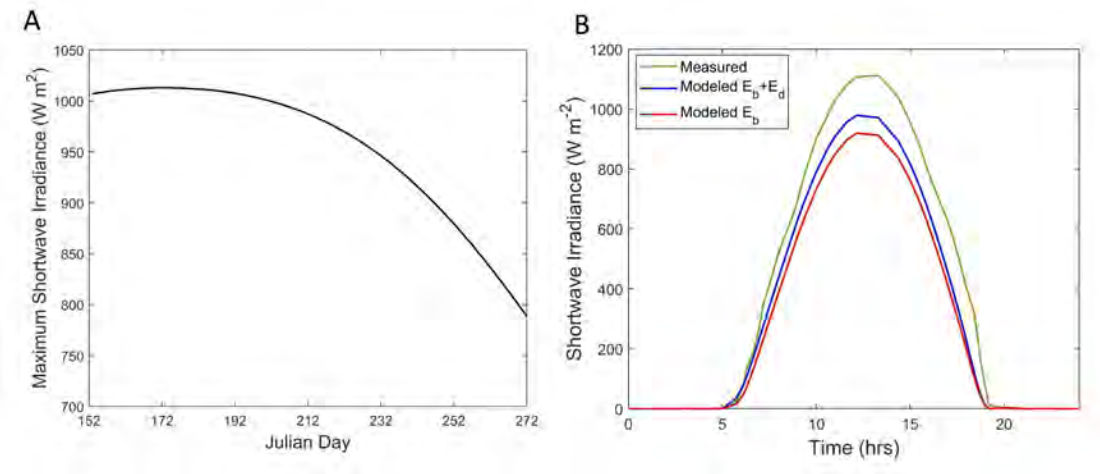

Figure 3.9: Simulated short-wave surface-irradiance and irradiance components used in simulations. (A) Maximum ablation-season variation in short-wave surface irradiance over the Baltoro Glacier. (B) Diurnal variation in short-wave irradiance compared to field measurements by Mihalcea et al. [6] on July 24th 2004. Shortwave irradiance is computed over the wavelength range of $0.3\mu m$ to $3\mu m$.

3.5.2 Ablation Rates

There are no reliable measurements of ablation rate as a function of debris-thickness available for the Baltoro Glacier, therefore, the overall accuracy of our modeled result is tested using field measurements on multiple Himalayan glaciers, including Barpu Glacier [1], Khumbu Glacier [2], and Rakhiot Glacier [3]. The simulated surface ablation rate as a function of debris-thickness is reasonably similar to that of other Himalayan glaciers (Figure. 3.10). The critical debris-thickness at which the sub-debris ablation rate equals that of bare-ice usually ranges from 0.02 to 0.1 m [23]. Several studies have measured the critical thickness for Himalayan glaciers (e.g., 0.02 m on Barpu glacier [1], 0.05 m on Khumbu glacier [2]). Our simulated critical debris-thickness is 0.03 m, which falls into a reasonable range.

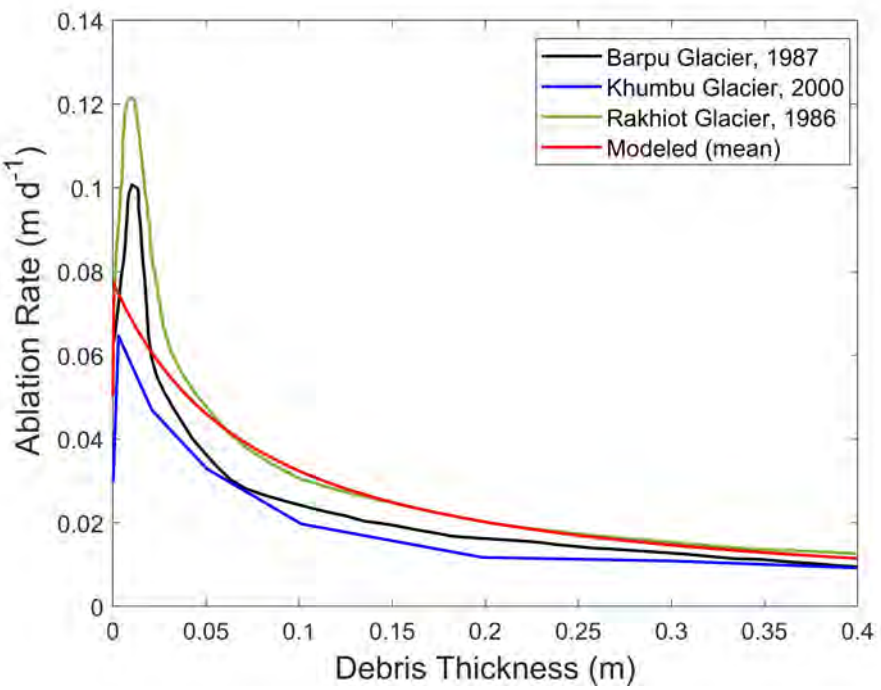

Figure 3.10: June-averaged simulated ablation rate (red) compared to field measurements in the ablation season on other Himalayan glaciers (including Barpu Glacier [1], Khumbu Glacier [2], and Rakhiot Glacier [3]).

The distributed surface ablation rates simulated over the Baltoro Glacier are compared with the results of Mihalcea et al. [4](Figure 3.11), which are computed based on remotely-sensed surface temperature. Both results show suppressed ablation in the terminus region and higher ablation around inter-moraine valleys. The simulated ablation rates have a lower mean magnitude ($0.0223 md^{-1}$ versus $0.0260 md^{-1}$), and have higher spatial variability (standard deviation 0.0171 md^{-1} versus 0.0164 md^{-1}), but in general, they are in good agreement with the remote-sensing-based results.

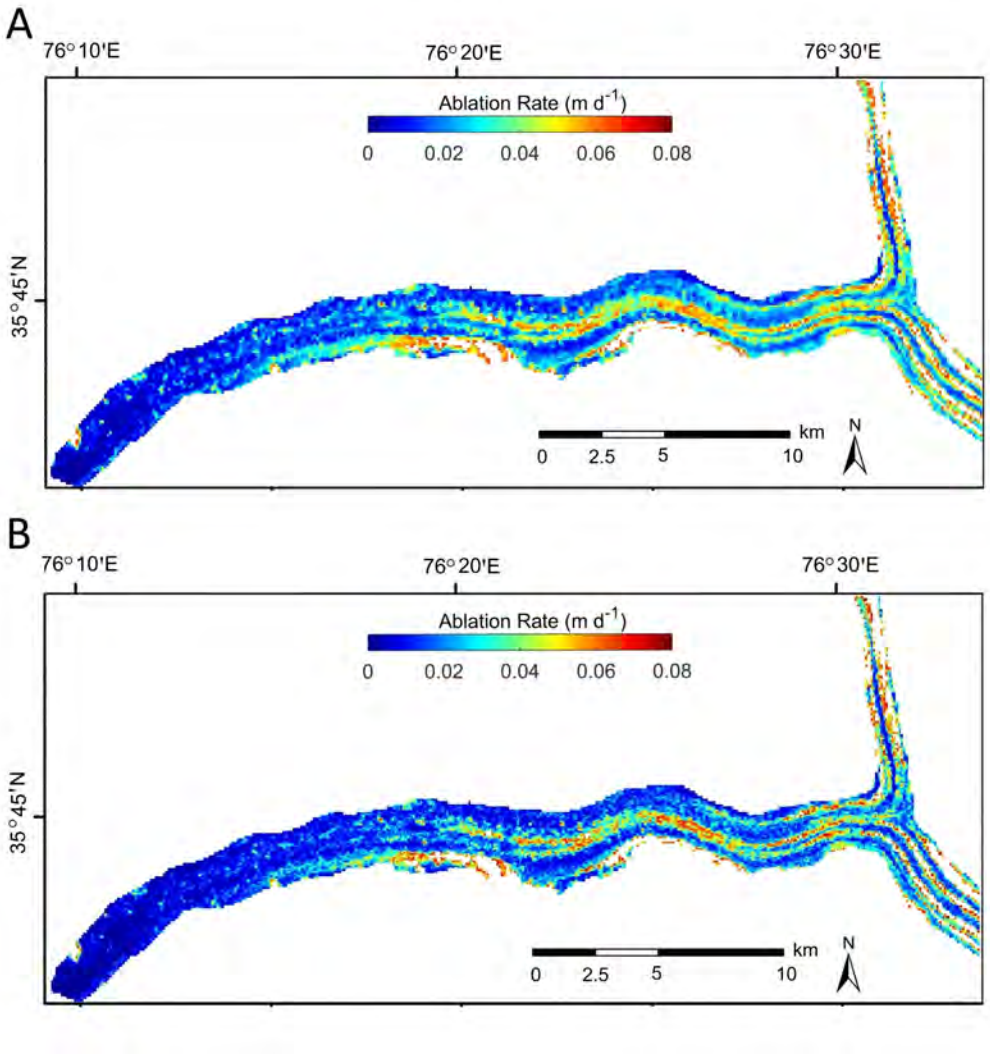

Figure 3.11: Simulated and remote-sensing estimates of ablation rates for the Baltoro Glacier. (A) Remote-sensing estimates of ablation rates for the Baltoro Glacier from Mihalceo et al. [4]. (B) Simulated ablation rates for the Baltoro Glacier. Both results are based on the same initial debris-thickness distribution as previously discussed and were produced to represent rates on August 14. 2004. Note that a major limitation of the remote-sensing-based approach is that it can only estimate instantaneous ablation rates due to the lack of continuous satellite data.

3.5.3 Supraglacial Debris Flux

The gravity-driven debris flux is sensitive to local topographic changes that can be significant during the ablation season due to melting ice. Figure 3.12 shows two locations on the simulated glacier surface (based on the modern-day topographic conditions of the Baltoro Glacier) where the

ablation rate dramatically varied due to the change in debris-thickness. The decrease in debris-thickness can be found at boundaries of depression zones, such as on the ice-cliffs, where debris rapidly migrates down a slope, as ice-cliffs or ice topography becomes steeper due to differential melting. An increase in debris-thickness can occur towards the center of depression zones, such as in a supraglacial lake depression, where debris accumulates under gravity.

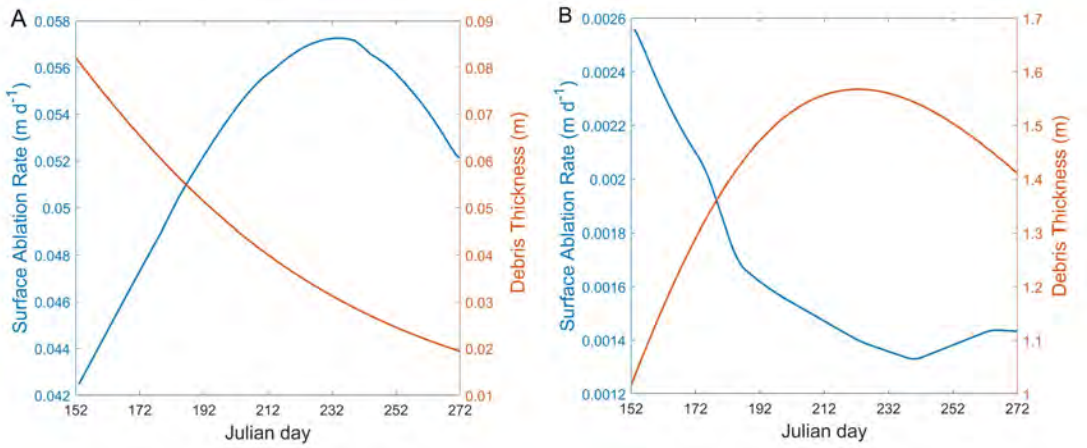

Figure 3.12: Simulated debris-thickness and ablation rate over the ablation season. (A) A grid cell (35^o 44'N, 76^o 21'E) with decreasing debris-thickness and an increasing and then decreasing ablation rate; (B) A grid cell (35^o 42'N, 76^o 12'E) with increasing and then decreasing debris-thickness and generally decreasing ablation rate. Gravity-driven debris transport governs the change in debris-thickness and can be a major controlling factor in the temporal variation of ablation rates.

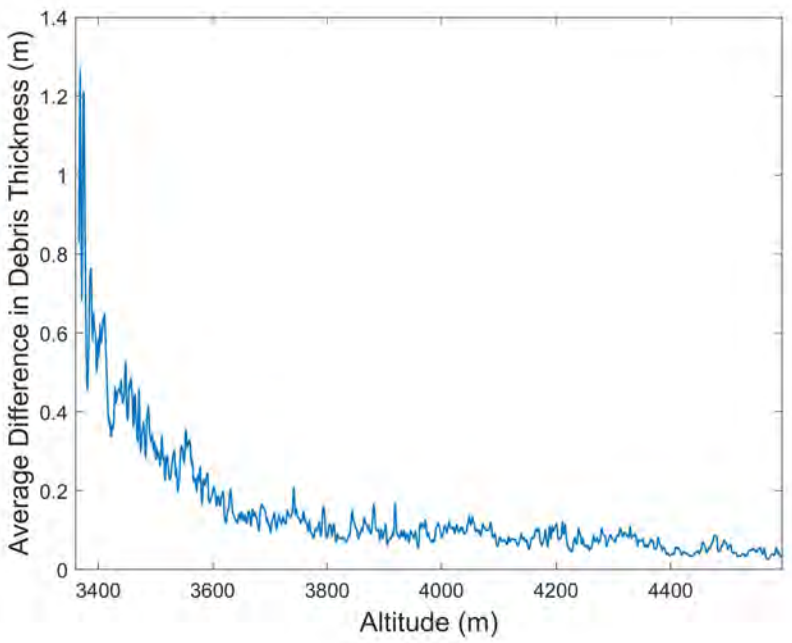

Figure 3.13: The change of debris-thickness as a function of altitude over the ablation season. Simulation is based on the modern-day conditions of the Baltoro Glacier (scenario HTD-1).

The difference between initial debris depths and final debris-thickness at the end of a simulation suggests that the lower ablation zone exhibits the highest magnitude of debris transport variations (Figure 3.13). This result is in agreement with the work by Gibson et al. [23], in which they found that the majority of debris-thickness change occurred in the lower ablation zone and around moraines from 2004 to 2012. They also estimated that the annual debris-thickness change is around -0.2m to 0.4m. Our modeled magnitude (-0.03m on average) is within the range but on the lower side, which is mainly due to the model's omission of sediment flux caused by ice flow.

3.5.4 Numerical Experiment 1: Surface Ablation and Topography for Bare-Ice

Surface topography influences the magnitude of irradiance and debris distribution, which governs surface ablation rates. In this experiment, we investigated the variation in surface ablation rate for different topographic conditions, by simulating ablation on bare-ice surfaces (in order to rule out debris influence) with varying topographic conditions based on four scenarios (BI 1- 4), as

listed in Table 3.2. Figure 3.14 compares the spatio-temporal averaged diurnal ablation rates and cumulative ice-volume loss for the four scenarios, and Figure 3.15 shows the spatial distribution of cumulative ice loss in meters of water equivalent (m w.e.) over the 120-day ablation season.

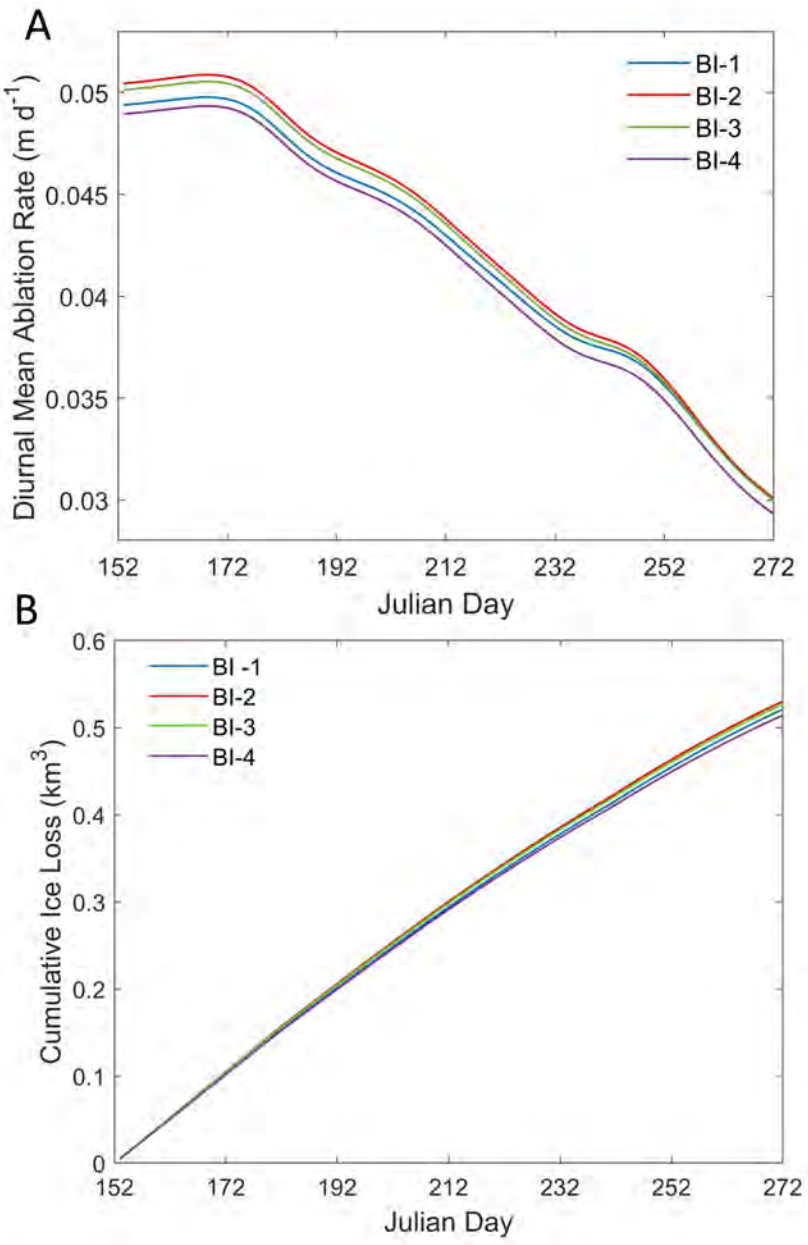

Figure 3.14: Ablation rate and ice-loss variations over the ablation season for scenarios BI 1-4 (BI 1 is the bare-ice glacier with modern-day topography, BI 2-4 represent hypothetical scenarios with increasing spatial frequency of topographic variation). (A) Averaged diurnal ablation rates over the ablation season. (B) Cumulative ice-volume loss over the ablation season.

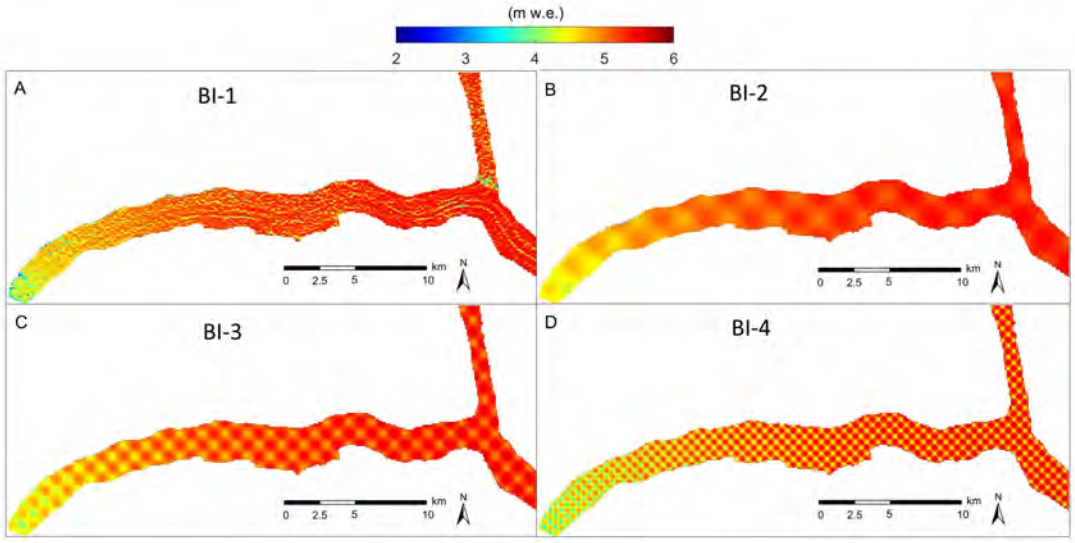

Figure 3.15: Cumulative ice loss over the ablation season for a bare-ice glacier with different topographic conditions. (A) Modern-day topography from DEM. (B) Low-frequency topographic variation (spatial frequency = $0.002m^{-1}$). (C) Medium-frequency topographic variation (spatial frequency = $0.004m^{-1}$). (D) High-frequency topographic variation (spatial frequency = $0.008m^{-1}$).

Simulation results indicate that both the diurnal mean ablation rate and the cumulative ice loss decrease as the spatial frequency of topographic variation becomes higher. The variability in ablation across the simulations is higher early in the ablation season compared to later in the ablation season (Figure 3.14A). This is due to higher surface irradiance in the early portion of the season, and less surface irradiance in the later portion of the season given changes in solar geometry and atmospheric attenuation. The spatial patterns clearly show the topographic control on surface ablation such that the ablation rate is higher on the hummocks and lower in the depression areas.

This simulation study demonstrates that local topographic effects governs the ablation rates even without supraglacial debris. The decrease in ablation rate on the more complex topography is due to the reduced irradiance caused by terrain self-shadowing and potential cast shadows depending upon the solar geometry and local relief. This demonstrates that local topographic variations on a glacier surface can significantly influence the ablation rate and ice-mass loss.

3.5.5 Numerical Experiment 2: Ablation Rate and Topography for Heterogeneous Debris

The actual debris-thickness distribution on a glacier can be very heterogeneous in nature. To better understand how heterogeneous debris conditions coupled with topographic variations governs surface ablation, we simulate surface ablation under 4 different types of topography (HTD 1-4 as listed in Table 3.2). Figure 3.16 compares the spatio-temporal averaged diurnal ablation rates and cumulative ice-volume loss for the four scenarios, and Figure 3.17 depicts the spatial distribution of cumulative ice-loss in meters of water equivalent (m w.e.) over the 120-day ablation season. Figure 3.18 shows the debris-thickness distribution at the end of the ablation season for each scenario.

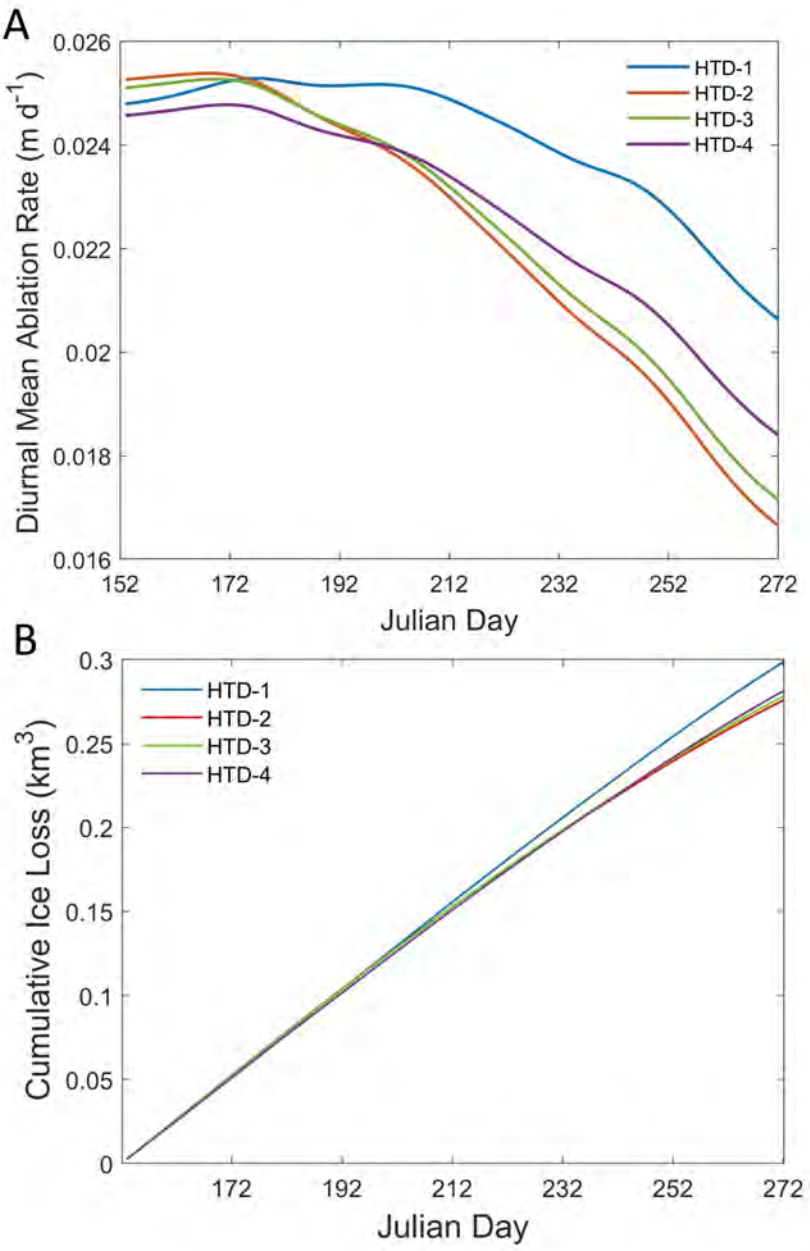

Figure 3.16: Ablation rate and ice-loss variations over the ablation season for HTD1-4 (HTD 1 is the debris-covered glacier with modern-day topography, HTD 2-4 represent hypothetical scenarios with increasing spatial frequency of topographic variation). (A) Spatio-temporal averaged diurnal ablation rate over the ablation season. (B) Cumulative ice-volume loss over the ablation season.

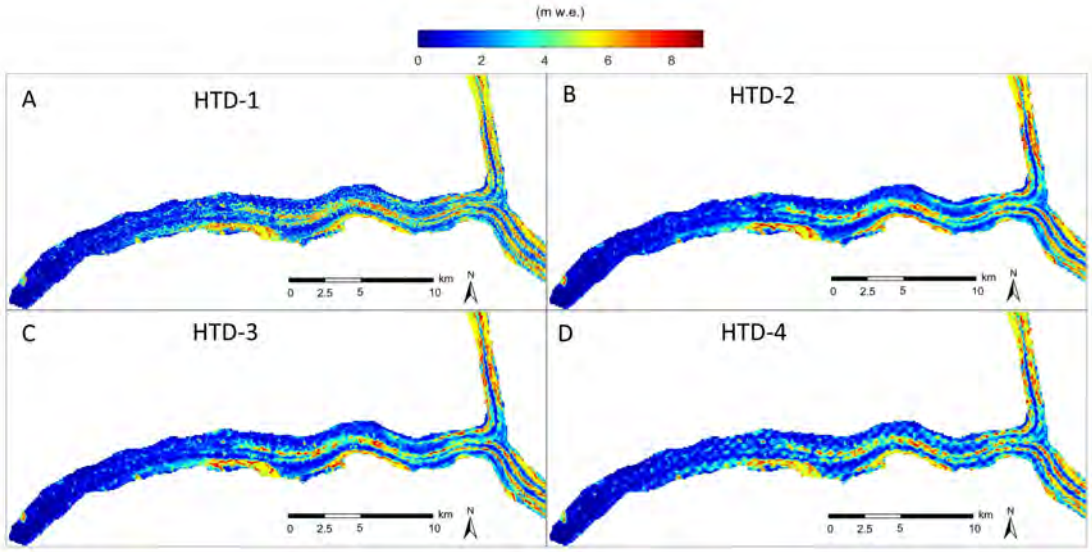

Figure 3.17: Cumulative ice loss over the ablation season for heterogeneous debris simulation scenarios. (A) Modern-day topography from DEM. (B) Low-frequency topographic undulations (spatial frequency = $0.002m^{-1}$). (C) Moderate-frequency topographic undulations (spatial frequency = $0.004m^{-1}$). (D) High-frequency topographic undulations (spatial frequency = $0.008m^{-1}$).

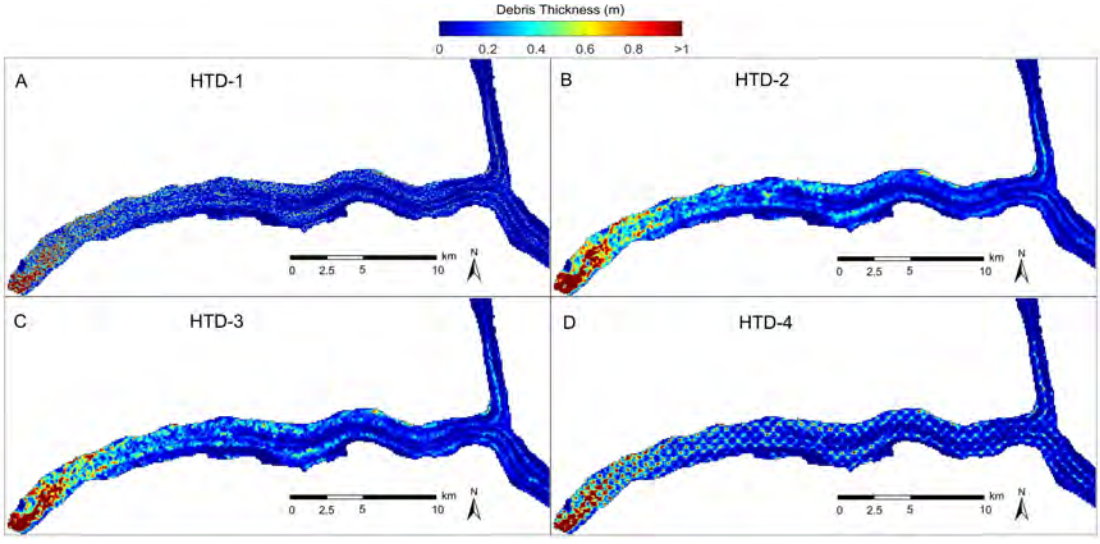

Figure 3.18: Debris-thickness distribution at the end of the ablation season for each simulation scenario. The topographic effect on debris distribution is most pronounced when the spatial frequency of topographic undulations is high (HTD-4).

Numerical results suggests that a debris-covered glacier responds to local radiative forcing differently from a bare-ice glacier, such that the mean ablation rate increases as the spatial frequency of topographic variation becomes higher (from $0.0223md^{-1}$ on HTD-2 to $0.0227md^{-1}$ on HTD-4), given that higher-frequency variation and steeper slopes generates a higher sediment flux that reduces the debris depth which increases the ablation rate. Figure 3.18 depicts the increase in thin debris-depth areas, as the spatial frequency of topographic variation becomes higher. Topographic self-shadowing also affects a debris-covered glacier similar to a bare-ice glacier, however, those depression zones on a debris-covered glacier exhibit minimal ablation even without shading, because thick debris accumulates in those depressions due to the gravitational debris flux, therefore, this mechanism makes the glacier less sensitive to topographic self-shadowing as compared to a bare-ice glacier.

To better compare and contrast the two baseline simulations BI-1 and HTD-1, we show a monthly comparison between them in Figure 3.19. Based on the comparison, it is clear that the overall ice-mass loss for simulation BI-1 is higher than simulation HTD-1, however, these simulations show the potential for debris-covered glaciers to exhibit greater spatial variability in ice-mass loss. For example, the terminus region, which is covered by thick debris, exhibits much lower ice-mass loss compared to inter-moraine valleys, where ice-loss is greater, compared to a bare-ice glacier, due to the melt-enhancing effects of thin debris.

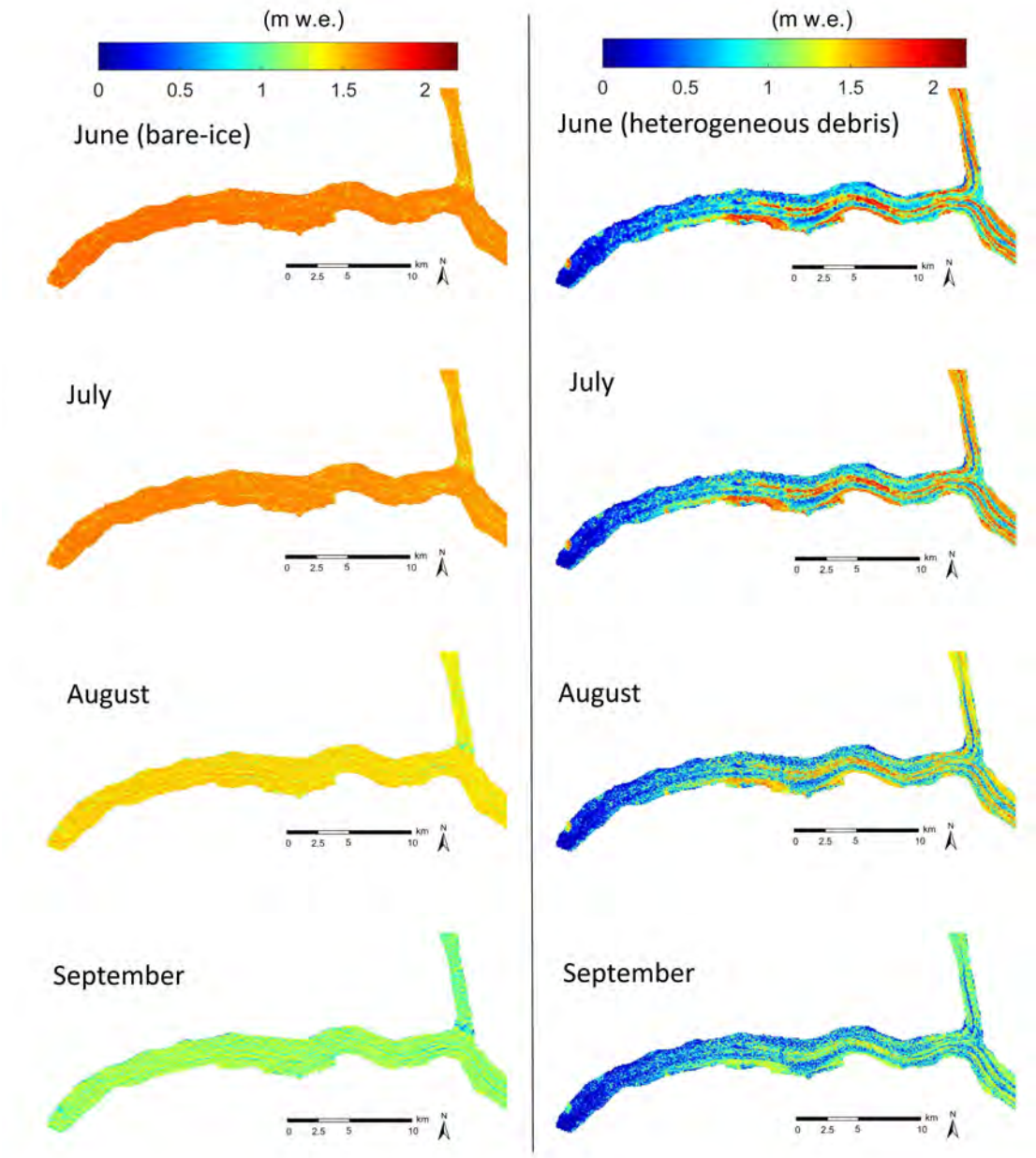

Figure 3.19: Comparison of monthly-averaged surface ablation for simulation BI-1 (left column) and simulation HTD -1 (right column). Note that the overall ice-mass loss for BI-1 is higher, but the spatial heterogeneity in mass loss (i.e., ablation) is much higher on this debris-covered glacier. It is important to note that other processes that can contribute to ice-mass loss (e.g., supraglacial lakes) have not been accounted for in these simulations.

3.5.6 Numerical Experiment 3: Ablation Rate Variation Due to Debris Thicknesses and Sediment Flux Rate

In this group of simulation experiments, we investigate ablation rate variation caused by varying debris thicknesses and sediment flux rates. Specifically, Nine scenarios with different debris-thickness (only vary in the parallel ice-flow direction) and flux rate combinations (HMD 1-9 as listed in Table 3.2) are simulated and compared. Figure 3.20 shows cumulative ice loss for each scenario over the ablation season, and Figure 3.21 is a comparison of spatio-temporal-averaged ablation rates for all nine scenarios.

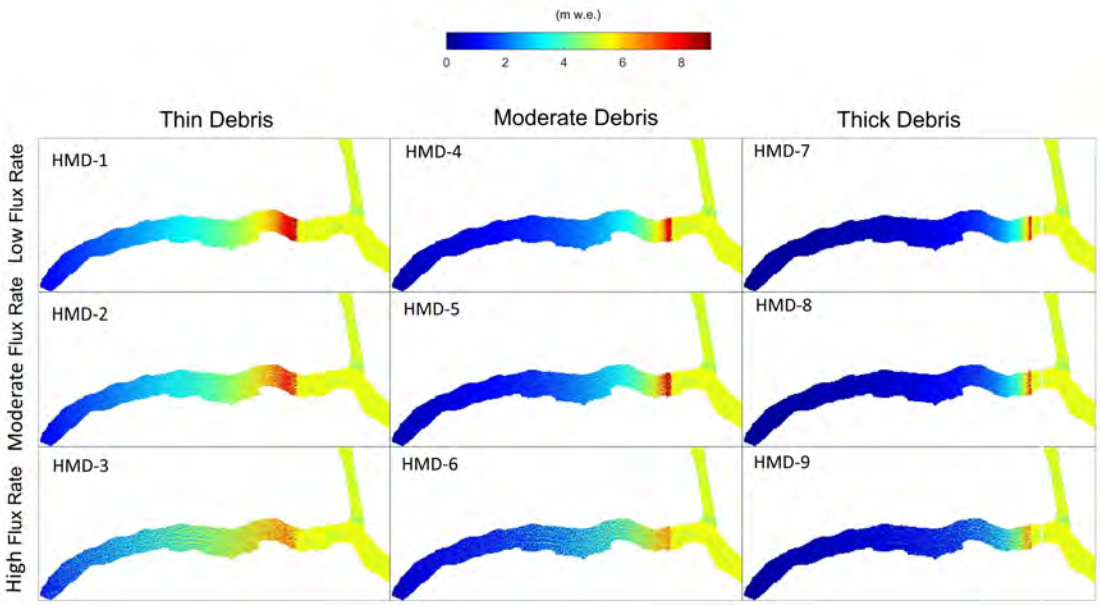

Figure 3.20: Cumulative ice loss over the ablation season for the Baltoro Glacier given different debris thicknesses and debris-flux rates. Note that the simulations in each column have the same initial debris-thickness, and simulations in each row have the same sediment-flux rate. The high magnitude transition zone in the upper portion of the glacier corresponds to the areas that exhibit the thin-debris effect which dramatically increases ablation rate as shown in Figure 3.10.

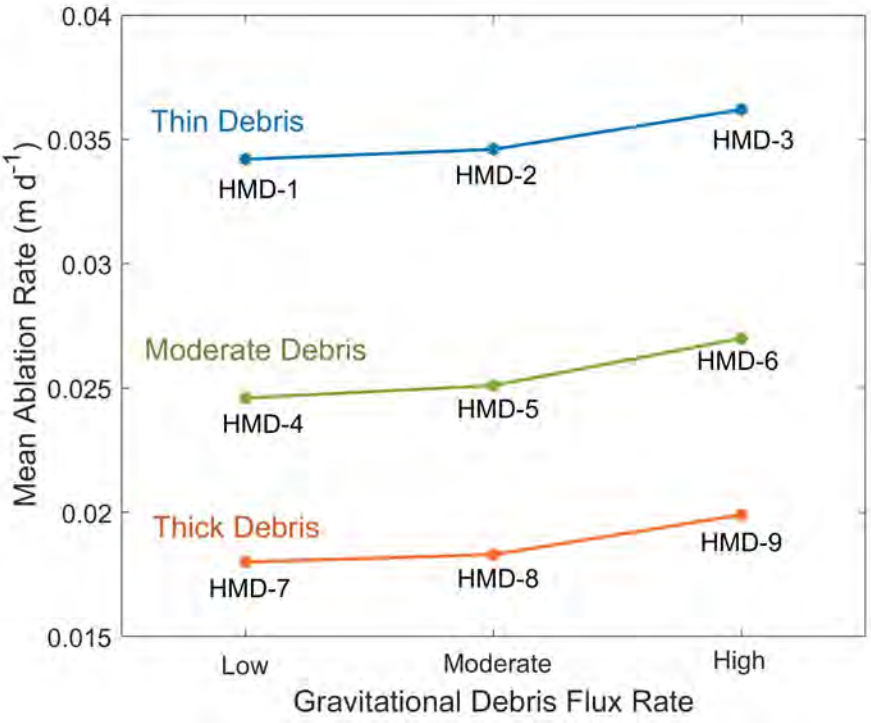

Figure 3.21: Comparison of spatio-temporal averaged ablation rates over the ablation season for scenarios with different debris thicknesses and debris flux rates (HMD 1-9 as shown in Figure 3.20).

These simulation experiments reveal that debris-thickness significantly governs the magnitude of ablation rates. The mean ablation rate on a glacier with thin debris (HMD-2) is 37.8% higher than that on a glacier with moderate debris thicknesses (HMD-5), and 89.1% higher than that on a glacier with thick debris cover (HMD-8). Gravitational debris flux rate also controls surface ablation by altering the spatial distribution of debris-thickness. The results show a continuous increase in mean ablation rates and a decrease in minimum ablation rates as the transport rate of the gravitational sediment flux increases. This strongly suggests that a higher gravitational sediment flux rate causes an increase in the overall surface ablation, which is the result of larger geographic areas of thin-debris and bare-ice exposed by the debris flux.

3.6 Discussion

3.6.1 Glacier Surface Topography

Glacier surface topography acts as an important controlling factor in surface ablation. Unlike many existing models in which the surface topography is held as constant (e.g. [4, 49]), our model accounts for the evolution of topography due to melting (e.g., the spatially-averaged surface downwasting simulated for the HTD-1 scenario is 2.89m over the ablation season). Based on the simulations of different topographic conditions, we found that the altitude, slope angle and slope azimuth angles control ablation by regulating the surface irradiance and gravitational debris flux.

Results strongly suggests that debris-covered glaciers and bare-ice glaciers respond differently to variations in surface topography. For a bare-ice glacier, higher-frequency topographic variation decreases the overall surface ablation (Figures 3.14, 3.15), which is mostly likely due to the reduced irradiance caused by the more significant terrain self-shading and potential cast shadows depending upon the solar geometry and local relief. For a debris-covered glacier, however, the mean ablation rate increases as the spatial frequency of topographic variations becomes higher (Figures 3.16, 3.17), and topographic forcing becomes more pronounced towards the end of the ablation season. This is mainly because surface topography governs the distribution of debris-thickness through the process of gravitational sediment transport, and more significant sediment redistribution occurs on a highly variable surface that accumulates debris into many depression areas, such as supraglacial lakes. Rapid debris thinning occurs on high-altitude non-depression areas (e.g., ice-cliffs around supraglacial lakes) causing enhanced ice melting. The topographic variations in our simulations caused up to 7% change in ice loss for the Baltoro glacier over the ablation season. We speculate that this value could be higher if there are more dramatic changes in topography over longer time periods, especially when a glacier exhibits active ice-flow or surge behavior. We therefore conclude that topographic forcing on glacier surface ablation can be significant and the topography-controlled irradiance and gravitational debris flux should be accounted for in ablation models for debris-covered glaciers.

3.6.2 Debris Thickness and Debris Flux

Our controlled simulations indicate that debris-thickness is the most significant factor governing surface ablation that we evaluated, and the distribution of debris-thickness should be modeled as a dynamic process by accounting for gravity-driven debris flux on a changing topography. Only then the surface ablation can be reasonably estimated for a debris-covered glacier. We have shown that the gravity-driven debris flux is active given a changing ice topography throughout the ablation season. For certain locations on a glacier surface, debris-thickness can vary significantly over the ablation season (more than 1m, Figure 3.13), which dramatically alters the ablation rate (Figures 3.10, 3.12). We also demonstrated that a higher sediment flux rate increases the total and spatial variability of surface ablation (Figure 3.20), which is most likely due to the larger geographic area of thin-debris and bare-ice exposed by debris transport under gravity. Most existing models, however, assume static debris-thickness during the simulation period (e.g., [4, 49, 24]), which increases the uncertainty in estimating the surface ablation rate.

Results also indicate the processes that govern the ablation rate over time represents a highly non-linear response to an increase in radiative forcing and debris-thickness, such that thick debris cover generally suppresses melting, while a thin debris cover can significantly enhance ice melting due to the minimal insulation and the high energy absorption given the lower albedo, which is in agreement with field studies (e.g., [76, 3, 2, 66]). The lowering of surface albedo is mostly due to the mixing with meltwater at locations where debris is thin, and simulations suggest that the spatio-temporal variation in surface albedo should also be accounted for in ablation models for debris-covered glaciers.

3.6.3 Differential Ablation

Several studies have reported or predicted an accelerated downwasting of Baltoro Glacier [32, 23, 19], and have indicated that the distribution of ablation rates on a debris-covered glacier is spatially heterogeneous [38, 27, 17]. Quantitative analysis of our simulation results, which include surface ablation, debris-thickness distribution and surface topography, suggests that there

is no linear relationship between elevation and surface ablation rate for this glacier, as the influence of altitude predominately governs the atmospheric attenuation parameter regulating the direct irradiance, and the magnitude of this parameter (i.e., altitude) is rather small compared to local and mesoscale topographic effects on the surface irradiance. This is in agreement with the field measurements on the Baltoro Glacier, where the measured ablation rate can be three times higher than its neighboring areas, even at the same elevation [6]. Clearly, surface irradiance and debris conditions strongly regulate ablation.

The ablation zone was found to exhibit high ablation rates that corresponded to geographic areas with thin debris cover (Figures 3.17, 3.18), This demonstrates the melt-enhancing effect of thin debris and moisture, which reveals that debris-covered ice can melt faster than bare-ice when the debris-thickness is less than the critical thickness. We also found that thin debris-depth areas also exhibit relative low albedo ("dirty ice") because meltwater can easily saturate a thin layer of debris and significantly reduce albedo.

Using modern-day topographic conditions in our simulations of the Baltoro Glacier, we found that zones of rapid melting associated with a thin debris layer can spatially represent over 15% of the glacier surface area, which on average exhibited higher ablation rates (about 1.5 times higher) than the mean value for the whole glacier. The high temporal variability in surface melting (aside from the diurnal and seasonal irradiance variation) is governed by debris flux, that is controlled by a constantly changing local topographic conditions. We also see a large difference in ablation rates between medial moraines and inter-moraine valleys due to heterogeneous debris-thickness (Figures. 3.11), which is also confirmed by field observations [55]. All of these findings indicate that the high degree of differential downwasting of a debris-covered glacier is strongly linked with the high spatial heterogeneity of debris-thickness, which is regulated by topography and debris flux. It is necessary to state that the model presented in this paper still underestimates the differential surface ablation because it does not account for more complicated processes involved with supraglacial lakes, englacial melting and precipitation-caused melting, which also contribute to the high-degree differential downwasting of debris-covered glaciers [38].

3.6.4 Feedback Mechanisms

Feedback mechanisms exist between multiple surface processes discussed in this model that may significantly govern surface-ablation dynamics. This feedback involves the coupling of topography, surface melting, irradiance and debris flux (Figure 3.22). Simulations suggest that, in the ablation season, glacier surface topography can change significantly due to differential melting. The altered surface topography from ablation controls the debris flux and influences surface irradiance, which in turn, controls the surface ablation rates.

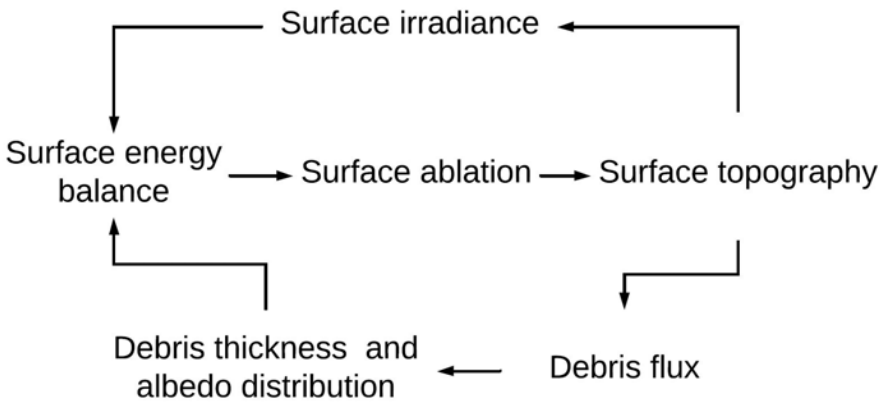

Figure 3.22: Diagram illustrating the feedback mechanisms involving multiple surface processes and surface morphology that can locally accelerate melting on debris-covered glaciers.

The alteration and evolution of surface topography is significant in a debris-covered glacier model. Our simulation results, based on the realistic topographic and debris load conditions of the Baltoro Glacier, show an average surface thinning of 2.9m during the ablation season, not accounting for mass inputs.

In certain locations on a glacier surface, this mechanism could form a positive feedback that accelerates melting. Positive feedbacks have been identified in our simulations at multiple locations, such as around supraglacial lakes (and potentially ice cliffs) where thin debris enhances melting and can potentially facilitate lake expansion and further ice-cliff retreat [20, 27]. These locations

on a glacier may be more sensitive to radiative forcing than we previously thought, due to a high degree of differential downwasting and feedbacks.

3.6.5 Model Assumptions and Limitations

This model simulates the surface ablation patterns and morphological changes under radiative forcing over one ablation season. It is not a climate-driven, annual (or longer term) mass-balance model that accounts for precipitation forcing and ice-flow dynamics. Therefore, the effects of precipitation, atmospheric variations, altitude changes due to ice flow, ice-flow sediment transport, and refreezing are neglected. Due to these limitations, the modeled surface ablation only reflects the potential magnitude of ablation caused by solar radiation, which is also underestimated (adjacent-terrain irradiance not accounted for), because precipitation can cause significant melting in the ablation season, and debris cover can contribute to heating surface water before it percolates through debris cover. As for debris flux, this model only accounts for short-term gravity-driven debris flux and neglects the advection of debris due to ice flow. This model also does not account for supraglacial lakes, which also contribute to the underestimation of the actual melting since supraglacial lakes generally absorb more heat than supraglacial debris, and lake expansion and lake water outflow can further accelerate surface melting. For future improvements to this work, we plan to develop a supraglacial lake model to better address this important process.

3.7 Conclusions

In this study, we use a radiation-driven model to understand how gravitational debris flux, debris-thickness, and surface topography govern surface ablation dynamics of debris-covered glaciers. From a methodological perspective, this model enables a more accurate characterization of surface ablation than existing models because: 1) Local and meso-scale topographic effects of surface irradiance are accounted for; 2) Gravity-driven debris flux on a changing ice topography is accounted for; 3) The melt-enhancing effect of thin debris is accounted for; 4) Surface temperature is continuously modeled rather than being restricted by instantaneous remote-sensing data; and 5) A sediment mineral and meltwater mixing model is used to account for the dynamic variation of glacier

surface albedo. Multiple numerical experiments based on the actual and hypothetical topography and debris-load conditions of the Baltoro Glacier were conducted to achieve a more comprehensive understanding of ablation dynamics on debris-covered glaciers. Based on numerical simulations, we identified and discussed three major factors that govern ablation rate: 1) Debris-thickness; 2) Gravitational debris flux; and 3) Surface topography. Specifically, we draw the following conclusions:

1. Topographic forcing on surface ablation is non-negligible for debris-covered glaciers because glacier surface topography controls irradiance and gravitational debris flux, and a constantly changing ice topography alters the debris flux and irradiance, thereby representing complex surface ablation dynamics.

2. Debris-covered glaciers and bare-ice glaciers respond differently to variations in surface topography. For a bare-ice glacier, high-frequency topographic variations decrease the overall surface ablation, which is due to the reduced irradiance caused by local topographic effects and terrain self-shadowing. For a debris-covered glacier, high-frequency topographic variations increase the overall surface ablation caused by an accelerated gravitational debris flux, which generally promotes larger geographic areas of thin-debris and bare-ice that results in higher ablation.

3. The Gravity-driven supraglacial debris flux plays an important role in debris-thickness redistribution which governs ablation. Debris transport variations tend to increase the overall surface ablation. Gravity-driven debris flux is a therefore a necessary component in ablation models for debris-covered glaciers.

4. A debris-covered glacier can exhibit high spatio-temporal variability in ablation due to heterogeneous debris-thickness that is governed by the debris flux. A bare-ice glacier under the same condition exhibits higher overall ablation, but exhibits much less spatio-temporal variability.

5. Surface ablation dynamics on a debris-covered glacier is regulated by system couplings and feedbacks between surface morphology, melting, and debris flux. The complex interactions between these processes may explain the observed accelerated ablation on some Karakoram glaciers, although other processes are also thought to contribute to such observations.

4. MODELING SUPRAGLACIAL LAKE DEVELOPMENT AND EVOLUTION ON DEBRIS-COVERED GLACIERS

4.1 Abstract

Supraglacial lakes play a significant role in the ablation dynamics of a debris-covered glacier. There is, however, little known about their contribution to glacier-surface ablation and the factors that govern lake development and evolution, because most existing models neglect supraglacial lake-water ablation and fail to characterize the couplings between irradiance, sediment fluxes and topographic evolution that regulates meltwater production. Such limitations often lead to an underestimation of ablation on debris-coved glaciers and introduces uncertainty in our assessments of glacier sensitivity to climate forcing. In this study, we investigate the dynamics of supraglacial lakes on debris-coved glaciers using a more comprehensive numerical model that characterizes the energy-balance of lakes, meltwater drainage and ponding, topographic evolution, and gravitational debris-flux. Simulations based on the modern-day and hypothetical conditions of the Baltoro Glacier suggest that: 1) Supraglacial lakes make a significant contribution to the total loss of ice mass and that the spatial variability of glacier-surface thinning is very high. Simulation over the ablation zone of the Baltoro Glacier shows that supraglacial lakes can be responsible for at least 22.78% of the total ice loss over the ablation season. Lake expansion is also responsible for a glacier's non-linear response to radiative forcing, because the lakes-water induced melting increases ablation as lakes expand, as a result, the glacier becomes more sensitive to radiative forcing towards the end of the ablation season. 2) Gravitational debris-flux controls the growth rate of supraglacial lakes by governing debris thickness and ablation rates around lakes, as a faster debris-flux dramatically decreases debris thickness on adjacent topography, which increases ablation and facilitates lake expansion. 3) The overall surface-slope of a glacier controls lake formation by affecting the supraglacial water storage and drainage patterns, such that a steeper slope gradient increases meltwater discharge and decreases storage. Simulations provide a possible explanation

to why supraglacial lakes are more abundant in the lower to mid ablation zone of glaciers. 4) The presence of supraglacial lakes increases the nonlinearity of a glacier's response to radiative forcing, which is represented as an acceleration in ablation rate, total ice-mass loss, and the lowering of surface altitude. These nonlinear responses may suggest the beginning of a critical transition of the glacier system that signifies an increasing level of glacier sensitivity to climate change.

4.2 Introduction

Supraglacial lakes play an important role in glacier mass-balance and glacial hydrology [37, 38, 39, 36]. Debris-covered glaciers (DCGs) can exhibit a relatively large number of supraglacial water bodies in the Himalaya [23], and those lakes and ponds are likely to grow rapidly given projections of atmospheric warming [75], which will have a significant impact on the regional water and hydro-power supply [39]. Large supraglacial lakes can also be destructive, as glacier-lake outburst floods (GLOFs) originate from DCGs in the Himalayas, and have caused injuries, deaths and property damage to downstream villages [41, 162]. Therefore, we require a better understanding of the processes and feedback dynamics that govern supraglacial lake formation, evolution and permanency to better assess regional water resources and geohazard conditions and potential impacts.

Supraglacial lake properties and lake spatial topological conditions also provide valuable insights into the nature of glacier sensitivity to climate change [41, 19, 23]. Field studies in the Himalaya have suggested that the spatial density of supraglacial ponds may be related to the degree of downwasting in the ablation zone due to more efficient heat absorption and lake-related englacial ablation [52, 43]. Most existing studies on supraglacial lakes focus on field measurements or remote-sensing-based mapping, which do not permit a quantitative assessment of supraglacial lake development, evolution, and the impact on glacier ablation dynamics. For example, we do not know what percentage of ice-mass loss is due to the presence of supraglacial lakes, and what are the factors and processes that control lake expansion. Therefore, a numerical ablation model that accounts for lake dynamics is sorely needed to investigate the influence of supraglacial lakes on the ablation dynamics of DCGs.

The development of supraglacial lakes on a DCG is not only governed by meltwater drainage and filling, but is also strongly controlled by topographic conditions and the debris-flux, which can operate at a faster rate during the ablation season due to the presence of surface water. Studies have suggested that the morphological changes on a glacier surface also contributes to the increasing number of supraglacial lakes [94, 52]. For example, the undulating surface and the gentle slope of the lower-mid ablation zone on a DCG encourages the formation of supraglacial lakes in depression areas [38, 75, 39, 42, 43], and the expansion of lakes further lowers the slope and creates more depressions, which, in turn, facilitate the formation of more lakes. Unfortunately, topographic influences on supraglacial lake development have not been adequately characterized in existing models, therefore, we do not have a quantitative understanding of multi-scale topographic effects on supraglacial lake development.

The gravitational debris-flux around supraglacial lakes also plays an important role in lake expansion. A rapid debris-flux can decrease the debris thickness on many ice slopes and ice-cliffs, which results in the generation of more meltwater, which promotes lake expansion [54, 27, 90]. This process is also coupled with topographic variation and ablation dynamics that may form a positive feedback to further accelerate lake expansion. Unfortunately, the gravitational debris-flux is not accounted for in most existing models, which restricts our capability to better understand lake evolution and thinning on DCGs.

Most existing DCG models neglect the development and evolution of supraglacial lakes due to the complexity of the aforementioned processes. These limitations often lead to an underestimation of ablation on DCGs. This could be, for example, one of the reasons why current models cannot explain the increasing number of supraglacial water bodies and accelerated downwasting observed on some debris-covered Himalayan glaciers (e.g., [31, 16]).

The main objective of this study is to provide insights into the above issues by simulating meltwater production, drainage and the genesis of supraglacial lakes and their evolution using numerical modeling. Specific research objectives are: 1) Develop a numerical model for DCGs that integrates meltwater production, surface drainage, supraglacial lake ablation, topographic evo-

lution, debris transport, and the coupling mechanisms between them; 2) Quantify the potential impact of supraglacial lakes on ice-mass loss and glacier thinning based on the simulations of the Baltoro Glacier in the central Karakoram Himalaya; 3) Understand how gravitational debris-flux govern supraglacial lake expansion; and 4) Investigate surface morphological conditions that govern supraglacial lake formation using simulations.

4.3 Background

Supraglacial lakes usually form along englacial conduits or in the lower-mid ablation zone where glacier-profile slopes are relatively low and topographic depressions are present [41, 54, 133, 27]. Large lakes on Himalayan glaciers can be a few kilometers across [39]. Supraglacial meltwater is usually transported via complex channel networks during the ablation season and can be temporarily stored in supraglacial lakes [36]. A typical lifespan for a supraglacial lake on Himalayan glaciers is a few years, during which they can form, grow, merge and be completely drained when they intersect with englacial conduits [70, 25]. Many supraglacial lakes are hydrologically connected [163, 42, 43], and large lakes usually have higher connectivity with other lakes, and most of them exhibit periodic filling and drainage processes [39].

Supraglacial lakes and adjacent ice cliffs are considered zones of rapid melting on DCGs [38, 54, 27, 164, 40, 90]. Their contribution to the total ice-mass loss is significant because supraglacial lakes and thin debris on ice cliffs exhibit relatively lower albedo than surrounding areas [8], which allows them to absorb more solar energy, rapidly melting the ice and expanding the lake zone area. Furthermore, water ablation can laterally erode the ice into the topography creating an ice-mass overhang that can collapse due to gravity, such that the calving process creates lake ice-bergs, more ice cliffs, and further expands the zone of rapid melting. Previous studies have estimated that the ablation rates around lakes can be one- or two-orders of magnitude higher than that of most debris-covered areas [38, 52, 40]. Most lakes also contribute to a significant amount of englacial ablation by warm-water outflow [38, 52, 164, 90]. Therefore, supraglacial lakes can be a significant contributor to the total ice-mass loss of a glacier. Furthermore, a very dense spatial distribution of lakes often increases downwasting, as they form a large number of englacial channels and the

collapse of the englacial channel roofs creates new lakes and further accelerates ablation in a positive feedback fashion.

The evolution of supraglacial lakes is thought to be controlled by a coupled system involving ablation, topography, englacial drainage conditions, sediment fluxes and surface albedo. Studies have identified relatively rapid sediment flow down ice-cliffs during their backwasting [20], which explains why the lake-facing slopes usually have a thinner debris cover that enhances melting, creating steeper slopes and rapid backwasting of ice-cliffs. The debris-load distribution adjacent to lakes can absorb short-wave radiation such that high surface temperatures produce significant emission of long-wave radiation that is part of the adjacent-terrain irradiance that also facilitates rapid backwasting, and ultimately further lake expansion [54, 164]. In addition, the temperature of lake water is affected by the adjacent debris-covered area [39]. Researchers also suggest that the albedo of an ice-cliff can change over time, such that given the active sediment flow and the mixing with meltwater, a lower albedo can further enhance the melting and facilitate lake expansion [27]. Consequently, multiple feedbacks can accelerate lake development, expansion and loss of glacier ice [70, 52].

4.4 Methods

4.4.1 Data

In this study, we conduct numerical simulations over the ablation zone of the Baltoro Glacier (Figure 4.1). The Baltoro Glacier is a notable debris-covered glacier located in the central Karakoram in Pakistan, and is one of the largest temperate glaciers in the world outside the polar regions. Baltoro Glacier is an ideal glacier for lake simulation studies because quantitative estimates of surface ablation rates, debris-thickness distribution and surface morphological maps (including supraglacial lakes) over the Baltoro Glacier have been produced from field measurements and remote-sensing analysis (e.g., [6, 4, 127, 23]).

Initial surface topography conditions and land-surface parameters were derived from a 30m digital elevation model, which was generated based on the use of stereo-correlation from ASTER

(Advanced Spaceborne Thermal Emission and Reflection Radiometer) satellite imagery using SILCAST software. The initial surface temperature was acquired from the ASTER surface-kinetic temperature product. All ASTER data were acquired in the middle of the ablation season (August 14, 2004, ID 00308142004054614) in order to maintain temporal consistency and facilitate calibration with the field measurements acquired at that time by Mihalcea et al. [6]. The temporal variation (diurnal and seasonal) in air temperature over the study area was derived from published results [147, 151], and a vertical lapse rate of $0.0065 Km^{-1}$ is used following Reid and Brock [13] to account for the decrease in air-temperature with increasing elevation.

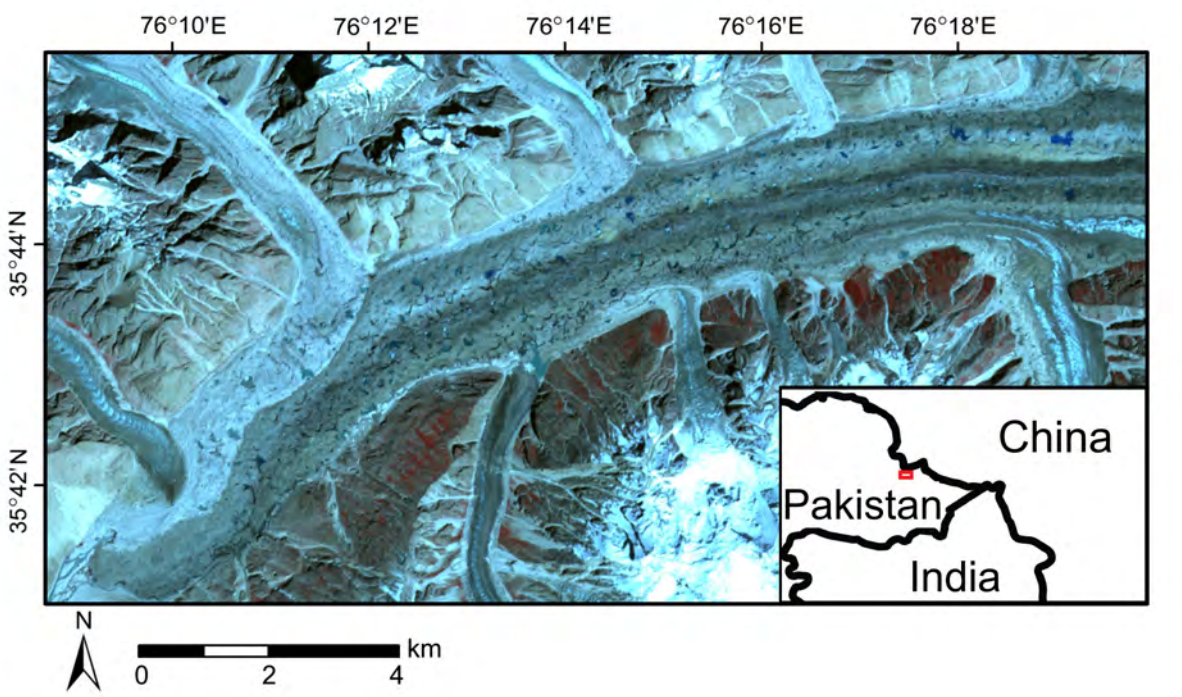

Figure 4.1: ASTER (Advanced Spaceborne Thermal Emission and Reflection Radiometer) false-color composite image (VNIR bands) of the ablation zone of the Baltoro Glacier located in the central Karakoram in Pakistan. Note the large number of supraglacial lakes in the ablation zone (imagery acquired on August 14, 2004).

4.4.2 Surface Ablation Model

Glacier-surface meltwater production is computed based on the surface energy balance and ablation model developed in Chapter 3 (Equations 3.1-3.15), which accounts for the short-wave irradiance, surface energy balance at the debris-ice interface, temporal variation in surface albedo, and topographic evolution. This model provides more reasonable ablation estimates compared to existing models, because: 1) Local and meso-scale topographic effects of surface irradiance are accounted for; 2) Surface temperature is continuously modeled rather than being restricted by instantaneous remote-sensing data; and 3) A sediment mineral and meltwater mixing model is used to account for the temporal variation of glacier-surface albedo.

4.4.3 Sediment Fluxes

Supraglacial sediment movement is a critical process that influences surface ablation dynamics on a DCG because it controls the thickness and mineralogical distribution of supraglacial sediments which governs the ablation rate. In this study, gravitational sediment fluxes are simulated using the model developed in Chapter 3 (Equations 3.16-3.23), which accounts for internal friction and basal resistance. The flux rate is controlled by a tuning parameter M, as defined in Equation 3.19. This sediment-transport component is integrated into the ablation model such that the changes in local topography due to ice melting at each iteration will influence the magnitude and direction of the sediment fluxes.

4.4.4 Lake Ablation Model

The ablation process due to supraglacial lakes is more complex than sub-debris or ice melting because lake water can store and transport energy. In this study, we use the energy-balance model developed by Sakai et al. [38] as the basis for simulating the ablation caused by supraglacial lakes. This lake energy-balance model can be written as:

$$Q_s + Q_l + Q_h + Q_e + Q_{in} - Q_{out} - \Delta Q_t - Q_d = 0, \tag{4.1}$$

where Q_s, Q_l, Q_h, Q_e are components of the net heat flux at the lake surface as defined in Chapter 3. Q_{in} is the input heat flux from meltwater inflow into the lake and, Q_{out} is the output heat flux due to water outflow from the lake. We assume all water exchange occurs on the glacier surface due to unknown englacial conditions. We neglect Q_{in} and Q_{out} in our simulations because they do not exist under our assumption of constant water temperature. Q_d is the conductive heat flux into the ice beneath the water surface that causes ablation, and ΔQ_t is the change in heat storage of the lake, which can be computed as:

$$\Delta Q_t = \frac{c_w \rho_w \Delta T_w \Delta V_w}{\Delta t}, \tag{4.2}$$

where c_w, ρ_w, T_w are the specific heat, density and temperature of lake water respectively, and they are held as constants in our simulations, and ΔV_w is the lake-volume change. We assume a turbulent well-mixed water for the entire lake, such that the water temperature does not change with depth [165].

Because ice is at melting temperature while in contact with lake water, the ablation rate beneath the lake surface can be computed as [53, 45]:

$$M_l = \frac{Q_d}{\rho_i L_f}, \tag{4.3}$$

where ρ_i is the density of ice, and L_f is the latent heat of fusion for ice as described in Chapter 3.

The topography is altered by lowering the elevation by Δz_i after each iteration (with a time step of Δt) based upon the ablation rate and surface slope angle (θ_t):

$$\Delta z_i = M_l \Delta t cos\theta_t, \tag{4.4}$$

Note that this model does not account for calving around the perimeter of a supraglacial lake caused by lateral ablation, which is a process that also contributes to the lateral expansion of lakes, because calving is governed by other processes (e.g., gravitational acceleration and ice-mass stresses caused by debris load, topography of the ice and ice-flow dynamics) that are beyond the

scope of this study, and cannot be characterized using our 2-D representation scheme.

4.4.5 Supraglacial Drainage Model

In the ablation zone, numerous water channels form on glacier surfaces that allow efficient meltwater drainage [36, 42]. A supraglacial drainage model that characterizes water-depth variation is necessary in order to simulate supraglacial lake formation and to estimate meltwater runoff. Based on the ablation model and the DEM of the glacier surface, we numerically simulate the supraglacial drainage conditions in the ablation season using the approach by Lüthje et al. [8]. This model is a second-order differential solution accounting for topography-controlled flow path, surface lowering due to melting, and variations in water level (h_w), and has been successfully utilized to model the evolution of supraglacial lakes on Greenland ice-sheet margin [8]. This model can be written as:

$$\frac{\partial h_w}{\partial t} = He(h)(\frac{\rho_i M_l}{\rho_w} - D\nabla \cdot (h_w \nabla z_i)), \tag{4.5}$$

where t is time, $He(h)$ is a Heaviside function to prevent negative water level, ρ_w is the density of water, D is a tuning parameter that controls the water-flow speed, and z_i is ice-surface elevation which is updated at each iteration based on Equation 4.4.

Equation 4.5 is implemented using an adaptive time-step finite differencing approach to ensure stability during long-period simulation, such that the time-step for each iteration is a dynamic function of the surface gradient (∇z_i), cell size (ds) and the remaining time (t_r) for the simulation:

$$\Delta t = min(\frac{ds^2}{4max(\nabla z_i)}, t_r), \tag{4.6}$$

Meltwater travels much slower on a debris-covered surface as compared to that on a bare-ice surface due to the impediment caused by sediments. Top account for this effect, the tuning parameter D is adjusted to be equal to 0.0015 for supraglacial sediment following the method by Lüthje et al. [166]. Note that this model does not account for englacial or subglacial drainage dynamics, therefore, meltwater is either stored on the glacier surface (in lakes or streams) or eventually

drains off of the surface at the terminus or lateral margins as surface runoff. We also estimate supraglacial discharge by recording the total volume of meltwater that is drained from the glacier terminus region.

4.4.6 Simulation Scenarios

Three groups of scenarios (Table 4.1) are simulated over the ablation season in 2004 to answer our research questions.

The first group of simulations (S1-S2) investigates the contribution of supraglacial lakes to the overall surface ablation and differential thinning. To quantify the ablation caused by lakes, we simulate and compare two scenarios: S1: a debris-covered glacier with supraglacial lakes, and S2: a debris-covered glacier without supraglacial lakes.

The second group of simulations (S3-S8) addresses the evolution of individual lakes and the influence of gravitational sediment flux on ice-cliff retreat and lake expansion. Gravitational sediment flux plays an important role in lake expansion because an increased debris-flux rate tends to increase the meltwater production on a debris-covered glacier as demonstrated in Chapter 3, and supraglacial lakes evolution could be more sensitive to the debris-flux due to the steep slopes around them. Specifically, we simulate the expansion of supraglacial lakes on different topography and with different debris-flux rates.

The third group of scenarios (S9-S11) investigates how the glacier-profile slope angle influences supraglacial meltwater drainage and lake formation. These simulations were designed to provide quantitative evidence to support the hypothesis that a gentle glacier-profile slope angle facilitates the formation of supraglacial lakes [41]. Specifically, we simulate surface drainage condition and estimate discharge for glacier surfaces with 3 different glacier-profile slope angles at 2^{o}, 5^{o}, and 10^{o} (the slope of the best-fit-plane of the whole glacier surface topography).

Simulation	Lakes	Surface Topography	Debris-Flux Rate
S1	Yes	Modern-day	Moderate
S2	No	Modern-day	Moderate
S3	Yes	HU	Low
S4	Yes	HU	Moderate
S5	Yes	HU	High
S3'	Yes	HF	Low
S4'	Yes	HF	Moderate
S5'	Yes	HF	High
S6	Yes	Modern-day	Low
S7	Yes	Modern-day	Moderate
S8	Yes	Modern-day	High
S9	Yes	Gentle slope (2^o)	Moderate
S10	Yes	Moderate slope (5^o)	Moderate
S11	Yes	Steep slope (10^o)	Moderate

Table 4.1: List of simulation scenarios used to provide insight into the impacts of glacier lakes on ice-mass loss and surface morphometry. The M value (Equation 3.19) for low, moderate, and high debris-fluxes are 0.99, 0.95, and 0.90 respectively. HU represents the hypothetical topography with undulations (Figure 4.2A), and HF represents the hypothetical topography that is flat (Figure 4.2B).

4.4.7 Initial Conditions

The initial surface topography, debris thickness, debris mineralogical composition, and atmospheric temperature discussed in Chapter 3 are used in this study. All scenarios start with a dry surface and we assume there is no precipitation, tributary glacier input, englacial meltwater storage or englacial transport throughout the simulations, such that all supraglacial lakes are created via the accumulation of meltwater generated on the glacier surface given radiation forcing. For

scenarios S3, S4 and S5, the initial topography is an inclined surface with topographic variations (a hummocky surface; Figure 4.2A) and a 0.5m thick debris load. For scenarios S3', S4' and S5', the initial topography is changed to an inclined surface without any undulations (Figure 4.2B). For scenarios S6, S7 and S8, a subset of the actual topography on the Baltoro Glacier is used (Figure 4.2C).

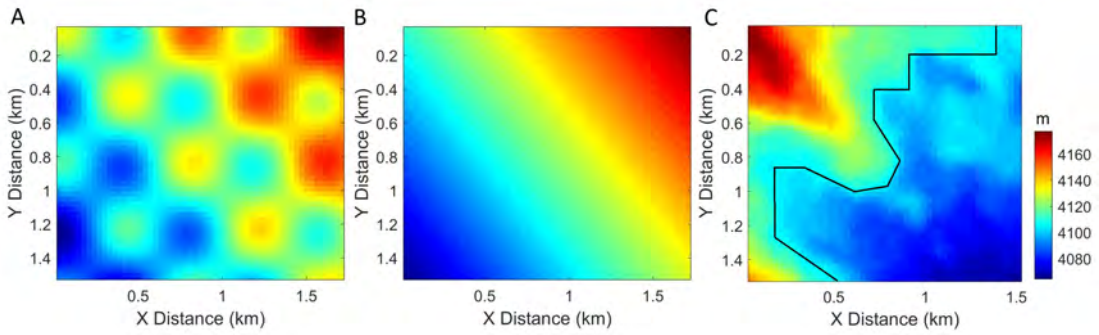

Figure 4.2: The ice-surface topography used in simulations S3-S8. (A) A hypothetical surface with undulations used as the initial topography for scenarios S3, S4 and S5. (B) A hypothetical flat surface is used as the initial topography for scenarios S3', S4' and S5'. (C) A subset of the actual topography on the Baltoro Glacier is used as the initial topography for scenarios S6, S7 and S8. The black line represents the location of an ice-cliff.

The albedo of supraglacial lakes (α) is estimated using the approach by Taylor and Feltham [7] and Lüthje et al. [8]. Based on which, the albedo is a function of lake-water depth (h_w):

$$\alpha = \frac{9702 + 1000e^{3.6h_w}}{-539 + 20000e^{3.6h_w}}, \tag{4.7}$$

Figure 4.3 shows the change in lake albedo as a function of water depth.

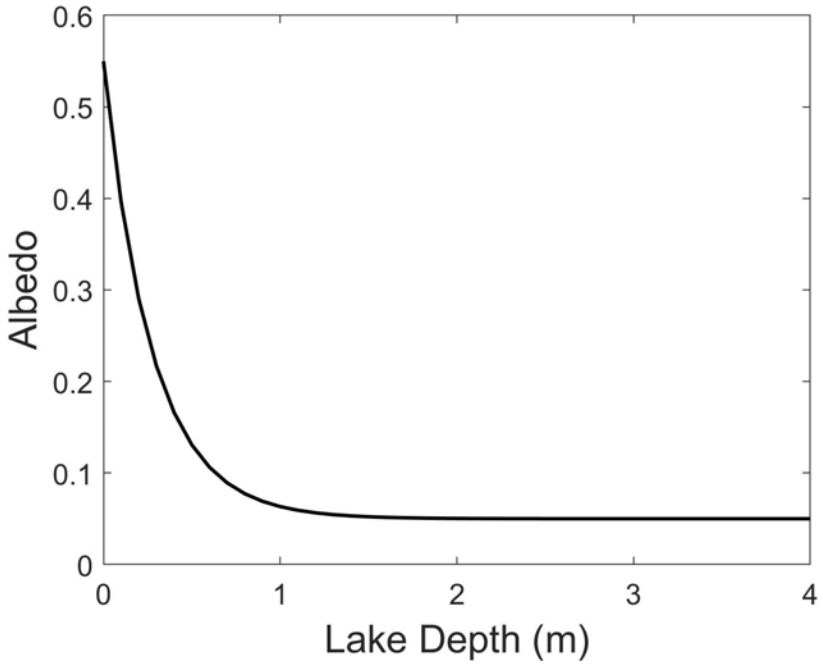

Figure 4.3: Lake-surface albedo as a function of water depth based on Taylor and Feltham [7] and Lüthje et al. [8].

4.5 Results

4.5.1 Supraglacial Drainage and Lake Formation

Supraglacial drainage conditions control the water-depth distribution on the glacier surface. We simulate the supraglacial water-depth variations in the ablation zone over the ablation season in 2004. Figure 4.4 shows the initial and final water-depth distribution on the glacier surface. The final water-depth distribution reveals a large number of supraglacial lakes and water channels. They are less abundant in the immediate terminus region because the debris is very thick in that area and the water level does not reach the top the debris column. Marginal streams are also revealed in Figure 4.4B, and the simulation result highlights both inter-moraine and valley-marginal channels, bounded by the valley wall and glacier, on both sides of the glacier. These zones represent lower surface altitudes where meltwater can accumulate and flow towards the terminus under the influence of gravity.

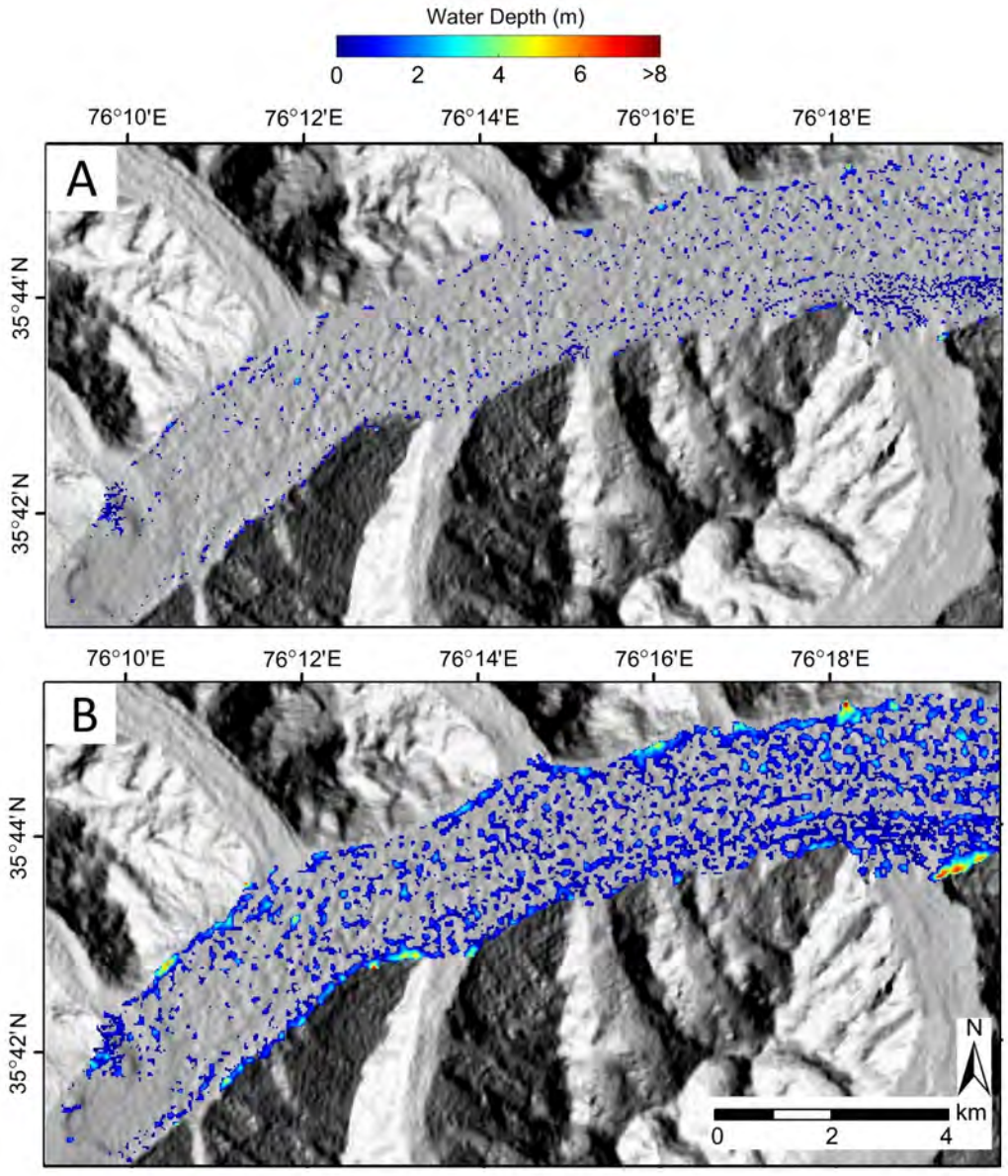

Figure 4.4: Simulated surface water depth in the ablation zone of the Baltoro Glacier. (A) The water-depth distribution after one day of simulation (12PM on the June 1st 2004). (B) The final water-depth distribution (12PM on the September 28th 2004). In our simulation, the surface is considered dry if the water level at that grid cell does not reach the top of debris column.

A comparison between the simulation result and published remote-sensing analysis [23] reveals that simulation results produce higher estimates of lake frequency and area compared to the remote-sensing results (Table 4.2). These results could be caused by many factors, both process

and methodology related, for example, the quality of data, and the use of thresholding can influence remote-sensing-based inventory results. Furthermore, the dominant factor most likely is the neglection of englacial conduits that reduce the volume of surface water by englacial drainage.

	N_l	A_l (km^2)
Simulated	250-300	1.74
Published [23] (based on remote sensing)	160-240	1.07

Table 4.2: Number (N_l) and area (A_l) of simulated supraglacial water bodies (streams and channels are not included) on the ablation zone of the Baltoro Glacier as compared to published results based on remote-sensing analysis of imagery acquired on August 14, 2004.

4.5.2 Surface Ablation Due to Supraglacial Lakes

To understand how supraglacial lakes govern surface ablation, we computed ablation rates in the ablation zone over the ablation season. Figure 4.5 compares the mean surface ablation rates (temporally averaged over the ablation season) between lake-present and no-lake scenarios (simulation S1 and S2), while Figure 4.6 compares the standard deviation that highlights temporal variability between the two scenarios. The magnitude and spatial distribution of simulated sub-debris ablation rates have been validated using the field measurements by Mihalcea et al. [6, 4] as discussed in Chapter 3. By comparing the two scenarios, we can see that lakes create numerous melting hotspots on the glacier surface and increased the spatial heterogeneity of surface ablation. The temporal standard deviations (Figure 4.6) reveal that the ablation rates for lakes also exhibit very high temporal variability over the ablation season, which suggests that supraglacial lakes are more sensitive to the seasonal variation in radiative forcing than other areas on the glacier surface.

Table 4.3 compares the statistics of the two simulated scenarios, which demonstrates that the presence of supraglacial lakes significantly increased the magnitude and spatial variability of surface ablation. The lakes on average accounts for 7.57% of the surface area, but they contributed

22.78% of the total ice-mass loss over the simulated period, and the ablation rates beneath the lake water are on average 5.6 times higher than the average for non-lake areas. This strongly suggests that supraglacial lakes can significantly increase ice-mass loss on a DCG, and high spatial variation in the ablation rates caused by lakes and ponds suggests that supraglacial lakes are also responsible for the high-magnitude heterogeneous thinning observed on many large DCGs (e.g., the Khumbu Glacier [38] and the Baltoro Glacier [6]).

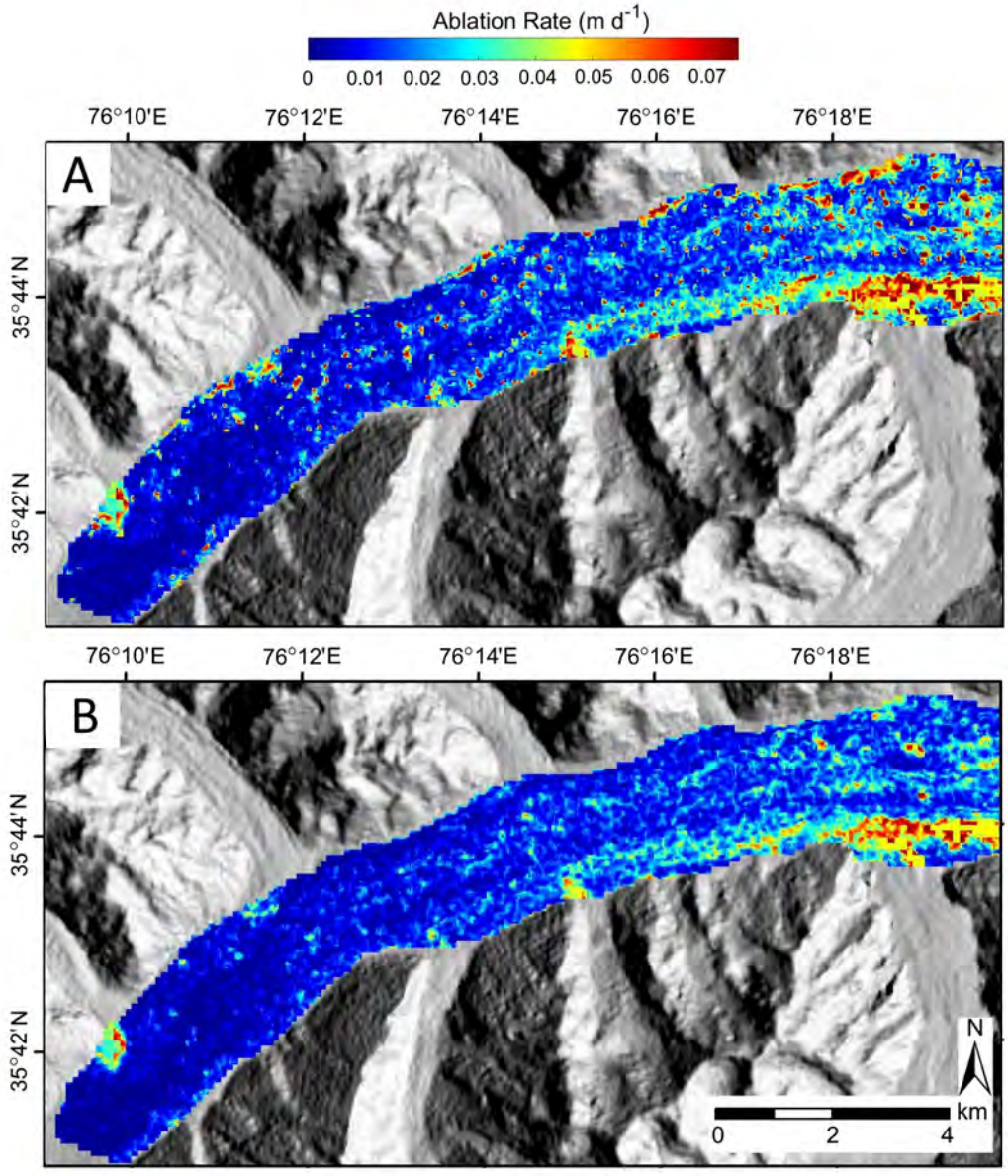

Figure 4.5: Simulated surface ablation rates in the ablation zone of the Baltoro Glacier (averaged over 120-day ablation season). (A) The supraglacial lake present scenario (S1). (B) The no-lake scenario (S2).

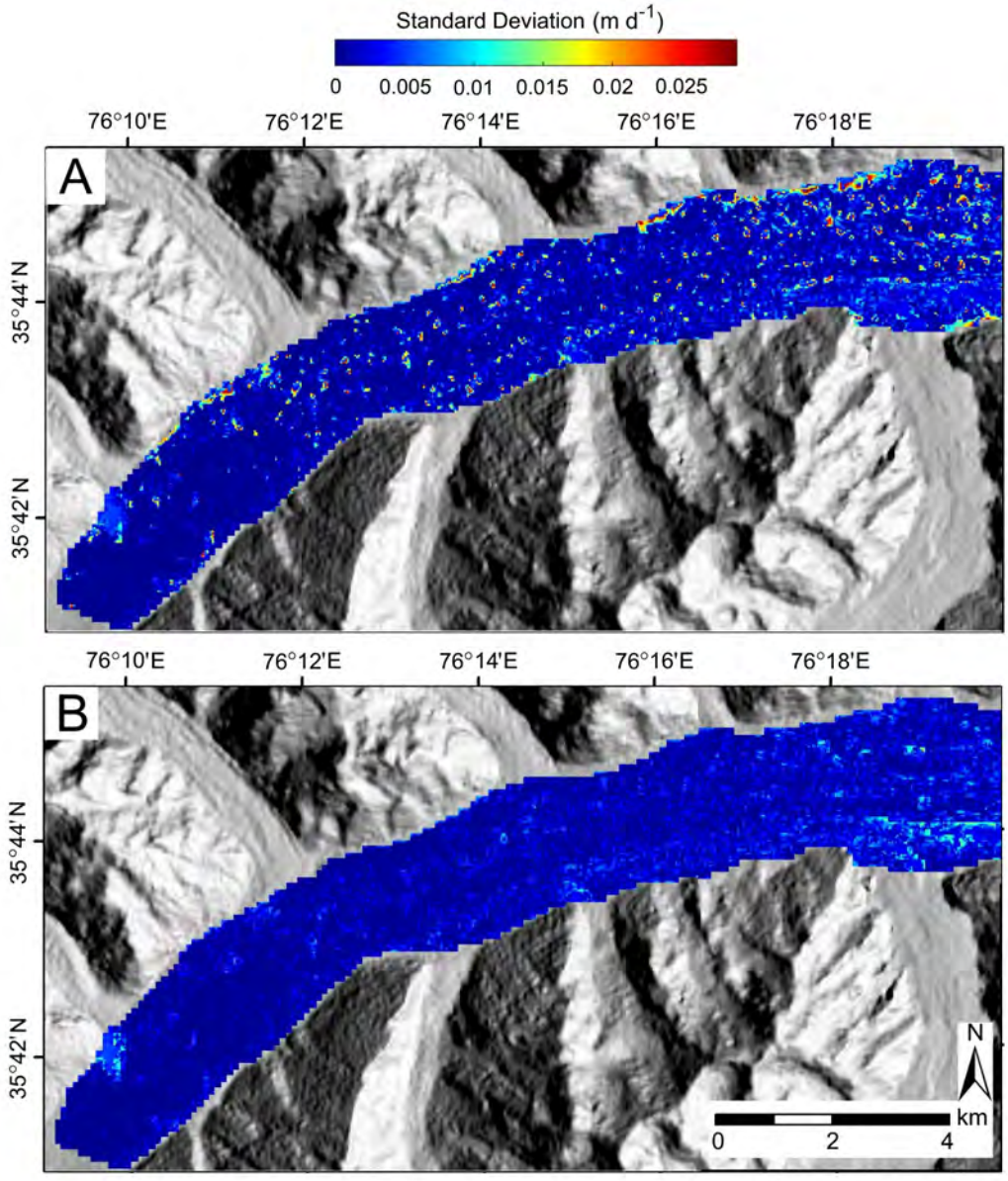

Figure 4.6: Standard deviation of surface ablation rate variations over the ablation season using a temporal interval of one month. for (A) The supraglacial lake present scenario (S1). (B) The no-lake scenario (S2). Note that most high magnitude areas correspond to supraglacial lakes that formed over different temporal stages.

Scenario	$\bar{M}_s$ (md^{-1})	σ_{M_s} (md^{-1})	$\bar{M}_l$ (md^{-1})	$A_l\%$	$M_l\%$
S1 (with lakes)	0.0180	0.0168	0.0661	7.57%	22.78%
S2 (wihtout lakes)	0.0139	0.0126	0.0118 (debris)	0.00%	0.00%

Table 4.3: Spatial statistical comparison between simulations S1 (with lakes) and S2 (without lakes). $\bar{M}_s$ represents mean surface ablation rate, σ_{M_s} represents the standard deviation of surface ablation rate, $\bar{M}_l$ represents the mean ablation rate beneath lake surface, $A_l\%$ represents the area fraction of lakes, and $M_l\%$ represents the fraction of lakes' contribution to total surface ablation. The ablation rates are temporally averaged over the ablation season first, and then the statistics are computed over the glacier surface.

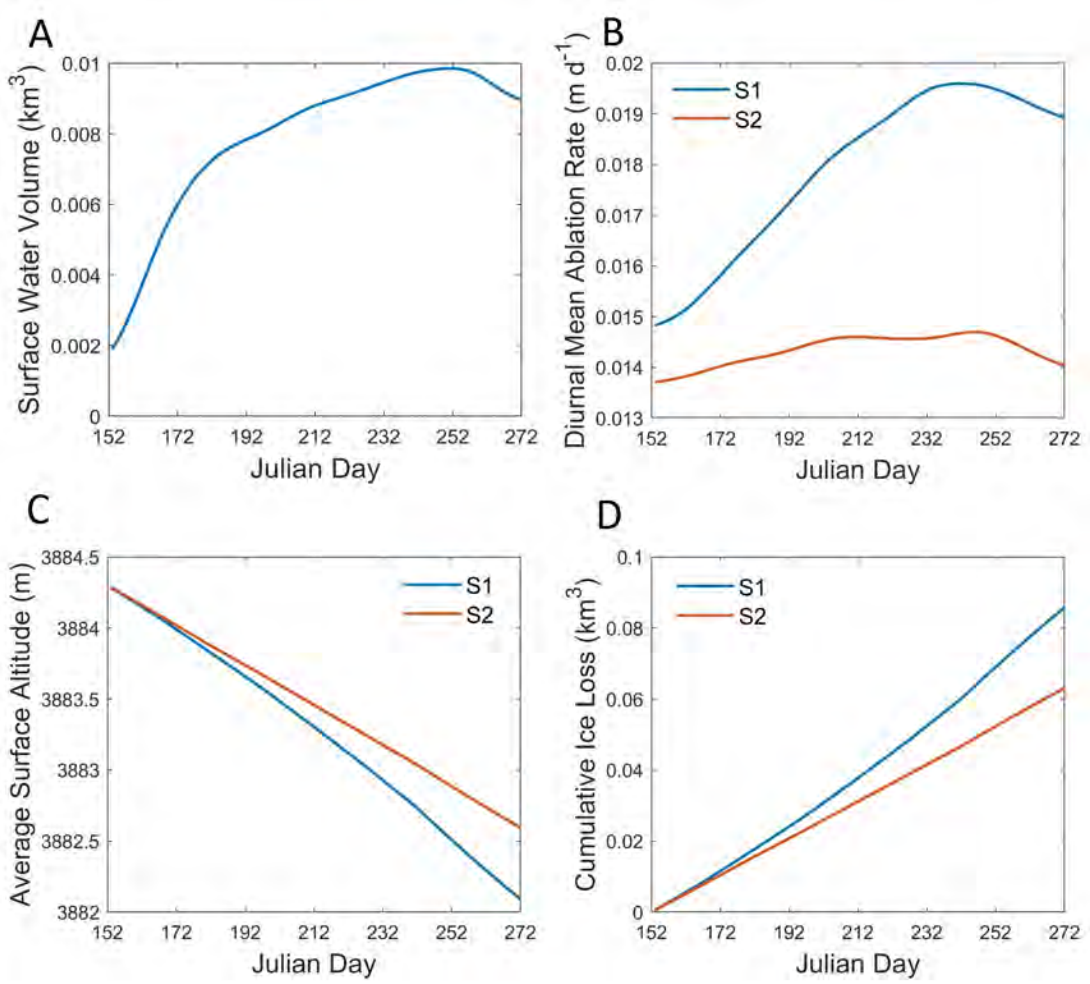

Figure 4.7: temporal variation in glacier surface conditions over the ablation season.(A) Temporal variation in total lake volume. (B) Temporal variation in diurnal mean ablation rate. (C) Temporal variation in average surface altitude. (D) Temporal variation in cumulative ice-volume loss.Note the non-linear variations when supraglacial lakes are present (S1)

Figure 4.7 depicts the variation in supraglacial water volume, and provides temporal comparisons between the two scenarios from three perspectives: The diurnal mean ablation rate (Figure 4.7B); The average glacier-surface altitude (Figure 4.7C); The cumulative ice-mass loss (Figure 4.7D). Simulation results suggest that the presence of meltwater and lake expansion dramatically accelerate the overall ice loss in the ablation zone, and the magnitude progressively increases towards the end of the ablation season because of lake evolution, although the magnitude of ablation decreases after early September, which is most likely caused by the decrease in the magnitude of

irradiance. Figure 4.7 also depicts that lake evolution causes a nonlinear decrease in glacier-surface altitude and that the degree of nonlinear change is most likely related to the spatial density of lakes on a glacier. Consequently, the nature of cumulative ice-mass loss is also nonlinear. We would expect that the nonlinearity can cause dramatic change over longer periods of time if the lakes remain on the surface over decadal time frames. These results strongly suggest that the formation and evolution of supraglacial lakes represents a key indicator of a glacier's overall sensitivity to radiative forcing.

4.5.3 Debris Flux and Lakes

Supraglacial lakes expand during the ablation season, and the growth rate is closely linked with debris-thickness distributions around the lakes [75]. To understand how debris-thickness variation controls the growth of a lake and how lake evolution controls sediment fluxes and ablation, we conduct simulations using three different gravitational debris-flux rates based on hypothetical and actual surface topography (S3-S8).

Figure 4.8 depicts simulated supraglacial lake evolution (water-depth distribution) for simulations S3-S5 on three different dates, using hypothetical topography consisting of equally-spaced periodic variations (Figure 4.2A). Simulations show the expansion of lakes in the depression areas with an increase in size and depth over time for each scenario. The comparison between S3 (low flux rate scenario), S4 (moderate flux rate scenario), and S5 (high flux rate scenario) indicates a positive correlation between gravitational debris-flux rate and lake size. A higher flux rate increases lake size and water volume, and also generates higher connectivity between the lakes. This is because a faster debris-flux can dramatically decrease debris thickness on adjacent slopes, which enhances ablation and facilitates meltwater production and lake expansion. Figure 4.9 compares the mean water depth and volume over time for the three scenarios. All scenarios show a non-linear increase in water depth and especially volume, which indicates accelerated lake expansion. The difference between scenarios becomes more pronounced in the later portion of the ablation season, as the steepening of adjacent slopes and the availability of meltwater most likely increases the flux rate and lake expansion. This represents a positive feedback that could lead to nonlinear increases

in ice-mass loss and lake expansion.

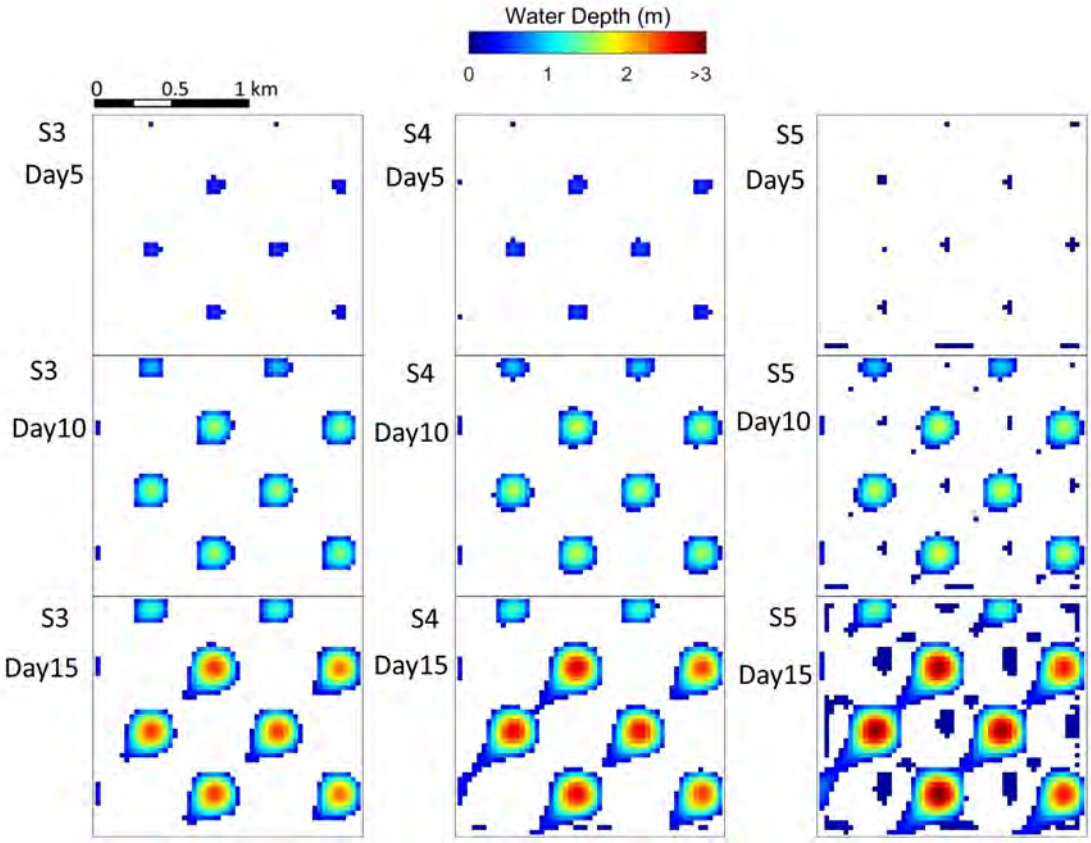

Figure 4.8: Simulated supraglacial lake evolution (water-depth distribution) on hypothetical topography (Figure 4.2A) under different gravitational debris-flux rates. Left column: S3 (low flux rate scenario, M=0.99). Mid column: S4 (moderate flux rate scenario, M=0.95). Right column: S5 (high flux rate scenario, M=0.90). The simulations start on June 1st , 2004.

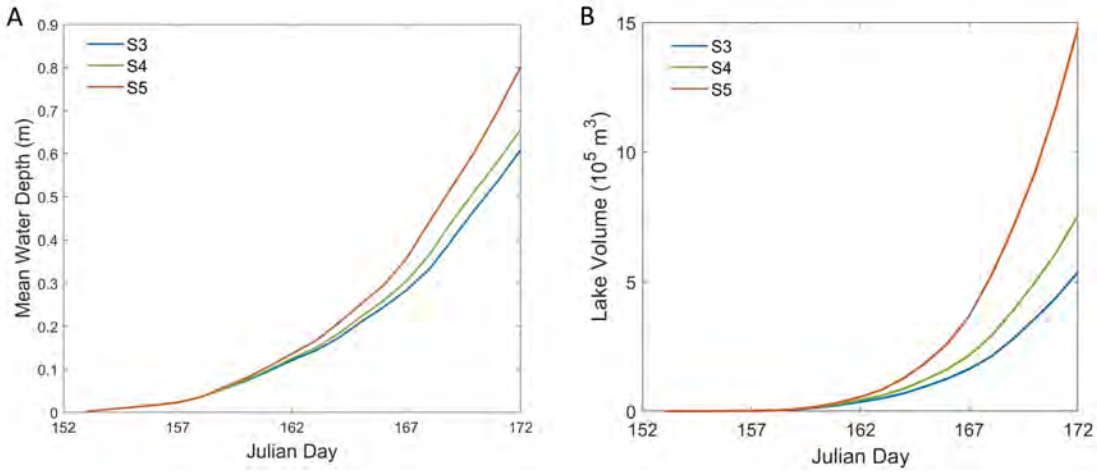

Figure 4.9: Mean lake-water (A) depth and (B) volume over the ablation season for scenarios S3-S5. The non-linear increase in water depth and volume indicates accelerated lake expansion during the ablation season.

We then simulated lake formation on an inclined surface without any topographic undulations (S3', S4' and S5'), and simulations revealed no lake formation, as there are no topographic depressions for meltwater to accumulate. These simulations are based on unrealistic topography but they demonstrate that topographic depressions are necessary for lake formation. On the surface of an actual DCG, there are numerous depressions that would eventual accumulate water, and serve as the basis for lake growth and evolution.

To achieve a more realistic simulation, we performed a similar numerical experiment based on modern-day surface topography, and focused on a subarea on the Baltoro Glacier (Figure 4.2C) where lakes are surrounded by steep slopes (outlined in Figure 4.2C). Here we simulated lake evolution under three different debris-flux rates (S6-S8). Figure 4.10 shows the increase in lake-water area and depth over time. These results also revealed a positive correlation between the gravitational debris-flux rate and lake size, a faster sediment flux generating larger areas of thin debris on the ice-cliffs and around the lake, thereby enhancing melting, and producing additional meltwater that accelerates lake expansion. Figure 4.11 compares the mean water depth and total lake volume over time for different debris-flux rates, which depicts a non-linear increase in water depth and

an even more non-linear increase in lake volume. This is most likely due to an accelerated lake expansion caused by the positive feedback between debris-flux, topography, meltwater production and surface ablation.

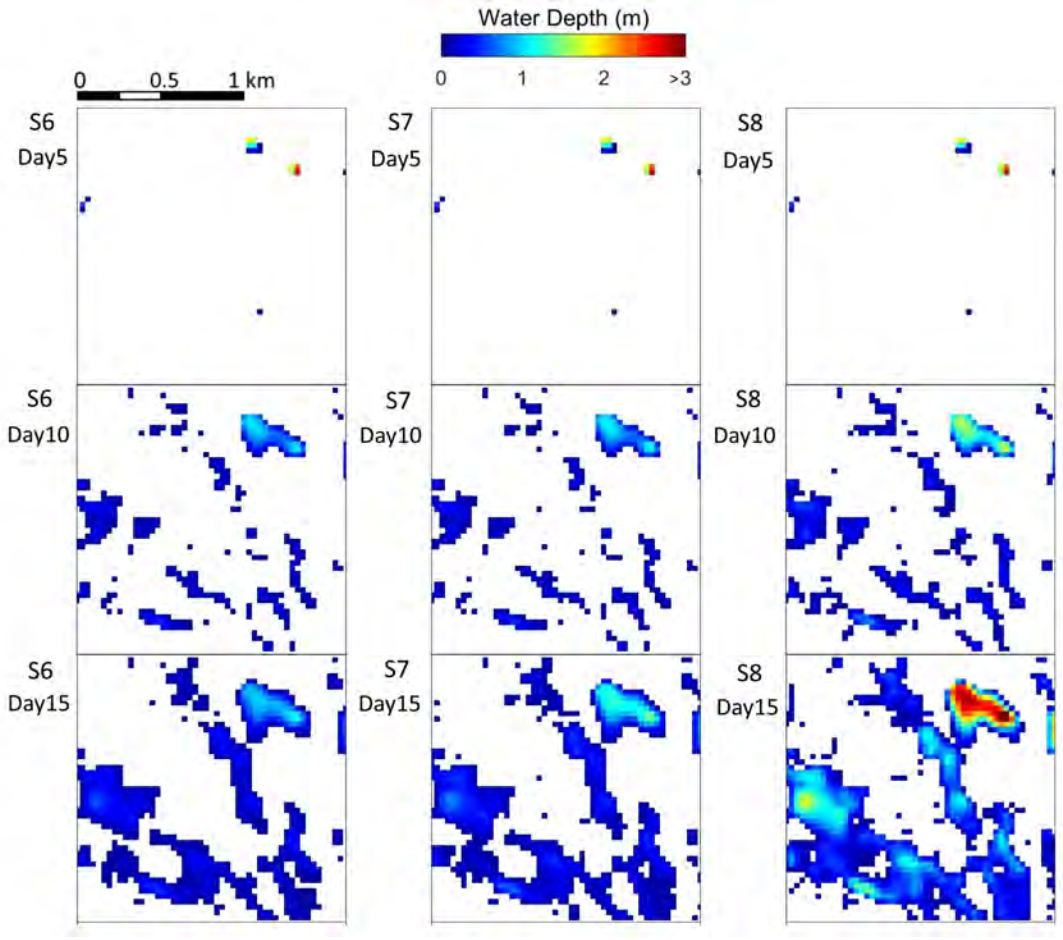

Figure 4.10: Simulated supraglacial water-depth on a subarea of the Baltoro Glacier (Figure 4.2C) under different gravitational debris-flux rates. Left column: S6 (low flux rate scenario, M=0.99). Mid column: S7 (moderate flux rate scenario, M=0.95). Right column: S8 (high flux rate scenario, M=0.90). The simulations start on June 1st, 2004.

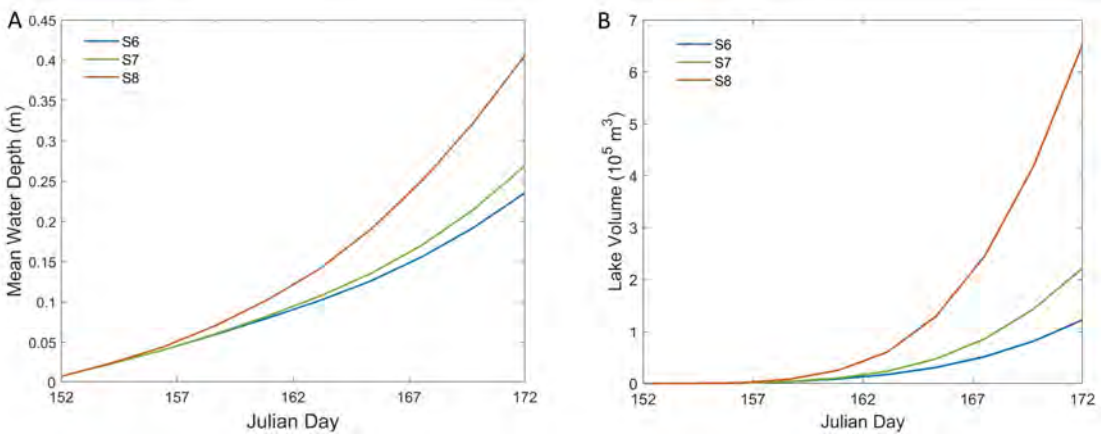

Figure 4.11: Mean water (A) depth and (B) volume over the ablation season for S6-S8 based on the modern-day glacier topography. Results show a positive correlation between gravitational debris-flux rate and lake size. Accelerated lake expansion is revealed by the non-linear increase in water depth and lake volume.

Supraglacial lake evolution is also controlled by lateral sub-water surface ablation and the retreat of ice-cliffs. The debris load usually gets thinner over time as adjacent slopes and ice-cliff becomes steeper (Figure 4.12) which potentially leads to faster retreat if the orientation of the ice-cliff is facing the solar azimuth direction. Figure 4.13 compares the mean ablation rate at lake boundaries (considered to be ice cliffs) as a function of debris thickness for scenarios S6, S7 and S8. Results show the thinning of debris at lake boundaries caused by an increase in debris-flux rate, and the thinning of debris accelerates melting on these slopes that facilitates lake expansion, and expansion creates steeper slopes, which in turn increases the debris-flux rate. These results reveal that lake formation further enhances debris-flux variability which controls meltwater and lake expansion is a positive feedback fashion.

Figure 4.12: A field photo of a debris-covered ice cliff and a small supraglacial lake on the Baltoro Glacier during the summer of 2005 (photo credit: Andrew B.G. Bush, 2005, with permission). Note that the debris cover on the ice cliff is thinner than adjacent areas and exhibits a relatively high moisture content due to meltwater production.

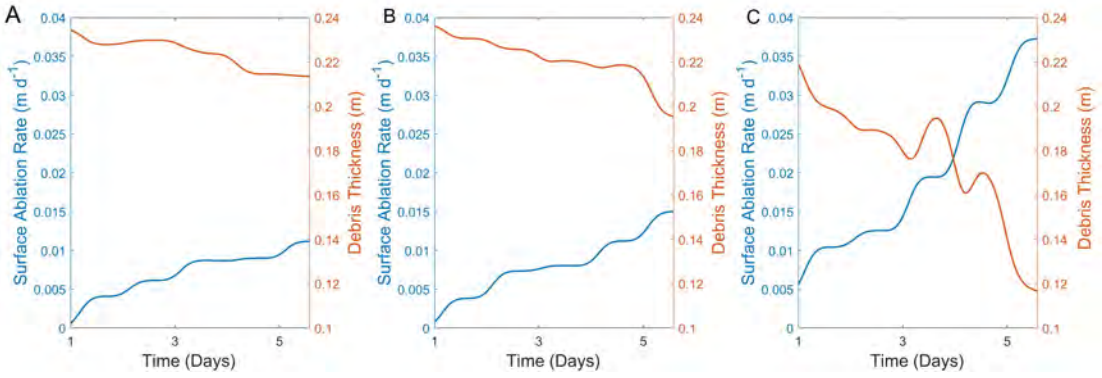

Figure 4.13: Mean ablation rate versus debris thickness at lake boundaries (the potential ice-cliff as marked in Figure 4.2C) under different debris-flux rates. (A) A low flux rate scenario (S6; M=0.99) , (B) A moderate flux rate scenario (S7; M=0.95); and (C) A high flux rate scenario (S8; M=0.90).

Note that over annual or decadal time frames, englacial drainage is a controlling mechanism on lake size, as most supraglacial lakes start to drain rapidly when they intersect englacial conduits [75]. Therefore, a lake cannot infinitely expand, and this simulation only serves as a demonstration of supraglacial lake expansion before it encounters an englacial drainage channel.

4.5.4 Topography and Supraglacial Discharge

Field studies have suggested that the overall glacier slope gradient in the ablation zone controls the formation of supraglacial lakes, such that most lakes exist over areas exhibiting relative gentle slope [41, 54, 133, 27, 40]. To understand and quantify the effect of glacier slope gradient variations on supraglacial lake formation and drainage, we performed 3 numerical experiments on glacier surfaces with three different slope gradients (Figure 4.14A, scenarios S9: slope angle = 2^o, S10: slope angle = 5^o and S11: slope angle = 10^o) and investigated the variations in discharge. Note that slope here refers to the overall slope gradient of the entire glacier in the ablation zone (i.e., the slope of the best-fit plane of the entire glacier. Not the local slope). The 2^o scenario represents a realistic topographic condition of the study area, and scenarios S10 and S11 represent hypothetical high-slope conditions. Simulations show a decrease in surface water volume (Figure 4.14B), and an increase in meltwater discharge (Figure 4.14C) as the glacier-profile gradient gets higher. Note that the simulations start with an initial dry surface, so rapid filling process lasted for about 25 days before surface water storage became stable. The total amount of meltwater produced is kept constant across all three scenarios, such that surface slope is the only factor that is responsible for the difference in discharge.

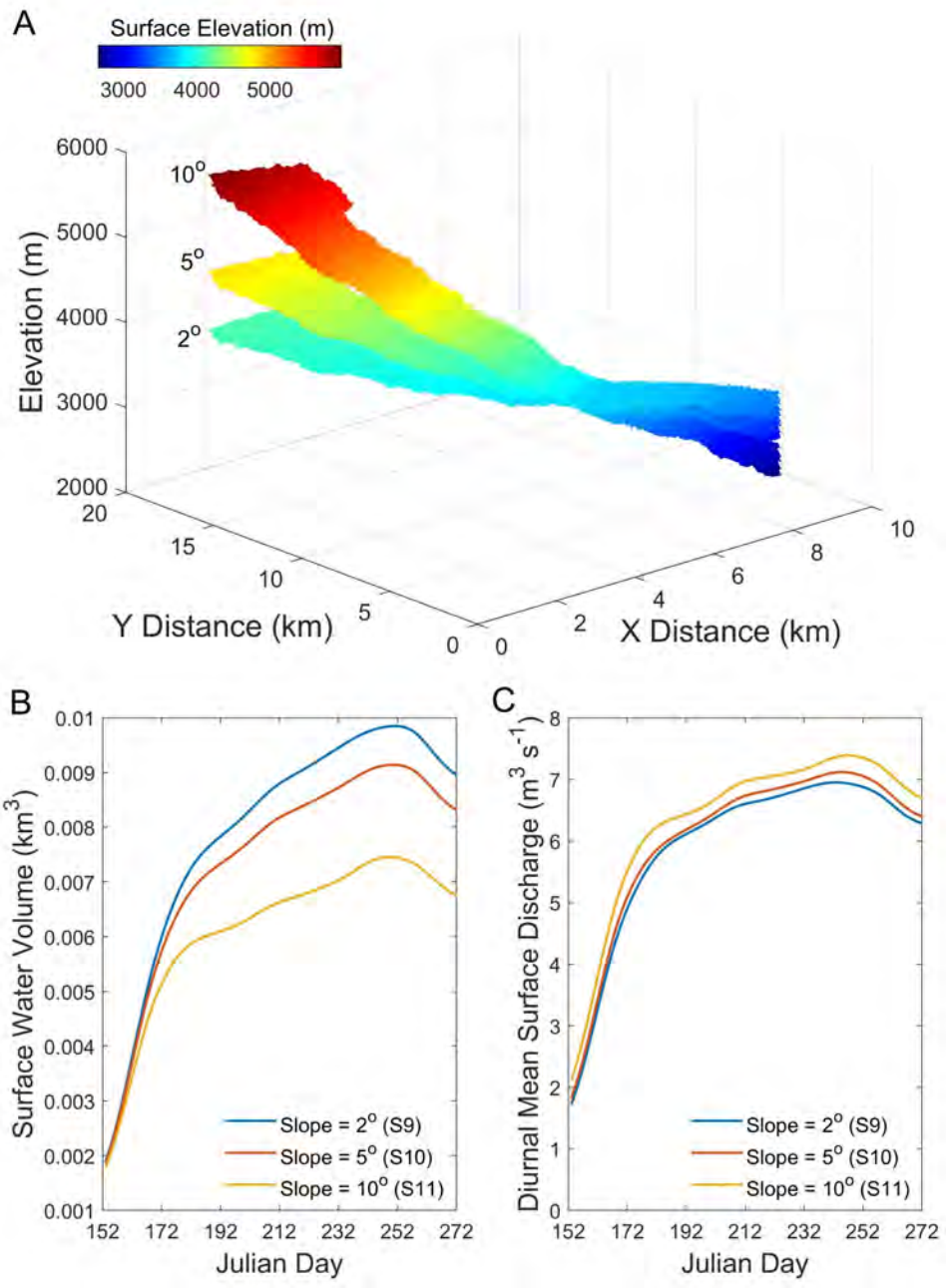

Figure 4.14: Glacier-profile gradient control on supraglacial discharge (lakes are accounted for). (A) Surface elevation conditions given different slope angles used in simulations S9-S11. (B) The volume of meltwater stored on the glacier surface over time for simulations S9-S11. (C) Diurnal mean surface discharge for simulations S9-S11. Note the decrease in surface water volume and the increase in discharge as the profile gradient gets higher.

Scenario	$\bar{V_s}$ (km^3)	$A_l\%$	$\bar{d}$ (m^3s^{-1})
S9	0.0080	7.57%	5.94
S10	0.0074	6.78%	6.07
S11	0.0062	4.82%	6.36

Table 4.4: Statistical comparison between the gentle-slope scenario (S9), the moderate-slope scenario (S10), and the steep-slope scenario (S11) based on the discharge simulations. $\bar{V_s}$ represents the mean volume of meltwater stored on the glacier surface over the ablation season, $A_l\%$ represents the area percentage of lakes at the end of ablation season, and $\bar{d}$ represents the mean diurnal surface meltwater discharge over the ablation season.

The increasing discharge given steeper slopes (Figure 4.14, Table 4.4) suggests that overall surface slope has a significant control on supraglacial drainage efficiency. As the slope increases from 2° to 10°, the total volume of meltwater stored on the surface decreased by 22.50%, the area percentage of lakes decreased by 36.33%, and as a result, the mean diurnal surface meltwater discharge over the ablation season increased by 7.07%. Supraglacial discharge is indicative of supraglacial lake formation because higher discharge means lower water storage on the glacier surface, which inhibits lake expansion based on our assumption of no englacial filling and drainage. The lower drainage efficiency on lower gradient indicates a higher water-storage capacity on the glacier, which is a favored condition for lake formation. These numerical results provide a quantitative explanation for the observed abundance of supraglacial lakes in ablation zones that exhibit relatively low gradients.

4.6 Discussion

4.6.1 Ablation and Lakes

Although supraglacial lakes and surrounding ice cliffs only make up a very small portion of the glacier surface area, they are responsible for a significant amount of ablation that is disproportionate to their area (Table 4.3). Simulation over the ablation zone of the Baltoro Glacier suggests that at least 22.78% of ice loss is related to lake-related ablation. This is in agreement with many

field observations (e.g., [38, 54, 27, 167, 164, 40, 90]). For example, Anderson [167] estimated that about 30% of net mass loss from the ablation zone of the Kennicott Glacier in Alaska is due to the retreat of ice cliffs. Supraglacial lakes cause high-magnitude ablation and ice-mass loss for two reasons: 1) Lakes efficiently absorb solar energy due to the low albedo of water [38, 8]. The energy can be effectively used for ice melting because heated lake water can easily percolate through porous debris. Sakai et al. [38] estimated that the absorbed heat per unit area for supraglacial lakes is about 7 times higher than the average for the entire debris-covered area, and our simulations indicate that the ablation rates beneath the lake surface are on average 5.6 times higher than debris-covered ice in the ablation zone. 2) The deepening of ice-surface depressions due to lake development can potentially cause faster debris transport around lakes, as more and more debris translocate and accumulate in the lake. Surrounding ice-cliffs are usually covered by a very thin layer of debris, which enhances rather than inhibits ablation. The presence of lakes also increases the spatial heterogeneity of ablation and collectively, they can facilitate glacier thinning as the size and spatial density of supraglacial lakes vary greatly on glacier surfaces. Supraglacial lakes are also responsible for the nonlinear increase in the ice-mass loss and lake volume over time, as depicted in Figures 4.7, 4.9, and 4.11, which indicates that the glacier surface tends to be more sensitive to radiative forcing when lakes are present.

It is extremely important to recognize that our simulation results depict an ablation nonlinear response to radiative forcing when supraglacial lakes are accounted for, which can be characterized as an acceleration in ablation rate, total ice-mass loss, and general lowering of surface altitude based upon lake frequency and spatial density distributions (Figure 4.7). This is potentially caused by a lake's status or "stage of development", such that more rapid change is likely to occur in the later portions of the ablation season, as it reaches its yearly maximum extend and depth. As such, a nonlinear response to radiative forcing may represent the beginning of a critical transition of the glacier system that further signifies the surface ablation-lake expansion feedback. The collective feedback mechanisms associated with supraglacial lake formation and evolution may be a sensitivity metric that indicates the rapid downwasting of alpine debris-covered glaciers.

4.6.2 Supraglacial Drainage and Discharge

The supraglacial fluvial system drains meltwater from the glacier surface to the englacial system and the adjacent ablation valleys [36]. Based on numerical simulations, we identified a large number of supraglacial lakes, ponds and water channels that formed (Figure 4.4), similar to what have been reported in field studies (e.g., [42, 28]). Another noticeable feature revealed by the simulation is the presence of inter-moraine water flow and marginal streams (Figure 4.4), which can be relative wide and more continuous, assuming that the water does not flow into the englacial system. This is in agreement with field observations that suggest suprafluvial streams and ablation valley streams can exist over long-distances in active marginal and sub-marginal channels [42].

The gentle glacier profile slope scenario (S9) in Figure 4.14 represents the simulated discharge from the ablation zone of the Baltoro Glacier as a function of time, and we consider our modeled discharge to be the lower limit of actual discharge because we do not account for englacial or subglacial melting and drainage. Given that this simulation assumes a relatively less porous debris cover over the entire glacier surface, our simulation results represent a relatively slow drainage situation. It should also be noted that the total runoff does not represent the total meltwater production from the glacier, due to surface storage and the large amount of englacial water storage and other ablation and hydrological processes [36].

4.6.3 Supraglacial Lake Expansion and Feedback Mechanisms

Based on our simulations, we identified two important feedback mechanisms that govern lake expansion on a DCG (Figure 4.15): 1) The lake size-ablation rate feedback. As the lake grows bigger, it absorbs more solar energy which in turn accelerates ablation rate that leads to further expansion of the lake. 2) The ice-cliff retreat-lake expansion feedback. As the lake-facing slope melts much faster due to the melt-enhancing effect of thin-debris, surrounding slopes becomes steeper, which leads to further thinning of the debris cover, and the lowering of albedo due to increased moisture content, which in turn, accelerates the melting of surrounding slopes and ice cliffs. This process has been described in previous studies [27, 28], and this model provides the

first numerical solutions to partially simulate this feedback mechanism.

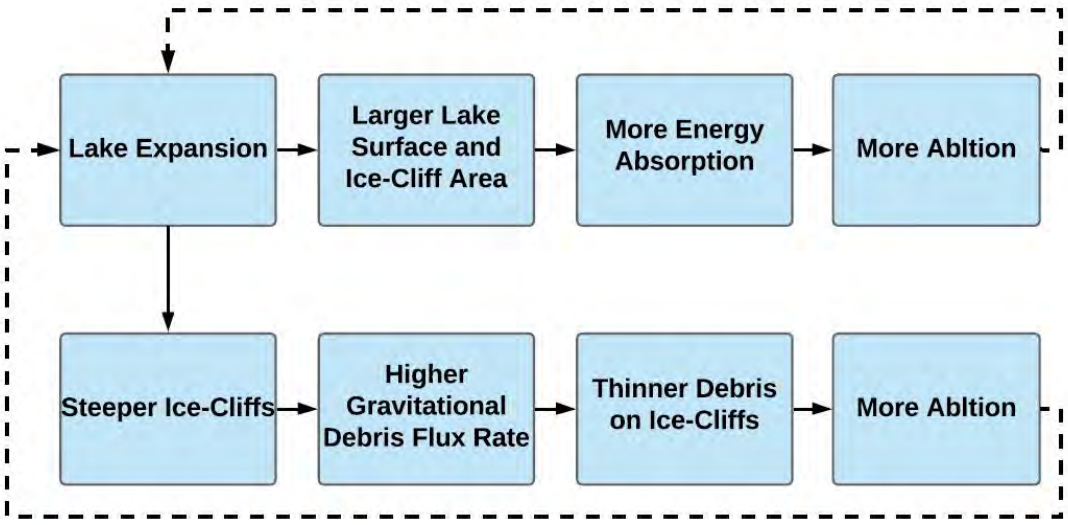

Figure 4.15: Diagram illustrating the positive feedbacks identified in this study that can accelerate supraglacial lake expansion on debris-covered glaciers.

The glacier surface topography also controls lake formation. Numerical simulations show the decrease in surface water storage with a higher gradient (Figure. 4.14, Table 4.4), which has been confirmed with field observations that indicate that glaciers with gentle surface gradient in the ablation zone frequently exhibit more lakes and often facilitate the formation of new lakes [41]. In addition to slope gradient, topographic depressions caused by differential ablation and surface water flow are also necessary for lake formation, as indicated by our simulations S3'-S5', because they provide a topographic sink for meltwater to accumulate. The depressions are ubiquitous on DCGs because of high spatial variability in ice topography, debris thickness and ablation rate [6, 4, 49, 19].

Collectively, favorable environmental conditions for supraglacial lake development on a DCG include relatively low surface gradient, presence of multi-scale topographic depressions, and high gravitational debris-flux, facilitated by the presence of meltwater and rapidly changing ice topog-

raphy. Under these conditions, supraglacial lakes can form and expand rapidly if no englacial drainage occurs.

4.6.4 Assumptions and Limitations

Our simulations investigate supraglacial lake dynamics over one ablation season. This model does not account for precipitation forcing and ice-flow, which are known to regulate glacier mass balance, sediment fluxes and surface topography over a multi-year time scale [36, 50]. Therefore, our simulations are not suitable for characterizing ablation dynamics and lake development over longer time periods, as other processes must be accounted for. Multi-year simulations that account for these processes are addressed in Chapter 5.

This model neglects adjacent-terrain irradiance, which could cause significant ablation on steep ice-cliffs. The fluvial sediment transport that could potentially increase surface ablation is also not accounted for. In addition, this model assumes no sub-lake-water-level lateral ablation that causes calving and lake expansion because of iceberg contribution. This model also neglects englacial filling and drainage, which are considered a dominant controlling factors for many supraglacial lakes [70, 75, 42]. Furthermore, this model does not account for the formation of supraglacial lakes due to the collapse of water channel roofs, which has been described in previous studies [38]. The ablation caused by warm lake water outflow is also neglected and the water temperature is assumed to be constant. Collectively, our simulation underestimates the amount of ice-mass loss and the glacier's non-linear response to radiative forcing.

4.7 Conclusions

Supraglacial lakes play a significant role in the ablation dynamics of a debris-coved glacier. Little is known about their contribution to glacier surface ablation and lake and glacier morphological evolution, as multiple processes and feedback mechanisms associated with lake formation and evolution have not be accounted for in glacier models. In this study, we investigated the dynamics of supraglacial lakes formation and evolution on the Baltoro Glacier in the central Karakoram in Pakistan. We developed a relatively comprehensive numerical model that characterizes the energy-

balance of lakes and the glacier surface, meltwater drainage and ponding, topographic evolution, and the gravitational debris-flux. We also identified and evaluated the influences of debris-flux and topography on supraglacial lake evolution. Simulation results based on the Baltoro Glacier and various hypothetical scenarios indicate that:

1. Supraglacial lakes make a significant contribution to the total surface ablation. Simulations reveal that supraglacial lakes can be minimally responsible for approximately 22.78% of the total ice-mass loss in the lower ablation zone over an ablation season. We found that lake formation and expansion processes represent a nonlinear response to radiative forcing, as a lake influence can operate over a variety of spatial scales, with lakes having a more significant influence on ice-mass loss towards the end of the ablation season when the lakes reach their yearly maximum extend.

2. Gravitational debris-flux partially controls the expansion rate of supraglacial lakes by governing the surrounding debris thickness and ablation rates, such that a faster debris-flux can dramatically decrease the debris thickness of adjacent slopes, which increases ablation and facilitates meltwater production and lake expansion. Lake expansion also increases debris-flux rate by steepening the adjacent slopes, which forms a positive feedback that accelerates surface ablation and lake expansion.

3. The overall slope gradient of a glacier partially controls the magnitude of supraglacial discharge, and influences lake formation, such that at steeper slopes, discharge increases and surface-water storage capacity decreases. Relatively high topographic variation also encourages lake formation. Therefore, supraglacial lake formation may be initiated given differential ablation and downwasting coupled with less ice-mass flux, that decreases the slope gradient and facilitates more meltwater production and accumulation in multi-scale topographic depressions.

4. A debris-covered glacier can exhibit a nonlinear response to radiative forcing when supraglacial lakes are accounted for. The nonlinearity is represented as an acceleration in ablation rate, total ice-mass loss, and the lowering of surface altitude. These nonlinear responses may indicate the beginning of a critical transition of the glacier system that signifies the glacier's increasing level of sensitivity to climate forcing.

5. UNDERSTANDING DEBRIS-COVERED GLACIER-CLIMATE SENSITIVITY IN THE CENTRAL KARAKORAM USING ICE-FLOW AND INTEGRATED MODELING

5.1 Abstract

Recent studies have not achieved a general consensus on how debris-covered glaciers (DCGs) in the Karakoram Himalaya respond to climate change. A major question that remains unsolved is how to determine DCG sensitivity to climate forcing because most of them have stable terminus positions due to heavy debris loads, and many "anomalous" glacier responses to climate cannot be explained by existing models due to the use of oversimplified parameterizations and inappropriate assumptions. To address this issue, we developed a more comprehensive numerical model that accounts for ice-flow, ablation, debris-flux, supraglacial lakes, basal erosion, topographic evolution, and multiple feedbacks. Simulation results based on the Baltoro Glacier are analyzed in a tipping-element and tipping-point framework to understand the sensitivity of DCG system to forcing factors. Specifically, we found that: 1) Ice-flow is a critical component that controls the overall dynamics of a DCG because it governs the supraglacial and englacial debris advection, surface topography, glacier erosion, and ice-mass flux from the accumulation zone. 2) DCGs in the Karakoram are actively responding to radiative forcing. More tipping points are identified in a DCG system than in a debris-free glacier system. These tipping points are early indicators of critical transitions that are represented as rapid nonlinear changes in ablation rate and supraglacial lake volume, ice volume, ice-flow speed, and mass balance, and most of the identified tipping points appear after 9 years based on the simulation of the Baltoro Glacier. 3) Our results highlight the positive feedback between lake expansion and ablation which may be the main cause for many nonlinear transitions found in the DCG system. Under the perturbations of positive feedbacks, subsystems of a DCG may experience more critical-state transitions over time that make some DCGs exhibit higher level of sensitivity to radiative forcing than debris-free glaciers, which could be an explanation to the "debris-covered glacier anomaly".

5.2 Introduction

Debris-covered glaciers (DCGs) in the high-mountain Asia play a critical role in governing water resources, natural hazards, mountain geodynamics and landscape evolution [10, 11, 12, 13, 14]. Recent studies have not achieved a general consensus on how these DCGs respond to climate variations [15, 16, 9]. For example, most researchers agree that debris insulation makes the glacier less sensitive to climate change (e.g., [45, 4, 13]), while other observations and simulations, however, show that some DCGs have exhibited accelerated thinning despite the presence of supraglacial debris [31, 32, 16], and some DCGs show an increase in annual ice-flow velocity fields [35, 9]. These "anomalous" glacier responses to climate cannot be explained by existing models, and researchers have attribute that to the oversimplified parameterizations and inappropriate assumptions used in these models [9].

It is difficult to determine if the DCGs are actively responding to climate change because most of them have stable terminus positions due to heavy debris loads. Glacier dynamic states (e.g., stable, retreating, or advancing termini) and mass balance conditions may not accurately reflect the spatio-temporal changes in ice-flow velocities, surface ablation rates, and morphology. This complexity is largely due to the fact that the dynamics of a DCG is governed by numerious interactions between internal and external processes that include climate, mass balance, ice-flow, debris-flux, supraglacial ponding, basal erosion and topographic evolution [119, 19, 17]. Most modeling work on debris-covered glaciers, however, only focuses on a single aspect of the system, such as surface mass balance (e.g., [45, 4, 13, 16]) rather than characterizing the system as a whole. There are two major limitations associated with these studies: 1) Isolating a small number of processes out of the full system increases uncertainty in results, as system couplings and feedbacks can significantly affect glacier dynamics [17, 18]. 2) These studies are often limited in spatio-temporal scale [167], because they rely on instantaneous remote-sensing data or field measurements, such that they do not support multi-year or longer-term simulations in which the glacier conditions (such as ice thickness, debris distribution and topography) would change dramatically. Therefore, in order to study DCG responses to forcing factors, a model must account for all the major glacier

components and address the feedbacks and nonlinear relationships between them.

Ice-flow acts as a bridge connecting all major components of the glacier system, and it has a significant impact on long-term glacier dynamics, as it controls flow velocity, ice topography and glacier geometry which are the foundations for assessing glacier responses to forcing factors [50]. Ice-flow plays a particularly important role in a DCG system because it also controls debris production and transport on the glacier which governs glacier mass balance [17, 18]. Unfortunately, little is known about the dynamics involved, and existing models (e.g., [18]) use over-simplified glacier conditions to simulate the feedback between ice-flow and mass balance. Therefore, we do not know the rates, the pathways and the associated time scales of supraglacial and englacial debris transport due to ice-flow on an actual DCG and how that affects glacier mass balance.

A major question that remain unsolved is how to determine DCG sensitivity to climate forcing, as the traditional mass balance approach overlooks many processes and feedbacks that amplify glacier response to climate, especially for DCGs. Tipping-point analysis could be a promising approach to take, because it helps identify significant positive feedbacks or nonlinear transitions that indicate system sensitivity to forcing factors, and it has been successfully used to study many similar systems that are complex and difficult to predict [168, 169, 170]. Tipping points refer to some critical threshold locations in space and/or time where a small perturbation can cause a large response of the system [168, 169]. This type of nonlinear transition is usually due to positive feedbacks which governs the dynamics of a DCG system (such as the ablation – lake expansion feedback). In this study we evaluate DCG-climate sensitivity based on tipping point analysis and focus on the magnitude and timescale of nonlinear responses and positive feedbacks that signify current or future rapid changes of the glacier system.

The main objectives of this study include: 1) Quantify the impact of ice-flow on glacier mass balance and debris transport. 2) Assess the sensitivity of a DCG system to radiative forcing. This will be achieved by integrating important processes, components (including ice-flow, ablation, debris-flux, supraglacial lake expansion, basal erosion and topographic evolution), and their feedback mechanisms into a more complete numerical model. Simulation results are then analyzed in

a tipping-point framework to evaluate for rapid nonlinear changes in major glacier subsystems to determine if DCGs are more sensitive to radiative forcing than debris-free glacier systems. Simulation results combined with tipping-point analysis are used to determine what aspects of the system may be the early indicators of rapid change to provides new insights into glacier-climate dynamics in the central Karakoram Himalaya.

5.3 Background

5.3.1 Ice-Flow Dynamics

Ice-flow modeling describes the movement of glacier mass by simulating velocities and geometry changes (length, width and thickness) of a glacier. Modeling glacier motion is the key for understanding glacier dynamics [50] and plays a fundamental role in prognostic glacier simulation. For a debris-covered glacier, ice-flow not only governs its velocity and geometry, but also controls debris production and transport. Studies (e.g. [35, 68, 96]) have suggested that the ice-flow can still be very active on a heavily debris-covered glacier even though its terminus is stable (not retreating or advancing).

The flow velocity of a glacier is governed by ice thickness, which is determined by surface and bed topography. Unlike the wide availability of DEMs, accurate bed topography is difficult to estimate, therefore, the knowledge of bed topography is essential in ice-flow models [50]. Direct measurements of the bed topography heavily depend on geophysical surveys (e.g. seismic, radio sounding), which are usually time-consuming and expensive [97]. Numerical modeling, on the other hand, provides different solutions to this problem. For example, studies have indicated that ice thickness can be estimated from mass conservation equation using apparent mass-balance distribution in the ice-flow catchments [98]. Mass-balance distribution, however, can be difficult to estimate, especially for debris-covered glaciers. Therefore, many modelers use surface velocities to infer ice thickness (e.g. [99, 97]), and associated optimization approaches have also been developed to improve accuracy [100]. Many of these methods are discussed briefly by [101], who concluded that ice thickness estimates are strongly dependent on the quality of input data, and

the choice of parameters, therefore, large uncertainty exist in most ice thickness estimates. The glacier velocity distribution and geometry evolution can be modeled using the shallow ice approximation (SIA) once the ice thickness is known [102, 103, 104, 18]. Generally, SIA assumes no debris cover and non-sliding at the bed. It is a second-order approximation approach and produces reasonable results compared to observations of large ice sheets (e.g., [106, 107]). Some recent studies, however, argue that modeling glaciers in steep mountain ranges can be inaccurate using the traditional SIA due to complex topography [108]. An ice-flow model also serves as the foundation for simulating glacier erosion. Herman et al. [103] indicated that the integration of ice-flow and erosion models can accurately delineate the evolution of alpine valleys, and their simulation results successfully characterized erosion patterns governed by glacial cycles, which demonstrated the capability to study alpine geomorphology. More advanced ice-flow models also take basal melt and temperature adjusted ice properties into account and are mathematically more suitable for long-term high-resolution simulation (e.g., [104]).

Ice-flow not only transports ice, but also transports debris from active erosion zone to depositional basins [50]. A complete picture of glacial debris transport consists of surface debris, englacial debris and basal debris [78]. Due to our limited knowledge of basal processes, most numerical models only consider the supraglacial and englacial debris transport (e.g. [18]). The most recent ice-flow-based debris transport model was developed by Anderson and Anderson [18]. They modeled englacial and supraglacial debris advection under a steady debris input to understand the mechanisms in the debris–glacier–climate system. Simulations indicated that debris has significant control on glacier length and gradients of ice discharge, ice thickness, and surface velocities. They also demonstrated that there are strong connections between ice-flow and glacier mass balance distribution due to the transport of debris.

5.3.2 Tipping Elements and Glacier Systems

Tipping elements refer to large-scale components of the Earth system that may pass a critical threshold in the spatial and-or temporal transition of system states, where a small perturbation can cause a large response, and those critical thresholds are called “tipping points” [168]. Tipping

points are considered as important early warning signals [168, 171] and tipping-elements analysis provides valuable insights into system sensitivity to climate change [168].

Tipping-point analysis has been used to study system sensitivity to forcing factors in climate, geomorphological and ecological systems [168, 172, 171] because tipping-point analysis is able to capture the key information (e.g., spatio-temporal scale, controlling parameters and critical values) in system responses that are governed by positive feedbacks and nonlinear transitions [168, 169, 170]. Most importantly, studies have demonstrated that tipping-point analysis is particularly useful in understanding cryosphere-climate sensitivity. Lenton et al. [168] suggests that Arctic summer sea-ice, Greenland and Antarctic ice sheets are among the most important tipping elements in Earth's climate system. Sea-ice area and ice sheet volume exhibit tipping mostly due to the positive feedbacks within the system, for example, the ice-albedo positive feedback governs multiple state transitions of sea-ice cover [173]. The positive feedback between ice altitude, melting, and increasing surface temperature causes nonlinear state transitions in the volume of the Greenland ice sheet [168]. Consequently, we might expect that tipping-point analysis of alpine glaciers can also be very important as they are governed by climate forcing and exhibit numerous positive feedbacks related to controlling factors [36, 15, 9].

Another advantage of tipping-point analysis is the capability of detecting early warning signals [168, 171]. Many studies have found that tipping points can predict critical-state changes in systems such as ice and snow cover, ocean circulation, soil moisture and forest cover [168, 172, 171]. These early warning signals are extremely valuable in policy-making regarding sustainability, food security, natural hazards, and climate change [168, 171].

From a methodological perspective, statistical metrics have been used in tipping-point analysis to identify locations in space and time that are considered important system transitions. Many metrics have been used to detect tipping points including autocorrelation, variance, skewness, standard deviation, thresholding, Kurtosis, BDS test and many model-based indicators. Among these metrics, autocorrelation and variance are the two most widely used indicators [171]. The autocorrelation and variance theoretically should increase when the system approaches a critical transition

[172, 171], and several studies have successfully detected system tipping points using autocorrelation and variance [174, 175, 176, 177, 178].

In this study, tipping-point analysis is used to analyze glacier-subsystem dynamic transitions as a proxy for glacier sensitivity to radiative forcing because traditional metrics such as terminus states (e.g., stable, retreating, or advancing) and mass balance estimates may not accurately reflect the DCG's sensitivity to climate forcing. These metrics characterize the overall magnitude of glacier geometry and mass gain/loss and do not account the dynamic spatio-temporal changes in process rates and glacier subsystems. As a climate-driven system controlled by subsystem couplings and feedbacks [38, 52, 17], a DCG system represents an ideal target for tipping-point analysis similar to ice sheets where tipping-point analysis has been successfully used.

We characterize the fundamental tipping elements and subsystem/system components that most likely will exhibit tipping points. Table 5.1 itemizes the tipping elements for a DCG system, which features multiple subsystems, control parameters and critical values and scale dependencies in terms of spatial and temporal transition scales, that govern glacier sensitivity to change. The climate system includes irradiance (E), precipitation (P), and air temperature (T_a), that are the main forcing factors. Five subsystems are evaluated for a DCG: surface ablation, ice volume, supraglacial lakes, ice-flow, and mass balance. Finally, the system is also influenced by tectonics including uplift and deformation. Understanding the timescale and spatial scale of state transitions is important because they allow us to compare with other tipping elements in the climate system, and rank the sensitivity of each tipping element to climate change to help us decide which one needs the greatest attention. Unfortunately, we do not know the spatial and temporal scales of such transitions and the associated critical values (β_{crit}) for most of the subsystems, and this study will provide the first attempt to evaluate them.

Tipping Element	Subsystems	Main Control Parameters	Spatial Scale: β_{crit}	Timescale: β_{crit}
Climate System	Irradiance (E)	Orbit, cosi, z	$\frac{dE}{dz} : NA$	$\frac{dE}{dt} : NA$
	Precipitation (P)	V_w, ρ_w, v_{wind}	$\frac{dP}{dz} : NA$	$\frac{dP}{dt} : NA$
	Air temperature (T_a)	Orbit, Gases, z	$\frac{dT_a}{dz} : NA$	$\frac{dT_a}{dt} : NA$
Glaciological System	Ablation (a)	E, z, h_d, V_{lw}	$\frac{da}{dz}$: ?	$\frac{da}{dt}$: ?
	Ice volume (V_i)	a, P, v_i	$\frac{dV_i}{dz}$: ?	$\frac{dV_i}{dt}$: ?
	Lakes (V_{lw})	a, θ_t	$\frac{dV_{lw}}{dz}$: ?	$\frac{dV_{lw}}{dt}$: ?
	Ice-flow (v_i)	V_i, H, θ_t	$\frac{dv_i}{dz}$: ?	$\frac{dv_i}{dt}$: ?
	Mass balance (MB)	a, V_{lw}, V_i, h_d	$\frac{dMB}{dz}$: ?	$\frac{dMB}{dt}$: ?
Tectonics	Uplift			
	Deformation	NA	NA	NA

Table 5.1: Composition of the tipping elements in a DCG system. The spatial and temporal scales of critical transitions are not known with any certainty. z is glacier surface elevation, V_w and ρ_w are the volume and density of atmospheric water vapor respectively, v_{wind} is wind speed, h_d is debris thickness, H is ice thickness, θ_t is the slope of the glacier. NA represents parameters and scales that are not evaluated in this study.

5.4 Methods

5.4.1 Data

In this study, we based our simulations on the actual conditions of the Baltoro Glacier in the central Karakoram. The Baltoro Glacier is an ideal simulation target because quantitative estimates of surface ablation rates, debris-thickness and supraglacial lake distributions have been produced (e.g., [6, 4, 127, 23]). As one of the largest debris-covered glaciers in the world, its surface velocity can be easily derived from satellite imageries [35].

Initial surface topography conditions and land-surface parameters were derived from a 30m digital elevation model (DEM), the DEM was generated based on the use of stereo-correlation

from ASTER satellite imagery using SILCAST software. The glacier surface velocity (Figure 5.1) is estimated from Landsat-8 satellite imageries using the Co-registration of Optically Sensed Images and Correlation (COSI-Corr) software package [5] from a Landsat-8 OLI panchromatic image pair acquired on September 15, 2004 and September 2, 2005.

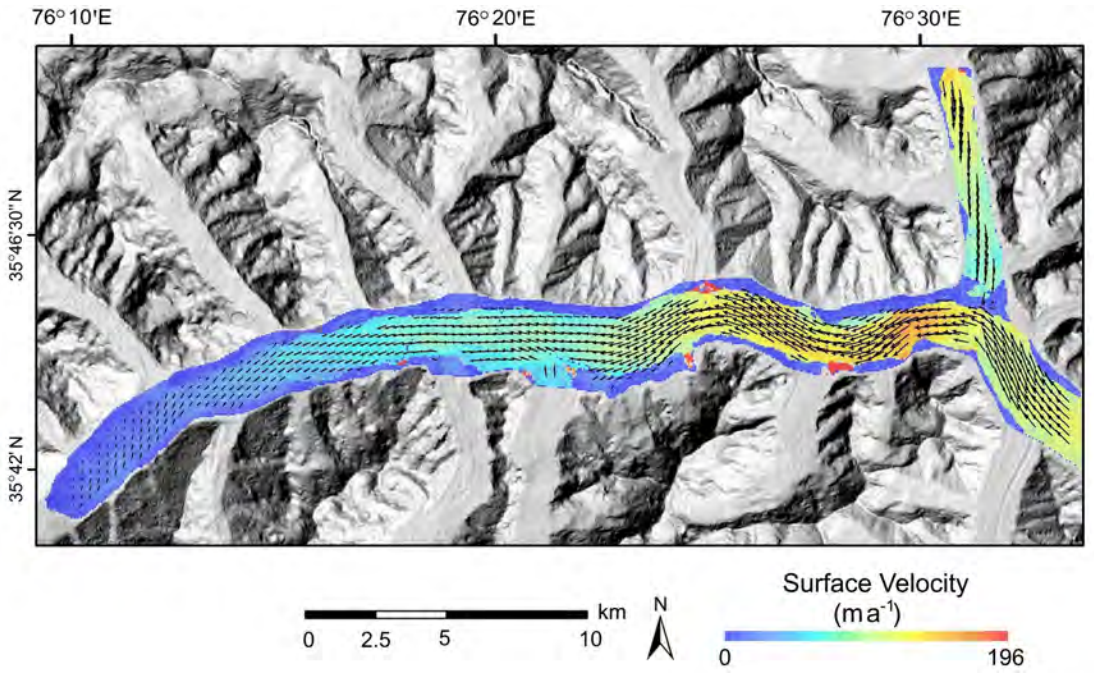

Figure 5.1: Initial surface velocity of the Baltoro Glacier estimated from a Landsat-8 OLI panchromatic image pair acquired on September 15, 2004 and September 2, 2005.

The climate data used in this study accounts for the monthly variations in air temperature and precipitation, which are based on the ERA-Interim100 regional average temperature and precipitation for the period 1989–2007 over the Karakoram, provided by Farinotti et al. [9]. (Figure 5.2). For multi-year simulations, the air temperature is adjusted using the Representative Concentration Pathway (RCP) 8.5 model [32] to account for projected atmospheric warming.

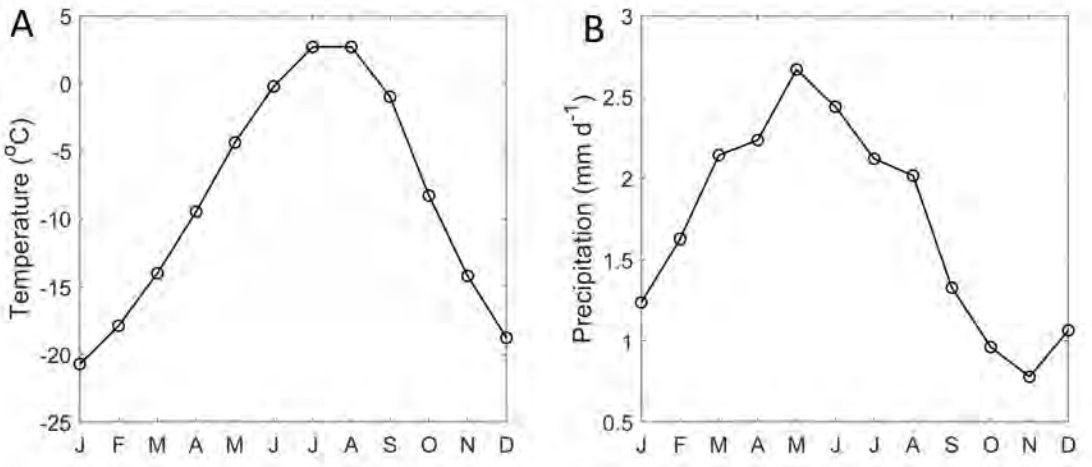

Figure 5.2: Temperature and precipitation trends used for simulations over the Baltoro Glacier. (A) Monthly air temperature varation. (B) Precipitation in the Karakoram region from 1989–2007 (after Farinotti et al. [9]).

5.4.2 Modeling

5.4.2.1 Surface Ablation

The surface ablation dynamics is simulated based on the surface energy balance and ablation model developed in Chapter 3 (equations 3.1 - 3.15), which accounts for shortwave irradiance, surface energy balance at debris-ice interface, surface albedo variation, and topographic evolution. This model provides more accurate ablation estimates compared to existing models, because: 1) Local and meso-scale topographic effects of surface irradiance are accounted for; 2) Surface temperature is continuously modeled rather than being restricted by instantaneous remote-sensing data; and 3) A sediment mineral and meltwater mixing model is used to account for the dynamic variation of glacier-surface albedo. Supraglacial sediment movement is a critical process that influences surface ablation dynamics on a DCG because it controls the thickness and mineralogical distribution of supraglacial sediments which governs ablation. In this study, gravitational sediment fluxes are simulated using the model developed in Chapter 3 (equation 3.16 - 3.23).

5.4.2.2 *Supraglacial Lakes*

This model accounts for supraglacial lakes as they have a significant impact on the ablation dynamics of a DCG. The ablation caused by supraglacial lakes are simulated using the model described in Chapter 4 (equation 4.1 – 4.4). The formation and development of lakes are also controlled by surface drainage conditions which is simulated using the supraglacial drainage model described in Chapter 4 (equation 4.5 – 4.6).

5.4.2.3 *Ice-Flow Dynamics*

Ice-flow characterizes the velocity field, mass distribution and debris transport of the glacier [17, 18]. The mass-continuity equation is the foundation of an ice-flow model:

$$\frac{\partial H}{\partial t} = M_g - \nabla \cdot \mathbf{Q}, \tag{5.1}$$

where H is the ice thickness, and M_g is the glacier mass balance. The flow of ice is characterized by a velocity field (u_x,u_y,u_z), which consists of the vertical velocity u_z and the horizontal velocities $\mathbf{U}$(u_x,u_y). The horizontal ice flux $\mathbf{Q}$ is a product of ice thickness and the vertically averaged horizontal velocity $\overline{\mathbf{U}}$:

$$\mathbf{Q} = \overline{\mathbf{U}} H. \tag{5.2}$$

Based on the widely used shallow-ice approximation (SIA) [102, 36], the horizontal velocity field (assuming non-sliding) can be written as [104]:

$$(u_x, u_y) = -\frac{2A(\rho_i g)^n}{n+1}[H^{n+1} - (z_i - z)^{n+1}] \mid \nabla z_i \mid^{n-1} \nabla z_i, \tag{5.3}$$

where u_x is the parallel-to-flowline component of the velocity field, u_y is the perpendicular-to-flowline component of the velocity field, A is the ice-flow factor (ice softness), which is assumed to be a constant ($9.5066 \times 10^{-24} Pa^{-3} s^{-1}$) in this study, ρ_i is the density of ice, g is gravitational acceleration, n is the stress exponent (a typical value of $n = 3$ is used), z is the elevation at which

the velocity is computed (such that $H-z$ is the depth within the ice), and z_i is ice-surface elevation.

Glacier surface velocities can be used to infer ice thickness [97, 99], in this study, ice thickness is estimated from the remote-sensing derived surface velocity by solving equation (5.3) at glacier surface:

$$H = \left[\frac{(n+1)u_x}{2A(\rho_i g sin\theta_t)^n}\right]^{\frac{1}{n+1}}, \tag{5.4}$$

where θ_t is overall slope angle of the glacier, which is assumed to be equal to the slope of the best-fit plane of the glacier surface. Figure 5.3 is the estimated ice thickness from the remote-sensing derived surface velocity using this equation.

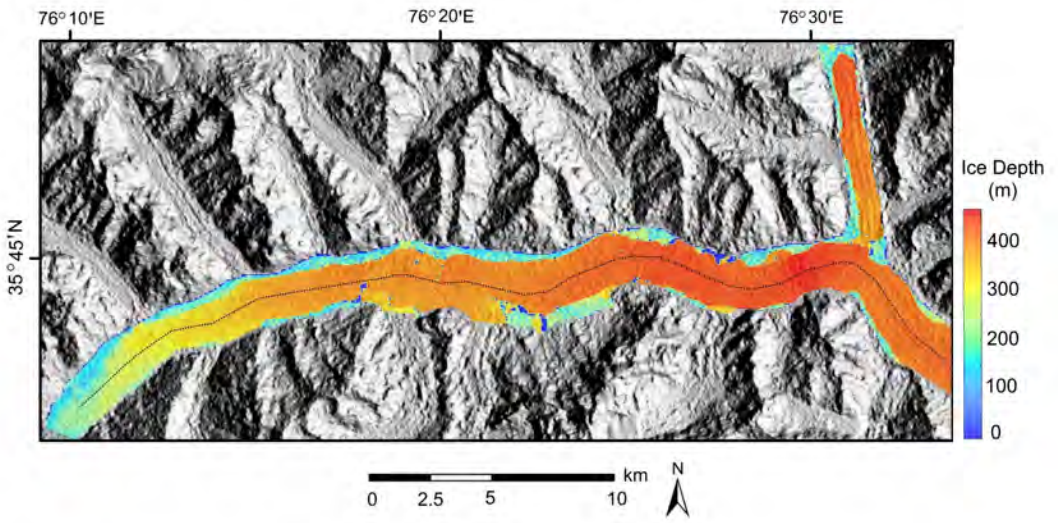

Figure 5.3: Modeled ice thickness for Baltoro Glacier superimposed on shaded-relief map. The black line in the center of the glacier represents the glacier flowline.

Based on the incompressibility of ice and non-sliding assumption, the vertical velocity at given depth z along the flowline can be computed by integrating the horizontal velocity [104]:

$$u_z = -\int_0^{H-z} \nabla \cdot u_x d\zeta, \tag{5.5}$$

After substituting equation (5.2) and equation (5.3) into equation (5.1), we have the equation that describes the rate of ice-thickness change over time under the SIA:

$$\frac{\partial H}{\partial t} = M_s + \nabla \cdot (\frac{2A(\rho_i g)^n}{n+1} H[H^{n+1} - (z_i - z)^{n+1}] \mid \nabla z_i \mid^{n-1} \nabla z_i). \tag{5.6}$$

This equation is implemented using an adaptive time-step finite differencing approach [104] to ensure stability during long-period simulation. Englacial ice velocity is modeled based on equations 5.3 and 5.5 along the flowline, and serve as a basis for englacial debris transport simulations. Figure 5.4 shows the modeled velocity profiles on horizontal and vertical directions respectively. Note that in this study, the transverse component of the horizontal velocity is neglected, therefore, the direction of the horizontal velocity is parallel to the flowline.

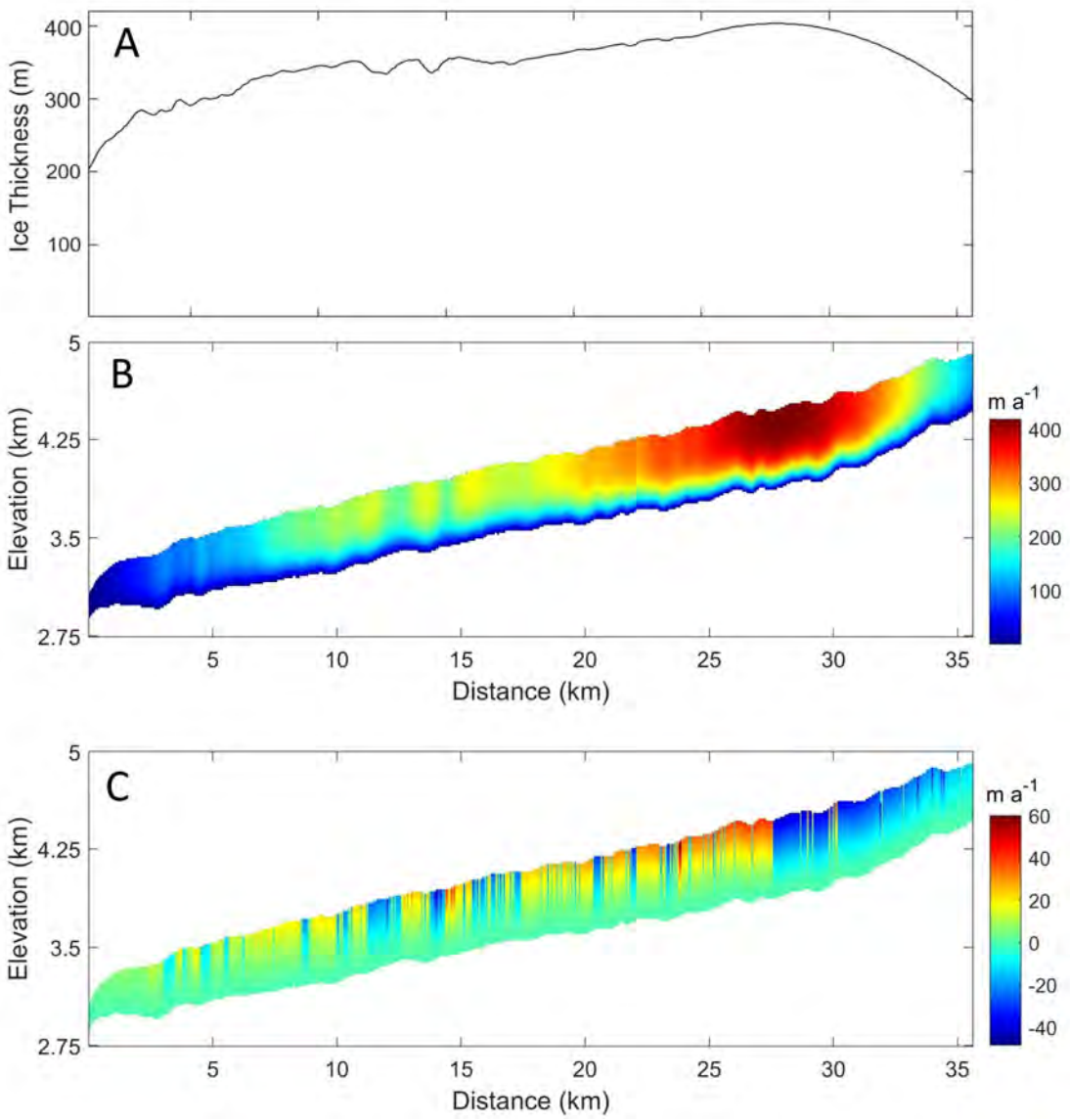

Figure 5.4: Modeled ice thickness and englacial ice-flow velocity profiles along the flowline of the Baltoro Glacier. (A) Ice thickness distribution along the flowline. (B) Horizontal ice-flow speed distribution based on equation5.3. (C) Vertical ice-flow speed distribution (positive on upward direction) based on equation5.5.

5.4.2.4 Debris Advection

The transport of supraglacial debris from high-altitude regions to the terminus under ice-flow is governed by the velocity field at the glacier surface. This type of mass movement can be modeled as an advection process:

$$\frac{\partial h_d}{\partial t} = -\nabla \cdot (h_d \mathbf{u_s}), \tag{5.7}$$

where h_d is the thickness or concentration of surface debris, t is time, and $\mathbf{u_s}(u_x, u_y)$ is surface ice-flow velocity. Similarly, englacial debris can also be modeled as an advection process following the approach by Anderson and Anderson [18]:

$$\frac{\partial C}{\partial t} = -\frac{\partial (u_x C)}{\partial x} - \frac{\partial (u_z C)}{\partial z} - \frac{C}{h_c}\frac{\partial h_c}{\partial t} - \frac{u_x C}{h_c}\frac{\partial h_c}{\partial x}, \tag{5.8}$$

where C is the debris concentration in each cell and u_x and u_z are the horizontal and vertical ice velocities, respectively. h_c is the cell height in a given ice column. The first and second terms on the right represent the advection process. The third and fourth terms represent the variations of debris concentration due to vertical and longitudinal ice thickness changes. The use of advection is valid for glacial debris transport because advection is defined as the transport of a substance due to the bulk motion of a fluid, and glacier ice is a form of a viscoelastic fluid that is the basis for all modern glacier modeling studies.

Supraglacial debris input is accounted for using constant headwall and sidewall deposition rates, specifically, a headwall erosion rate of $5 mma^{-1}$ and a sidewall erosion rate of $1 mma^{-1}$ are used based on the 1-8mma^{-1} range suggested by Anderson and Anderson [18]. Note that this model does not account for ice and debris input from tributaries. Also note that this approach does not support 3-dimensional englacial debris transport as the transverse component of the flow velocity is not accounted for. Therefore, englacial debris transport is only simulated on the profile along the flowline.

5.4.2.5 Basal Erosion

Basal erosion is accounted for in this model as it modifies topography and contributes debris in the glacier system. Glacial erosion is thought to scale with ice-sliding velocity at the ice-bedrock interface, and the erosion rate ε can be written as [109, 112]:

$$\varepsilon = K_g u_{bs}^{l}, \tag{5.9}$$

where K_g is the glacial erosion constant, which is set to be 0.01 following Tomkin and Braun [112], u_{bs} is the basal-sliding velocity (in this case, it is always a non-negative value along the flow line), the exponent l is taken to be 1 based on [111, 112]. The basal-sliding velocity is estimated as [113]:

$$u_{bs} = u_0 e^{1-\frac{\tau_c}{\tau_b}}, \tag{5.10}$$

where u_0 is the typical sliding velocity ($5 - 20myr^{-1}$), τ_c is the reference basal stress ($10^5 Pa$), and τ_b is the basal shear stress, which is computed as [36]:

$$\tau_b = C\rho_i g H \theta_t, \tag{5.11}$$

where C is a constant to account for effects of sidewall drag, which is set to be 0.75 following Anderson and Anderson [18].

5.4.3 Model Integration

In order to more accurately characterize a DCGs' response to forcing factors, the model used in this study is an integration of all the important processes, components, and their feedback mechanisms (Figure 5.5). Specifically, this model accounts for the radiation-driven surface ablation, gravitational debris-flux, debris mixing, and supraglacial lake development as discussed in previous chapters. These components are then integrated into the ice-flow framework, which accounts for glacier mass movement, supraglacial and englacial debris advection, basal erosion, and topographic evolution.

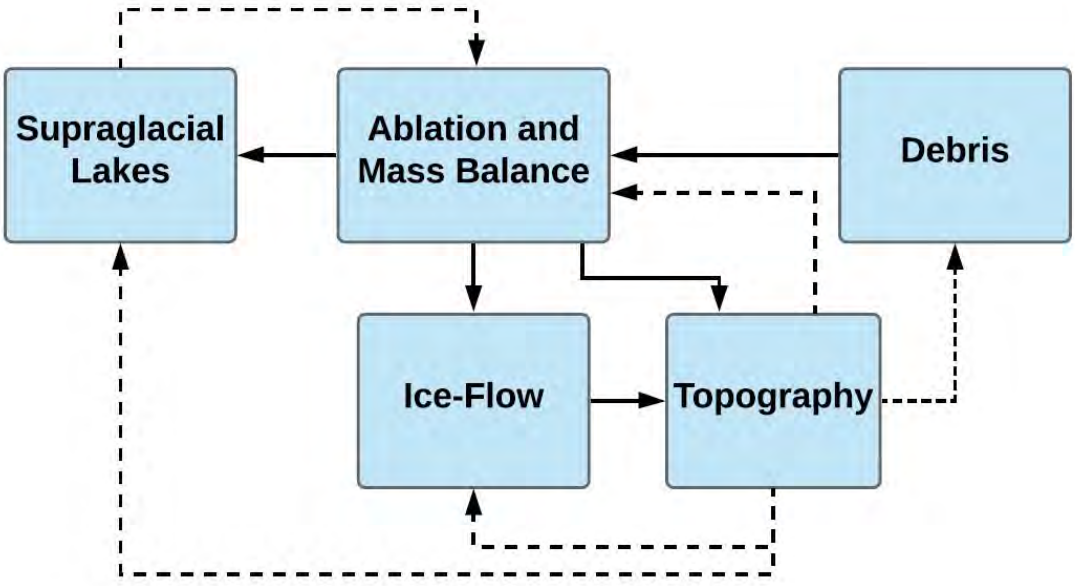

Figure 5.5: Diagram illustrating the key components of the model and the feedbacks (dashed lines) between them. Positive feedbacks are important components in the model because they can lead to critical-state transitions in subsystems that signify a glacier's increasing sensitivity to climate change.

5.4.4 Tipping-Point Analysis

The glacier's sensitivity to climate forcing is evaluated using tipping-point analysis. Specifically, we identify tipping points that serve as early indicators of critical state transitions in major subsystems (as listed in Table 5.1). We analyzed both temporal variations and spatial variations for each subsystem. From a temporal perspective, spatially averaged values are presented as a function of time. From a spatial perspective, the data is averaged temporally, and then presented as a function of altitude using the spatial mean with a 30m altitude bin. The curves are also preprocessed using a Gaussian filter to remove local high frequency variations.

A tipping point index (I) that combines autocorrelation (AC) and the coefficient of variance (COV) is used to identify tipping points. The metrics AC and COV were selected because they are the two most widely used tipping point indicators, and are easy to compute and involve less subjectivity than threshold-based metrics. Theoretically, both AC and COV should increase when

the system approaches a critical transition [172, 171]. We define the index as:

$$I = \begin{cases} S_{AC} \cdot S_{COV}, & \text{if } S_{AC} > 0 \text{ and } S_{cov} > 0 \\ 0, & \text{if } S_{AC} \leq 0 \text{ or } S_{cov} \leq 0 \end{cases} \tag{5.12}$$

where S_{AC}, S_{COV} are the slope angles (positive for an increasing trend) within a sliding window for the autocorrelation and coefficient of variance respectively. All metrics are calculated using a sliding window with a size of 1/16 of the original data length. Second derivative is also used to help signify state changes in system because tipping points are early warning signals, such that the critical transition is represented as a sign change of the second derivative that follows the tipping point.

5.4.5 Simulation Scenarios

Multiple scenarios (Table 5.2) are simulated to better understand DCGs' responses to ice-flow and climate variations over time. These simulation scenarios are divided into three groups based on the associated research objectives.

The first group contains a 100-year simulation (S5.1) that addresses the influence of ice-flow on debris transport and basal erosion. Specifically, this 100-year simulation is performed with an adaptive-time-step approach (the average time-step is 0.1 year) under a constant mass balance condition, and we focus on three aspects of this simulation: 1) The magnitude and timescale of supraglacial debris transport due to ice-flow; 2) The pathways and timescale of englacial debris (originated from headwall erosion) transport due to ice-flow; 3) The magnitude of basal erosion and the timescale for basal debris (originated from basal erosion) to emerge on glacier surface.

The second group of simulations (S5.2a - S5.3b) investigates the influence of ice-flow on glacier mass balance and surface morphometry. They are simulated for 10 years at two-hour time step. Specifically, S5.2a and S5.2b represent the default simulations with ice-flow under debris-covered condition and debris-free condition respectively, S5.3a and S5.3b represent the simulations without ice-flow under debris-covered condition and debris-free condition respectively. The tip-

ping point analysis focuses on simulations S5.2a and S5.2b, which represent the realistic scenarios for DCG and DFG respectively.

Simulation	Debris-load	Ice-flow	Time step	Simulation period
S5.1	Debris-covered	Yes	Varying (0.1-yr in average)	100 years
S5.2a	Debris-covered	Yes	2-hr	10 years
S5.2b	Debris-free	Yes	2-hr	10 years
S5.3a	Debris-covered	No	2-hr	10 years
S5.3b	Debris-free	No	2-hr	10 years

Table 5.2: List of simulation scenarios used to provide insight into the impacts of ice-flow on glacier dynamics.

5.5 Results

5.5.1 Supraglacial Debris Transport due to Ice-flow

The advection of supraglacial debris due to the ice velocity field is simulated over the Baltoro Glacier (Figure 5.6) starting from 2004 using the initial debris distribution, surface velocity and ice thickness estimates.

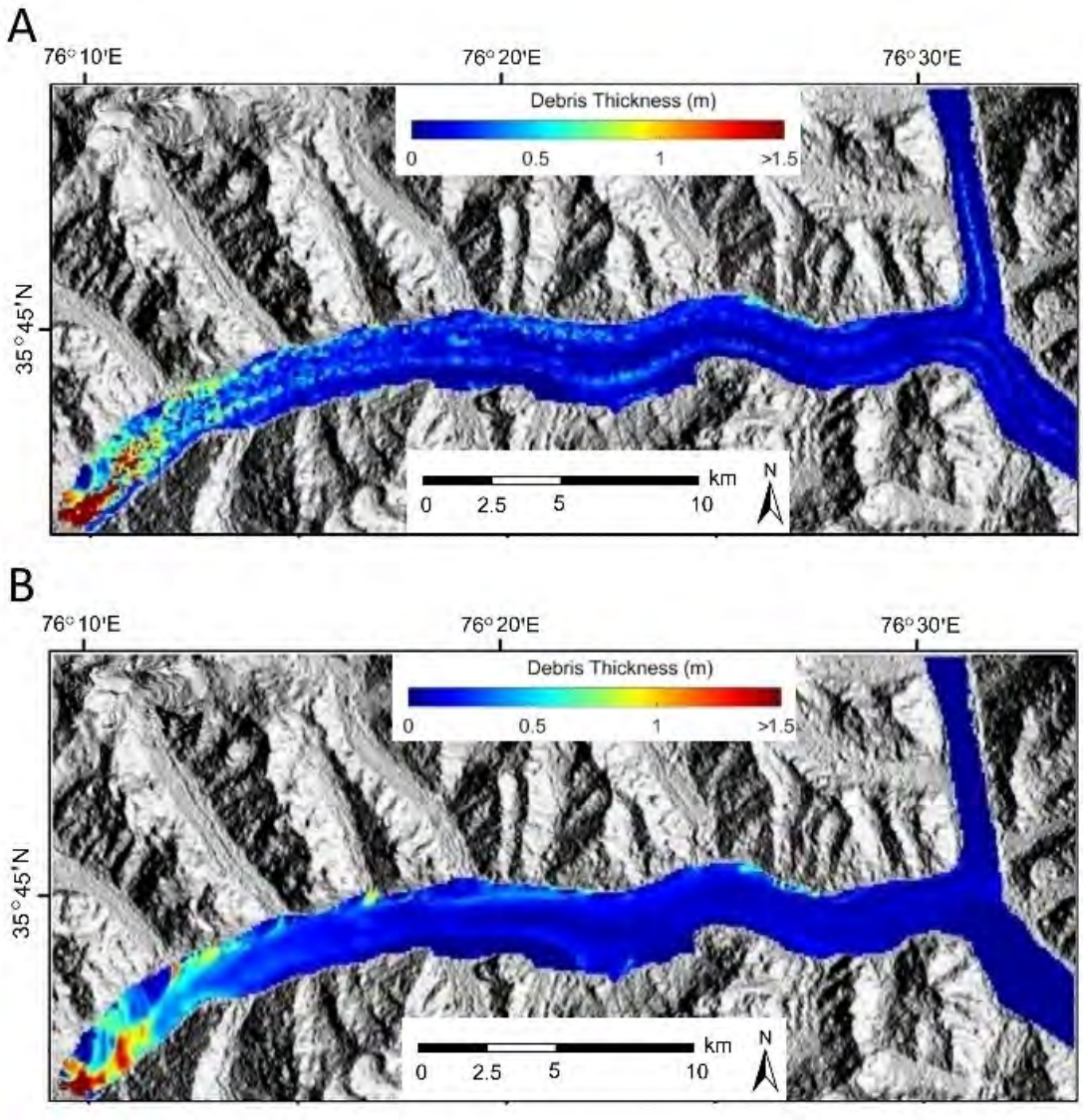

Figure 5.6: Simulated advective supraglacial debris transport (represented by debris thickness distribution) due to ice-flow on the Baltoro Glacier. (A) The initial debris-thickness distribution. (B) The debris-thickness distribution after 50 years.

Figure 5.6 shows the variation of supraglacial debris distribution in 50 years. Result indicates that terminal debris is not completely stagnant, supraglacial sediments can still exit the glacier from the terminus (although very slowly). Based on this simulation of the Baltoro Glacier, the average supraglacial debris-flux rate is 5554 m^3a^{-1}. The actual flux rate could be higher because other processes such as the fluvial system and gravitational sediment flux will also contribute to

the transport of sediments.

5.5.2 Basal Erosion and Englacial Debris Transport

We simulate the englacial debris transport and basal erosion along the flowline profile of the Baltoro Glacier over 100 years to understand the pathways and associated time scales of englacial debris transport that originated from headwall erosion and basal erosion.

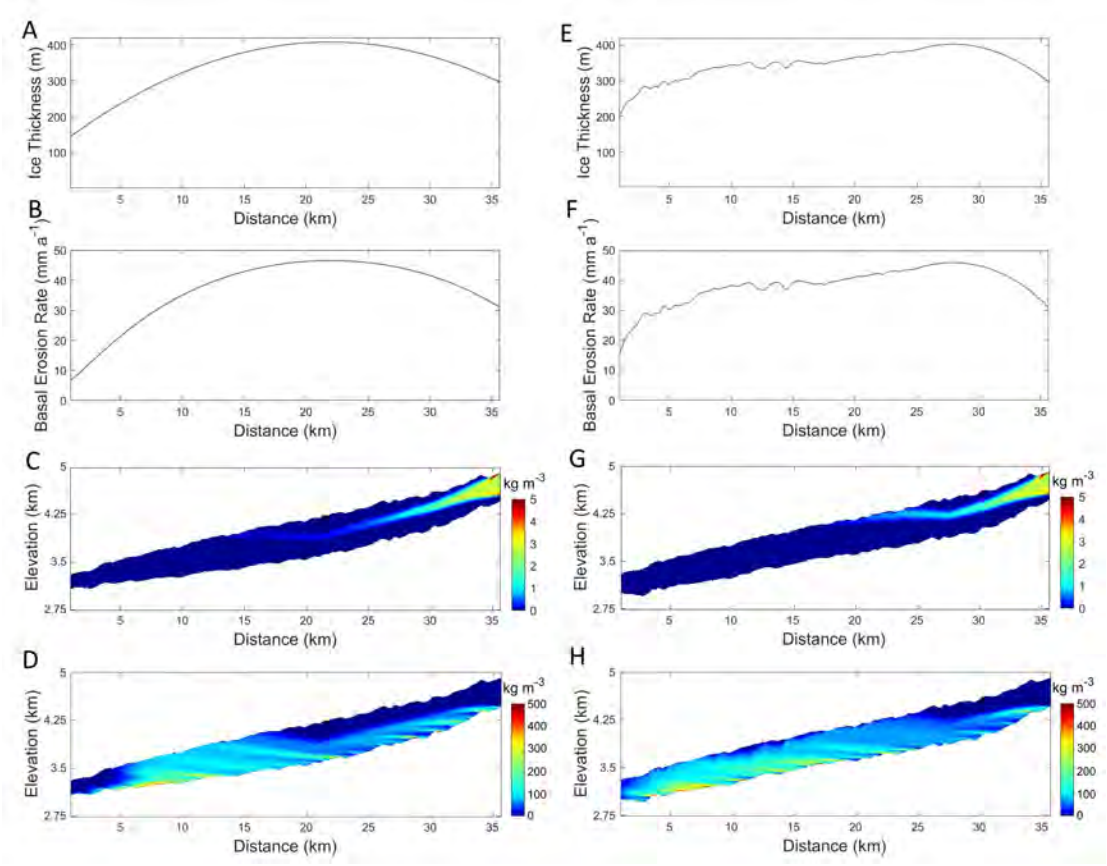

Figure 5.7: Englacial debris transport and basal erosion simulations along the flowline of the Baltoro Glacier. (A) Hypothetical ice thickness distribution along the flowline. (B) Simulated basal erosion rates. (C) Simulated englacial debris concentration for debris originated from headwall. (D) Simulated englacial debris concentration for debris originated from basal erosion. E-H represent the simulation based on a more realistic (remote-sensing surface velocity derived) ice thickness. The simulations start with no englacial debris and the results represent the debris conditions after 100 years

Simulations suggest that the basal erosion rate (Figure 5.7B, F) is highly correlated with ice thickness (Figure 5.7A, E), such that the highest erosion rate (46mm per year) corresponds to the maximum ice thickness, which is typically located near the equilibrium-line altitude (ELA), because thick ice near the ELA causes faster ice flow that magnifies erosion. This correlation between the ice-thickness distribution and erosion rate is known to exist on most alpine glaciers [115, 116].

Figure 5.7C, G and Figure 5.7D, H show the distribution of englacial debris that originated from headwall and basal erosion respectively, and table 5.3 lists the time it took for the englacial debris to first emerge at the surface under each scenario. As the ice thickness starts to decrease below the ELA, englacial debris loads are advected towards the glacier surface. The location of the ELA affects the emergence location of englacial debris, such that if there is a greater distance between the ELA and the headwall (Figure 5.7C), the englacial debris loads travel a longer distance before they emerge on the surface at lower altitudes. If the ELA is closer to the headwall (Figure 5.7G), the englacial debris loads travel a shorter distance, and therefore they can emerge on the surface at higher altitudes. The high ELA scenario also creates larger altitude range for basal debris to emerge on the surface (Figure 5.7H as compared to Figure 5.7D). The englacial debris distribution also suggests that more englacial debris will be exposed as surface ablation accelerates, and the surface debris concentration is likely to increase over time as indicated by many studies (e.g., [93, 80, 18]).

ELA Location	Debris Source	Surface Emergence
Low (Figure 5.7 C)	Headwall erosion	68 years
High (Figure 5.7 G)	Headwall erosion	36 years
Low (Figure 5.7 D)	Basal erosion	37 years
High (Figure 5.7 H)	Basal erosion	37 years

Table 5.3: Timescale for englacial debris to first emerge on glacier surface under different scenarios.

5.5.3 Ice-flow and Mass Balance

Ice-flow redistributes the glacier mass [36]. To quantify the impact of ice-flow on the glacier mass balance, simulations with and without ice-flow are compared. The influence of ice-flow on mass balance is reflected by ice volume differences.

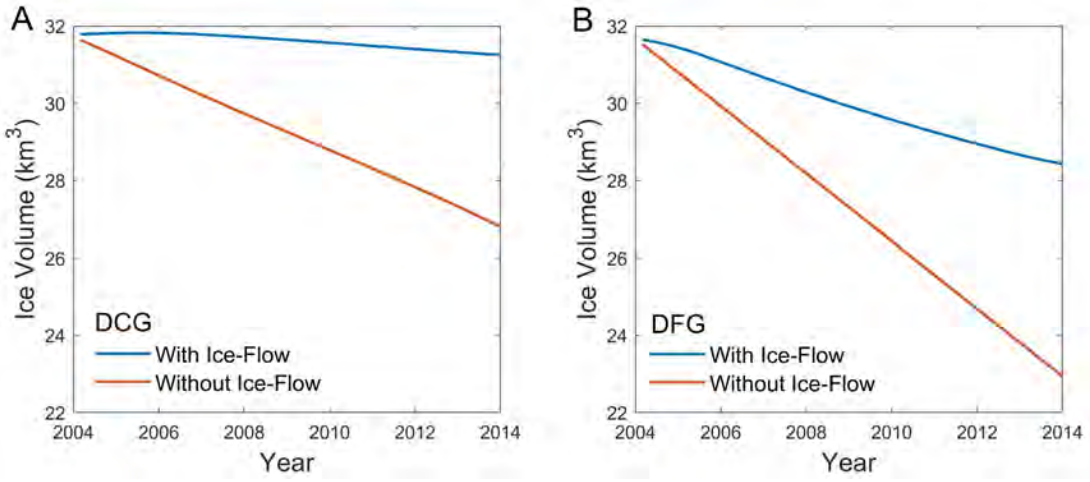

Figure 5.8: The impact of ice-flow on glacier mass balance is reflected by ice volume differences between the simulations with and without ice-flow. The difference is mostly due to ice mass influx from the accumulation zone. The neglection of mass influx in a pure ablation model can cause a significant overestimation of the ice volume loss.

Figure 5.8 demonstrates that ice-flow has a significant impact on ice volume change. For the DCG and the DFG, the ice volume losses are overestimated by $4.45km^3$ and $5.48km^3$ respectively if the ice-flow is neglected, because ice-flow transports large amount of ice mass from the accumulation area into the ablation zone. Neglection of mass influx causes an overestimation of the ice volume loss, and this overestimation becomes more and more significant as the time scale of the simulation expands. Simulations suggest that ice-flow also influences the surface ablation rate (Figure 5.9A) and surface topography (Figure 5.9B). There is slight increase in ablation when ice-flow is accounted for, which is mostly likely due to more active debris-flux and topographic changes caused by the ice-flow.

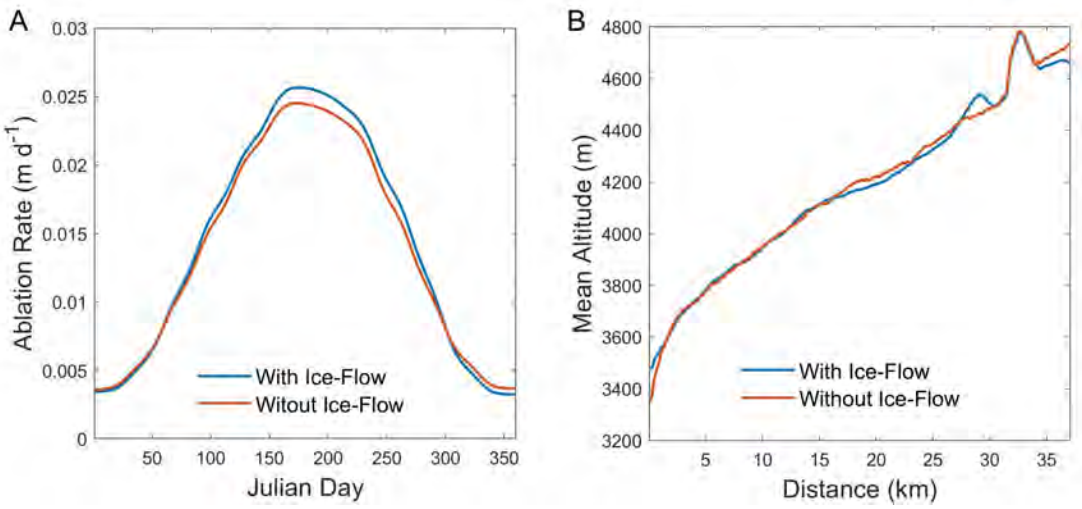

Figure 5.9: Simulated ablation rate and surface altitude variations as a function of including and not including ice-flow.(A) Comparison of the mean ablation rates on a DCG with and without ice-flow. (B) Comparison of mean glacier surface altitudes on a DCG with and without ice-flow at the end of a one-year simulation.

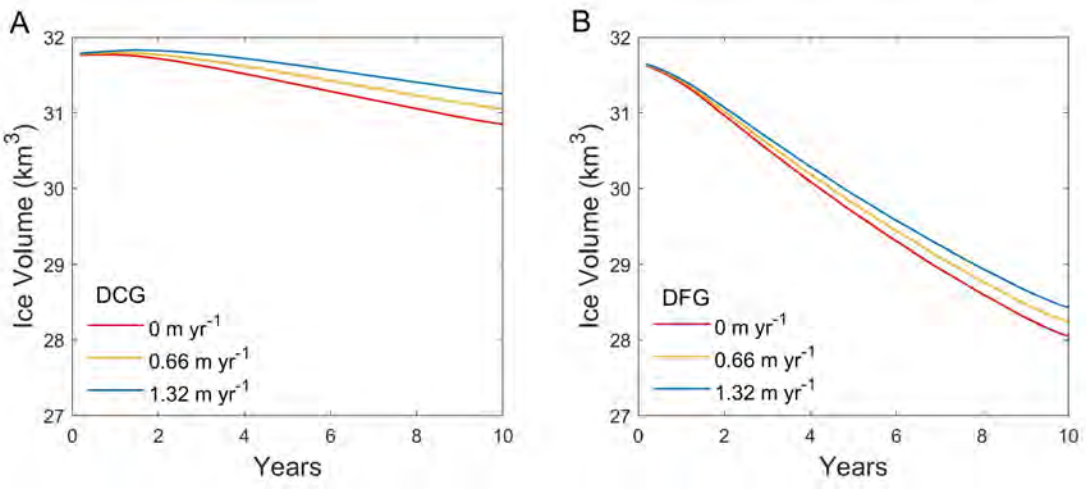

Figure 5.10: Ice volume variations in response to different levels of precipitation rates in the accumulation zone. The debris-covered glacier (DCG) is slightly more sensitive to the change in precipitation than the debris-free glacier (DFG).

Simulations under different precipitation rates (Figure 5.10) suggest that the DCG is slightly

more sensitive to variations in precipitation than the DFG. Both glaciers show positive correlation between ice volume and precipitation rate. The ice volume of the DCG increases by $0.180km^3$ as response to a 1m increase in annual precipitation, which is slightly higher than the $0.173km^3$ on the DFG. A DCG may be slightly more sensitive to precipitation change possibly due to the fact that the reduced ice-flow velocity and the lower ablation rate in the ablation zone of a DCG delays the transport and melting of newly accumulated ice.

5.5.4 Tipping-Point Analysis

5.5.4.1 Surface Ablation

The surface ablation variability in response to climate forcing is evaluated using tipping-point analysis on temporal variations over one ablation season (Figure 5.11) and over a 10 year period (Figure 5.12). A tipping point is identified using the tipping-point index (I), and the critical-transition zone is highlighted with a gray box, which represents a major state change (as indicated by the second derivative). Tipping-point analysis is conducted for both DCG and DFG simulations. Tipping points were also identified based on critical transitions in spatial variations (Figure 5.13).

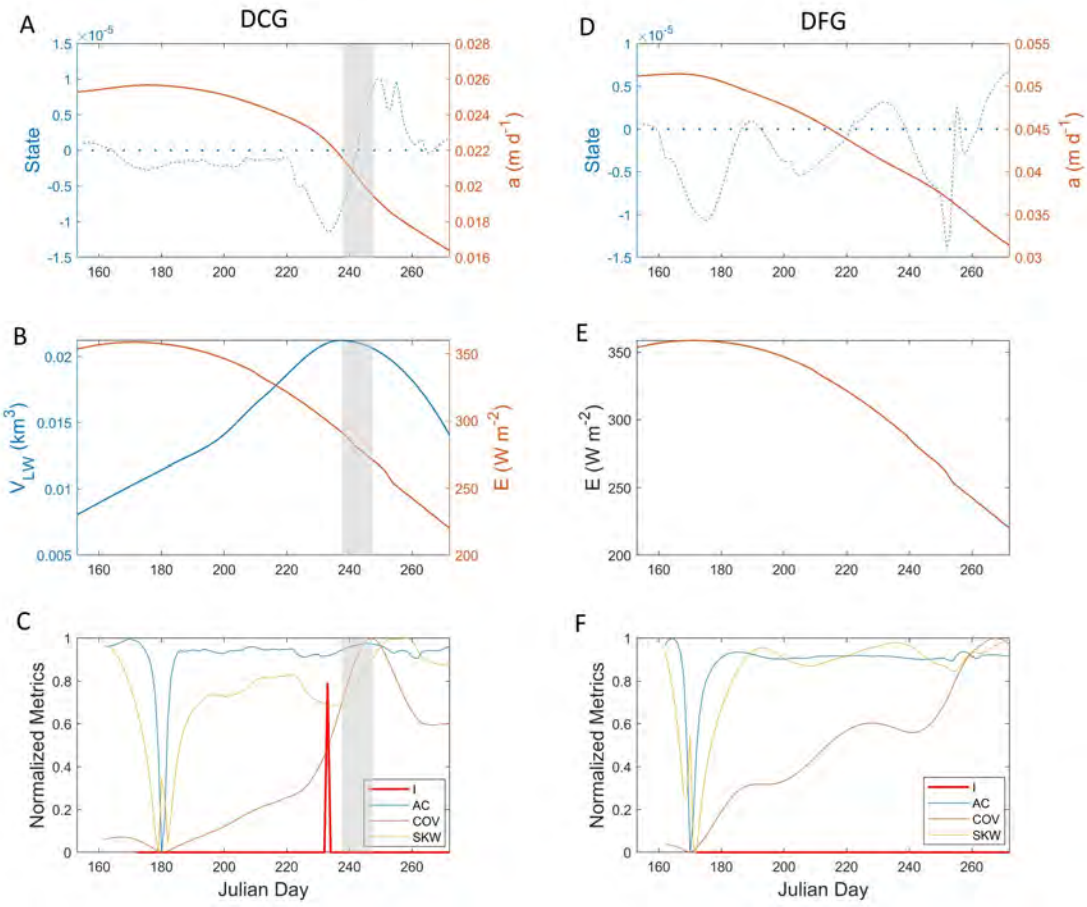

Figure 5.11: Tipping-point analysis results for surface-ablation variations in debris-covered glacier (DCG; column 1) and debris-free glacier (DFG; column 2) simulations over the ablation season. (A) Ablation rate variations (a) over the ablation season. The dashed line is the second derivative and represents state transitions. The gray zone highlights the critical transition. (B) The main control parameter governing the transition is the variation in lake-water volume (V_{LW}). (C) Transition index and metrics used for identifying tipping points for the DCG simulation. (D) Ablation rate variations over the ablation season. (E) The trend of ablation rate is controlled by surface irradiance (E), but no state transitions are found. (F) Transition index and metrics used for identifying tipping points for the DFG simulation.

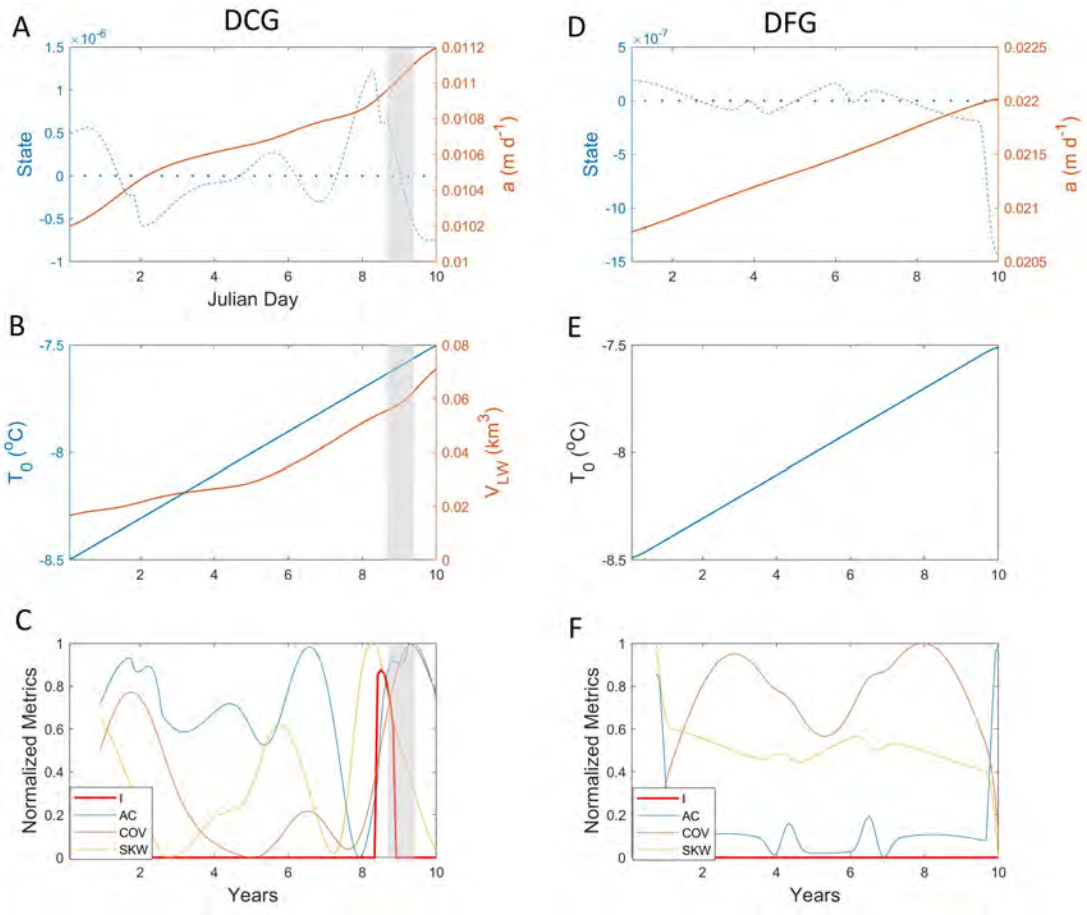

Figure 5.12: Tipping-point analysis results for surface-ablation variations in debris-covered glacier (DCG; column 1) and debris-free glacier (DFG; column 2) simulations over a 10-year time period. (A) Ablation rate variations (a) over ten years. The dashed line is the second derivative and represents state transitions. The gray zone highlights the critical transition. (B) The main control parameter governing the transition is the variation in lake-water volume (V_w). (C) Transition index and metrics used for identifying tipping points for the DCG simulation. (D) Ablation rate variations over 10 years. (E) The trend of ablation rate is controlled by Atmospheric temperature (T_0), but no state transitions are found. (F) Transition index and metrics used for identifying tipping points for the DFG simulation. The ablation rate for the DCG simulation exhibits a critical transition that appears at approximately 9 years.

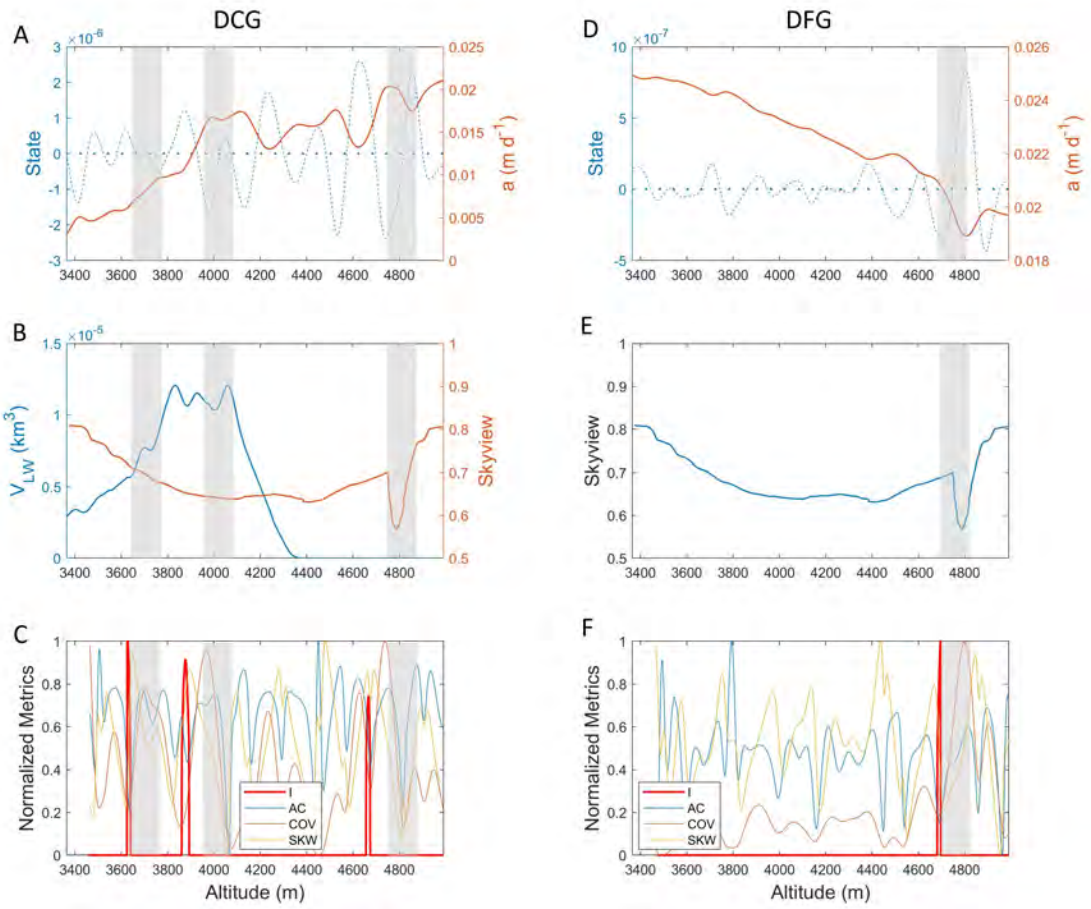

Figure 5.13: Tipping-point analysis results for surface-ablation variations in debris-covered glacier (DCG; column 1) and debris-free glacier (DFG; column 2) simulations over the altitude range of the Baltoro Glacier. (A) Ablation rate variations (a) as a function of altitude. The dashed line is the second derivative and represents state transitions. The gray zone highlights the critical transition. Note that three transitions were identified. (B) The main control parameters governing the transitions are the variation in lake-water volume (V_{LW}) and the skyview coefficient. (C) Transition index and metrics used for identifying tipping points for the DCG simulation. (D) Ablation rate variations as a function of altitude. Note that one transition was found. (E) The control parameter for the state transition is the skyview coefficient. (F) Transition index and metrics used for identifying tipping points for the DFG simulation.

Tipping-point analysis on the ablation variations (Figures 5.11-5.13) suggests that: 1) The ablation rate on DCG exhibits a major state transition in the late ablation season due to the presence of supraglacial lakes. Tipping points were not found for the DFG simulation over the ablation season, which suggests that ablation is more sensitive to the seasonality of radiative forcing on a

DCG due to ablation-lake positive feedback. 2) The decadal ablation variation on a DCG exhibits a critical transition after 9 years, most likely due to the increased supraglacial lake volume, however, no tipping point was found on for the DFG simulation. For the DCG simulation, ablation variations exhibited a high-degree of non-linearity over a decade time period. 3) From a spatial-transition perspective (Figure 5.13), three tipping points were identified for the DCG simulation, and only one was found for the DFG simulation. Note that the larger number of tipping points in the ablation zone given a DCG simulation, suggests that debris-load variations and the presence of supraglacial lakes make a DCG more sensitive to ablation variations given radiative forcing.

5.5.4.2 Lake Volume

The evolution of supraglacial lakes is represented as the variation of lake water volume over time. The nonlinear increase of the lake water volume was identified using tipping-point analysis, and the state transition zones are highlighted by the gray boxes. Figure 5.14 shows the temporal and spatial variations in lake volume over one decade. The expanding lakes contribute to the DCG's nonlinear responses to radiative forcing that do not exist in DFG simulations, as a DFG in the same setting typically have very few supraglacial lakes [23].

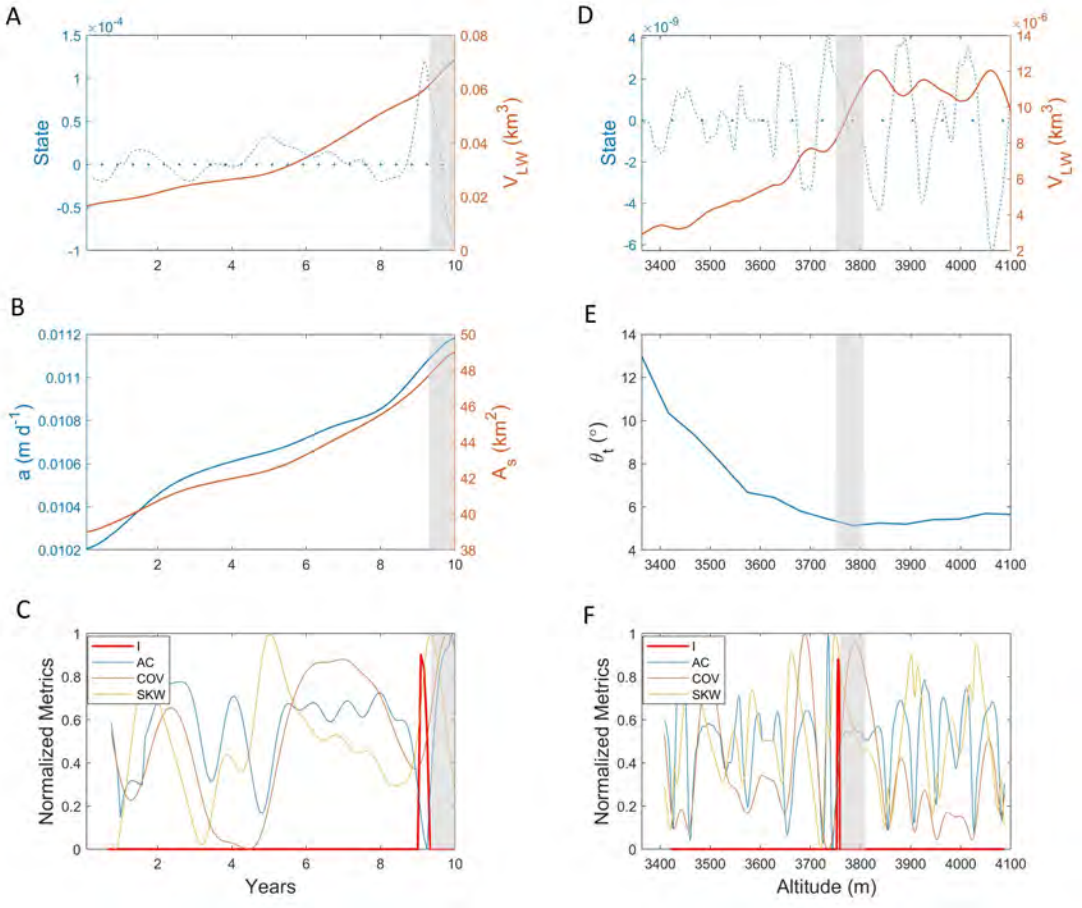

Figure 5.14: Tipping-point analysis results for lake-water volume variations on the Baltoro Glacier from a temporal perspective (column 1), and from a spatial perspective (column 2). (A) Lake-water volume (V_{LW}) variations over ten years. The dashed line is the second derivative and represents state transitions. The gray zone highlights critical transitions. (B) The main control parameter governing the transition is the variation in surface area (A_s) and ablation rate (a). (C) Transition index and metrics used for identifying the tipping point. (D) Lake-water volume variations as a function of altitude. (E) The state transition is controlled by the glacier surface slope (θ_t) that permits ponding. (F) Transition index and metrics used for identifying the tipping point.

The temporal variation of supraglacial lake volume shows a tipping point after about 9 years (Figure 5.14A) due to the increased ablation rate. Expanded lakes can further enhance ablation, therefore, there is a positive feedback between lake expansion and ablation which makes the DCG more sensitive to radiative forcing over time. The spatial variation of supraglacial lake volume (assuming lakes only exist in the ablation zone) exhibits a critical transition between 3700m to

3800m (Figure 5.14D), which corresponds to the transition from heavily debris-covered terminus to the flatter area where lakes become abundant. Based on remote-sensing analysis, Gibson et al.[23] estimated that the area of supraglacial water bodies tripled from 2001 to 2012, and our simulation result shows that the total lake volume in 2014 is about 3.5 times the total lake volume in 2004, which is in a good agreement with the remote-sensing result.

5.5.4.3 Ice Volume and Ice-Flow Speed

The cumulative glacier response to climate forcing is represented as ice volume and flow speed changes over time. Figure 5.15 and Figure 5.16 show the tipping-point analysis results on ice volume and flow speed for DCG and DFG simulations over 10 years. The spatial comparison of ice-flow speed between the DCG and the DFG is shown in Figure 5.17.

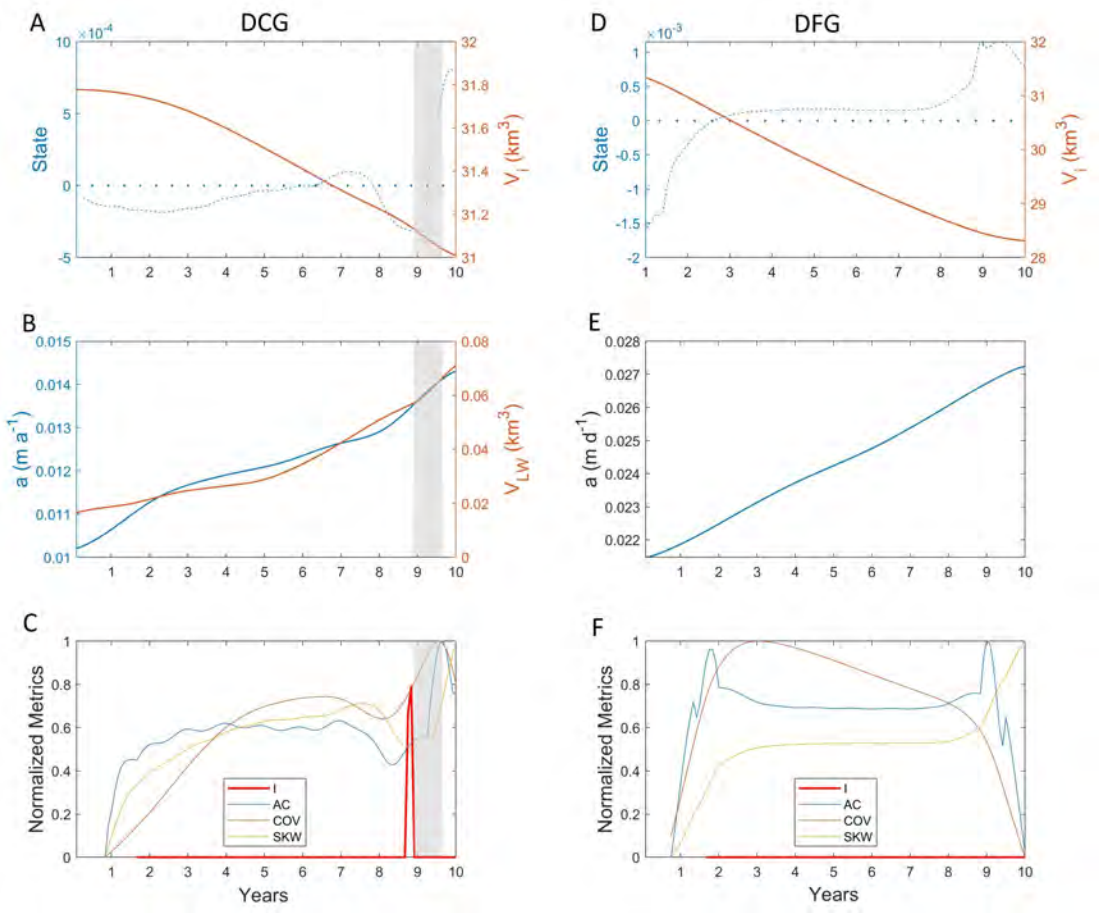

Figure 5.15: Tipping-point analysis results for ice-volume variations in debris-covered glacier (DCG; column 1) and debris-free glacier (DFG; column 2) simulations over a 10-year time period. (A) Ice-volume variations (V_i) over ten years. The dashed line is the second derivative and represents state transitions. The gray zone highlights critical transitions. (B) The main control parameter governing the transition is the variation in lake-water volume (V_{LW}) and ablation rate (a). (C) Transition index and metrics used for identifying tipping points for the DCG simulation. (D) Ice-volume variations over 10 years. (E) The trend of ice-volume variations is controlled by surface ablation rate (a), but no state transitions are found. (F) Transition index and metrics used for identifying tipping points for the DFG simulation.

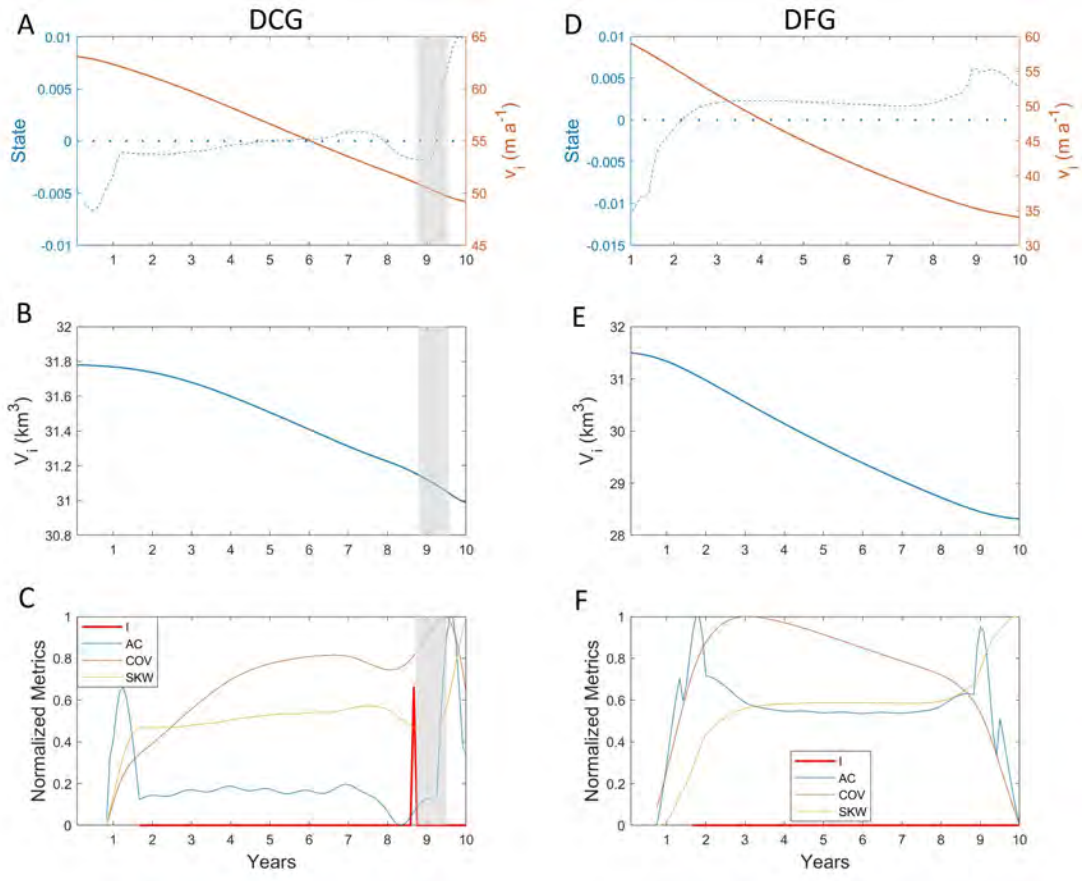

Figure 5.16: Tipping-point analysis results for average ice-velocity variations in debris-covered glacier (DCG; column 1) and debris-free glacier (DFG; column 2) simulations over a 10-year time period. (A) Ice-velocity variations (v_i) over ten years. The dashed line is the second derivative and represents state transitions. The gray zone highlights critical transitions. (B) The main control parameter governing the transition is the variation in ice volume (V_i). (C) Transition index and metrics used for identifying tipping points for the DCG simulation. (D) Ice-velocity variations over 10 years. (E) The trend of ice-velocity variations is controlled by ice volume (V_i), but no state transitions are found. (F) Transition index and metrics used for identifying tipping points for the DFG simulation. The ice-flow speed in the DCG simulation exhibits a critical transition after 9 years.

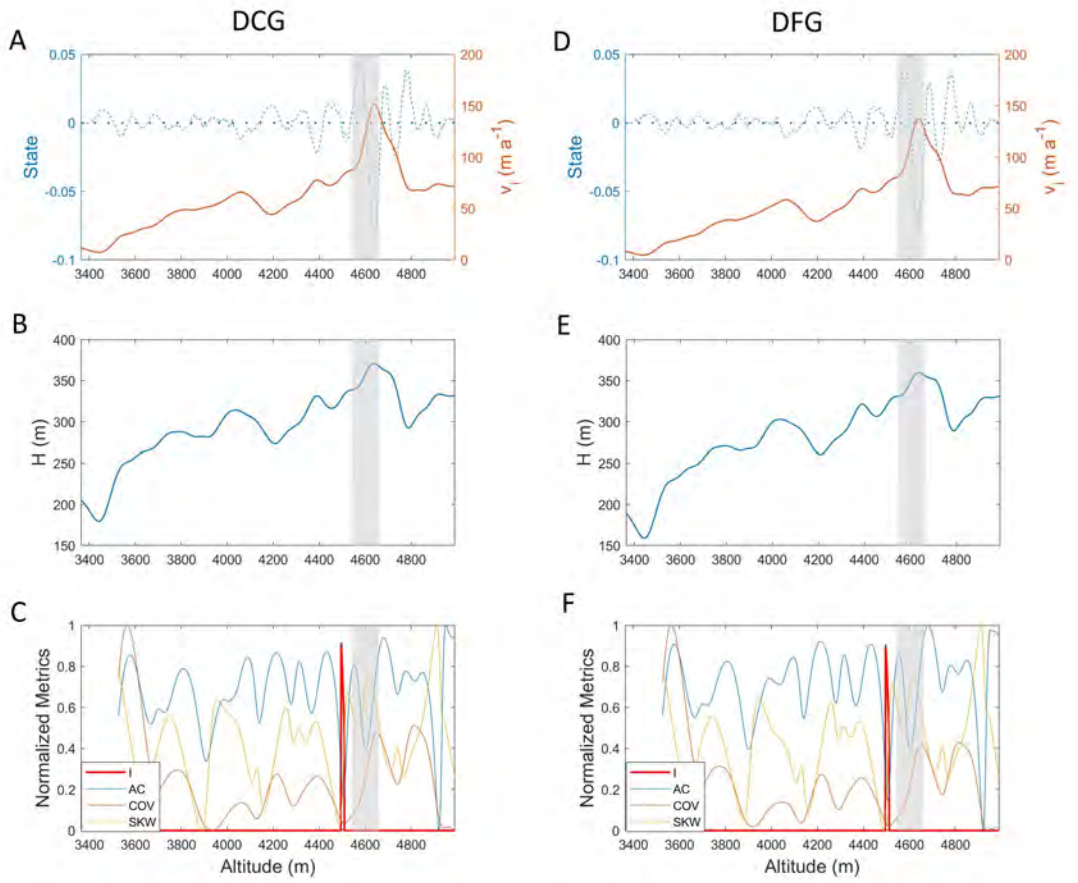

Figure 5.17: Tipping-point analysis results for average ice-velocity variations in debris-covered glacier (DCG; column 1) and debris-free glacier (DFG; column 2) simulations over the altitude range of the Baltoro Glacier. (A) Ice-velocity variations (v_i) as a function of altitude. The dashed line is the second derivative and represents state transitions. The gray zone highlights the critical transition. (B) The main control parameter governing the transition is the ice depth (H). (C) Transition index and metrics used for identifying tipping points for the DCG simulation. (D) Ice-velocity variations (v_i) as a function of altitude. (E) The main control parameter governing the transition is the ice depth (H). (F) Transition index and metrics used for identifying tipping points for the DFG simulation.

Results show that the ice volume for the DCG simulation exhibits a critical transition after about 9 years (Figure 5.15), which indicates a "speed up" in ice loss due to increased ablation. The ice-flow speed is highly correlated with ice volume and therefore shows the same transition as in the ice volume (Figure 5.16). From a spatial perspective (Figure 5.17), both DCG and DFG simulations show the same tipping point at about 4500m due to the increase in ice thickness near

the ELA. The ice loss on the DFG is of a higher magnitude but gradually slows down and no tipping points were found (Figure 5.15D), whereas the ice loss on the DCG is increasing (Figure 5.15A), most likely due to the positive feedback between ablation and supraglacial lake expansion that accelerates ice loss.

5.5.4.4 Mass Balance

Mass balance is a critical factor that characterizes the overall glacier response to climate forcing, and here we compared the mean mass balance for the DCG and DFG simulations. Figure 5.18 depicts tipping-point analysis results on the temporal variation of mean mass balance (averaged over the entire glacier) over a 10-year period. Figure 5.19 depicts the spatial transition in mass balance (as a function of altitude) for the DCG and DFG simulations.

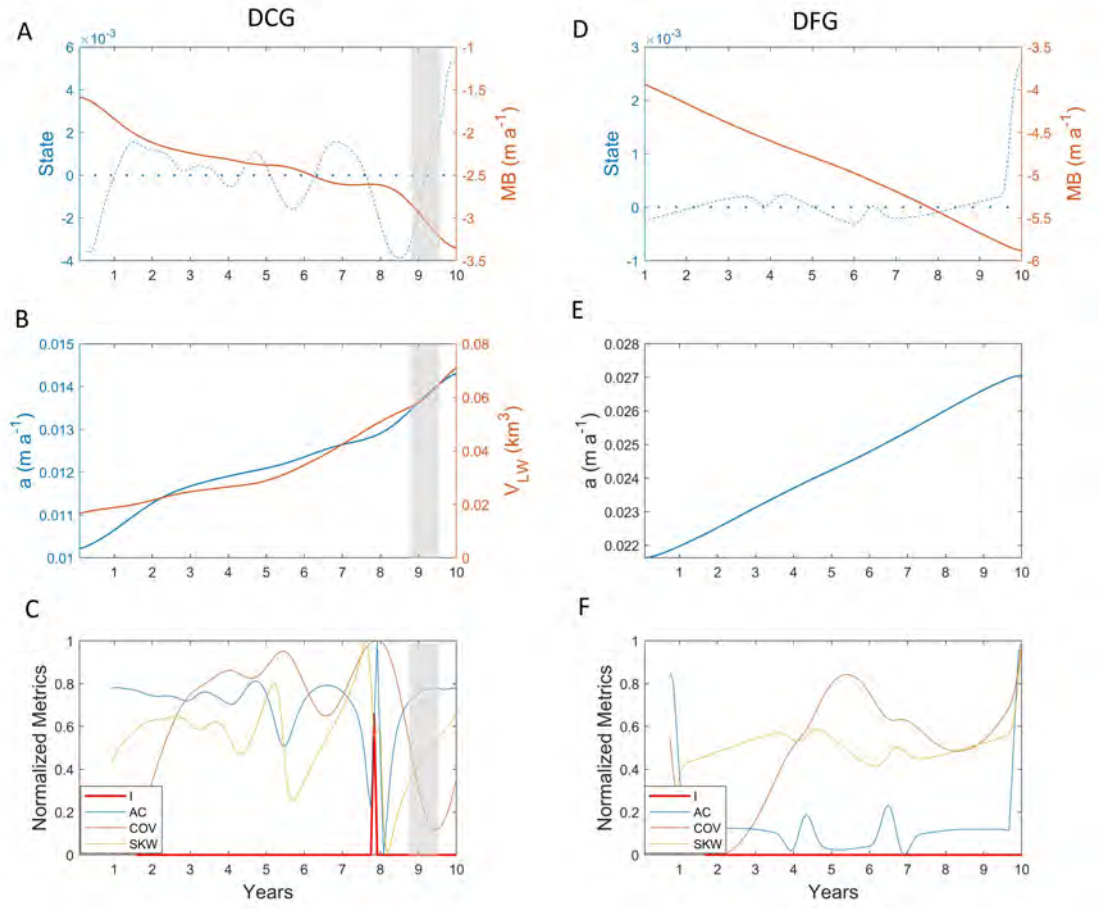

Figure 5.18: Tipping-point analysis results for mass-balance variations in debris-covered glacier (DCG; column 1) and debris-free glacier (DFG; column 2) simulations over a 10-year time period. (A) mass-balance variations (MB) over ten years. The dashed line is the second derivative and represents state transitions. The gray zone highlights critical transitions. (B) The main control parameters governing the transition is the variation in lake-water volume (V_{LW}) and ablation rate (a). (C) Transition index and metrics used for identifying tipping points for the DCG simulation. (D) Mass-balance variations over 10 years. (E) The trend of mass-balance variations is controlled by ablation rate (a), but no state transitions are found. (F) Transition index and metrics used for identifying tipping points for the DFG simulation. The mass-balance of the DCG simulation exhibits higher nonlinearity as compared to the DFG simulation.

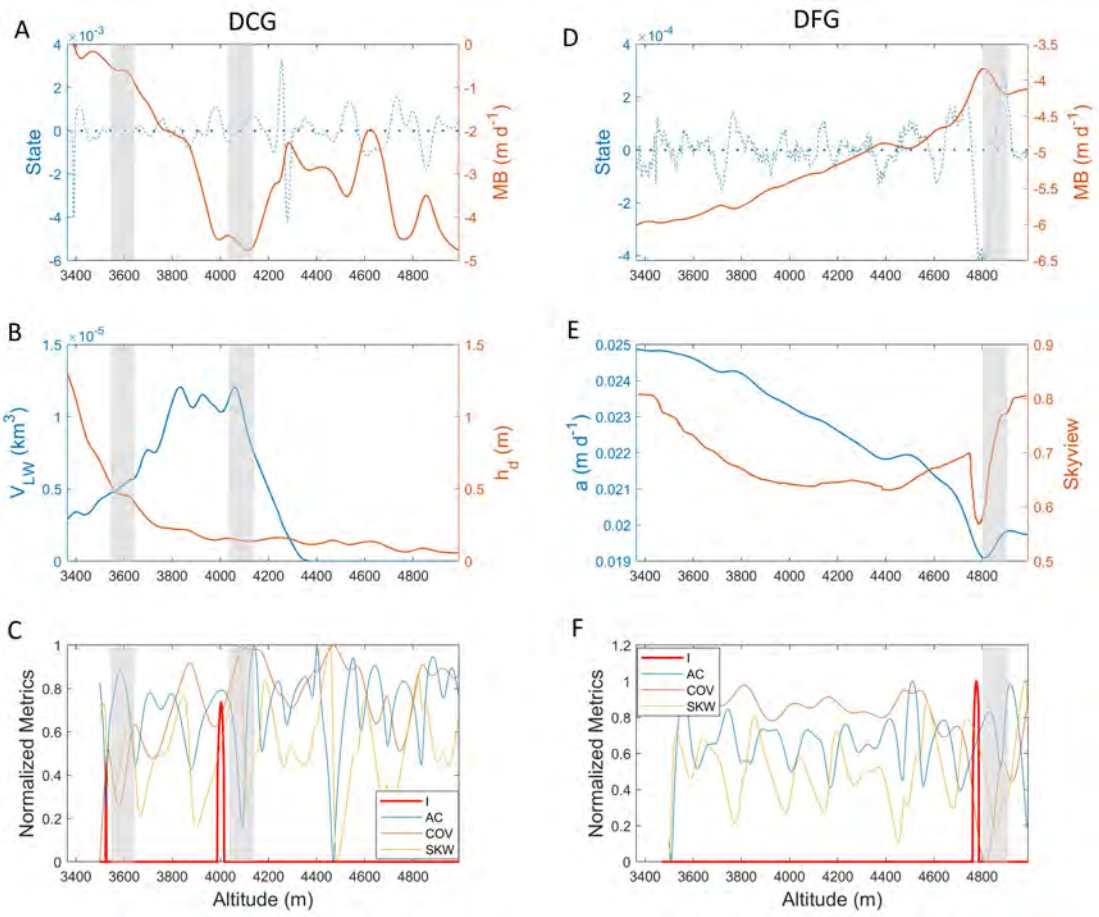

Figure 5.19: Tipping-point analysis results for mass-balance variations in debris-covered glacier (DCG; column 1) and debris-free glacier (DFG; column 2) simulations over the altitude range of the Baltoro Glacier. (A) mass-balance variations (MB) as a function of altitude. The dashed line is the second derivative and represents state transitions. The gray zone highlights the critical transitions. (B) The main control parameter governing the transition is the lake-water volume (V_{LW}) and debris depth (h_d). (C) Transition index and metrics used for identifying tipping points for the DCG simulation. (D) Mass-balance variations as a function of altitude. (E) The main control parameters governing the transition is ablation rate (a) that is controlled by the skyview coefficient. (F) Transition index and metrics used for identifying tipping points for the DFG simulation.

Mass balance variations for a DCG simulation also exhibit a critical transition after 9 years (Figure 5.18A), and the new state represents an accelerated decrease in mass balance due to the rapid increase in ablation rate and supraglacial lake volume (Figure 5.18B). No tipping points were found for the DFG simulation. From the spatial perspective, the DFG simulation exhibits a critical transition at about 4800m due to a rapid decrease in ablation rate likely caused by topographic

shielding as indicated by the skyview coefficient (Figure 5.19E), and the sudden drop in skyview is most likely due to the high-magnitude glacial erosion at this altitude, because the paleo-ELA zone of the Baltoro Glacier may be located at this altitude, and maximum erosion is typically found near the ELA [115, 116]. This demonstrates another significant topographic control on the glacier mass balance. Two tipping points were found for the DCG simulation, and they are located in the ablation zone where the mass balance is governed by the distribution of debris and supraglacial lakes (Figure 5.19B). This suggests that a DCG exhibits much higher spatial variability in mass balance due to heterogeneous debris and supraglacial lakes in the ablation zone. These result reveal a more rapid nonlinear decrease in mass balance for the DCG which suggests that a DCG may exhibit a higher level of sensitivity to climate forcing than a DFG.

5.6 Discussion

5.6.1 Ice Flow

Ice-flow plays a critical role in glacier dynamics because: 1) It governs the large-scale supraglacial and englacial debris transport that directly influences surface ablation; 2) It alters surface topography which affects other components in the system; 3) It is responsible for glacier erosion which governs bed topography over long periods of time, and erosion controls debris production; 4) It governs ice-mass flux from the accumulation area, which controls the ice volume of the glacier. Simulations demonstrated that ice-flow significantly governs the total ice volume variations of the glacier (Figure 5.8).

Ice thickness is the most important parameter that governs ice-flow dynamics, and the distribution of ice thickness also controls the pathways of englacial transport [18]. Based on simulations (Figure 5.7), englacial debris starts to advect towards the glacier surface as the ice thickness gradually decrease below the ELA. The location of the ELA affects the emergence location of englacial debris, such that if the ELA is further away from the debris source, the englacial debris travels a longer distance before it emerges on the surface at lower altitudes. If the ELA is closer to the debris source, the englacial debris travels a shorter distance, and therefore it emerges on the sur-

face at a higher altitude. The surface debris concentration is likely to increase over time because more englacial debris will be exposed due to surface ablation [93, 80, 18]. From a methodological perspective, we made improvements on the existing model by Anderson and Anderson [18], such that the model now accounts for basal debris and non-flat bed topography. The elongated englacial debris paths (Figure 5.7) also provide an explanation for the observed englacial debris bands inside many DCGs [80, 50].

Simulations based on the Baltoro Glacier suggest that englacial debris may be able to emerge on the glacier surface in about 40 years, and the transport paths are expected to be sensitive to basal topography which is controlled by erosion. The average supraglacial debris-flux rate due to ice-flow advection is $5554 m^3 a^{-1}$, which is a reasonable estimate, as a previous study has reported a debris-flux rate range of 0 - $12000 m^3 a^{-1}$ for the Baltoro Glacier [23].

The simulated basal erosion rate along the flowline of the Baltoro Glacier is $37.6 mm a^{-1}$ on average with a maximum of $46 mm a^{-1}$. This result has a high degree of uncertainty due to the many unknown basal conditions and processes (e.g., basal hydrology and quarrying) that are not accounted for, but the magnitude is within the widely accepted 0-$100 mm a^{-1}$ range [179, 180].

5.6.2 Glacier Sensitivity to Climate Forcing

Simulation results and tipping-point analysis indicate that the DCGs in the Karakoram are most likely actively responding to radiative forcing, even though their terminus positions are much more stable than DFGs due to debris loads. The overall dynamics of a DCG is more complex than that of a DFG because many nonlinear processes and feedbacks significantly influence the system. For example, the interactions between debris-flux, supraglacial lake and surface topography can cause a dramatic increase in ice loss during the ablation season as demonstrated in Chapter 4. As in many climate-driven systems, the accumulation of these nonlinear perturbations could lead to tipping points which indicate significant transitions of system state [172, 171]. These critical state transitions in the DCG system have not been addressed in previous studies also because most existing models only partially characterize glacier systems or relay on oversimplified assumptions, which overlook the accumulation of small nonlinear perturbations that could eventually change

glacier-system state, and govern glacier sensitivity to climate change. Therefore, we argue that the traditional metrics such as dynamic states (e.g., stable, retreating, or advancing termini) and mass balance estimates may not accurately reflect a DCG's sensitivity to climate forcing, because these metrics focus on magnitudes rather than the dynamic spatio-temporal changes in process rates and glacier subsystems.

We identified many tipping points in a DCG system that were not found in DFG simulations. These tipping points correspond to critical transitions that characterize rapid nonlinear increases in ablation (Figures 5.11, 5.12), supraglacial water volume (Figure 5.14), and decreases in ice volume (Figure 5.15), ice-flow speed (Figure 5.16), and mass balance (Figures 5.18, 5.19). These transitions may occur in major glacier subsystems approximately around 8-9 years based on the simulations of the Baltoro Glacier. Our result highlighted the positive feedback between lake expansion and ablation which may be the main cause for the appearance of tipping points. From a spatial perspective, there are also more tipping points identified for DCG simulations compared to DFG simulations (Figures 5.13, 5.19) suggest that a DCG exhibits much higher spatial variability in ablation due to heterogeneous debris and supraglacial lakes. Collectively, results indicate that even though the magnitude of ice loss on a DFG is typically higher, a DCG shows more critical state transitions and higher spatio-temporal variability in process rates and internal system variation, which suggest that a DCG can exhibit a higher level of sensitivity to radiative forcing than a DFGs.

Tipping point analysis provided insight into the "debris-covered glacier anomaly" [33], which states that some DCGs exhibit accelerated thinning despite the presence of debris load [31, 16]. This can then be explained as the transition into a new state in which the glacier becomes more sensitive to the warming atmosphere and positive feedbacks that locally accelerate ablation.

Some glacier-system responses and feedbacks may operate at very large timescales, and future research is needed to determine if more tipping points exist and if we can identify these early indicators of system change at longer (multi-decade and multi-century) timescales.

5.6.3 Assumptions and Limitations

Simulations in this study do not account for the entire accumulation area which feeds ice mass to the glacier. Therefore, the results show less sensitivity to the regional precipitation forcing than actual conditions. The initial ice thickness is estimated from surface velocity based on a first-order SIA approach which could be inaccurate if the basal topography is rugged [108]. Headwall and basal erosion are considered as the only debris sources in the model, which could be an underestimate of the actual debris input, because there are many other processes such as landslides, rockfall, and tributary inflow also contribute debris deposition on and into the glacier [50].

From the ablation dynamics perspective, many complicated processes that are known to influence glacier ablation such as the melting caused by precipitation, englacial ablation and drainage, refreezing, and sublimation are not accounted for. As a result, the simulation underestimates both the magnitude and the nonlinearity of the actual ablation.

This work does not address system sensitivity to climate change at scales longer than one decade due to the computational complexity, and it is possible that many significant system tipping points will appear over much longer timescales. Future research should focus on discovering those critical transitions using century-scale simulations.

5.7 Conclusions

In this study, numerical simulations based on the Baltoro Glacier in the Karakoram Himalaya are used to understand the role of ice-flow in glacier mass balance and debris transport, and to assess DCG sensitivity to climate forcing. The simulations account for important processes, components (including ice-flow, ablation, debris-flux, supraglacial lake expansion, basal erosion and topographic evolution), and their feedback mechanisms. Results are analyzed from a tipping-element and tipping-point framework to understand the sensitivity of a DCG system to forcing factors. Specifically, we draw the following conclusions:

1. Ice-flow is a critical component that controls the overall dynamics of a DCG because it governs the supraglacial and englacial debris advection; alters surface topography; governs glacier

erosion; and controls ice mass flux from the accumulation zone which regulates the ice volume of a glacier.

2. It takes about 40 years on the Baltoro Glacier for basal debris to emerge on the glacier surface. Englacial debris loads start to advected towards the glacier surface as the ice thickness gradually decrease below the ELA. The distance between the debris source and the ELA affects the time it takes for the englacial debris to emerge at the glacier surface.

3. DCGs in the Karakoram appear to be actively responding to radiative forcing. Results highlighted the positive feedback between lake expansion and ablation which may be the main cause for many tipping points found in the DCG system. Under the perturbations of positive feedbacks, a DCG may experience more state transitions over time that lead to an increasing level of sensitivity to radiative forcing, which may explain the "debris-covered glacier anomaly".

4. More tipping points were identified in the DCG system than in the DFG system. These tipping points were found to be early indicators of critical transitions that are represented as rapid nonlinear increases in ablation rate and supraglacial lake volume, and decreases in ice volume, ice-flow speed, and mass balance, and most of them appear within a decade (about 9 years) based on simulations of the Baltoro Glacier. Additional tipping points were identified from a spatial-transition perspective for DCG simulations. Collectively, the results indicate that even though the magnitude of ice loss on a DFG is typically higher, the subsystems of a DCG show more critical state transitions and higher variability (spatial and temporal), which suggest that DCGs are more sensitive to radiative forcing than previously thought, and some DCGs may exhibit higher sensitivity to climate forcing than DFGs.

6. SUMMARY AND CONCLUSIONS

6.1 Conclusions

This research focuses on understanding the nature of debris-covered glacier dynamics using numerical modeling to provided new insights into the sensitivity of a debris-covered glacier system to climate change in the central Karakoram. The major contribution of this research is the attempt to demonstrate that debris-covered glaciers in the central Karakoram may be more sensitive to radiative forcing than previously thought, based on better characterizations of climate-glacier processes, feedback mechanism and glacier-subsystem state transitions. Collectively, simulations and tipping-point analysis provide modeling results that support the concept of the "debris-covered glacier anomaly", which states that debris-covered glaciers can exhibit high-magnitude thinning despite the presence of debris loads [16, 31, 33]. Simulation results also suggest that a debris-covered glacier system is much more complex than a debris-free glacier system, such that traditional metrics such as terminus states (e.g., stable, retreating, or advancing) and mass balance estimates may not accurately reflect the debris-covered glacier's sensitivity to subsystem state changes.

Simulations suggest that debris-covered glaciers in the Karakoram are actively responding to climate forcing, even though we do not have adequate empirical data that provides insight into the radiative and precipitation forcing characteristics of the region. Simulation results strongly suggest that glacier-surface ablation rates are accelerating due to positive feedbacks and complex couplings between surface ablation, debris-flux, supraglacial lake development, and topographic evolution. The collective super-positioning of these nonlinear perturbations may significantly increase the level of glacier-subsystem sensitivity to climate forcing and result in system response tipping points which are early indicators of rapid change [172, 171]. To our knowledge, this is the first time this type of modeling and analysis has been applied to a debris-covered glacier, and the results suggest that glaciers in the eastern Himalaya may have significantly evolved past major tipping points, in terms of supraglacial lake development and evolution. In the Karakoram, it appears that only

the largest glaciers with relatively shallow slope profiles exhibit surface conditions indicative of critical thresholds that are related to supraglacial lake development and heterogeneous thinning. Climate-glacier simulations revealed a significant number of spatio-temporal system tipping points for debris-covered glacier systems compared to debris-free glacier systems. These results strongly suggest that debris-covered glacier systems may exhibit more critical-state transitions and may be more sensitive to climate forcing than debris-free glaciers. These findings validate the initial research hypotheses and represents an entirely different perspective on climate-glacier dynamics in High Mountain Asia, and can help explain theories of the Karakoram Anomaly and the "debris-covered glacier anomaly".

This research also evaluated multiple factors that have significant impacts on glacier dynamics but are often neglected in existing models, such as debris-flux and supraglacial lake development. These factors form positive feedbacks that locally accelerate melting and lead to high spatio-temporal variability in ablation rates. This research also highlighted a debris-covered glacier's response to topographic forcing, which has not been explored in previous studies. Results suggest that a more complex surface topography increases ablation on a debris-covered glacier by enhancing debris-flux and supraglacial lake formation.

From a methodological perspective, the model developed in this research is more comprehensive than other existing debris-covered glacier models to date. The parametrization schemes account for numerous processes, feedback mechanisms and forcing factors that have been neglected or over-simplified in existing glacier system models. Examples include the use of a radiation-transfer model that accounts for local and meso-scale topographic effects of surface irradiance; a relatively comprehensive debris transport system including gravity-driven debris-flux and ice-flow driven debris-flux; mineral spectral reflectance mixing and temporal surface albedo variation caused by sediment flux, meltwater drainage and supraglacial lake expansion; basal-debris production and advection; and topographic controls on englacial debris transport. Therefore, this model enables the simulation of subsystem couplings and feedbacks between multiple parameters, processes and subsystems, many of which have never been discussed in the existing literature.

Finally, new insights gained from this research will contribute to scientific inquiry and practical problem solving related to meltwater production, geohazards, geodynamics, geomorphology, and glaciology issues in the Karakoram Himalaya. The numerical models developed in this research will facilitate future efforts to assess the response of debris-covered glaciers to climate change.

6.2 Summary of Findings

1. Surface ablation dynamics of a debris-covered glacier (DCG):

The surface ablation dynamics on a DCG is significantly controlled by debris-thickness, debris-flux, supraglacial lakes, and topographic conditions, such that a DCG can exhibit high spatio-temporal variability in ablation due to supraglacial lake development and heterogeneous debris-thickness distribution. A debris-free glacier (DFG) under the same conditions exhibits much less spatio-temporal variability in surface ablation.

The gravitational supraglacial debris-flux plays an important role in debris-thickness redistribution which governs ablation. Faster debris transport tends to expose more thin-debris and bare-ice area that increases the overall surface ablation. Gravitational debris-flux is a therefore a necessary component in ablation models for DCGs.

Topographic forcing on surface ablation is non-negligible for DCGs because glacier surface topography controls irradiance and gravitational debris-flux, and a constantly changing ice topography makes the ablation process more dynamic. DCGs and DFGs respond differently to variations in surface topography. For a DFG, high-frequency topographic variations decrease the overall surface ablation, which is due to the reduced irradiance caused by local topographic effects and terrain self-shadowing. For a DCG, high-frequency topographic variations increase the overall surface ablation caused by an accelerated gravitational debris-flux, which generally promotes larger geographic areas of thin-debris and bare-ice that results in higher ablation.

2. Supraglacial lake dynamics on a debris-covered glacier:

Supraglacial lakes make a significant contribution to the total surface ablation. Simulations over the Baltoro Glacier reveal that supraglacial lakes can be minimally responsible for approximately 22.78% of the total ice-mass loss in the lower ablation zone over an ablation season. We

found that lake formation and expansion processes represent a nonlinear response to radiative forcing, as a lake influence can operate at local and regional scales, with lakes having a more significant influence on ice-mass loss towards the end of the ablation season when the lakes reach their yearly maximum extend. Therefore, supraglacial lakes contribute to the glacier's nonlinear response to radiative forcing, and the nonlinearity is represented as an acceleration in ablation rate, total ice-mass loss, and the lowering of surface altitude. These nonlinear responses may indicate the beginning of a critical transition of the glacier system that signifies the glacier's increasing level of sensitivity to climate forcing.

Gravitational debris-flux partially controls the expansion rate of supraglacial lakes by governing the surrounding debris-thickness and ablation rates, such that gravitational debris-flux decreases debris-thickness of adjacent slopes, which increases ablation and facilitates lake expansion. The expanded lakes also increase debris-flux rate by steepening the adjacent slopes, which forms a positive feedback that accelerates surface ablation and lake expansion.

Topography also plays an important role in lake formation by controlling supraglacial drainage and discharge, such that given a higher glacier-profile gradient, discharge increases and surface-water storage capacity decreases. Relatively high topographic variation also encourages lake formation by providing depressions for water to accumulate. Therefore, supraglacial lake formation may be initiated given more heterogeneous distribution of ablation and downwasting coupled with a gentle surface profile slope that facilitate meltwater production and accumulation in local-scale topographic depressions.

3. Ice-flow dynamics on a debris-covered glacier:

Ice-flow is a critical component that controls the overall dynamics of a DCG because it governs the supraglacial and englacial debris advection, glacier erosion, topographic variation and ice-mass flux from the accumulation zone which controls the ice volume of a glacier.

Englacial debris can be elevated towards the glacier surface as the ice thickness gradually decrease below the ELA. The distance between the debris source and the ELA affects the time it takes for the englacial debris to emerge at the glacier surface. It takes about 40 years on the Baltoro

Glacier for basal debris to emerge on the glacier surface. The surface debris concentration is likely to increase over time as more englacial debris gets exposed on the surface.

4. Debris-covered glacier sensitivity to radiative forcing:

Simulation results suggest that DCGs in the Karakoram are actively responding to radiative forcing. Results highlighted the positive feedback between lake expansion and ablation which may be the main cause for many tipping points found in DCG subsystems. Under the perturbations of positive feedbacks, a DCG may experience more state transitions over time that lead to an increasing level of sensitivity to radiative forcing, which may explain the "debris-covered glacier anomaly".

More tipping points are identified in DCG simulations than in DFG simulations, and these tipping points are early indicators of critical transitions that are characterized as rapid nonlinear increases in ablation rate and supraglacial lake volume, and decreases in ice volume, ice-flow speed, and mass balance, and most of them appear within a decade time period (about 9 years). Tipping points were identified for spatio-temporal transitions in DCG simulations, with less transitions identified for DFG simulations. Collectively, the results indicate that even though the magnitude of ice loss on a DFG is typically higher, a DCG shows more critical-state transitions and higher spatio-temporal variability, which suggest that DCGs are more sensitive to climate change than previously thought, and some DCGs may exhibit higher sensitivity to radiative forcing than DFGs.

6.3 Future Work

A major direction of future work is to expand the research in terms of evaluating a wider range of the spatio-temporal scale dependencies that govern glacier dynamics. Simulations over a longer period of time are needed to determine if there are more significant system state transitions because some subsystems respond to forcing factors at larger timescale, such as the erosion-topography-ice-flow feedback, the coupling between debris, mass balance and ice dynamics [18], and the effects of basal processes [110, 50].

Simulations over different geographic areas are also needed to better understand the spatially variable response of Himalayan glaciers to climate change [119, 15]. Glaciers under different

climate, topographic and debris-load conditions need to be compared to determine what are the dominant factors that caused the spatial variations in glacier sensitivity to climate change over the Himalaya [119].

Future efforts should also explore: 1) The impacts of englacial and basal hydrology on the glacier dynamics; 2) The role of tributary glaciers; 3) Additional debris sources; 4) Different debris-flux behaviors, such as non-turbulent plastic behavior versus fluid behavior [50], and the hydrological controls on debris transport [89]; 5) Full 3D velocity modeling that accounts for rugged bed topography and debris-covered stagnant termini; and 6) Precipitation-related ablation that is caused by debris heating and warm-water percolation.

Improving the quality of initial input data is also crucial for future work. Most glacier surface features and properties that are used for initial conditions in simulations can be estimated from remote-sensing data. Future simulations need to use latest high-quality remote-sensing products, as the spatial resolution of data limits the accuracy of initial conditions (e.g., topography, debris-thickness and supraglacial lake distribution), thereby governing the uncertainties in simulation results. High-resolution spatio-temporal data can also be very useful for validation, which represents another research direction for future studies.

REFERENCES

[1] M. I. Khan, "Ablation on barpu glacier, karakoram himalaya, pakistan a study of melt processes on a faceted, debris-covered ice surface," *Master Thesis*, 1989.

[2] R. B. Kayastha, Y. Takeuchi, M. Nakawo, and Y. Ageta, "Practical prediction of ice melting beneath various thickness of debris cover on khumbu glacier, nepal, using a positive degree-day factor," *IAHS-AISH P*, vol. 264, pp. 71–81, 2000.

[3] L. Mattson, "Ablation on debris covered glaciers: an example from the rakhiot glacier, punjab, himalaya.," *Intern. Assoc. Hydrol. Sci.*, vol. 218, pp. 289–296, 1993.

[4] C. Mihalcea, C. Mayer, G. Diolaiuti, C. D'agata, C. Smiraglia, A. Lambrecht, E. Vuillermoz, and G. Tartari, "Spatial distribution of debris thickness and melting from remote-sensing and meteorological data, at debris-covered baltoro glacier, karakoram, pakistan," *Annals of Glaciology*, vol. 48, pp. 49–57, 2008.

[5] S. Leprince, S. Barbot, F. Ayoub, and J.-P. Avouac, "Automatic and precise orthorectification, coregistration, and subpixel correlation of satellite images, application to ground deformation measurements," *IEEE Transactions on Geoscience and Remote Sensing*, vol. 45, no. 6, pp. 1529–1558, 2007.

[6] C. Mihalcea, C. Mayer, G. Diolaiuti, A. Lambrecht, C. Smiraglia, and G. Tartari, "Ice ablation and meteorological conditions on the debris-covered area of baltoro glacier, karakoram, pakistan," *Annals of Glaciology*, vol. 43, pp. 292–300, 2006.

[7] P. Taylor and D. Feltham, "A model of melt pond evolution on sea ice," *Journal of Geophysical Research: Oceans*, vol. 109, no. C12, 2004.

[8] M. Lüthje, L. Pedersen, N. Reeh, and W. Greuell, "Modelling the evolution of supraglacial lakes on the west greenland ice-sheet margin," *Journal of Glaciology*, vol. 52, no. 179, pp. 608–618, 2006.

[9] D. Farinotti, W. W. Immerzeel, R. J. de Kok, D. J. Quincey, and A. Dehecq, "Manifestations and mechanisms of the karakoram glacier anomaly," *Nature Geoscience*, vol. 13, no. 1, pp. 8–16, 2020.

[10] M. P. Bishop, J. F. Shroder Jr, R. Bonk, and J. Olsenholler, "Geomorphic change in high mountains: a western himalayan perspective," *Global and Planetary change*, vol. 32, no. 4, pp. 311–329, 2002.

[11] U. Kamp Jr, K. Haserodt, and J. F. Shroder Jr, "Quaternary landscape evolution in the eastern hindu kush, pakistan," *Geomorphology*, vol. 57, no. 1-2, pp. 1–27, 2004.

[12] Y. B. Seong, L. A. Owen, C. Yi, and R. C. Finkel, "Quaternary glaciation of muztag ata and kongur shan: Evidence for glacier response to rapid climate changes throughout the late glacial and holocene in westernmost tibet," *Geological Society of America Bulletin*, vol. 121, no. 3-4, pp. 348–365, 2009.

[13] T. D. Reid and B. W. Brock, "An energy-balance model for debris-covered glaciers including heat conduction through the debris layer," *Journal of Glaciology*, vol. 56, no. 199, pp. 903–916, 2010.

[14] W. W. Immerzeel, L. P. Van Beek, and M. F. Bierkens, "Climate change will affect the asian water towers," *Science*, vol. 328, no. 5984, pp. 1382–1385, 2010.

[15] T. Bolch, A. Kulkarni, A. Kääb, C. Huggel, F. Paul, J. G. Cogley, H. Frey, J. S. Kargel, K. Fujita, M. Scheel, *et al.*, "The state and fate of himalayan glaciers," *Science*, vol. 336, no. 6079, pp. 310–314, 2012.

[16] K. Fujita, A. Sakai, *et al.*, "Modelling runoff from a himalayan debris-covered glacier," *Hydrol. Earth Syst. Sci*, vol. 18, no. 7, pp. 2679–2694, 2014.

[17] A. V. Rowan, D. L. Egholm, D. J. Quincey, and N. F. Glasser, "Modelling the feedbacks between mass balance, ice flow and debris transport to predict the response to climate change of debris-covered glaciers in the himalaya," *Earth and Planetary Science Letters*, vol. 430, pp. 427–438, 2015.

[18] L. S. Anderson and R. S. Anderson, "Modeling debris-covered glaciers: response to steady debris deposition," *The Cryosphere*, vol. 10, no. 3, p. 1105, 2016.

[19] I. D. Dobreva, M. P. Bishop, and A. B. Bush, "Climate–glacier dynamics and topographic forcing in the karakoram himalaya: concepts, issues and research directions," *Water*, vol. 9, no. 6, p. 405, 2017.

[20] D. I. Benn and L. A. Owen, "Himalayan glacial sedimentary environments: a framework for reconstructing and dating the former extent of glaciers in high mountains," *Quaternary International*, vol. 97, pp. 3–25, 2002.

[21] M. P. Bishop, J. F. Shroder Jr, and J. D. Colby, "Remote sensing and geomorphometry for studying relief production in high mountains," *Geomorphology*, vol. 55, no. 1-4, pp. 345–361, 2003.

[22] D. Egholm, S. Nielsen, V. K. Pedersen, and J.-E. Lesemann, "Glacial effects limiting mountain height," *Nature*, vol. 460, no. 7257, pp. 884–887, 2009.

[23] M. J. Gibson, N. F. Glasser, D. J. Quincey, C. Mayer, A. V. Rowan, and T. D. Irvine-Fynn, "Temporal variations in supraglacial debris distribution on baltoro glacier, karakoram between 2001 and 2012," *Geomorphology*, vol. 295, pp. 572–585, 2017.

[24] T. Reid, M. Carenzo, F. Pellicciotti, and B. Brock, "Including debris cover effects in a distributed model of glacier ablation," *Journal of Geophysical Research: Atmospheres*, vol. 117, no. D18, 2012.

[25] J. Gulley and D. Benn, "Structural control of englacial drainage systems in himalayan debris-covered glaciers," *Journal of Glaciology*, vol. 53, no. 182, pp. 399–412, 2007.

[26] A. Sakai and K. Fujita, "Formation conditions of supraglacial lakes on debris-covered glaciers in the himalaya," *Journal of Glaciology*, vol. 56, no. 195, pp. 177–181, 2010.

[27] T. Reid and B. Brock, "Assessing ice-cliff backwasting and its contribution to total ablation of debris-covered miage glacier, mont blanc massif, italy," *Journal of Glaciology*, vol. 60, no. 219, pp. 3–13, 2014.

[28] K. E. Miles, B. Hubbard, D. J. Quincey, E. S. Miles, T. D. Irvine-Fynn, and A. V. Rowan, "Surface and subsurface hydrology of debris-covered khumbu glacier, nepal, revealed by dye tracing," *Earth and Planetary Science Letters*, vol. 513, pp. 176–186, 2019.

[29] D. Scherler, B. Bookhagen, and M. R. Strecker, "Hillslope-glacier coupling: The interplay of topography and glacial dynamics in high asia," *Journal of Geophysical Research: Earth Surface*, vol. 116, no. F2, 2011.

[30] M. P. Bishop, R. Bonk, U. Kamp Jr, and J. F. Shroder Jr, "Terrain analysis and data modeling for alpine glacier mapping," *Polar Geography*, vol. 25, no. 3, pp. 182–201, 2001.

[31] A. Kääb, E. Berthier, C. Nuth, J. Gardelle, and Y. Arnaud, "Contrasting patterns of early twenty-first-century glacier mass change in the himalayas," *Nature*, vol. 488, no. 7412, pp. 495–498, 2012.

[32] W. Immerzeel, F. Pellicciotti, and M. Bierkens, "Rising river flows throughout the twenty-first century in two himalayan glacierized watersheds," *Nature geoscience*, vol. 6, no. 9, pp. 742–745, 2013.

[33] F. Salerno, S. Thakuri, G. Tartari, T. Nuimura, S. Sunako, A. Sakai, and K. Fujita, "Debris-covered glacier anomaly? morphological factors controlling changes in the mass balance, surface area, terminus position, and snow line altitude of himalayan glaciers," *Earth and Planetary Science Letters*, vol. 471, pp. 19–31, 2017.

[34] K. Hewitt, "The karakoram anomaly? glacier expansion and the 'elevation effect,'karakoram himalaya," *Mountain Research and Development*, vol. 25, no. 4, pp. 332–340, 2005.

[35] L. Copland, S. Pope, M. P. Bishop, J. F. Shroder, P. Clendon, A. Bush, U. Kamp, Y. B. Seong, and L. A. Owen, "Glacier velocities across the central karakoram," *Annals of Glaciology*, vol. 50, no. 52, pp. 41–49, 2009.

[36] K. M. Cuffey and W. S. B. Paterson, *The physics of glaciers*. Academic Press, 2010.

[37] A. G. Fountain and J. S. Walder, "Water flow through temperate glaciers," *Reviews of Geophysics*, vol. 36, no. 3, pp. 299–328, 1998.

[38] A. Sakai, N. Takeuchi, K. Fujita, and M. Nakawo, "Role of supraglacial ponds in the ablation process of a debris-covered glacier in the nepal himalayas," *IAHS PUBLICATION*, pp. 119–132, 2000.

[39] R. L. Wessels, J. S. Kargel, and H. H. Kieffer, "Aster measurement of supraglacial lakes in the mount everest region of the himalaya," *Annals of Glaciology*, vol. 34, pp. 399–408, 2002.

[40] S. Thompson, D. I. Benn, J. Mertes, and A. Luckman, "Stagnation and mass loss on a himalayan debris-covered glacier: processes, patterns and rates," *Journal of Glaciology*, vol. 62, no. 233, pp. 467–485, 2016.

[41] J. M. Reynolds, "On the formation of supraglacial lakes on debris-covered glaciers," *IAHS publication*, pp. 153–164, 2000.

[42] D. I. Benn, S. Thompson, J. Gulley, J. Mertes, A. Luckman, and L. Nicholson, "Structure and evolution of the drainage system of a himalayan debris-covered glacier, and its relationship with patterns of mass loss," *The Cryosphere*, 2017.

[43] E. S. Miles, J. Steiner, I. Willis, P. Buri, W. W. Immerzeel, A. Chesnokova, and F. Pellicciotti, "Pond dynamics and supraglacial-englacial connectivity on debris-covered lirung glacier, nepal," *Frontiers in Earth Science*, vol. 5, p. 69, 2017.

[44] M. Rankl, C. Kienholz, and M. Braun, "Glacier changes in the karakoram region mapped by multimission satellite imagery," *The Cryosphere*, vol. 8, no. 3, pp. 977–989, 2014.

[45] L. Nicholson and D. I. Benn, "Calculating ice melt beneath a debris layer using meteorological data," *Journal of Glaciology*, vol. 52, no. 178, pp. 463–470, 2006.

[46] B. Pratap, D. Dobhal, M. Mehta, and R. Bhambri, "Influence of debris cover and altitude on glacier surface melting: a case study on dokriani glacier, central himalaya, india," *Annals of Glaciology*, vol. 56, no. 70, pp. 9–16, 2015.

[47] B. W. Brock, C. Mihalcea, M. P. Kirkbride, G. Diolaiuti, M. E. Cutler, and C. Smiraglia, "Meteorology and surface energy fluxes in the 2005–2007 ablation seasons at the miage

debris-covered glacier, mont blanc massif, italian alps," *Journal of geophysical research: atmospheres*, vol. 115, no. D9, 2010.

[48] E. Collier, L. Nicholson, B. Brock, F. Maussion, R. Essery, and A. Bush, "Representing moisture fluxes and phase changes in glacier debris cover using a reservoir approach," *The Cryosphere*, vol. 8, no. 4, pp. 1429–1444, 2014.

[49] Y. Zhang, K. Fujita, S. Liu, Q. Liu, and T. Nuimura, "Distribution of debris thickness and its effect on ice melt at hailuogou glacier, southeastern tibetan plateau, using in situ surveys and aster imagery," *Journal of Glaciology*, vol. 57, no. 206, pp. 1147–1157, 2011.

[50] D. Benn and D. J. Evans, *Glaciers and glaciation*. Routledge, 2014.

[51] K. R. MacGregor, R. S. Anderson, and E. D. Waddington, "Numerical modeling of glacial erosion and headwall processes in alpine valleys," *Geomorphology*, vol. 103, no. 2, pp. 189–204, 2009.

[52] D. Benn, T. Bolch, K. Hands, J. Gulley, A. Luckman, L. Nicholson, D. Quincey, S. Thompson, R. Toumi, and S. Wiseman, "Response of debris-covered glaciers in the mount everest region to recent warming, and implications for outburst flood hazards," *Earth-Science Reviews*, vol. 114, no. 1-2, pp. 156–174, 2012.

[53] M. Nakawo and G. J. Young, "Field experiments to determine the effect of a debris layer on ablation of glacier ice," *Annals of Glaciology*, vol. 2, pp. 85–91, 1981.

[54] A. Sakai, M. Nakawo, and K. Fujita, "Distribution characteristics and energy balance of ice cliffs on debris-covered glaciers, nepal himalaya," *Arctic, Antarctic, and Alpine Research*, vol. 34, no. 1, pp. 12–19, 2002.

[55] C. L. Fyffe, T. D. Reid, B. W. Brock, M. P. Kirkbride, G. Diolaiuti, C. Smiraglia, and F. Diotri, "A distributed energy-balance melt model of an alpine debris-covered glacier," *Journal of Glaciology*, vol. 60, no. 221, pp. 587–602, 2014.

[56] M. P. Bishop, B. W. Young, J. D. Colby, R. Furfaro, E. Schiassi, and Z. Chi, "Theoretical evaluation of anisotropic reflectance correction approaches for addressing multi-scale

topographic effects on the radiation-transfer cascade in mountain environments," *Remote Sensing*, vol. 11, no. 23, p. 2728, 2019.

[57] P. S. Chavez *et al.*, "Image-based atmospheric corrections-revisited and improved," *Photogrammetric engineering and remote sensing*, vol. 62, no. 9, pp. 1025–1035, 1996.

[58] M. Z. Jacobson and M. Z. Jacobson, *Fundamentals of atmospheric modeling*. Cambridge university press, 2005.

[59] C. Gueymard *et al.*, *SMARTS2: a simple model of the atmospheric radiative transfer of sunshine: algorithms and performance assessment*. Florida Solar Energy Center Cocoa, FL, 1995.

[60] R. E. Bird and C. Riordan, "Simple solar spectral model for direct and diffuse irradiance on horizontal and tilted planes at the earth's surface for cloudless atmospheres," *Journal of climate and applied meteorology*, vol. 25, no. 1, pp. 87–97, 1986.

[61] J. Dozier, J. Bruno, and P. Downey, "A faster solution to the horizon problem," *Computers & Geosciences*, vol. 7, no. 2, pp. 145–151, 1981.

[62] R. E. Rossi, J. L. Dungan, and L. R. Beck, "Kriging in the shadows: geostatistical interpolation for remote sensing," *Remote Sensing of Environment*, vol. 49, no. 1, pp. 32–40, 1994.

[63] R. Dubayah and P. M. Rich, "Topographic solar radiation models for gis," *International journal of geographical information systems*, vol. 9, no. 4, pp. 405–419, 1995.

[64] P. T. Giles, "Remote sensing and cast shadows in mountainous terrain," *Photogrammetric engineering and remote sensing*, vol. 67, no. 7, pp. 833–840, 2001.

[65] R. Dadic, R. Mott, M. Lehning, and P. Burlando, "Wind influence on snow depth distribution and accumulation over glaciers," *Journal of Geophysical Research: Earth Surface*, vol. 115, no. F1, 2010.

[66] S. Adhikary, N. Masayoshi, K. Seko, and B. Shakya, "Dust influence on the melting process of glacier ice: experimental results from lirung glacier, nepal himalayas," in *Debris-covered Glaciers: Proceedings of an International Workshop Held at the University of Washington in Seattle, Washington, USA, 13-15 September 2000*, no. 264, p. 43, IAHS, 2000.

[67] Y. Zhang, Y. Hirabayashi, K. Fujita, S. Liu, and Q. Liu, "Heterogeneity in supraglacial debris thickness and its role in glacier mass changes of the mount gongga," *Science China Earth Sciences*, vol. 59, no. 1, pp. 170–184, 2016.

[68] D. Quincey, L. Copland, C. Mayer, M. Bishop, A. Luckman, and M. Belo, "Ice velocity and climate variations for baltoro glacier, pakistan," *Journal of Glaciology*, vol. 55, no. 194, pp. 1061–1071, 2009.

[69] G. Jouvet, M. Picasso, J. Rappaz, M. Huss, and M. Funk, "Modelling and numerical simulation of the dynamics of glaciers including local damage effects," *Mathematical Modelling of Natural Phenomena*, vol. 6, no. 5, pp. 263–280, 2011.

[70] D. I. Benn and F. Lehmkuhl, "Mass balance and equilibrium-line altitudes of glaciers in high-mountain environments," *Quaternary International*, vol. 65, pp. 15–29, 2000.

[71] L. A. OWEn and E. Derbyshire, "The karakoram glacial depositional system," *Zeitschrift für Geomorphologie*, vol. 76, no. Suppl., pp. 33–73, 1989.

[72] R. S. Anderson, "A model of ablation-dominated medial moraines and the generation of debris-mantled glacier snouts," *Journal of Glaciology*, vol. 46, no. 154, pp. 459–469, 2000.

[73] M. P. Bishop, J. F. Shroder Jr, and J. L. Ward, "Spot multispectral analysis for producing supraglacial debris-load estimates for batura glacier, pakistan," 1995.

[74] M. P. Bishop, A. B. Bush, L. Copland, U. Kamp, L. A. Owen, Y. B. Seong, and J. F. Shroder Jr, "Climate change and mountain topographic evolution in the central karakoram, pakistan," *Annals of the Association of American Geographers*, vol. 100, no. 4, pp. 772–793, 2010.

[75] D. Benn, S. Wiseman, and K. Hands, "Growth and drainage of supraglacial lakes on debris-mantled ngozumpa glacier, khumbu himal, nepal," *Journal of Glaciology*, vol. 47, no. 159, pp. 626–638, 2001.

[76] G. Östrem, "Ice melting under a thin layer of moraine, and the existence of ice cores in moraine ridges," *Geografiska Annaler*, vol. 41, no. 4, pp. 228–230, 1959.

[77] N. Reznichenko, T. Davies, J. Shulmeister, and M. McSaveney, "Effects of debris on ice-surface melting rates: an experimental study," *Journal of Glaciology*, vol. 56, no. 197, pp. 384–394, 2010.

[78] M. J. Hambrey, D. J. Quincey, N. F. Glasser, J. M. Reynolds, S. J. Richardson, and S. Clemmens, "Sedimentological, geomorphological and dynamic context of debris-mantled glaciers, mount everest (sagarmatha) region, nepal," *Quaternary Science Reviews*, vol. 27, no. 25-26, pp. 2361–2389, 2008.

[79] T. Bolch, M. F. Buchroithner, J. Peters, M. Baessler, and S. Bajracharya, "Identification of glacier motion and potentially dangerous glacial lakes in the mt. everest region/nepal using spaceborne imagery," *Natural Hazards and Earth System Sciences*, vol. 8, no. 6, pp. 1329–1340, 2008.

[80] M. P. Kirkbride and P. Deline, "The formation of supraglacial debris covers by primary dispersal from transverse englacial debris bands," *Earth Surface Processes and Landforms*, vol. 38, no. 15, pp. 1779–1792, 2013.

[81] S. Thakuri, F. Salerno, C. Smiraglia, T. Bolch, C. D'Agata, G. Viviano, and G. Tartari, "Tracing glacier changes since the 1960s on the south slope of mt. everest (central southern himalaya) using optical satellite imagery," 2014.

[82] M. Juen, C. Mayer, A. Lambrecht, H. Han, and S. Liu, "Impact of varying debris cover thickness on ablation: a case study for koxkar glacier in the tien shan," *The Cryosphere*, vol. 8, no. 2, p. 377, 2014.

[83] D. R. Rounce, O. King, M. McCarthy, D. E. Shean, and F. Salerno, "Quantifying debris thickness of debris-covered glaciers in the everest region of nepal through inversion of a subdebris melt model," *Journal of Geophysical Research: Earth Surface*, vol. 123, no. 5, pp. 1094–1115, 2018.

[84] M. S. Pelto, "Mass balance of adjacent debris-covered and clean glacier ice in the north cascades, washington," *Iahs Publication*, pp. 35–42, 2000.

[85] P. Buri, E. S. Miles, J. F. Steiner, W. W. Immerzeel, P. Wagnon, and F. Pellicciotti, "A physically based 3-d model of ice cliff evolution over debris-covered glaciers," *Journal of Geophysical Research: Earth Surface*, vol. 121, no. 12, pp. 2471–2493, 2016.

[86] H. Chen and C. Lee, "Numerical simulation of debris flows," *Canadian Geotechnical Journal*, vol. 37, no. 1, pp. 146–160, 2000.

[87] C.-Z. Qin and L. Zhan, "Parallelizing flow-accumulation calculations on graphics processing units—from iterative dem preprocessing algorithm to recursive multiple-flow-direction algorithm," *Computers & Geosciences*, vol. 43, pp. 7–16, 2012.

[88] T. van Woerkom, J. F. Steiner, P. D. Kraaijenbrink, E. Miles, and W. W. Immerzeel, "Sediment supply from lateral moraines to a debris-covered glacier in the himalaya," *Earth Surface Dynamics*, vol. 7, pp. 411–427, 2019.

[89] N. Spedding, "Hydrological controls on sediment transport pathways: implications for debris-covered glaciers," *IAHS publication*, pp. 133–142, 2000.

[90] J. R. Mertes, S. S. Thompson, A. D. Booth, J. D. Gulley, and D. I. Benn, "A conceptual model of supra-glacial lake formation on debris-covered glaciers based on gpr facies analysis," *Earth Surface Processes and Landforms*, vol. 42, no. 6, pp. 903–914, 2017.

[91] L. Huang, Z. Li, H. Han, B. Tian, and J. Zhou, "Analysis of thickness changes and the associated driving factors on a debris-covered glacier in the tienshan mountain," *Remote Sensing of Environment*, vol. 206, pp. 63–71, 2018.

[92] R. J. Braithwaite and O. B. Olesen, "Response of the energy balance on the margin of the greenland ice sheet to temperature changes," *Journal of glaciology*, vol. 36, no. 123, pp. 217–221, 1990.

[93] A. Kellerer-Pirklbauer, "The supraglacial debris system at the pasterze glacier, austria: spatial distribution, characteristics and transport of debris," *Zeitschrift für Geomorphologie, Supplementary Issues*, vol. 52, no. 1, pp. 3–25, 2008.

[94] D. J. Quincey and N. F. Glasser, "Morphological and ice-dynamical changes on the tasman glacier, new zealand, 1990–2007," *Global and Planetary Change*, vol. 68, no. 3, pp. 185–197, 2009.

[95] S. H. Mernild and B. Hasholt, "Climatic control on river discharge simulations, mittivakkat glacier catchment, ammassalik island, se greenland," *Hydrology Research*, vol. 37, no. 4-5, pp. 327–346, 2006.

[96] D. Quincey, M. Braun, N. F. Glasser, M. Bishop, K. Hewitt, and A. Luckman, "Karakoram glacier surge dynamics," *Geophysical Research Letters*, vol. 38, no. 18, 2011.

[97] R. McNabb, R. Hock, S. O'Neel, L. A. Rasmussen, Y. Ahn, M. Braun, H. Conway, S. Herreid, I. Joughin, W. Pfeffer, *et al.*, "Using surface velocities to calculate ice thickness and bed topography: a case study at columbia glacier, alaska, usa," *Journal of Glaciology*, vol. 58, no. 212, pp. 1151–1164, 2012.

[98] D. Farinotti, M. Huss, A. Bauder, M. Funk, and M. Truffer, "A method to estimate the ice volume and ice-thickness distribution of alpine glaciers," *Journal of Glaciology*, vol. 55, no. 191, pp. 422–430, 2009.

[99] P. Gantayat, A. V. Kulkarni, and J. Srinivasan, "Estimation of ice thickness using surface velocities and slope: case study at gangotri glacier, india," *Journal of Glaciology*, vol. 60, no. 220, pp. 277–282, 2014.

[100] M. Morlighem, E. Rignot, H. Seroussi, E. Larour, H. Ben Dhia, and D. Aubry, "A mass conservation approach for mapping glacier ice thickness," *Geophysical Research Letters*, vol. 38, no. 19, 2011.

[101] D. Farinotti, D. Brinkerhoff, G. K. Clarke, J. J. Fürst, H. Frey, P. Gantayat, F. Gillet-Chaulet, C. Girard, M. Huss, P. W. Leclercq, *et al.*, "How accurate are estimates of glacier ice thickness? results from itmix, the ice thickness models intercomparison experiment," *The Cryosphere Discussions*, 2016.

[102] L. Morland and I. Johnson, "Steady motion of ice sheets," *Journal of Glaciology*, vol. 25, no. 92, pp. 229–246, 1980.

[103] F. Herman and J. Braun, "Evolution of the glacial landscape of the southern alps of new zealand: Insights from a glacial erosion model," *Journal of Geophysical Research: Earth Surface*, vol. 113, no. F2, 2008.

[104] E. Bueler and J. Brown, "Shallow shelf approximation as a "sliding law" in a thermo-mechanically coupled ice sheet model," *Journal of Geophysical Research: Earth Surface*, vol. 114, no. F3, 2009.

[105] J. Savage and W. Paterson, "Borehole measurements in the athabasca glacier," *Journal of Geophysical Research*, vol. 68, no. 15, pp. 4521–4536, 1963.

[106] R. Greve, "Application of a polythermal three-dimensional ice sheet model to the greenland ice sheet: response to steady-state and transient climate scenarios," *Journal of Climate*, vol. 10, no. 5, pp. 901–918, 1997.

[107] A. Fowler, "Glaciers and ice sheets," in *The Mathematics of Models for Climatology and Environment*, pp. 301–336, Springer, 1997.

[108] D. L. Egholm, M. F. Knudsen, C. D. Clark, and J. E. Lesemann, "Modeling the flow of glaciers in steep terrains: The integrated second-order shallow ice approximation (isosia)," *Journal of Geophysical Research: Earth Surface*, vol. 116, no. F2, 2011.

[109] J. Braun, D. Zwartz, and J. H. Tomkin, "A new surface-processes model combining glacial and fluvial erosion," *Annals of Glaciology*, vol. 28, pp. 282–290, 1999.

[110] N. R. Iverson, D. Cohen, T. S. Hooyer, U. H. Fischer, M. Jackson, P. L. Moore, G. Lappegard, and J. Kohler, "Effects of basal debris on glacier flow," *Science*, vol. 301, no. 5629, pp. 81–84, 2003.

[111] J. M. Harbor, "Numerical modeling of the development of u-shaped valleys by glacial erosion," *Geological Society of America Bulletin*, vol. 104, no. 10, pp. 1364–1375, 1992.

[112] J. H. Tomkin and J. Braun, "The influence of alpine glaciation on the relief of tectonically active mountain belts," *American Journal of Science*, vol. 302, no. 3, pp. 169–190, 2002.

[113] M. A. Kessler, R. S. Anderson, and G. M. Stock, "Modeling topographic and climatic control of east-west asymmetry in sierra nevada glacier length during the last glacial maximum," *Journal of Geophysical Research: Earth Surface*, vol. 111, no. F2, 2006.

[114] D. R. Montgomery and M. T. Brandon, "Topographic controls on erosion rates in tectonically active mountain ranges," *Earth and Planetary Science Letters*, vol. 201, no. 3-4, pp. 481–489, 2002.

[115] F. Herman, F. Beaud, J.-D. Champagnac, J.-M. Lemieux, and P. Sternai, "Glacial hydrology and erosion patterns: a mechanism for carving glacial valleys," *Earth and Planetary Science Letters*, vol. 310, no. 3-4, pp. 498–508, 2011.

[116] P. Steer, R. S. Huismans, P. G. Valla, S. Gac, and F. Herman, "Bimodal plio–quaternary glacial erosion of fjords and low-relief surfaces in scandinavia," *Nature Geoscience*, vol. 5, no. 9, pp. 635–639, 2012.

[117] M. Dühnforth, R. S. Anderson, D. Ward, and G. M. Stock, "Bedrock fracture control of glacial erosion processes and rates," *Geology*, vol. 38, no. 5, pp. 423–426, 2010.

[118] S. V. Ugelvig, D. L. Egholm, and N. R. Iverson, "Glacial landscape evolution by subglacial quarrying: A multiscale computational approach," *Journal of Geophysical Research: Earth Surface*, vol. 121, no. 11, pp. 2042–2068, 2016.

[119] D. Scherler, B. Bookhagen, and M. R. Strecker, "Spatially variable response of himalayan glaciers to climate change affected by debris cover," *Nature geoscience*, vol. 4, no. 3, pp. 156–159, 2011.

[120] E. Berthier, H. Vadon, D. Baratoux, Y. Arnaud, C. Vincent, K. Feigl, F. Remy, and B. Legresy, "Surface motion of mountain glaciers derived from satellite optical imagery," *Remote Sensing of Environment*, vol. 95, no. 1, pp. 14–28, 2005.

[121] E. W. Burgess, R. R. Forster, and C. F. Larsen, "Flow velocities of alaskan glaciers," *Nature communications*, vol. 4, no. 1, pp. 1–8, 2013.

[122] B. H. Raup, L. M. Andreassen, T. Bolch, and S. Bevan, "Remote sensing of glaciers," *Remote Sensing of the Cryosphere*, pp. 123–56, 2015.

[123] M. Fahnestock, T. Scambos, T. Moon, A. Gardner, T. Haran, and M. Klinger, "Rapid large-area mapping of ice flow using landsat 8," *Remote Sensing of Environment*, vol. 185, pp. 84–94, 2016.

[124] F. Paul, C. Huggel, and A. Kääb, "Combining satellite multispectral image data and a digital elevation model for mapping debris-covered glaciers," *Remote sensing of Environment*, vol. 89, no. 4, pp. 510–518, 2004.

[125] A. Brenning, "Benchmarking classifiers to optimally integrate terrain analysis and multispectral remote sensing in automatic rock glacier detection," *Remote Sensing of Environment*, vol. 113, no. 1, pp. 239–247, 2009.

[126] N. Karimi, A. Farokhnia, L. Karimi, M. Eftekhari, and H. Ghalkhani, "Combining optical and thermal remote sensing data for mapping debris-covered glaciers (alamkouh glaciers, iran)," *Cold Regions Science and Technology*, vol. 71, pp. 73–83, 2012.

[127] M. P. Bishop, J. F. Shroder, G. Ali, A. B. Bush, U. K. Haritashya, R. Roohi, M. A. Sarikaya, and B. J. Weihs, "Remote sensing of glaciers in afghanistan and pakistan," in *Global land ice measurements from space*, pp. 509–548, Springer, 2014.

[128] A. Luckman, D. Quincey, and S. Bevan, "The potential of satellite radar interferometry and feature tracking for monitoring flow rates of himalayan glaciers," *Remote sensing of Environment*, vol. 111, no. 2-3, pp. 172–181, 2007.

[129] A. Shukla and I. Ali, "A hierarchical knowledge-based classification for glacier terrain mapping: a case study from kolahoi glacier, kashmir himalaya," *Annals of Glaciology*, vol. 57, no. 71, pp. 1–10, 2016.

[130] S. Ojha, K. Fujita, A. Sakai, H. Nagai, and D. Lamsal, "Topographic controls on the debris-cover extent of glaciers in the eastern himalayas: Regional analysis using a novel high-resolution glacier inventory," *Quaternary International*, vol. 455, pp. 82–92, 2017.

[131] M. Gibson, N. Glasser, D. J. Quincey, A. V. Rowan, and T. Irvine-Fynn, "Changes in glacier surface cover on baltoro glacier, karakoram, north pakistan, 2001–2012," *Journal of Maps*, vol. 13, no. 2, pp. 100–108, 2017.

[132] D. M. Rippin, A. Pomfret, and N. King, "High resolution mapping of supra-glacial drainage pathways reveals link between micro-channel drainage density, surface roughness and surface reflectance," *Earth Surface Processes and Landforms*, vol. 40, no. 10, pp. 1279–1290, 2015.

[133] W. Immerzeel, P. Kraaijenbrink, J. Shea, A. Shrestha, F. Pellicciotti, M. Bierkens, and S. De Jong, "High-resolution monitoring of himalayan glacier dynamics using unmanned aerial vehicles," *Remote Sensing of Environment*, vol. 150, pp. 93–103, 2014.

[134] P. S. Hill, J. P. Syvitski, E. A. Cowan, and R. D. Powell, "In situ observations of floc settling velocities in glacier bay, alaska," *Marine Geology*, vol. 145, no. 1-2, pp. 85–94, 1998.

[135] A. Ahlstrøm, S. B. Andersen, F. Nick, C. Reijmer, R. van de Wal, and A. Hubbard, "Seasonal velocities of eight major marine-terminating outlet glaciers of the greenland ice sheet from continuous in situ gps instruments," *Earth system science data discussions*, vol. 6, no. 1, pp. 27–57, 2013.

[136] T. A. Scambos, M. J. Dutkiewicz, J. C. Wilson, and R. A. Bindschadler, "Application of image cross-correlation to the measurement of glacier velocity using satellite image data," *Remote sensing of environment*, vol. 42, no. 3, pp. 177–186, 1992.

[137] R. Bindschadler, M. Fahnestock, P. Skvarca, and T. Scambos, "Surface-velocity field of the northern larsen ice shelf, antarctica," *Annals of Glaciology*, vol. 20, pp. 319–326, 1994.

[138] M. Frezzotti, A. Capra, and L. Vittuari, "Comparison between glacier ice velocities inferred from gps and sequential satellite images," *Annals of Glaciology*, vol. 27, pp. 54–60, 1998.

[139] A. N. Evans, "Glacier surface motion computation from digital image sequences," *IEEE Transactions on Geoscience and Remote Sensing*, vol. 38, no. 2, pp. 1064–1072, 2000.

[140] A. Kääb, "Combination of srtm3 and repeat aster data for deriving alpine glacier flow velocities in the bhutan himalaya," *Remote Sensing of Environment*, vol. 94, no. 4, pp. 463–474, 2005.

[141] F. Ayoub, S. Leprince, and J.-P. Avouac, "Co-registration and correlation of aerial photographs for ground deformation measurements," *ISPRS Journal of Photogrammetry and Remote Sensing*, vol. 64, no. 6, pp. 551–560, 2009.

[142] Z. Chi, *Investigation of Glacial Dynamics in the Lambert Glacier-Amery Ice Shelf System (LAS) Using Remote Sensing*. PhD thesis, 2012.

[143] V. Kumar, G. Venkataramana, and K. A. Høgda, "Glacier surface velocity estimation using sar interferometry technique applying ascending and descending passes in himalayas," *International Journal of Applied Earth Observation and Geoinformation*, vol. 13, no. 4, pp. 545–551, 2011.

[144] F. Casu, M. Manzo, and R. Lanari, "A quantitative assessment of the sbas algorithm performance for surface deformation retrieval from dinsar data," *Remote Sensing of Environment*, vol. 102, no. 3-4, pp. 195–210, 2006.

[145] T. Strozzi, U. Wegmuller, L. Tosi, G. Bitelli, and V. Spreckels, "Land subsidence monitoring with differential sar interferometry," *Photogrammetric engineering and remote sensing*, vol. 67, no. 11, pp. 1261–1270, 2001.

[146] L. Liu, L. Jiang, Y. Sun, H. Wang, C. Yi, and H. Hsu, "Morphometric controls on glacier mass balance of the puruogangri ice field, central tibetan plateau," *Water*, vol. 8, no. 11, p. 496, 2016.

[147] E. Collier, T. Mölg, F. Maussion, D. Scherer, C. Mayer, and A. Bush, "High-resolution interactive modelling of the mountain glacier-atmosphere interface: an application over the karakoram," *The Cryosphere*, vol. 7, no. 3, p. 779, 2013.

[148] J. Oerlemans, "Quantifying global warming from the retreat of glaciers," *Science*, vol. 264, no. 5156, pp. 243–245, 1994.

[149] J. Dozier and J. Frew, "Rapid calculation of terrain parameters for radiation modeling from digital elevation data," *IEEE Transactions on Geoscience and Remote Sensing*, vol. 28, no. 5, pp. 963–969, 1990.

[150] B. Y. Liu and R. C. Jordan, "The interrelationship and characteristic distribution of direct, diffuse and total solar radiation," *Solar energy*, vol. 4, no. 3, pp. 1–19, 1960.

[151] P. Reggiani, G. Coccia, and B. Mukhopadhyay, "Predictive uncertainty estimation on a precipitation and temperature reanalysis ensemble for shigar basin, central karakoram," *Water*, vol. 8, no. 6, p. 263, 2016.

[152] F. Li, D. L. Jupp, M. Thankappan, L. Lymburner, N. Mueller, A. Lewis, and A. Held, "A physics-based atmospheric and brdf correction for landsat data over mountainous terrain," *Remote Sensing of Environment*, vol. 124, pp. 756–770, 2012.

[153] O. Hungr, "A model for the runout analysis of rapid flow slides, debris flows, and avalanches," *Canadian Geotechnical Journal*, vol. 32, no. 4, pp. 610–623, 1995.

[154] O. Hungr and N. Morgenstern, "Experiments in high velocity open channel flow of granular materials," *Géotechnique*, vol. 34, pp. 405–413, 1984.

[155] K. Hutter and S. Savage, "Avalanche dynamics: the motion of a finite mass of gravel down a mountain side," in *International symposium on landslides. 5*, pp. 691–697, 1988.

[156] T. G. Freeman, "Calculating catchment area with divergent flow based on a regular grid," *Computers & Geosciences*, vol. 17, no. 3, pp. 413–422, 1991.

[157] N. Takeuchi and Z. Li, "Characteristics of surface dust on ürümqi glacier no. 1 in the tien shan mountains, china," *Arctic, Antarctic, and Alpine Research*, vol. 40, no. 4, pp. 744–750, 2008.

[158] X. Yue, J. Zhao, Z. Li, M. Zhang, J. Fan, L. Wang, and P. Wang, "Spatial and temporal variations of the surface albedo and other factors influencing urumqi glacier no. 1 in tien shan, china," *Journal of Glaciology*, vol. 63, no. 241, pp. 899–911, 2017.

[159] J. Coakley, "Reflectance and albedo, surface," *Encyclopedia of the Atmosphere*, pp. 1914–1923, 2003.

[160] M. P. Bishop and J. D. Colby, "Topographic normalization of multispectral satellite imagery," *Journal of Glaciology*, vol. 55, pp. 131–146, 2011.

[161] S. Liang, "Narrowband to broadband conversions of land surface albedo i: Algorithms," *Remote sensing of environment*, vol. 76, no. 2, pp. 213–238, 2001.

[162] S. D. Richardson and J. M. Reynolds, "An overview of glacial hazards in the himalayas," *Quaternary International*, vol. 65, pp. 31–47, 2000.

[163] C. S. Watson, D. J. Quincey, J. L. Carrivick, and M. W. Smith, "The dynamics of supraglacial ponds in the everest region, central himalaya," *Global and Planetary Change*, vol. 142, pp. 14–27, 2016.

[164] E. S. Miles, F. Pellicciotti, I. C. Willis, J. F. Steiner, P. Buri, and N. S. Arnold, "Refined energy-balance modelling of a supraglacial pond, langtang khola, nepal," *Annals of Glaciology*, vol. 57, no. 71, pp. 29–40, 2016.

[165] H. Thomsen and N. Reeh, "Glaciological investigations at the margin of the inland ice northeast of jakobshavn, west greenland," *Grønl. Geol. Unders. Rapp*, vol. 130, pp. 102–108, 1986.

[166] M. Lüthje, D. Feltham, P. Taylor, and M. Worster, "Modeling the summertime evolution of sea-ice melt ponds," *Journal of Geophysical Research: Oceans*, vol. 111, no. C2, 2006.

[167] L. S. Anderson, "Glacier response to climate change: modeling the effects of weather and debris-cover," *Geological Sciences Graduate Theses and Dissertations.*, 2014.

[168] T. M. Lenton, H. Held, E. Kriegler, J. W. Hall, W. Lucht, S. Rahmstorf, and H. J. Schellnhuber, "Tipping elements in the earth's climate system," *Proceedings of the national Academy of Sciences*, vol. 105, no. 6, pp. 1786–1793, 2008.

[169] T. M. Lenton, "Environmental tipping points," *Annual Review of Environment and Resources*, vol. 38, pp. 1–29, 2013.

[170] Z. A. Thomas, "Using natural archives to detect climate and environmental tipping points in the earth system," *Quaternary Science Reviews*, vol. 152, pp. 60–71, 2016.

[171] P. K. Krishnamurthy R, J. B. Fisher, D. S. Schimel, and P. M. Kareiva, "Applying tipping point theory to remote sensing science to improve early warning drought signals for food security," *Earth's Future*, vol. 8, no. 3, p. e2019EF001456, 2020.

[172] V. Dakos, S. R. Carpenter, W. A. Brock, A. M. Ellison, V. Guttal, A. R. Ives, S. Kefi, V. Livina, D. A. Seekell, E. H. van Nes, *et al.*, "Methods for detecting early warnings of critical transitions in time series illustrated using simulated ecological data," *PloS one*, vol. 7, no. 7, 2012.

[173] R. Lindsay and J. Zhang, "The thinning of arctic sea ice, 1988–2003: Have we passed a tipping point?," *Journal of Climate*, vol. 18, no. 22, pp. 4879–4894, 2005.

[174] T. J. Hefley, A. J. Tyre, and E. E. Blankenship, "Statistical indicators and state–space population models predict extinction in a population of bobwhite quail," *Theoretical Ecology*, vol. 6, no. 3, pp. 319–331, 2013.

[175] A. J. Veraart, E. J. Faassen, V. Dakos, E. H. van Nes, M. Lürling, and M. Scheffer, "Recovery rates reflect distance to a tipping point in a living system," *Nature*, vol. 481, no. 7381, pp. 357–359, 2012.

[176] R. D. Batt, W. A. Brock, S. R. Carpenter, J. J. Cole, M. L. Pace, and D. A. Seekell, "Asymmetric response of early warning indicators of phytoplankton transition to and from cycles," *Theoretical ecology*, vol. 6, no. 3, pp. 285–293, 2013.

[177] S. R. Carpenter and W. A. Brock, "Rising variance: a leading indicator of ecological transition," *Ecology letters*, vol. 9, no. 3, pp. 311–318, 2006.

[178] G. Takimoto, "Early warning signals of demographic regime shifts in invading populations," *Population ecology*, vol. 51, no. 3, pp. 419–426, 2009.

[179] M. McClenaghan and R. Paulen, "Application of till mineralogy and geochemistry to mineral exploration," in *Past glacial environments*, pp. 689–751, Elsevier, 2018.

[180] S. J. Cook, D. A. Swift, M. P. Kirkbride, P. G. Knight, and R. I. Waller, "The empirical basis for modelling glacial erosion rates," *Nature communications*, vol. 11, no. 1, pp. 1–7, 2020.